Sound Findings on Hand Dynamics

Validation and Application of Ultrasound Speckle Tracking of Tendon and Nerve Dynamics

ir. drs. Jan-Wiebe H. Korstanje

Paranimfen: Mevr. dr. L.M.J.W. van Driel MSc and Ir. J.J.M. Korstanje

Printing: Optima Grafische Communicatie, Rotterdam, The Netherlands

ISBN: 978-94-6169-119-4

Sound Findings on Hand Dynamics

Validation and Application of Ultrasound Speckle Tracking of Tendon and Nerve Dynamics

Weerklinkende bevindingen over hand dynamica

Validatie en applicatie van ultrageluid speckle tracking van de pees en zenuw dynamica

Proefschrift

ter verkrijging van de graad van doctor aan de
Erasmus Universiteit Rotterdam
op gezag van de rector magnificus

Prof. dr. H.G. Schmidt

en volgens besluit van het College voor Promoties.
De openbare verdediging zal plaatsvinden op

woensdag 16 november 2011 om 11:30 uur

Ir. drs. Jan-Wiebe Herman Korstanje

geboren te Hoorn

Promotoren:	Prof. dr. H.J. Stam Prof. dr. S.E.R. Hovius
Overige leden:	Prof. dr. G.J. Kleinrensink Prof. dr. H.E.J. Veeger Dr. ir. J.G. Bosch
Copromotor:	Dr. R.W. Selles

Chapter 1
General Introduction

HISTORY IMAGING MODALITIES

The wish or need to capture body structures and motion in an image is a long-lasting quest. Already dating back 30,000 years ago, an image of a mammoth's heart painted on a cave wall was made by Aurignacian men[146]. Not until the late 1890s the first realistic imaging modality was invented, namely the static Roentgen or X-ray image by Wilhelm Conrad Roentgen[175].

Another imaging modality, based on the principle of using X-rays, is the computed tomography (CT) that was introduced in 1930 by Vallebona[73]. However, it took more than 40 years before the first clinical static CT image was made. The acquisition time of a single slide ranged from 4 to 8 minutes. Improvements in acquisition time followed in a rapid pace and within 10 years the first dynamic CT image sequences (and thus a movie) of a heart were made by the Boyd and colleagues [115]. However, while the dynamic CT images had a relatively high temporal resolution, they had a poor spatial resolution compared to static images.

Shortly after CT, ultrasound (US) was introduced, based on the principal of piezoelectricity first described in the 1880s by Pierre and Jacques Curie[73]. US was first applied during World War I to detect submarines. In the late 1930s, US was used for the first time in a clinical setting to detect tumors in the head using two single transducers, rendering a so-called A-mode "image"[73]. An A-mode "image" is basically a plot with on the y-axis the intensity of the received signal and on the x-axis the time or distance. In 1947 the first B-mode US scanner was developed, which was able to construct real static images[73]. A B-mode image is a 2D representation of an A-mode "image" after brightness modulation. After 20 years of research and development, in 1970, the first real time B-mode scanner was introduced[73].

Soon after the introduction of US in a clinical setting, nuclear magnetic resonance (NMR) was introduced in the field of chemistry in the late 1940s[73]. It was until the mid 1980s before the NMR was used in a clinical setting to static images[36]. Only a few years later the first dynamic NMR image sequences were acquired, called MR fluoroscopy[157].

The before mentioned imaging modalities are generally accepted modalities for anatomical imaging, although several other valuable imaging modalities exist, e.g. scintigraphy, single photon emission computed tomography (SPECT), and positron emission tomography (PET) scan. However, for capturing dynamic behavior of structures, several of these imaging modalities are less suitable than others. The following subchapter will discuss the most suitable imaging modalities for dynamic imaging of the hand.

DYNAMIC IMAGING OF THE HAND

Dynamic imaging of the hand and wrist would give valuable insight in the complex interaction between tendons, nerves, and their surrounding tissue during hand movements. Moreover, it could provide clinicians and therapists with valuable information to objectively diagnose patients, or to follow progress in patients over time. However, the dynamic behavior of the hand and its tendons and nerves is hard to capture with a clinical imaging modality, let alone to quantify its behavior. The first problem with imaging the dynamic behavior of the hand is the high physiological range of velocities. Velocities can go up to 30 mm/s[35], which is challenging for any clinical imaging modality to image real-time with a reasonable frame rate. Furthermore, when imaging the dynamic behavior of the hand or its tendons and nerves it is also important to maintain a reasonable image quality in order to analyze or track any given structure with reasonable accuracy.

Two key terms in describing the performance of an imaging modality are temporal resolution and spatial resolution. The temporal resolution refers to the ability of an imaging modality to visualize moving objects. In other words, it is a measure of the fastest object motion that can be detected. Thus, the higher the temporal resolution, the faster the imaging modality is able to produce separate images. This is also known as the frame rate of the measurement sequence. The spatial resolution refers to the ability of the imaging modality to discern be-

tween two different objects. So, generally speaking, it is desirable to have a high temporal resolution to achieve real-time imaging and high spatial resolution to achieve accurate tracking. Unfortunately, there is often a trade-off between the temporal resolution and spatial resolution. CT has the lowest temporal resolution, followed by MRI, and finally US, while for the spatial resolution, MRI has the lowest in-plane resolution, followed by CT, and finally US.

From the above, it is clear that US is the obvious choice for imaging hand dynamics with high spatial resolution and high temporal resolution. Nevertheless, it should be noted that US also has downsides, mainly a poor image quality and a small field-of-view (FOV). Speckle noise is the main contributor to the poor image quality of US images[191]. Speckle noise is seen as a smeared dotted texture, which is generated by the scattering of the US waves due to irregularities in the tissue much smaller than the wavelength of the US[191]. Although the speckle pattern does not resemble the underlying anatomical structure, it does have a distinct pattern for different tissues. Although speckle noise reduces image quality, it is the cornerstone of speckle tracking which is discussed in the next subchapter. In addition to the problem of speckle noise, the field-of-view (FOV is relatively small compared to MRI or CT. The FOV is the part that you can actually capture in an image. The limited FOV could potentially limit the length over which structures can be tracked. Because of the speckle noise and the small field of view, US images can be difficult to relate to their anatomical context[83,147].

US is not the only imaging modality used to study tendon and nerve dynamics in-vivo. The first in-vivo studies on tendon excursions used radiographs to image markers attached to the tendon[149,168,205,214]. Due to the harmful ionizing radiation and the lack of real-time imaging capabilities, new techniques were introduced. US Doppler was one of the first techniques to measure tendon and nerve dynamics in-vivo, as Doppler was readily available on clinical US scanners[29,81,173]. Part of the US Doppler research has been performed by Hans Soeters at the Department of Rehabilitation of the Erasmus MC in Rotterdam. An advantage of Doppler is its capability to measure real-time. A major disadvantage of Doppler is its moderate accuracy, mostly due to angle estimation errors. For Doppler measurements, the scan head needs to be positioned under an angle to accurately measure velocities and excursions. The larger the angle between the US beam and the structure to be imaged, the more prone the velocity and excursion estimations are to errors. This is because the Doppler frequency depends on the cosine of the angle, thus an angle of 80° with 1° measurement error will generate larger errors in the Doppler frequency (≈10%) than an angle approximating 45° with 1° measurement error (≈2%). To overcome the angle-dependency of Doppler, new techniques were developed based on US using the B-mode images to track structures[34]. This again has the advantage that it is capable of real-time imaging, but does not have the disadvantage of angle dependent errors.

Several studies focused on the development of these ultrasound tracking algorithms, mainly focusing on cardiac tracking[56,202] and some on nerve tracking[34]. The main challenge in using these algorithms for measuring dynamics of tendons and nerves lies in the optimization needed for soft tissue tracking, which leaves room for further optimization towards tendon tracking. Therefore, the first chapters (Chapters 2 and 3) will focus on the optimization and validation of speckle tracking algorithm specifically for measuring tendon displacement.

While Chapters 2 and 3 focus on the development of tendon and nerve tracking using ultrasound, the following chapters of this thesis will describe the application of these techniques to hand flexor tendon injuries, carpal tunnel syndrome (CTS), and on measuring the digital nerve, since ultrasound may have important benefits in the early detection of changes in hand dynamics using our novel US tracking algorithm.

Hand injuries are an important burden to society. The incidence rate of hand and wrist injuries is about 1,800 per 100,000 inhabitants in The Netherlands, which is comparable to the incidence rate in Northern Europe (1,500-3,800 per 100,000)[106]. Approximately 26% of the hand and wrist injuries involve tendon lesions or lacerations[212]. Although overall the treatment for flexor tendon injuries is successful, there are four main aspects that affect the success rate: 1) the kind of injury (e.g., the number of affected fingers and affected zone), 2) the surgical techniques used, 3) patient compliance in wearing their splint, and 4) the rehabilitation protocol[15,160,190,193].

The first aspect that influences success of treatment for flexor tendon injuries is the kind of injury. The number of injured fingers is negatively correlated with the success of treatment[193]. In zone II (Fig. 1: Overview of the different zones in the hand according to Verdan[201]), patients with single digit injuries overall have a higher active ROM for distal interphalangeal (DIP) joint and proximal interphalangeal (PIP) joint, higher satisfaction score, and less flexion contractures compared to patients with multiple digit injuries[193]. Furthermore, when looking at the success of treatment per zone, there is a wide range in success rates for zone II (64-91% good-excellent) and zone V (55-100% good-excellent)[10,25,39,84,111]. Obviously, results are difficult to compare as the before-mentioned four main aspects influence the results. Another problem which makes comparison difficult is the variety in scoring systems used, e.g. Buck-Gramcko[20], Strickland[178], and Modified Strickland[178]. However, the consensus is that zone II injuries are more often prone to poor outcome than zone V[10], probably due to factors such as better vascularization and less constrictive space in zone V compared to zone II[111].

The second aspect that influences success of treatment is the surgical technique. There are several different suture techniques used for end-to-end flexor tendon repair, e.g. the Bunnell stitch[21], Kessler stitch[98], 2-strand, 4-strand[129,179], 6-strand[114,161], and 8-strand[169]. Commonly, there are no differences in the suture technique applied in the different zones[111]. As can be seen from this list, the focus over the recent years has mainly been on the development of more core sutures (the multi-strand techniques) to increase the resilience against tendon loading. This seems reasonable because the 2-strand does not withstand light active gripping during week 1 through week 3 postoperative. In contrast, the 4-, 6-, and 8-strand techniques are better able to withstand forces of light active gripping from day one of rehabilitation[180] . However, a serious downside to multi-strand techniques is that increasing the number of core-sutures will likely increase the chance of extensively damaging the tendon[180]. Nevertheless, the rationale for developing multi-strand sutures is to allow early active mobilization protocols, as these protocols are associated with a lower risk of adhesion formation.

The third aspect that influences success of treatment is patient compliance[160]. Most patients with hand flexor tendon lacerations follow a 12-week mobilization program, during which patients must wear their mobilization splint continuously. Sandford et al. reported that 67% of these patients are non-compliant. Of these patients, 25% removed their splint daily, but mostly less than an hour (75%). Male patients showed a significant correlation with splint removal and might therefore be considered a high-risk group[160].

The last aspect that influences success of treatment is the mobilization protocol. The goal of rehabilitation is to regain hand function and prevent tendon adhesions[111]; this can be achieved by mobilization of the injured hand[67]. As shortly mentioned in the previous paragraph, mobilization protocols can influence rupture rate and risk of adhesion formation. Traditionally immobilization was preferred to prevent excessive stress on the repair site that could lead to a re-rupture of the tendon[67]. This, however, leads to a higher adhesion rate due to lacking tendon excursion during rehabilitation. Although not supported by firm scientific data, Duran and Houser (presented at the AAOS Symposium on Ten-

don Surgery in the Hand, 1975) proposed a minimum excursion of at least 5 mm to prevent firm adhesions. Two mainstream rehabilitation mobilization protocols can be distinguished to obtain tendon excursion, namely early active mobilization and passive mobilization[66,67]. The two most-commonly used protocols within the group of passive mobilization protocols are the modified Kleinert protocol and the four-finger protocol[63,96]. Both protocols pose an extension constraint on the metacarpophalangeal (MCP) joint, but still allow some flexion and extension of the MCP joint. In both protocols, patients actively extend their injured fingers, while flexion is achieved by an elastic band attached to the tip of the fingers (Fig. 2). The difference between the Kleinert protocol and the four-finger protocol is that the latter protocol uses elastic bands on all fingers on the injured side, in contrast to only the injured finger in the Kleinert protocol. The early active mobilization protocols, as in the passive mobilization protocols, still include an extension constraint, but in contrast to the passive mobilization protocol, patients are allowed to use their injured fingers without assistance of rubber bands albeit with low loads[66,67]. The advantage of early active mobilization over passive mobilization would be the increased tendon excursion leading to less adhesion, possibly at the expense of a higher re-rupture rate[58].

Evaluating the four main aspects influencing success rate after hand flexor tendon laceration, it is obvious that the kind of injury cannot be influenced during surgery and rehabilitation. It has also been reported that suture techniques have evolved to enable early active mobilization without an increased incidence of tendon ruptures[193]. However, it is still unclear what the biomechanical behavior of tendons is during different mobilization protocols. It could very well be that early active mobilization is not a necessity, but that optimization of a passive mobilization protocol can be sufficient to obtain enough tendon gliding to prevent adhesion formation. This is more elaborately discussed in Chapters 4 and 5.

Only a limited number of studies have attempted to describe or assess the biomechanical behavior of the tendons during the different rehabilitation protocols[78,128,149,189], with highly conflicting results. An extra complication in the assessment of the effects of rehabilitation protocols on tendon excursion is the complex interaction between the hand flexor tendons. This interaction exists due to fine meshed tissue connecting the different structures called the subsynovial connective tissue (SSCT) (Fig. 3). As the SSCT is very thin, its excursion has only been measured invasively and its biomechanical behavior with respect to the hand flexor tendons and the median nerve is still unknown. This has lead to the several questions concerning the SSCT and its interaction with the hand flexor tendons and the MN. For example, it is still unknown which rehabilitation protocols do actually achieve the 5 mm excursion suggested to prevent tendon adhesions. Furthermore, it is also unknown what the influence of the uninjured fingers is on the tendon excursion of the injured fingers as the hand flexor tendons are interconnected by SSCT and thereby could influence their individual dynamic behavior. Moreover, insight in the biomechanical behavior of the hand flexor tendons during different rehabilitation protocols can have an additive value in classifying rehabilitation protocols as it could help physicians and therapists in selecting the most appropriate rehabilitation protocol based on patients needs. The lack of the biomechanical understanding of the complex network of tendons, subsynovial connective tissue (SSCT), and pulleys on tendon excursion is the drive for this part of the thesis.

Although hand flexor tendon repair and rehabilitation are an obvious choice when looking at the clinical impact of biomechanical behavior of tendons, nerves, and SSCT, there is more to explore in terms of clinical impact. Several impairing diseases, such as carpal tunnel syndrome (CTS) and neuromas are associated with changes in biomechanical behavior of hand flexor tendon, nerves, or their SSCT and are therefore interesting to explore. The following subchapter

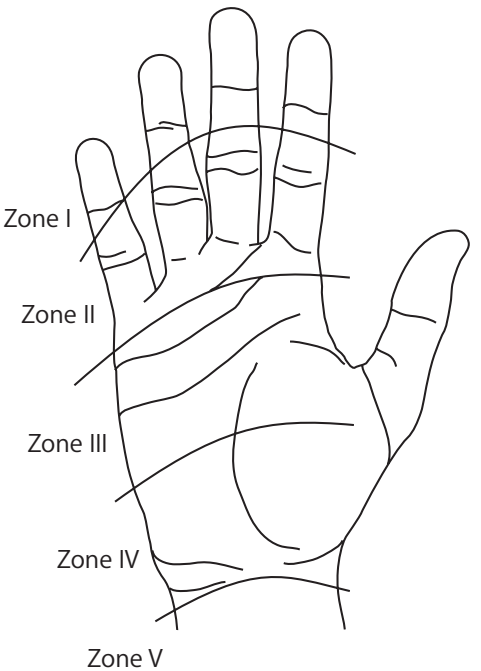

Figure 1. The different surgical zones in the palm of the hand defined by Verdan.

will discuss CTS and the clinical impact of changes in the biomechanical behavior of the hand flexor tendons, median nerve, and their SSCT in CTS patients, which is the topic of Chapters 6, 7, and 8.

Carpal tunnel syndrome (CTS) is one of the most common compression neuropathies. In CTS, it is assumed that compression of the median nerve (MN) under the transverse carpal ligament in the carpal tunnel leads to clinical symptoms. The estimated occurrence in the general population is around 1-4%, with the incidence for women ranging from 3-6% and for men from 1-3%, depending on the diagnostic criteria used[158]. The classical CTS patient is female in her 60s with overweight and complaints of pain or numbness in one or both hands[93,105,122,171,177]. Other risk factors for CTS are, amongst others, hypothyroidism and pregnancy[164].

The hallmark of classic CTS is pain or numbness and tingling of the area innervated by the MN. This includes the thumb (in 79% of cases), index finger (92%), middle finger (96%), and the radial half of the ring finger (83%)[177]. Typically, patients are awakened by nightly episodes of increased pain or numbness, which typically diminishes when shaking or wringing their hands. However, CTS does not seem to be limited to the first four digits. A number of patients present themselves with pain in the wrist, forearm, and sometimes even the shoulder[164].

Besides sensory symptoms, patients with severe CTS also show motor involvement with symptoms such as atrophy of the thumb muscles (abductor pollicis brevis, flexor pollicis brevis, and opponens pollicis) and, consequently, weakness of thumb opposition and abduction. Typically, patients can provoke symptoms by reading, writing, opening a jar, dressing, holding a phone or carrying bags[113,164].

There are several options to treat CTS. When symptoms are mild, a conservative treatment is preferred, which is either a hand brace or a corticosteroid injection[123,125]. Corticosteroids are effective in approximately 75% of patients and the maximal effect would be expected within a month. When repeating the injections about 50% of patients are still free of complaints after one year. If conservative treatment is not successful, surgical decompression is preferred. Surgical decompression is successful in approximately 75% of patients, while in approximately 8% of patients symptoms worsen; recurrence after successful decompression is rare. Although, if surgery is planned based on clinical symptoms alone, the success rate drops to approximately 50% or lower if patients are in the end stage of CTS[16]. Though treatment of CTS is reasonably successful CTS still results in significant morbidity[109]. The discrepancy between being diagnosed with CTS and the outcome after intervention might lie in the lacking burden of proof to confirm CTS. It might therefore be beneficial to further study the etiology of CTS.

The causes of CTS and many aspects of its etiology remain unclear. Although CTS is associated with an altered signal conduction of the MN, it is unclear what causes these changes. Hypotheses vary from increased pressure in the carpal tunnel to inflammation and fibrosis of the SSCT[32,44,61,116,185]. None of the above hypotheses completely explain the changes found in CTS patients and the symptoms associated with CTS.

Although commonly used, diagnosing CTS based on classic clinical symptoms is far from straightforward due to the large variety in clinical symptoms, how patients experience their symptoms, and the involvement of areas outside the innervation area of the MN. To objectify the CTS diagnosis, electrodiagnostic (EDX) studies, including nerve conduction studies (NCS) or electromyography (EMG), are often used.

Simpson was the first to report the usefulness of EDX studies in the diagnosis of CTS in 1956. Nowadays, EDX studies are commonly used to support the diagnosis of CTS and are often used as a gold standard, although it is a topic of debate[66,67,97]. However, in patients with clinically suspected CTS, the EDX study may be normal in 16-34% of the cases[90,164,210]. The limited sensitivity of EDX studies has lead to the use of imaging modalities such as MRI and US, to detect pathophysiological changes of the MN. It has been reported

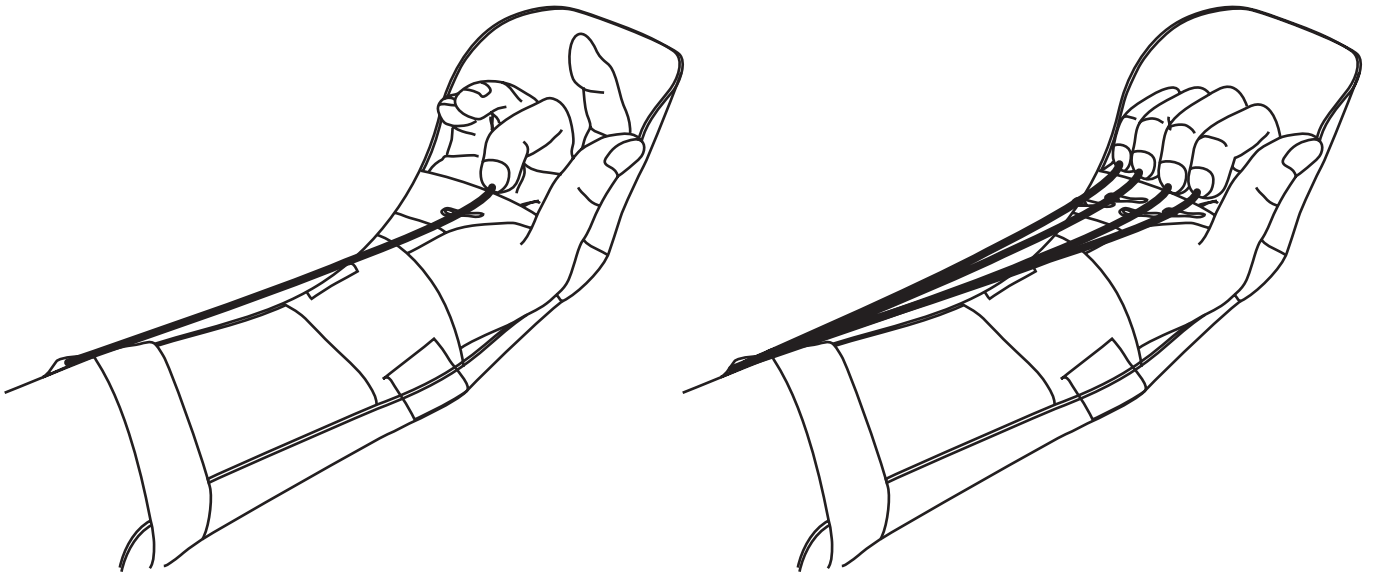

Figure 2. Two commonly used passive rehabilitation mobilization protocols used after hand flexor tendon reconstruction or repair. The left panel depicts the Kleinert mobilization protocol in which only the injured finger has a rubber band allowing passive movement of the injured finger. The right panel depicts the four-finger mobilization protocol defined by Silfverskiold and May in which all fingers, injured and uninjured, have a rubber band allowing passive movement. Note that both mobilization protocols allow active extension and that the metacarpophalangeal (MCP) joint has an extension constraint due to the splint.

CARPAL TUNNEL SYNDROME

that thickening of the MN is evident in CTS, which may be caused by a biological cascade due to the entrapment. This cascade comprises, amongst others, endoneural edema, demyelination, inflammation, fibrosis, and thickening of the perineurium and endothelium[153]. Besides the cross-sectional area (CSA) of the MN, a variety of parameters have been proposed to describe these changes such as the ratio of the CSA of the MN measured proximal and distal of the carpal tunnel or the flattening of the MN. One of the most predictive parameters has been the CSA, with a sensitivity of 0.70-0.88 and a specificity of 0.57-0.97[12,54]. However, the sensitivity and specificity vary largely between studies, which is mostly likely due to high intra- and interrater variability[54]. US is therefore considered less suitable to use as a diagnostic tool.

Besides transversal static imaging of the carpal tunnel, several studies proposed longitudinal imaging of the carpal tunnel and more specifically the MN and its surrounding tissue. A particularly promising approach is the assessment of the dynamics of the subsynovial connective tissue (SSCT) in CTS patients. The SSCT surrounds the MN and the hand flexor tendons in the carpal tunnel. It has been suggested that the SSCT might be fibrotic in CTS patients as part of the before-mentioned cascade initiated by the entrapment of the MN. As the SSCT might be fibrotic, this consequently might influence its effect on the dynamics of the MN and the hand flexor tendons[217,221].

Although several new potential diagnostic tools have been described, it is still not possible to diagnose CTS objectively and with high sensitivity and specificity. All current diagnostic tools lack the ability to assess the dynamics of the MN, while complaints mostly arise during daily activity. It might therefore be worthwhile to assess the dynamics of the MN in relation to CTS. The most suitable imaging modality would be ultrasonography, as this is the only modality capable of real-time imaging with high spatial and temporal resolution. Assessing the MN in both the transverse and longitudinal plane could give insight in whether the dynamics of the MN and the hand flexor tendons change due to fibrosis of the SSCT. Furthermore, it clarifies the influence of the hand flexor tendons on the dynamics of the MN on the CTS symptoms. Therefore, the aim is to identify prediction parameters using US and use these parameters to define prediction models to assess CTS.

DIGITAL NERVE

The previous sections discussed the tracking capabilities of the US tracking algorithm for relatively large structures such as the hand flexor tendons or the MN. As a next step in the development of speckle tracking, we evaluated its ability to study the dynamics of the much thinner digital nerve. This research was performed in cooperation with Dirk Jan van der Avoort of the Department of Plastic and Reconstructive Surgery at the Erasmus MC Rotterdam. His research focuses on the dynamics of the digital nerve in relation to painful neuromas. The first step towards describing the dynamics of the digital nerve is to investigate the US tracking capabilities when tracking the digital nerve in-vivo using our US tracking algorithm. In-vivo measurements of the dynamic behavior of digital nerves are difficult due to the small size of the digital nerves and possibly due to their small excursion during loading. We believe that with small alterations of the block matching technique presented in Chapters 2 and 3 it could be possible to study the dynamic behavior of the digital nerve. The aim of Chapter 9 is to assess the reproducibility of measurements of digital nerve excursions and thereby assess the robustness of our ultrasound block matching algorithm.

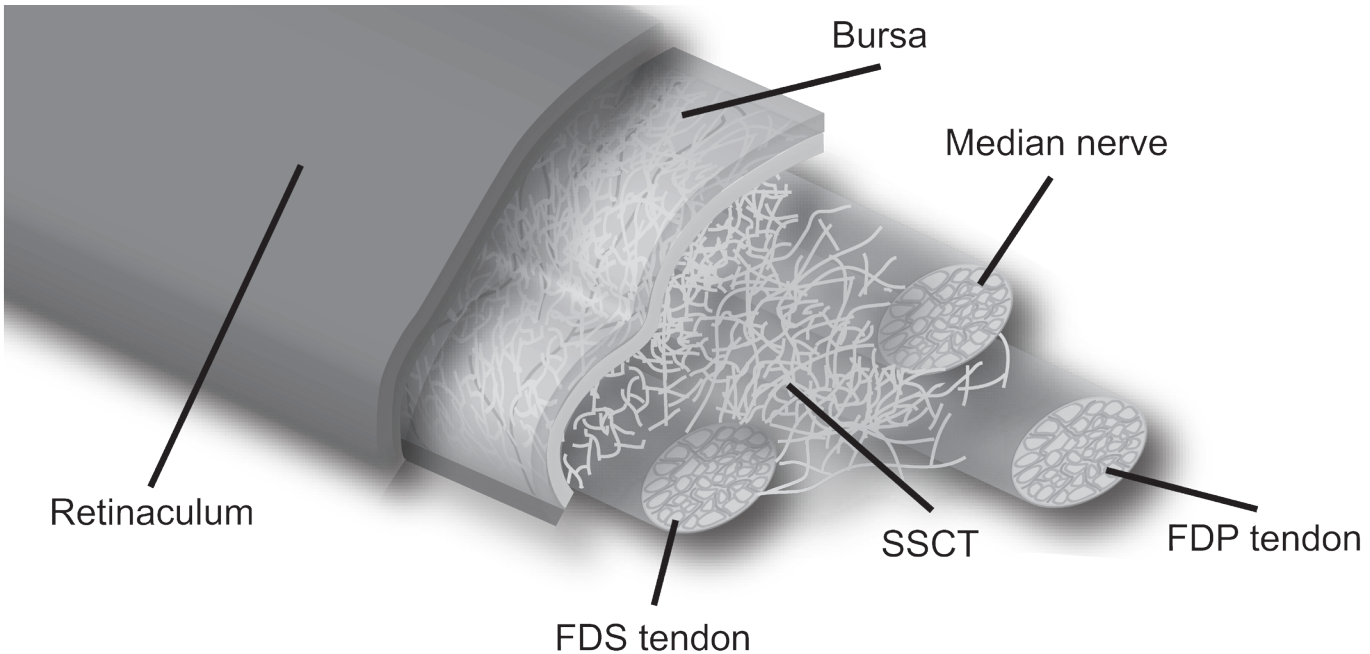

Figure 3. Expanded view of a part of the carpal tunnel, including retinaculum, bursa, median nerve, flexor digitorum profundus (FDP) tendon, flexor digitorum superficialis (FDS), and the subsynovial connective tissue (SSCT). This model shows the possibility of interaction between the hand flexor tendons, median nerve, and bursa facilitated by the SSCT. The SSCT is a fine meshed structure, which can be elongated easily compared to tendons and nerves under loading conditions.

The aim of this thesis is to provide more insight in normal and abnormal dynamic behavior of tendons and nerves in the hand using ultrasound as an objective measure and possibly as a diagnostic tool. To pursue this goal, the general aim can be divided into two sub questions:

1) Is it possible to quantify dynamic behavior of tendons and nerves in the hand during hand movements using ultrasound?

2) If so, is it possible to differentiate between normal and abnormal dynamic behavior for different diseases of the hand using ultrasound?

Chapters 2 and 3 describe the development and validation of our ultrasound tracking algorithm, which is capable of tracking small excursions in a broad range of velocities. The algorithm is based on the common block matching principle and is further extended and optimized to increase tracking accuracy. The algorithm was extensively validated in-vitro, ex-vivo, and in-vivo, assessing tracking accuracy and applicability towards clinical use.

The first clinical application of the algorithm was the assessment of hand flexor tendon excursions in relation to the finger joint angles during active and passive hand movement, which is described in Chapter 4. By assessing the excursions during different hand movements that resemble different rehabilitation protocols used after tendon reconstruction or surgery, this chapter studies the differences in tendon excursions between active and passive rehabilitation protocols. Based on this, we can specifically determine if active and passive rehabilitation protocols obtain sufficient tendon excursion to prevent tendon adhesions. The next step in assessing the effectiveness of different rehabilitation protocols in achieving sufficient tendon excursions is to investigate the influence of finger positions on tendon excursions, which is described in Chapter 5. As all hand flexor tendons are interconnected, it is reasonable to assume that the position of each finger influences the dynamic behavior of the other fingers. Therefore, the aim of Chapter 5 is to study the effect of the positions of the uninjured fingers on the excursion of the injured finger during different rehabilitation protocols.

The second clinical application is the assessment of nerve and tendon dynamics in carpal tunnel syndrome (CTS). Chapter 6 describes the feasibility of measuring different dynamic parameters in the carpal tunnel. Parameters such as the area, perimeter, and transversal excursion of the different hand flexor tendons and the MN under unloaded and loaded conditions might provide valuable insight in the etiology of CTS, but may also allow differentiating between normal and abnormal dynamic behavior. Chapters 7 assesses the differences in dynamic behavior between a healthy population and CTS patients in transversal US images. Chapter 8 assesses the dynamic behavior of CTS patients, comparing the most affected hand with the least affected hand in longitudinal US images. The aim is to develop a predictive model for diagnosing CTS using the different dynamic parameters and thereby introducing US as a diagnostic tool to assess CTS.

The third clinical application of the algorithm is the assessment of the dynamic behavior of the digital nerve, which is described in Chapter 9. During stretching of the entire nervous pathway, from the plexus brachialis to the MN to the small branches of the MN and finally to the digital nerve, the dynamic behavior of the digital nerve was investigated. The aim is to get insight in whether the dynamic behavior of the digital nerve might play a role in the development of painful neuromas.

Finally, the main findings, strengths, and weaknesses of this thesis are discussed in Chapter 10, in addition to the clinical implications and directions for future research.

Chapter 2
Dedicated Ultrasound Speckle Tracking to Study Tendon Displacement

Jan-Wiebe H. Korstanje
Ruud W. Selles
Henk J. Stam
Steven E.R. Hovius
Johan G. Bosch
Conference Proceedings SPIE: Medical Imaging 2009: Ultrasonic Imaging and Signal Processing; 7265:726505-772511.

Ultrasound can be used to study tendon and muscle movement. However, quantization is mostly based on manual tracking of anatomical landmarks such as the musculotendinous junction, limiting the applicability to a small number of muscle-tendon units. The aim of this study is to quantify tendon displacement without employing anatomical landmarks, using dedicated speckle tracking in long B-mode image sequences. We devised a dedicated two-dimensional multi-kernel block-matching scheme with subpixel accuracy to handle large displacements over long sequences. Images were acquired with a Philips iE33 with a 7 MHz linear array and a VisualSonics Vevo 770 using a 40 MHz mechanical probe. We displaced the flexor digitorum superficialis of two pig cadaver forelegs with three different velocities (4,10 and 16 mm/s) over 3 distances (5, 10, 15 mm). As a reference, we manually determined the total displacement of an injected hyperechogenic bullet in the tendons. We automatically tracked tendon parts with and without markers and compared results to the true displacement. Using the iE33, mean tissue displacement underestimations for the three different velocities were 2.5 ± 1.0%, 1.7 ± 1.1% and 0.7 ± 0.4%. Using the Vevo770, mean tissue displacement underestimations were 0.8 ± 1.3%, 0.6 ± 0.3% and 0.6 ± 0.3%. Marker tracking displacement underestimations were only slightly smaller, showing limited tracking drift for non-marker tendon tissue as well as for markers. This study showed that our dedicated speckle tracking can quantify extensive tendon displacement with physiological velocities without anatomical landmarks with good accuracy for different types of ultrasound configurations. This technique allows tracking of a much larger range of muscle-tendon units than by using anatomical landmarks.

Until today there is no suitable objective technique to accurately measure movement of a tendon in-vivo in the human body in absence of anatomical landmarks. Presently used ultrasound techniques manually or automatically track the motion of landmarks such as the musculotendinous junction to quantify tendon displacements[110,120]. This approach limits the applicability of the technique to a small number of muscle-tendon groups, thereby excluding, amongst others, the hand and wrist tendons. These flexor and extensor tendons play an important role in normal daily hand function and may be impaired due to, for example, trauma or degenerative diseases. Since both surgery and rehabilitation often focuses on regaining range of motion of the tendon and preventing tendon adhesions, direct measurement of tendon movement would be highly valuable[188].

While a number of block matching algorithms have been proposed to measure tendon movement, these techniques are all based on tracking a clearly identifiable anatomical landmark. In a number of tendons, the V-shaped musculotendinous junction is such a landmark[110,120]. This V- shape changes only slowly during motion, making it suitable for block matching. However, necessity of identifiable landmarks limits the applicability to a small number of sites. The musculotendinous junctions of the hand tendons, for example, are located in the lower arm, making landmark tracking impossible at the level of the carpal tunnel or more distal. Although some studies showed the possibility of tendon tracking without using a landmark, none of these studies were extensively validated in-vitro[34,141]. It is also unknown if different types of ultrasound modalities have any influence on tracking accuracy.

One of the first techniques to study hand tendon displacement in-vivo without anatomical landmarks was Color Doppler Imaging (CDI)[23,29,174]. While results showed good reproducibility,[23,29,174] Doppler only measures 1D velocities along the ultrasound beam. Since tendons generally move almost perpendicular to the ultrasound beam, these measurements are very sensitive for visual angle mismatch[18,139].

As an alternative to Color Doppler Imaging, 2D motion tracking based on speckle tracking block matching is one way to overcome angle dependency[17]. Speckle track block matching techniques use a predefined block or a so-called kernel that is selected from a frame and that contains one or more pronounced speckles. The kernel is used as a template with which a match has to be found in a predefined search region in a subsequent frame. The template will be compared to all translations possible in the search region. To quantify the match, different techniques can be used such as normalized cross-correlation (NCC), sum-of-absolute-difference (SAD) or sum-of-squared-difference (SSD)[56]. Block matching has been used extensively in cardiology for tracking cardiac wall motion to calculate displacement, strain and strain rate[139].

Since tracking of tendons poses specific challenges and requirements on speckle tracking, commercially available algorithms are not directly applicable for the use on tendons. For example, one of the specific problems is that most of the available tracking software in commercially available ultrasound machines do not support the use of high frequency linear probes. In addition, most tracking software is optimized for muscle tissue, with its specific speckle characteristics and kinetic behavior. The purpose of this study, therefore, is to implement and test a technique that objectively quantifies tendon displacement over longer distances at physiological speeds without using any anatomical landmarks.

Characteristics of ultrasound images of tendons

Associated with its function, tendons in the hand and wrist are thin, elongated stiff fibrous structures, which can displace over considerable distances (multiple centimeters) within a partially mobile sheath. The longitudinal fibers create a characteristic striated speckle pattern in ultrasound images with long thin lines parallel to the motion axis (see Figure 1). The tendon sheath (black arrows) is seen

Philips iE33 L9-3

VisualSonics Vevo770 RMV 704

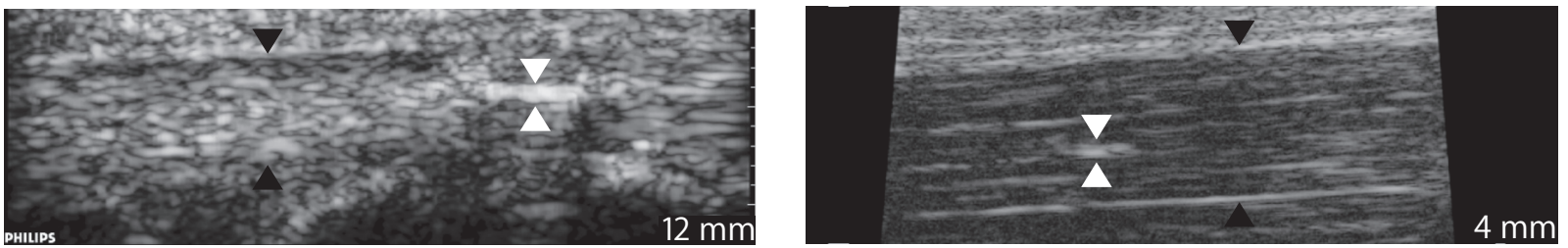

Figure 1. The fibrous structure of the tendon causes a striated speckle pattern in an ultrasound image. The sheath surrounding the tissue is seen as a hyperechogenic continuous line (▽). In a. the inserted aluminum platelet and in b. the inserted sphere is seen as a hyperechogenic triangle (▼).

as a continuous hyperechogenic line surrounding the tissue.

Tracking algorithm

Block matching uses a similarity measure, such as normalized cross-correlation (NCC), sum-of-absolute-difference (SAD) or sum-of-squared-difference (SSD), for frame-to-frame displacement analysis[34,62]. The assumptions for this technique are that frame-to-frame gray-level patterns changes are minimal and that the texture of interest should have sufficient unambiguous information[62]. The advantage of NCC over SAD and SSD is that NCC compensates for mean and standard deviation of the template and target signal of interest[56,202]. The downside of NCC is its higher computational load, making it less suitable for real-time implementation[202]. The advantage of SSD is that larger mismatches are more heavily weighted than small mismatches[202]. The advantage of SAD is its lower computational load compared to NCC and SSD. However, the performance differences between the similarity measures are quite small. Because our proposed technique is not bound to real-time processing and we aim for high accuracy, we chose NCC as our similarity measure.

Block matching suffers from an inherent tradeoff between accuracy and spatial resolution. Larger matching blocks decrease the ambiguity, which can result in lower matching errors. However, when motion fields change considerably in space or are non-rigid larger matching blocks often fail. This can be resolved by decreasing the matching blocks in size. Downside to smaller matching blocks is the higher susceptibility to noise and higher chance of mismatch due to ambiguity. This tradeoff can be resolved with a multilevel block matching approach[216]. However, tendons have a practically rigid motion field[29] and therefore multilevel block matching will not increase accuracy much.

A second limitation on the accuracy of displacement estimation is the quantization error. Block matching typically finds the optimal displacement in integer pixel steps. The quantization error can be reduced by using subpixel interpolation. Either the kernel and search region can be interpolated, or the output matrix of the similarity measure. The latter is much more efficient and widely applied. There are several subpixel interpolation schemes i.e. cubic spline fitting, parabolic fitting and grid slope[60,152,202,224]. The combination of the earlier discussed similarity measures SSD and NCC with spline fitting showed to be the best combination when looking at standard deviation for different subpixel shifts[202].

For tracking of tendon movement we devised a dedicated multi-kernel block-matching scheme with normalized cross-correlation (NCC) as similarity measure (see Figure 2). An elongated tracking region of interest (ROI) was placed manually within the tendon and frame-to-frame displacement is estimated by multiple overlapping kernels covering the ROI. Kernel size and shape were adapted to the typical speckle structure of tendons and optimal sizes were predetermined for each machine (see Table 1). We kept the frame-to-frame displacement in a predetermined range for different velocities in different acquisitions. For each kernel, all possible pixel displacements within the search region are evaluated with NCC. To increase displacement accuracy to subpixel level we used a 1:10 2D cubic spline interpolation scheme[60,152,224] (Matlab) on the NCC output matrix before peak detection. The 2D ROI displacement is calculated from all kernel displacements within the ROI above a predefined lower bound T by a correlation-weighted displacement vector average.

The ROI position was kept stationary in lateral (horizontal) and axial (vertical) direction, because the total tendon displacement is generally much larger than the image size over the typically long sequences (~1000 frames). Total displacement is estimated by integration of interframe displacements over all frames. For low speeds, the sequence is decimated over time by the factors given in table 1 to maintain the balance of reasonable interframe displacement without loss of correlation. In case there is negligible strain, this does not influence the results.

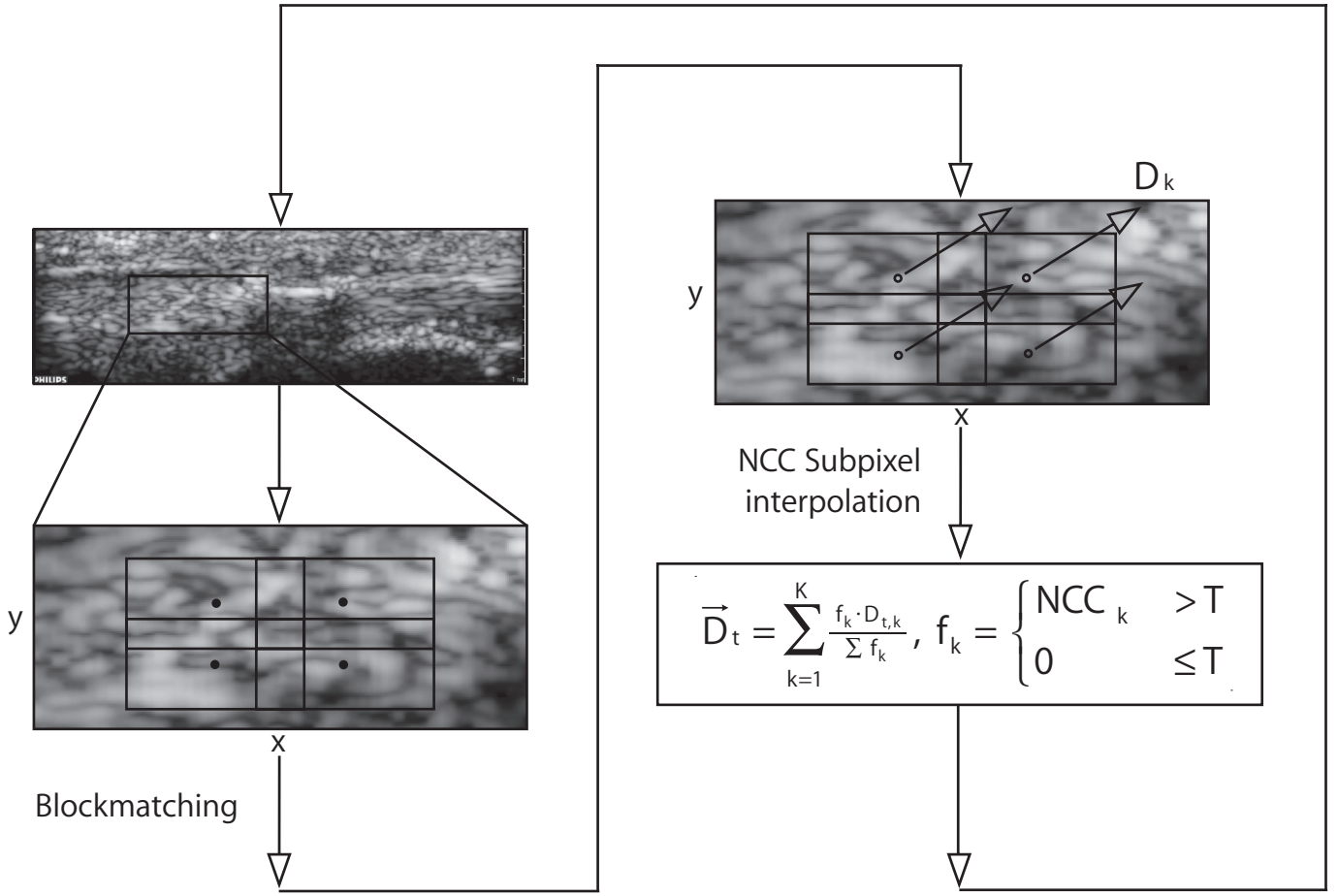

Figure 2. The developed algorithm, based on block matching with the normalized cross-correlation (NCC) as similarity measure. The user manually defines a region-of-interest (ROI) after which the algorithm automatically places a predefined number of kernels in the ROI. The algorithm automatically evaluates the different displacement estimates for each kernel. After subpixel interpolation of the NCC output matrix a correlation-weighted kernel displacement vector average is calculated. For each frame the ROI was kept stationary.

Experimental setup

To determine the accuracy of the developed algorithm, we designed an experimental setup to displace a cadaver porcine tendon with different displacements and velocities (see Figure 3). The porcine leg [11] was placed in an aluminum holder [1] and was fixated with two aluminum screws. The proximal flexor digitorum superficialis (FDS) was surgically undone of fascia, fibrous tissue and supportive tissue and was clamped in between two aluminum plates [4] using two small screws. The clamp was connected to a universal material testing machine [10] (Testometric AX M250-2.5KN, the Testometric Company Ltd., Lancashire, United Kingdom) via a stainless steel microcable [5] (0.27 mm diameter, 1770 N/mm^2 resistance, Carl Stahl MicroCables, Süssen, West-Germany) to minimize friction. The stainless steel wire was guided through a pulley [3], which was placed in an aluminum holder [2]. The pulley was adjustable in height for an optimal horizontal alignment with the tendon. Sutures [6] were attached to the FDS on one end and to a pullback-weight [8] of 705 grams at the other end. The sutures were guided over a metal rod [7] for spacing purposes. The counter weight preloaded the tendon to prevent slacking. The transducer [9] was fixated to minimize movement artifacts.

Ultrasound recordings and reference measurements

Tissue tracking was tested on the flexor digitorum superficialis tendon of two pig cadaver forelegs acquired with two very different ultrasound configurations: (a) the Philips iE33 using a L9-3 linear probe in harmonic mode with a center frequency of 7 MHz and a harmonic frequency of 3 MHz and (b) the VisualSonics Vevo 770 with a RMV 704 40 MHz mechanical probe. Images were acquired at 120 fps and 60 fps, respectively. Selected image regions of interest were 200 x 90 pixels, with 0.067 x 0.067 mm/pix (Philips iE33), and 140 x 70 pixels, with 0.020 x 0.020 mm/pix (VisualSonics Vevo 770). The difference in size of the region of interest is, besides a difference in resolution, due to the limited field-of-view of the VisualSonics Vevo 770. Because the marker has been inserted in the upper part of the tendon, the ROI could only be placed in the lower part of the tendon. The search region was kept the same as for the Philips configuration for comparison purposes. As a consequence, ROI was reduced in lateral direction. Sequences typically contained 100 to 1000 images.

To create a reliable ground truth for our proposed dedicated speckle tracking algorithm, an echogenic marker was injected into the tendons (see Figure 1, white arrows). Actual displacement of these markers within the ultrasound images were measured manually and used as a golden standard. For the VisualSonics Vevo770 configuration, we injected a 1mm diameter sphere (10% 0.3µm SiC particles suspended in epoxy) into the tendon. For the Philips iE33 configuration, an aluminum platelet of 5 mm x 5 mm x 1 mm was surgically inserted into the tendon. Because of different spatial resolutions, different types of markers were used. The tendon was displaced externally with a universal material testing machine with three different velocities (4 mm/s, 10 mm/s and 16 mm/s) and three different displacements (5 mm, 10 mm and 15 mm) for the Philips iE33 with forces ranging from 10 N up to 125 N. For the VisualSonics Vevo 770 only the first two displacements were performed. This is because the VisualSonics Vevo 770 has a limited field of view. For an accurate true displacement measurement the marker needed to be inside the field of view during the entire measurement. Each experiment was repeated after the porcine leg was removed and placed back into the aluminum holder. These experiments were also repeated with a different porcine leg. Due to logistic reasons, experiments with the VisualSonics Vevo 770 configuration had to be performed on another set of porcine legs than the experiments with the Philips iE33 configuration. However, the rest of the experimental setup was not changed in between experiments.

Due to tissue deformations and other mechanical effects, the external displacements and speeds applied by the universal material testing machine resulted in lower internal values within the tendons. Therefore, the universal material testing machine was not used as a reference for the displacement calculations.

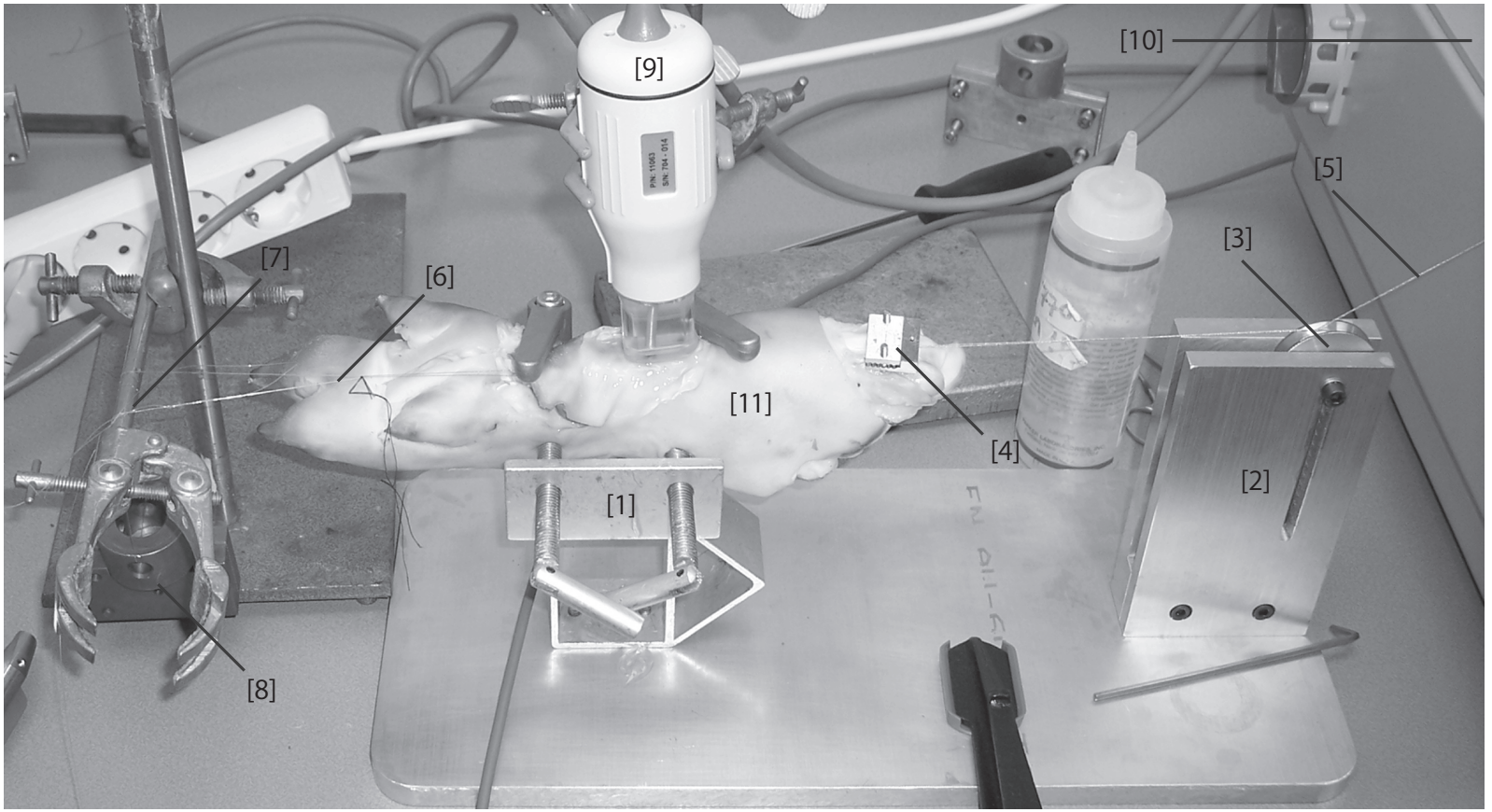

Figure 3. Experimental setup to fixate the porcine foreleg and displace the porcine tendon with different displacements and velocities.

Ultrasound imaging analysis

For tracking tendon tissue we used the block-matching scheme described above (see Figure 2), where the ROI was chosen such that it excluded the marker over the whole sequence. The ground truth displacement measurement was obtained by manually determining the position of the marker in the first frame and at the end of every flexion. The ground truth displacement is further referred to as true displacement. The marker was also tracked automatically to get an indication of the drift of the tracking algorithm itself. The same tracking algorithm was used, but the ROI was a narrow box (141 x 41 pix for the Philips iE33 and 71 x 17 pix for the VisualSonics Vevo 770) around the marker and moved with the marker, rather than being stationary.

Statistical analysis

To determine the errors of the speckle tracking, we calculated the difference between the true displacement and the tissue tracking. For all comparisons, we calculated absolute root mean squared (RMS) errors between both displacements and the relative errors by normalizing to the true displacement, expressed in percentages.

For each ultrasound configuration separately, we determined the accuracy of the speckle tracking algorithm by calculating the mean and standard deviation of the errors for all measurements combined. To assess different error sources, we compared the accuracy at the different velocities and different displacements for the two ultrasound modalities separately. To determine velocity dependent errors, we grouped all errors for the three velocities that we prescribed to the universal material testing machine (4, 10 and 16 mm/s). To determine displacement dependent errors, we grouped all measurements for the three displacements that we prescribed to the universal material testing machine (5, 10 and 15 mm) in case of the Philips iE33. For the VisualSonics Vevo 770, we grouped all measurements for the two displacements (5 and 10 mm).

Two observers have examined the ultrasound images twice by manually measuring the displacement of the marker. The intra- and inter-observer errors of these measurements were calculated using the technical error of measurement (TEM)[207]. The formula for TEM for comparison of two measurements or observations is:

$$TEM = \sqrt{\frac{\sum D^2}{2N}} \qquad \text{(Eq.2)}$$

where D represents the difference between two measurements or observations and N represents the number of replicates.

Figures 4A and 4B show typical results of the three different velocities for the Philips iE33 and the VisualSonics Vevo 770, respectively. As Figure 4 shows, all measured displacements differed considerably from the intended displacement of 10 mm that was prescribed to the universal material testing machine due to mechanical effects. This was the case for all prescribed displacements. We used the manually derived marker displacement as golden standard (true tendon displacement). Overall, differences between the true displacement, the tissue tracking and the marker tracking were small for all displacements. As discussed in the method section, the true displacement is calculated as the average manually-measured displacements of the marker by two observers. The intra- and interobserver errors (TEM) were 0.07 mm and 0.12 mm for the Philips iE33, respectively. For the VisualSonics Vevo 770 the intra- and interobserver errors were 0.06 mm and 0.08 mm[207].

Figure 5A shows the absolute errors of tissue tracking versus the true total tendon displacement for the three different velocities using the Philips iE33 and Figure 5B shows the absolute errors when using the VisualSonics Vevo 770. The absolute error for the Philips iE33 is slightly larger than for the VisualSonics Vevo 770. Both show an increase in the absolute error with increased displacement. The relative errors for the Philips iE33 and the VisualSonics Vevo 770 are shown in Figure 5c and d. The relative error for the Philips configuration is slightly larger than for the VisualSonics configuration.

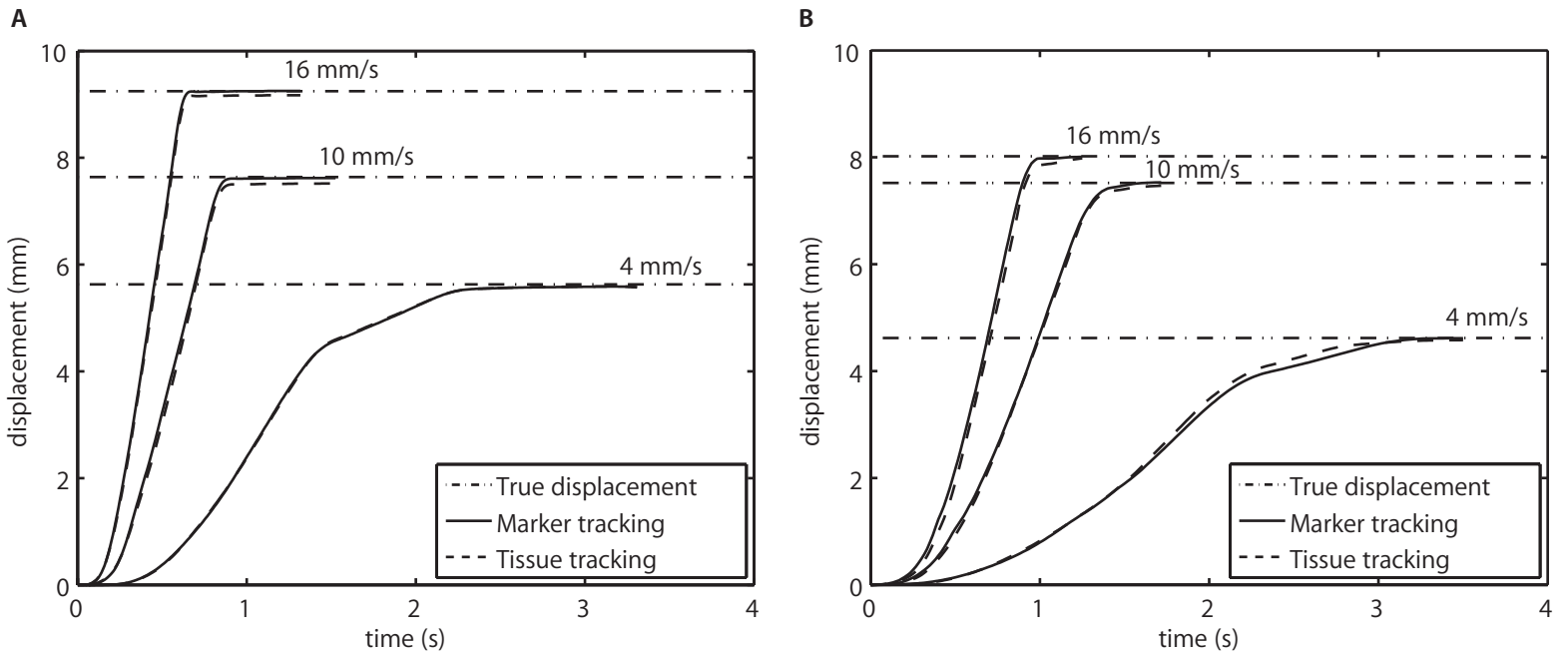

Figure 4. Typical displacement profile with a prescribed displacement of 10 mm for a. the Philips iE33 configuration and b.VisualSonics configuration.

The relative errors for both ultrasound modalities decrease with increasing displacement. When grouping all measurements for the Philips iE33, we found a mean (±standard deviation) tendon displacement of 9.2 (± 5.6) mm. The absolute error was 0.08 (± 0.09) mm and the relative error 1.3 (± 1.0) %. The mean tendon displacement for the VisualSonics Vevo 770 was 5.3 (± 2.7) mm. The absolute error was 0.7 (± 0.8) % and the relative error was 0.03 (± 0.02) mm. Since all errors are within the range of the interobserver error of the golden standard, these errors can be considered very small.

Figure 6 shows a modified Bland-Altman plot of the marker tracking and the tissue tracking for the Philips iE33 and the VisualSonics Vevo 770. The y-axis shows the difference between marker tracking and tissue tracking at different time intervals, thus from the start of the displacement up to the maximum displacement. The x-axis represents the mean of the marker tracking and tissue tracking at different time intervals. Each line represents one tracking sequence. The mean (±S.D.) difference between marker tracking and tissue tracking for the Philips iE33 was -0.06 (±0.2) mm. The mean difference only differed slightly for the different velocities. However, the standard deviations were 0.10 mm, 0.20 mm and 0.24 mm for 4 mm/s, 10 mm/s and 16 mm/s, respectively. The mean difference between marker tracking and tissue tracking for the VisualSonics Vevo 770 was 0.02 (±0.08) mm. Differences between the different velocities were small. These values correspond to differences of 1±4 pixels between marker and tissue tracking for both modalities.

Table 2 shows the mean total tendon displacement, absolute errors of tissue tracking and relative errors for the Philips iE33 and the VisualSonics Vevo 770. The errors are categorized by velocity related errors and displacement related errors. The mean displacements for both configurations increase with the velocity. For the Philips configuration, the absolute error for the lowest velocity was smaller than for the other two velocities. The corresponding relative error decreased with increasing velocity. Both absolute and relative errors differed only slightly between the Philips iE33 and the VisualSonics Vevo 770. The absolute and relative errors associated with displacement did not differ much for both configurations.

RESULTS

In this study, we implemented and tested a novel dedicated ultrasound speckle tracking algorithm to objectively quantify tendon displacement without the use of anatomical landmarks. The results showed that our proposed algorithm is highly reliable in objectively quantifying tendon displacements without the use of anatomical landmarks. The relative error of the complete tendon displacements, averaged over all displacements and velocities, was 1.3 % with a maximum error of 3.2 % for the Philips iE33 and 0.7 % with a maximum error of 1.9 % for the Visual Sonics Vevo 770.

The errors of the ultrasound measurements of tendon displacement in this study are lower than the methods reported earlier in the literature. For example, Buyruk et al.[23] used Color Doppler Imaging to study tendon displacement. In this study, the errors were up to 2 mm for displacements of maximally 11 mm (18 %). Lee et al.[110] used optical flow to study displacement of the musculotendinous junction of a cadaver gastrocnemius, reporting errors from 5 to 10 % during 30 mm displacements. When applied in-vivo, errors between automated tracking and manual tracking in this study ranged from 4 to 8 % during tendon displacements of about 20 mm.

A similar algorithm than the one proposed in this study, but applied to nerves instead of tendon, was described by Dilley et al.[34]. In this study a block matching scheme with NCC was used with only one large kernel. Accuracy of this algorithm was studied in-vivo with the ultrasound probe moving instead of the nerve moving, eliminating any deformation of the nerve during movement and the interaction between the nerve and its surrounding tissue[72]. Despite of this, errors were up to 10 % between automated tracking and a micromanipulator.

A limitation in the present study was that we used an inter-

DISCUSSION

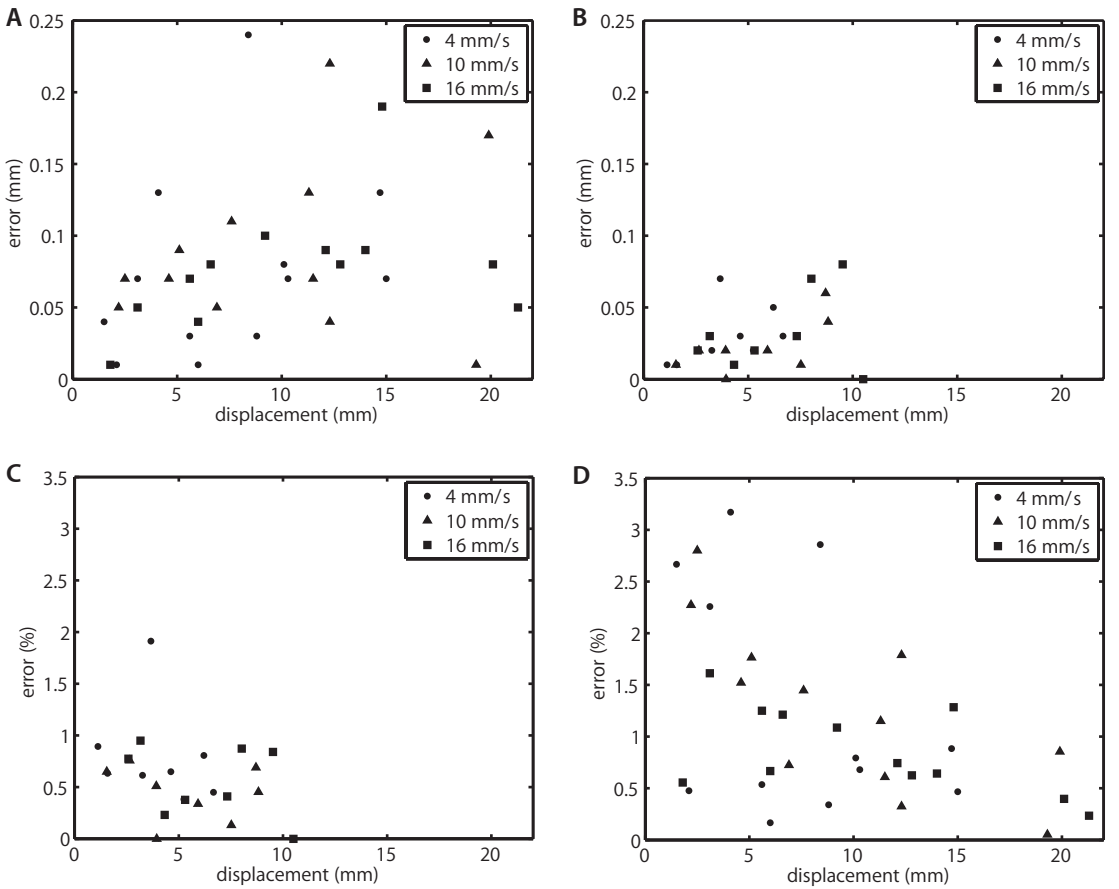

Figure 5. Absolute error of tissue tracking versus true displacement for A. the Philips iE33 and B. the VisualSonics Vevo 770. Relative errors versus true displacement for C. the Philips iE33 and D. the VisualSonics Vevo 770.

nal reference (the manual tracking and the marker tracking) rather than an external reference such as the movement of the universal material testing machine. We manually determined the position of the marker in the first frame and at the end of every flexion as a golden standard. The accuracy of this procedure is limited to typically one pixel, while the algorithm uses sub-pixel tracking. We found that the intra- and inter-observer errors of this reference for both ultrasound configurations were small (a few pixels). However, the error of the speckle tracking is in the same range, which makes it hard to tell whether tissue tracking was equally accurate as marker tracking. However, we can conclude that both tracking techniques perform very well. Another limitation is that inserting a marker into the tendon may have altered the tendon and its surrounding tissue. However, the tendons of this study in which the markers were injected showed neither visible damage nor any damage visible on the ultrasound recordings. The same holds for the surgically inserted markers. To prevent any distortion or damage, although not visible, we always tracked a region of the tendon outside the surgical field for the automated tracking.

Although the presented algorithm is largely automated, we manually selected the frame difference. The frame difference was defined as the number of frames between the two frames that were compared with block matching. When choosing this frame difference too low, we found that quantization errors would dominate the total error. On the other hand, when choosing this frame difference too high, decreased correlation would cause mismatches or loss of precision. The manual selection of frame difference was based on the maximum expected velocity. Another study on motion tracking found an underestimation for low frame differences and suggested to assess the pixel shift consistency over the different frame differences and the narrowness of the correlation peak[34]. The impact of the manually selected frame difference is very small, since marker tracking results and tissue tracking results were acquired with the same frame difference for comparison. However, for future use, this frame difference selection can be further automated to prevent human biasing and to improve the performance in sequences with varying or unknown motion velocity.

Another issue is the fact that it still needs to be assessed that the algorithm works for longer displacements (larger than the image size), which could not be evaluated with the current setup. A different model with multiple markers per tendon could help. Still, the present results suggest that absolute errors stay the same with longer displacements, and that relative errors decrease.

In conclusion, we have shown that our algorithm is capable of quantifying tendon displacements very accurately. The presented algorithm makes it possible to objectively quantify tendon displacement without making use of any anatomical landmark. The algorithm gave accurate measurements for velocities ranging from 4 mm/s up to 16 mm/s, making it applicable to track both healthy moving tendon as well as dysfunctional tendons. The algorithm proved to be applicable to very different types of ultrasound configurations. One of the implications of tracking tendons without using anatomical landmarks is that this technique broadens the applicability of tendon tracking to for example hand tendons. This makes it possible to study the mechanics of the hand more objectively and more precise and possibly quantify tendon dysfunction. Future efforts should be focused on automating frame different selection to increase objectivity. A human cadaver experiment would be the next step to validate this technique before finally using it in-vivo.

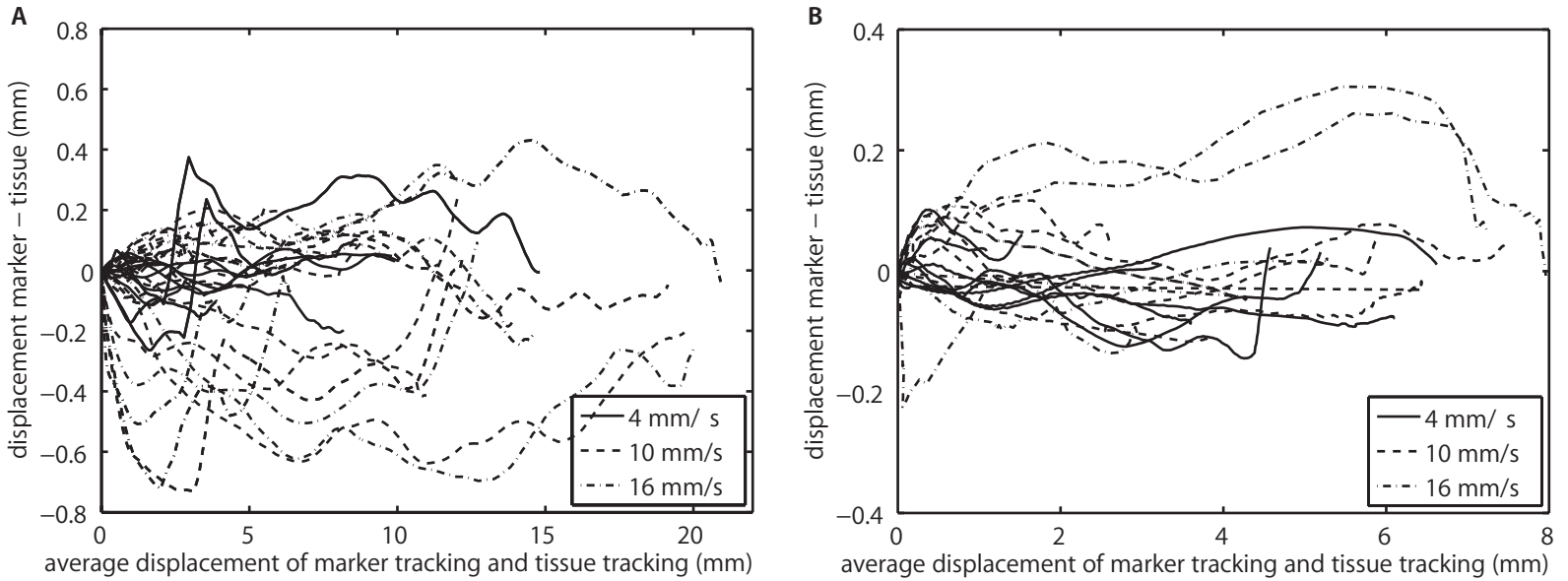

Figure 6. Modified Bland-Altman plot of the marker tracking and the tissue tracking for A. the Philips configuration and B. the Visual Sonics configuration. Each line represents one sequence tracking with at the x-axis the mean displacement and at the y-axis the difference between the displacements of marker tracking and tissue tracking.

Table 1. Technical details and general settings for the ultrasound scanners and algorithm.

	Philips iE33 L9-3	Visual Sonics Vevo 770 RMV704
Center frequency (MHz)	7	40
Focus (mm)	Centered to FOV	6 mm
Field of View (FOV) (H x V)(mm x mm)	59 x 19	10 x 10[§]
Millimeter-pixel ratio (mm/pix)	0.067	0.02
Number of kernels (horizontal x vertical)	6 (3 x 2)	6 (3 x 2)
Kernel size[†] (pix x pix)	101 x 51	141 x 71
Kernel size[†] (mm x mm)	6.8 x 3.4	2.8 x 1.4
Region of interest[†] (pix x pix)	200 x 90	145 x 75
Frame rate (fps)	120	60
Lower bound cross-correlation (T)	0.7	0.7
Frame difference[‡]	24/14/8	24/14/8
Expected maximal axial displacement a (pix)	20	20
Expected maximal lateral displacement b (pix)	100	160
Number of frames	200-1000	100-500

[†] Kernel size and region of interest are only for tissue tracking. For marker tracking kernel size and region of interest were sized to exactly fit around the marker.
[‡] Mentioned frame differences are for 4, 10 and 16 mm/s, respectively.
[§] Native field of view

Figure 7. Absolute and relative errors between true displacement and tissue tracking, categorized by velocity related and displacement related errors for the Philips iE33 L9-3 and the VisualSonics Vevo 770 RMV704

	Philips iE33 L9-3			VisualSonics Vevo 770 RMV704		
	Mean displacement (mm)	Absolute error (mm)	Relative error (%)	Mean displacement (mm)	Absolute error (mm)	Relative error (%)
Velocity related errors						
4 mm/s	7.5 (± 4.5)	0.04 (± 0.08)	2.5 (± 1.0)	4.0 (± 2.0)	0.03 (± 0.02)	0.8 (± 1.3)
10 mm/s	9.6 (± 5.9)	0.11 (± 0.12)	1.7 (± 1.1)	5.4 (± 2.8)	0.03 (± 0.02)	0.6 (± 0.3)
16 mm/s	10.6 (± 6.3)	0.09 (± 0.06)	0.7 (± 0.4)	6.3 (± 3.0)	0.03 (± 0.03)	0.6 (± 0.3)
Displacement related errors						
5 mm	3.5 (± 1.6)	0.08 (± 0.07)	1.3 (± 1.1)	3.4 (± 1.3)	0.02 (± 0.02)	0.7 (± 1.1)
10 mm	9.3 (± 3.2)	0.11 (± 0.11)	1.6 (± 1.0)	8.1 (± 2.4)	0.04 (± 0.02)	0.5 (± 0.3)
15 mm	15.0 (± 4.1)	0.09 (± 0.06)	1.0 (± 0.9)	n.a.	n.a.	n.a.

Chapter 3

Development and Validation of Ultrasound Speckle Tracking to Quantify Tendon Displacement

Jan-Wiebe H. Korstanje
Ruud W. Selles
Henk J. Stam
Steven E.R. Hovius
Johan G. Bosch

Journal of Biomechanics
2010
43:1373-1379

Ultrasound can be used to study tendon movement. However, measurement of tendon movement is mostly based on manual tracking of anatomical landmarks such as the musculo-tendinous junction, limiting the applicability to a small number of muscle-tendon units. The aim of this study was to quantify tendon displacement without anatomical landmarks using a speckle tracking algorithm optimized for tendons in long B-mode image sequences. A dedicated two-dimensional multi-kernel block-matching scheme with subpixel motion estimation was devised to handle large displacements over long sequences. The accuracy of the tracking on porcine tendons was evaluated during different displacements and velocities. Subsequently, the accuracy of tracking the flexor digitorum superficialis (FDS) of a human cadaver hand was evaluated. Finally, the in-vivo accuracy of the tendon tracking was determined by measuring the movement of the FDS at the wrist level. For the porcine experiment and the human cadaver arm experiment tracking errors were, on average, 0.08 and 0.05 mm, respectively (1.3% and 1.0%). For the in-vivo experiment the tracking error was, on average, 0.3 mm (1.6%). This study demonstrated that our dedicated speckle tracking can quantify tendon displacement at different physiological velocities without anatomical landmarks with high accuracy. The technique allows tracking over large displacements and in a wider range of tendons than by using anatomical landmarks.

Until today, there are only a limited number of validated techniques to measure tendon movement in-vivo in absence of an anatomical landmark such as the musculo-tendinous junction [49,118]. Presently used ultrasound techniques are mostly based on manual tracking of the displacement of landmarks such as the musculo-tendinous junction in B-mode images[6,110,119,120]. This approach limits the ability to measure tendon movement manually to a small number of muscle-tendon groups where this junction can be visualized repeatedly. In addition, it limits the motion measurement to the location of this junction and quantification of movements larger than the B-mode window size is impossible, as the junction will move outside of the image window.

Automated matching algorithms have been proposed to measure tendon movement. However, these techniques are also mostly based on tracking the musculo-tendinous junction. The V-shaped musculo-tendinous junction used in these studies changes only slightly during motion, making it suitable for automated tracking approaches. However, tracking tendon movement in absence of a musculo-tendinous junction may importantly increase the applicability of ultrasound measurement of tendon movement.

A number of studies have shown the possibility of using block matching techniques to measure tendon movement without an identifiable landmark[34,49,118,141,155]. However, these techniques were not extensively validated[34,118,141,154] or validated for other situations, such as for measuring small displacements only[49]. Block matching uses a predefined block of pixel data (a so-called kernel) that is selected from an image frame containing structural information such as one or more pronounced speckles. The kernel is used as a template that is matched to all possible corresponding blocks within a predefined search region in a subsequent frame. To quantify the match, measures such as normalized cross-correlation (NCC), sum-of-absolute-difference (SAD) or sum-of-squared-difference (SSD) can be used[56]. Block matching relies on the typical ultrasound speckle patterns, which are almost invariant under small displacements. Therefore, block matching techniques are frequently referred to as 'speckle tracking'. In addition to block matching, optical flow has also been used to study tissue displacement[34]. However, optical flow usually performs better if the displacement is small with respect to the speckle size, which is not the case for tendon tracking[62].

An important related research subject is elastography[27,118,139,208]. Classical elastography uses a similar approach as block matching, optical flow and RF analysis for tissue displacement estimation[130,144,156,200]. The estimated strain is calculated as the gradient of the displacement estimates. Elastography techniques evolved to overcome limitations of the original approach focusing on improving e.g. signal-to-noise ratio (SNR), sensitivity, and dynamic range. Although the general approach in classic elastography techniques may be applicable to our problem, the elastographic optimization will not provide accurate results for our application. The rationale behind this is that with strains larger than 2%, which is the case for tendons in general, the optimal window size is small[199]. Based on earlier findings by Korstanje et al. (2009), the window size is relatively large compared to the optimal window size for strain imaging. We therefore feel that the conditions are so different that a specialized approach is needed for tendon tracking. In addition, RF data is not helpful in our case since the use of RF data will specifically improve accuracy in axial direction (in the direction of the ultrasound beam). Tendon motion however, primarily takes place in the lateral direction, where RF analysis does not offer any advantage.

Tracking tendons poses specific requirements for designing a speckle tracking algorithm. Firstly, it requires a high accuracy and a long total tracking range. Secondly, frame-to-frame motion varies considerably, as tendons can move very fast or very slow. Due to large tendon motion over long ultrasound sequences, a tracked region can move out of the image. Another issue is the typical striated speckle pattern of tendons compared to other tissue, requiring very elongated blocks to capture a unique pattern. Furthermore, tendons

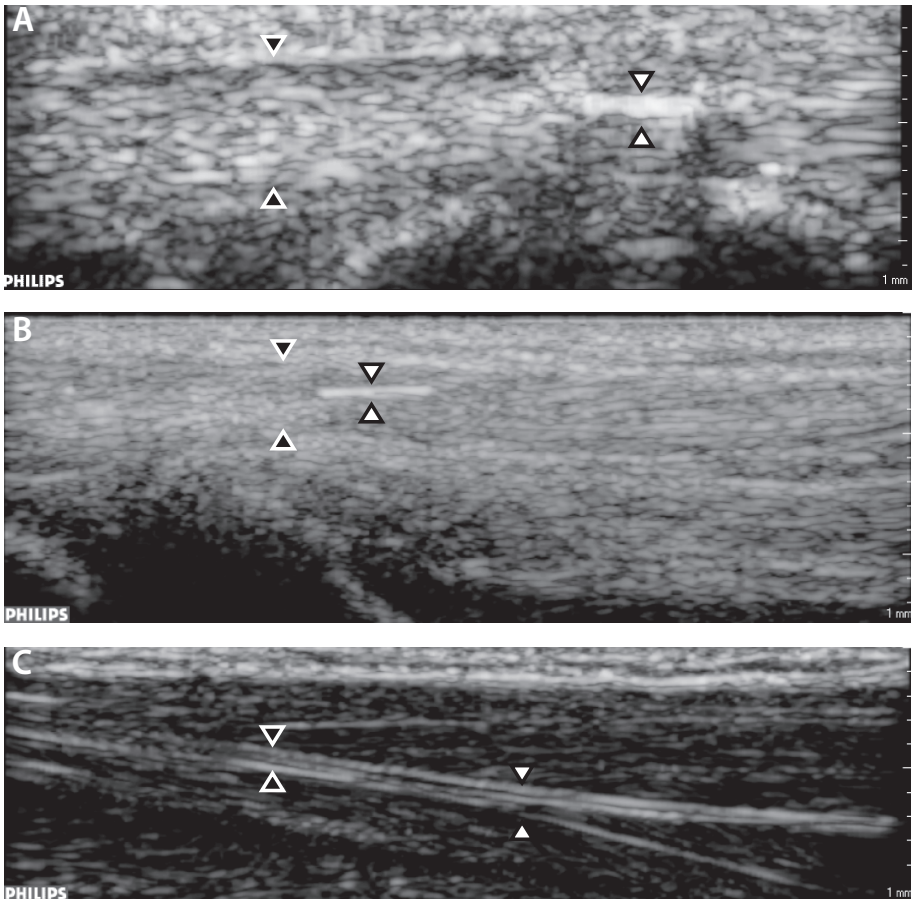

Figure 1. Example of the fibrous structure of the tendon, causing a striated speckle pattern in the ultrasound image. The sheath surrounding the tendon is seen as a hyperechogenic continuous line in all three images (▽). In 1A and B, the inserted aluminum platelet is seen as a hyperechogenic rectangle (▽). In 1C the musculotendinous junction is seen as a hyperechogenic v-shape (▽).

are very stiff compared to muscle with strains ranging from 0.06 to 0.8% at 0 to 50% of a maximum voluntary contraction[49]. The highly coherent motion of a tendon and the small deformations (large stiffness) can be exploited to improve the accuracy of the algorithm. A third requirement is that the size of the template (block) used to track a tendon should be chosen with care. While a large block will contain an unambiguous, unique pattern, during rapid motion the pattern in this block will slightly change due to small deformations, leading to a low correlation and an imprecise displacement estimate. Also, larger blocks are more susceptible to local problems such as shadowing. A small block is less susceptible to deformations and local artifacts, but it may have an ambiguous pattern. A combination like multilevel block matching[216] may reduce the problem of deformations but not of shadowing, which is a more pronounced problem in stiff tendons. A fourth requirement for a speckle tracking algorithm is that it should be able to deal both with small and large frame-to-frame displacements. For large displacements, similar deformation or decorrelation problems occur as described above for large block sizes. This can be handled by increasing the frame rate, so that the frame-to-frame displacement will be smaller. For very small displacements, correlation will be excellent but quantization errors will be relatively large since block matching typically finds the optimal displacement in integer pixels (typically the spatial resolution of the image). If the displacement is of the order of this integer step, this quantization error will be significant. Quantization errors can be reduced using subpixel interpolation of the output matrix of the similarity measure. Furthermore, reducing the frame rate, decimating the image sequence, or calculating displacements between frames further apart in the sequence (using a higher 'frame difference') will limit the quantization error. Fincham and Spedding (1997) showed that a suitable frame difference importantly increases accuracy.

Because of the above-mentioned specific requirements for tendon tracking, commercially available tracking algorithms are not directly applicable. The aim of this study was to extensively study the accuracy of a speckle tracking algorithm optimized for tracking tendon movement. The accuracy was determined over a range of physiological tendon displacements. First, the accuracy of the tracking was evaluated in cadaver porcine tendons during different displacements and velocities using inserted echogenic markers as a reference. Subsequently, the accuracy on the flexor digitorum superficialis (FDS) of a human cadaver hand was evaluated using inserted markers. Finally, the in-vivo accuracy was determined by measuring the FDS movement at wrist level with the musculo-tendinous junction of the FDS as a reference.

Proposed tracking algorithm

Tendons in the hand and wrist are thin, elongated stiff fibrous structures that can displace over considerable distances (multiple centimeters) within a partially mobile sheath. The longitudinal fibers create a characteristic striated speckle pattern in ultrasound images with long thin lines parallel to the motion axis (see Figure 1). The tendon sheath (black arrows) is seen as a continuous hyperechogenic line surrounding the tendon.

$$\rho_{nm}(k,l)=\frac{\sum_{i=-K}^{K}\sum_{j=-L}^{L}\left[F_1(n+i,m+j)F_2(n+k+i,m+l+j)\right]}{\left[\sum_{i=-K}^{K}\sum_{j=-L}^{L}\left[F_1(n+i,m+j)\right]^2\right]^{1/2}\left[\sum_{i=-K}^{K}\sum_{j=-L}^{L}\left[F_2(n+k+i,m+l+j)\right]^2\right]^{1/2}} \quad \text{(Eq.1)}$$

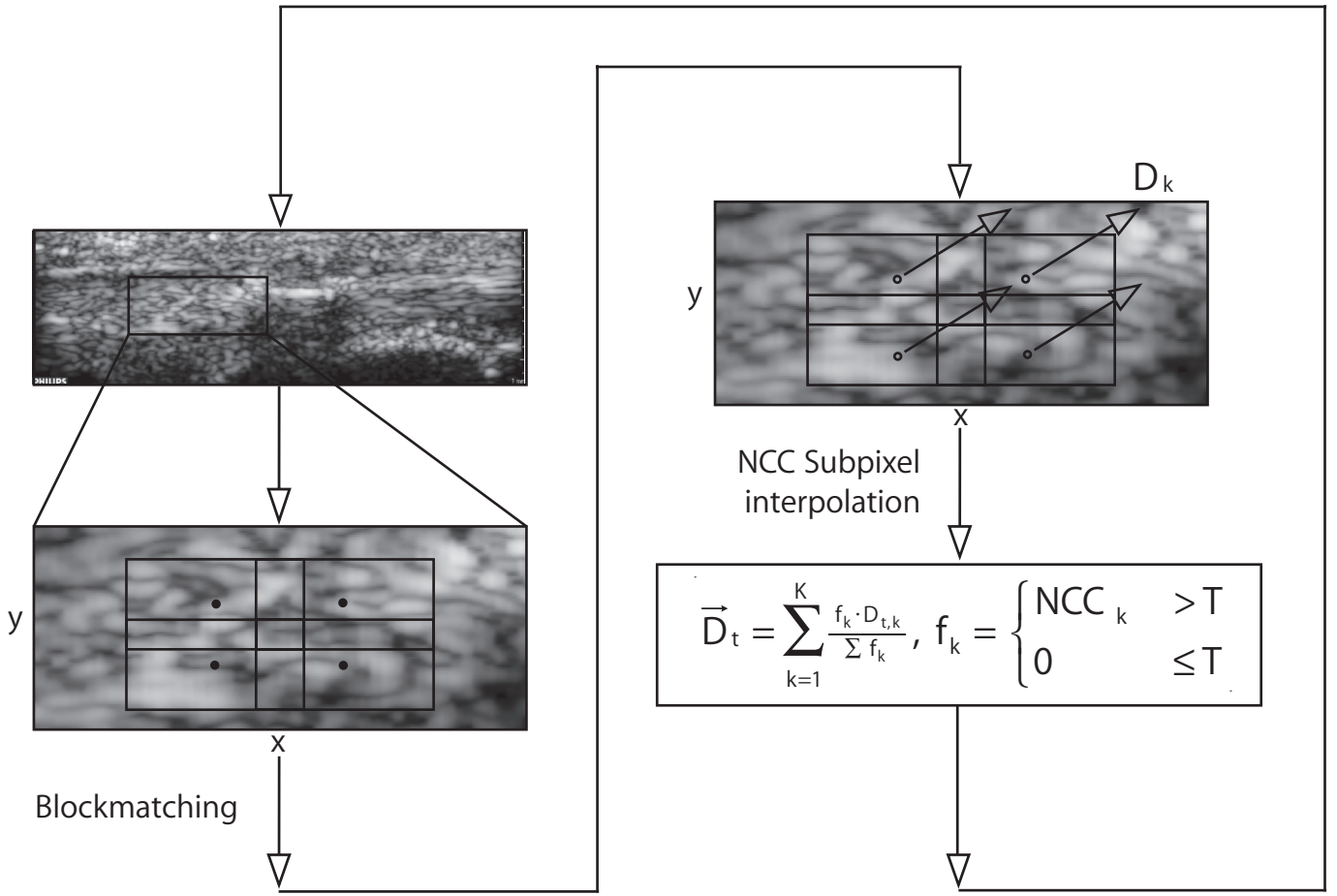

Figure 2. A schematic outline of the proposed algorithm, based on block matching with normalized cross correlation (NCC) as similarity measure. The user manually defines a region-of-interest (ROI) after which the algorithm automatically distributes a predefined number of kernels over the ROI. The algorithm automatically evaluates the different displacement estimates for each kernel. After subpixel interpolation of the NCC output matrix, a correlation-weighted kernel displacement vector average is calculated. For each frame the ROI was kept stationary.

Based on the considerations given in the Introduction, a multi-kernel block-matching scheme was devised specifically for tracking tendon movement with normalized cross-correlation (NCC)(Eq. 1) as similarity measure (see Figure 2). An elongated tracking region of interest (ROI) is placed manually within the tendon and frame-to-frame displacement is estimated using multiple overlapping small kernels. The algorithm was implemented using Matlab (R2007b).

The kernel size and shape were optimized to adapt to the typical speckle structure of tendons and the frame difference was optimized to increase accuracy[104]. To obtain the optimal kernel size we varied the kernel size in the x- and y-direction independently with the best choice being the kernel size with the highest tracking accuracy compared to the manual ground truth. This optimization was performed in phantom experiments and porcine cadaver experiments[104]. For this study we adopted these findings and verified whether tracking accuracy was comparable to earlier findings.

The frame difference was also optimized for our situation. As described by Dilley et al (2001), a higher frame difference will reduce quantization error in favor of tracking accuracy. On the other hand, a higher frame difference will also lead to more decorrelation. Therefore, we determined the optimal frame difference by increasing the frame difference up to the point where the NCC over the whole sequence was still above 0.7.

For each kernel, all possible integer pixel displacements within the search region were evaluated using NCC. To increase displacement accuracy to a subpixel level, a 1:10 2D cubic spline interpolation scheme[60,152,224] was used on the NCC output matrix before peak detection. The total 2D tissue displacement is calculated from all kernel displacements within the ROI with correlations above a predefined lower bound (see Table 1) using a correlation-weighted displacement vector average, such that unreliable estimates are discarded and the best estimates dominate the average. The lower bound of the NCC measure was adopted from earlier findings, such as by Farron et al (2009).

Because the total tendon displacement was often larger than the image size, the frame-to-frame tissue displacement was calculated in a fixed ROI. Thus, instead of conventionally moving the ROI along with the tissue, we used a fixed ROI with the tendon tissue moving through the ROI.

Total displacement was estimated by integration of interframe displacements over all frames. Assuming that strain is very small in tendons, this will be equivalent to the displacement of any point within the tendon.

For low speeds, the sequence was analyzed with a high frame difference (see Table 1) to maintain the balance of reasonable interframe displacement without loss of correlation. Although a high frame difference was selected, each frame was analyzed, creating multiple interleaved sets of frames. Each set was appointed a timestamp corresponding to the midpoint between the frames, e.g. the speed calculated from the frame at t=1.100s and t=1.300s is assigned to t=1.200s.

Experimental setup

To determine the accuracy of our algorithm, we first evaluated the FDS tendon displacement of two porcine legs. During this experiment, the porcine foreleg was fixated in an aluminum holder and the proximal part of the tendon was attached to a universal material testing machine (Testometric AX M250-2.5KN, the Testometric Company Ltd., Lancashire, United Kingdom) using a stainless steel microcable (0.27 mm diameter, Carl Stahl Micro-Cables, Süssen, West-Germany). The testing machine displaced the porcine tendon with three velocities (4, 10, and 16mm/s) and three displacements (5, 10, and 15mm) with forces ranging between 10 and 125N. Each experiment was repeated after the porcine leg was removed and placed back into the aluminum holder.

Due to tissue deformations and other mechanical effects, the displacement and speed of the testing machine could

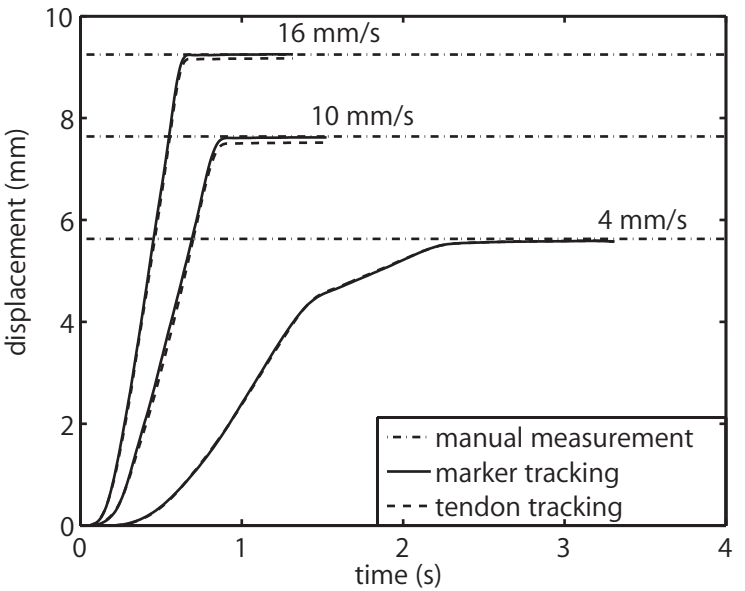

Figure 3. Typical time series for the three different velocities of the porcine leg experiment. The solid and striped lines indicate the profiles of the marker tracking and tendon (speckle) tracking. The horizontal dotted lines indicate the total displacement measured manually.

not be used as a reference measure for the local tendon displacement. Therefore, an echogenic marker (aluminum platelet of 5 x 5 x 1mm) was surgically inserted into the tendon (see Figure 1, white arrows) to serve as a ground truth measurement. Actual displacements of these markers within the ultrasound images were measured manually and were used as a golden standard.

After this experiment, we evaluated the accuracy on the FDS tendon of a human cadaver hand using the same marker and setup. We only evaluated the accuracy at the highest displacement velocity, as this was the worst-case scenario.

Finally, we determined the in-vivo accuracy of the tendon tracking by measuring the movement of the FDS tendon just proximal to the wrist since, at this location, we could use the musculo-tendinous junction as a reference. In this experiment, we asked two healthy subjects (one male, age 28 and one female, age 25) to actively move all fingers from flexion to extension and back at a comfortable speed. This procedure was repeated three times for each subject. The study was approved by the medical ethical committee of the Erasmus MC and subjects gave their written informed consent.

Ultrasound recordings

All recordings were acquired with a Philips iE33 (Philips Medical Systems, Best, the Netherlands) using a L9-3 linear probe in harmonic mode (fundamental frequency 3.7 MHz, harmonic 7.4 MHz). Images were acquired at 120 fps. Recordings were exported as uncompressed AVI files and imported into Matlab for further analyses. The ROI was positioned manually and was typically 148 by 80 pixels, with 0.067 by 0.067mm/pix for the porcine cadaver experiment and 0.043 x 0.043mm/pix for the human cadaver arm and the in-vivo experiment. Sequences typically contained 100 to 1000 images, depending on the displacement (from 4 to 30 mm) and velocity settings (from 4 to 16 mm/s). To minimize the amount of data we stopped the acquisition directly after each displacement.

Data comparison and statistical analysis

For the porcine experiment and the human cadaver experiment the ground truth displacement was obtained by manually determining the marker position in the first and last frame of every movement. In the in-vivo experiment, the ground truth displacement was obtained by manually determining the position of the musculo-tendinous junction at the beginning and end of each movement ('manual displacement measurement'). Two observers independently performed all manual measurements twice.

The marker was also tracked automatically ('marker tracking') to estimate the drift of the tracking algorithm using a slightly adapted version of the tracking algorithm. In this case, the ROI was a narrow box (141 x 41 pix) tightly surrounding the marker and moving with the marker rather than being stationary.

To determine the tendon tracking errors, the difference between the manual displacement measurement and the tendon tracking was calculated. For all comparisons, we calculated normalized root mean squared (RMS) errors between both displacements, expressed in percentages, by normalizing to the manual displacement measurement. In addition the mean and standard deviation of the errors for all manual measurements was calculated to determine the accuracy of the tendon tracking. To determine velocity dependent errors, all errors for the three velocities were grouped that were prescribed with the universal material testing machine (4, 10 and 16mm/s). To determine displacement-dependent errors, we grouped all measurements for the three displacements that we prescribed with the universal material testing machine (5, 10 and 15mm).

The intra- and inter-observer errors of these manual measurements were calculated for each experiment separately using the technical error of measurement (TEM)[207]:

where D represents the difference between two measurements or

$$TEM = \sqrt{\frac{\sum D^2}{2N}} \qquad \text{(Eq.2)}$$

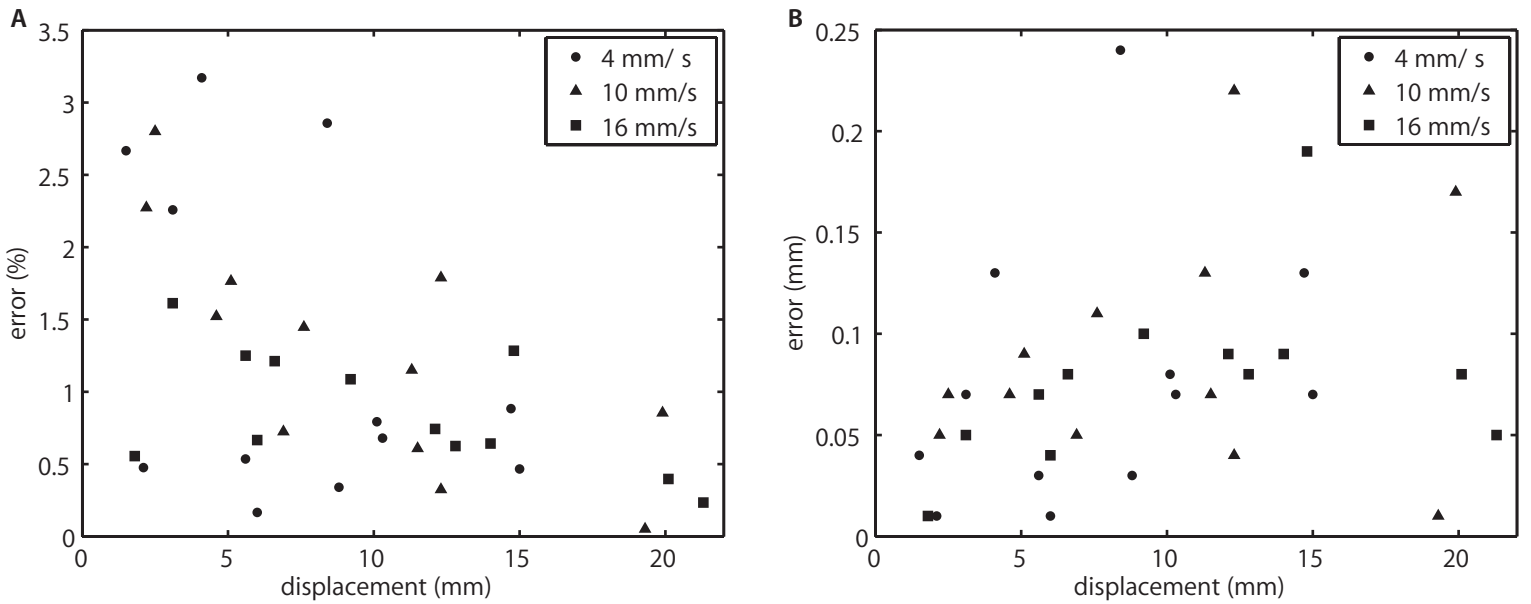

Figure 4. A. Relative errors between manual displacement measurement and tendon tracking for the porcine leg experiment. The different markers indicate the three different velocities imposed by the testing device. B. Absolute errors between manual displacement measurement and tendon tracking.

observations and N represents the number of replicates.

The typical examples of the three different velocities obtained during the porcine leg experiment demonstrate that differences between the manual displacement measurement, marker tracking, and tendon tracking were minimal (see Figure 3). When comparing all 36 displacements from this experiment, the relative errors between the manual displacement measurement and tendon tracking were maximally 3.2% with a mean of 1.3% (see Figure 4A). The relative error decreased for larger displacements, independently of the displacement velocity (see Figure 4A). The corresponding absolute errors of the displacements were all smaller than 0.23mm with a mean of 0.08mm, which is about 1 pixel (see Figure 4B).

The intra- and interobserver errors (TEM) between the manual displacement measurements (the golden standard) of both examiners in the porcine experiment were 0.07 and 0.12mm, indicating that the above-mentioned errors between tendon tracking and manual displacement measurement were mostly within the range of the interobserver error of the golden standard (see Table 2). Therefore, we cannot distinguish between errors in manually quantifying the tendon displacement and errors of the speckle tracking.

When studying the difference between marker tracking and tendon tracking over the complete displacement (figure 4B), typical differences between marker tracking and tendon tracking displacements were found ranging between -0.3 and 0.3mm (95% confidence interval). The mean error between marker tracking and tendon tracking was -0.06 (± 0.2)mm. The largest differences typically occurred only in the middle part of the trajectory for the high-velocity displacements, where the velocity reached its maximum (see Figure 5). The difference decreased again towards the end of the displacement, where the velocity was lower.

Results of the human cadaver arm experiment showed similarly small differences between the manual displacement measurement, marker tracking and tendon tracking as in the porcine experiment (see Figure 6). Again, the tracking errors (see Table 2) were within the range of the intra- and interobserver errors (TEM 0.09 and 0.12mm, respectively).

Displacement curves of the in-vivo measurements of the FDS indicated a more irregular movement pattern than for the cadaver experiments. This is because the active voluntary movements of the subjects were less regular than the machine-controlled porcine and human cadaver experiment. Since manual measurement of the musculo-tendinous junction was more difficult than for the echogenic markers, its intra- and interobserver errors were significantly larger (TEM 0.38 and 0.65mm, respectively). This may partly explain the larger errors of the tracking of the in-vivo tendon movement (see Table 2).

In this study, a novel ultrasound speckle tracking algorithm optimized for tendon tracking was implemented and tested to objectively quantify tendon displacement without the use of anatomical landmarks. The novelty of this algorithm is the use of multiple overlapping kernels and the use of a stationary region of interest (ROI). The use of multiple overlapping kernels can increase tracking accuracy under the assumption of a rigid body. The use of a stationary ROI will allow for tracking tendon displacements beyond the window size of the B-mode images. The results demonstrated that our proposed algorithm is highly reliable in objectively quantifying tendon displacements. For the porcine foreleg experiment, the relative error of the complete tendon displacements, averaged over all displacements and velocities, was 1.3%. The errors for the human cadaver arm experiment and the in-vivo experiment were similar to these results, indicating that the proposed technique is robust.

Our tracking setup has a higher accuracy than other studies reported (see Table 3). For example, Buyruk et al. (1998), using Color Doppler Imaging to study tendon displacement, reported er-

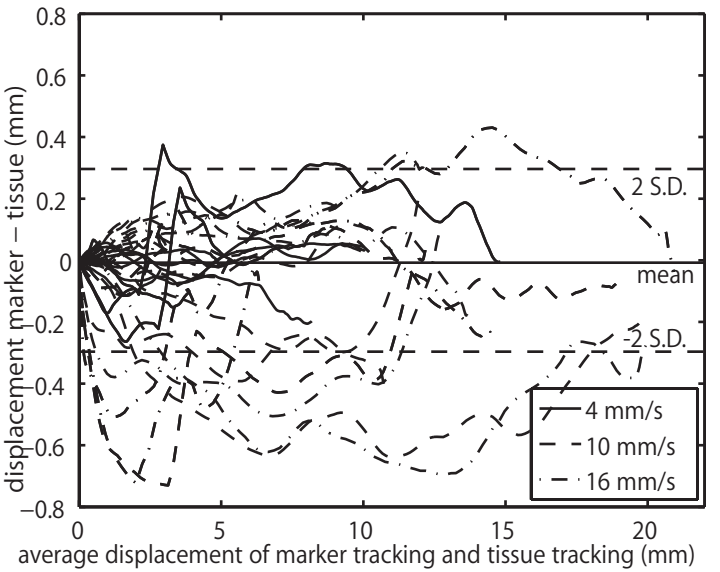

Figure 5. Modified Bland-Altman plot showing the difference in movement paths of the marker tracking and tendon tracking of all measurements. The x-axis represents the mean of the marker tracking and tendon tracking. The y-axis represents the difference between marker tracking and tendon tracking from the start of the displacement up to the maximum displacement. Each line represents a displacement curve.

rors up to 18% for displacements of maximally 11mm. Color Doppler imaging as used in their approach is generally less accurate compared to B-mode imaging or RF imaging[30,77]. Moreover, the in-vivo errors may in fact be larger since Buyruk only presented an in-vitro validation. Lee et al. (2008), using optical flow to measure the displacement of the gastrocnemius musculo-tendinous junction, reported errors of 4 to 8% during in-vivo tendon displacements of about 20 mm using a similar manual tracking of the junction as in the presented study. However, the reported errors only hold when tracking the musculo-tendinous junction and errors may increase when tracking only the tendon due to the more rapidly changing speckle patterns. Dilley et al. (2001), using block matching to measure nerve movement, reporting errors of up to 10%. However, as a reference, a micromanipulator was used that moved the scanhead instead of the tendon. This eliminates any interaction between tendons and surrounding tissue, rendering errors that can be much smaller than for the realistic situation.

A limitation in the present study was the use of an internal reference rather than an external reference such as the movement of the universal material testing machine. The position of the marker in the first frame and at the end of every flexion as a golden standard was manually determined. The accuracy of this procedure is principally limited to one pixel, apart from interpretation differences of the observers. The intra- and inter-observer errors of this manual reference were found to be quite small (mean 0.13mm, max. 0.65mm), and in the same range as the difference with the automated speckle tracking (both for marker and tissue tracking), implying that the automated speckle tracking was at least equally accurate as manual displacement measurement of the marker. Another limitation is that inserting a marker into the tendon may have altered the tendon and its surrounding tissue. However, the tendons showed neither visible damage nor any apparent damage on the ultrasound recordings. Moreover, we always tracked a region of the tendon outside the surgical field for the automated tracking. The assumption that the ROI or kernel does not deform for small frame-to-frame displacements is another limitation in this study. Evidently, the tendon undergoes stretching and relaxation during loading and unloading. These deformations will influence tracking accuracy, especially when averaging multiple kernel displacements. However, when choosing the kernel size and frame difference (and thus the frame-frame displacement) carefully, this influence can be minimized. A smaller kernel is less susceptible to deformations and local artifacts, but may have a more ambiguous pattern. Larger kernels contain a less ambiguous pattern, but are more susceptible to deformations[62]. Since tendons are very stiff, strain ranging from 0.06-0.8% during 0-50% of a maximum voluntary contraction[49], compared to muscle tissue, it is acceptable to increase the kernel size compared to the kernel size used with muscle tracking. Moreover, in this study we used a counterweight to preload the tendon to avoid buckling of the tendon. Preloading will also minimize load chances during displacements, therefore the assumption of no deformation during small frame-to-frame displacements will hold.

DISCUSSION

The typical transitory difference between tissue and marker tracking for the higher velocities shown in the modified Bland-Altman plot (see Fig. 5) may be due to a small time-misalignment between the marker and tendon tracking algorithms; given the tendon velocity, the transitory difference of 5-10 pixels is of the order of the frame-to-frame displacement for the chosen frame difference. We would dismiss strain as tendons are very stiff and the found differences were larger than expected by strain effects alone. We would also dismiss inertia differences in the tendon as a cause for difference, because the tendon is very stiff and the marker was firmly sutured into the tendon. For slower velocities, this 'time lag' was not obvious. For all velocities the most important result, the drift over the total trajectory, was very small, in the order of only one pixel.

Although the presented algorithm is largely automated, we manually selected the frame difference. In future research, ac-

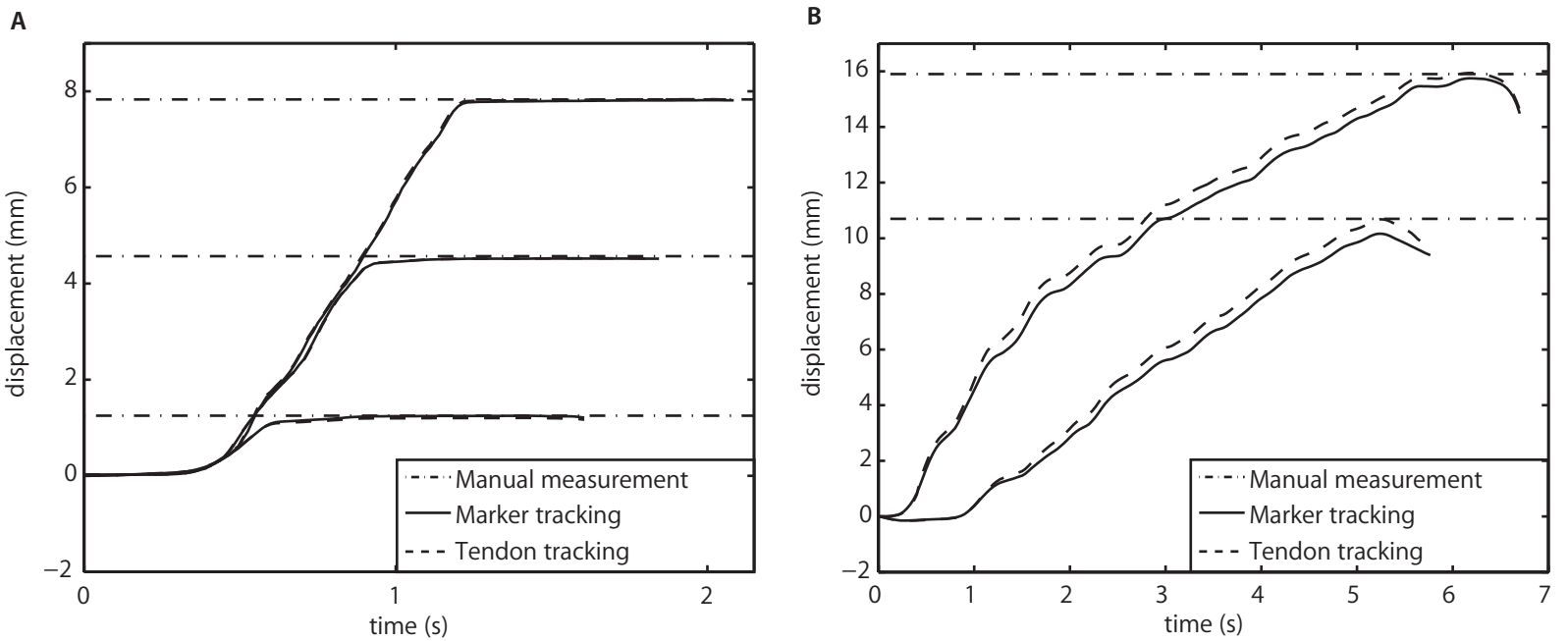

Figure 6. Typical results of tracking in A. a human cadaver arm at 16 mm/s and B. in-vivo on a human arm at pysiological velocty.

curacy of the block matching might be optimized by taking small frame differences for high speeds and large frame differences for low speeds and there are a number of options to automate this process. This would also further prevent human bias and improve the performance in sequences with varying or unknown motion velocity.

An important problem inherent to speckle tracking is out-of-plane motion, occurring when misaligning the probe with the longitudinal direction of the tendon. The larger the misalignment, the lower the cross-correlation will be, following a predictable smooth s-shaped drop-off[51,55,80]. In the porcine and human cadaver arm experiment, we used an inserted marker as reference. The marker's width was of the order of the tendon diameter, ensuring that small out-of-plane motions would have had little influence on the marker tracking, making it reliable as a reference. However, for the in-vivo experiment, we used the musculo-tendinous junction as a reference. Typically the musculo-tendinous is a biconcave structure[69], therefore out-of-plane motion will lead to displacement estimation errors. Results for the in-vivo experiment showed a more irregular motion pattern than for the cadaver experiments, which might indicate out of plane motion. However, the mean correlation coefficient of the normalized cross correlation was in the same range as for the porcine foreleg experiment and the human cadaver arm experiment. Therefore we concluded that the irregular motion would likely correspond to true irregular active voluntary finger movement of the subjects. If the case were out of plane motion or tissue deformation, this would have resulted in a lower correlation. Nevertheless, the musculo-tendinous junction should be avoided as a reference, which is possible with our proposed technique.

In summary, in this study, we have shown that the tracking algorithm is capable of quantifying tendon displacements very accurately. The presented algorithm allows objective quantification of tendon displacement without using anatomical landmarks. Since anatomical landmarks are not needed, this technique broadens the applicability of tendon tracking to a larger number of tendons, such as, for example, the long flexor tendons in the hand. The speckle tracking of tendon movement may have a range of different uses in biomechanical study. For example, it allows researchers and clinicians to acquire important biomechanical variables such as moment arms[88] and muscle or tendon shortening[140]. From a clinical point of view, it could help identify tendon adhesions after surgical repair or to study the effect of different nerve gliding exercises during rehabilitation after injury[174]. To calculate the moment arm it is necessary to measure the joint rotation as well, which is common clinical practice for rehabilitation specialists and therapists[5].

Table 1. Technical details and general settings for the ultrasound scanner and algorithm.

	Porcine experiment	Human cadaver experiment	Human arm experiment
Center (harmonic) frequency (MHz)		3.7 (7.4)	
Field of View (FOV) (H x V)(mm x mm)	46 x 12	46 x 13	46 x 11
Millimeter-pixel ratio[a] (mm/pix)	0.067	0.043	0.043
Number of kernels (horizontal x vertical)		6 (3 x 2)	
Kernel size[b] (pix x pix)	101 x 51	101 x 51	101 x 51
Kernel size[b] (mm x mm)	6.8 x 3.4	4.3 x 2.2	4.3 x 2.2
Region of interest[b] (pix x pix)		200 x 90	
Frame rate (fps)		120	
Lower bound cross-correlation (T)		0.7	
Frame difference[c]	24/14/8	8	1
Maximal axial displacement a (pix)		20	
Maximal lateral displacement b (pix)		100	
Number of frames		100-1000	

[a] Millimeter to pixel ratio was similar in lateral and axial direction.
[b] Kernel size and region of interest are only for tendon tracking. For marker tracking kernel size and region of interest were sized to exactly fit around the marker.
[c] Mentioned frame differences are for 4, 10 and 16 mm/s, respectively.

Chapter 4

Ultrasonographic Assessment of Middle Finger Tendon Excursion in Zone V during Passive and Active Tendon Gliding Exercises

Jan-Wiebe H. Korstanje
Ton R. Schreuders
Jors van der Sijde
Steven E.R. Hovius
Johan G. Bosch
Ruud W. Selles
Journal of Hand Surgery (Am)
2010
35:559-565

Cadaver and in-vivo studies report variable results for tendon excursion during active and passive hand movements. The purpose of this study was to measure middle finger flexor digitorum profundus tendon excursion during active and passive movement using high-resolution ultrasound images. Flexor digitorum profundus tendon excursion was measured at the wrist level in ten healthy subjects during full tip-to-palm active and passive flexion of the fingers. Passive movement was performed two ways: 1) straight-to-full fist: passive flexion starting at the metacarpophalangeal joint, followed by proximal interphalangeal and distal interphalangeal joint flexion; and 2) hook-to-full fist: passive flexion starting at the distal interphalangeal joint, followed by proximal interphalangeal and metacarpophalangeal joint flexion. Tendon excursion was measured using an in-house developed frame-to-frame analysis of high-resolution ultrasound images. Median flexor digitorum profundus excursion was 24.3 mm, 14.0 mm, and 13.6 mm for active fist, straight-to-full fist, and hook-to-full fist movements, respectively. Tendon excursions during active movements was significantly larger compared to excursions during passive movements (p=0.005). The adjusted median tendon excursion was 12.7 mm/100°, 7.5 mm/100°, and 7.4 mm/100° for active fist, straight-to-full fist, and hook-to-full fist movements, respectively. Adjusted tendon excursions during active movement were significantly larger compared to those achieved during passive straight-to-full fist movement (p=0.013). Adjusted tendon excursions during straight-to-full fist movements were significantly larger compared to those achieved during passive hook-to-full fist movement (p=0.017). Active motion produced 74 and 79% increases in excursions compared to both passive motions in healthy controls. The study results can serve as a reference for evaluating excursions in patients with tendon pathology, including those who have undergone tendon repair and reconstruction.

INTRODUCTION

Adhesion formation is a major problem following hand tendon surgery. Historically, three rehabilitation protocols have been used after flexor tendon repair: 1) immobilization, 2) early controlled mobilization or passive mobilization, and 3) early active mobilization[159,181,188]. Since immobilization is thought to contribute to tendon adhesion formation[19], Duran and Houser[38] introduced early controlled mobilization or passive mobilization protocols to minimize tendon adhesion formation. However, Manske [124] suggested there may not be sufficient tendon movement at the repair site during passive motion protocols and active motion was necessary. Strickland et al.[181] reported that early active mobilization can generate larger tendon excursions but is associated with an increased risk of tendon rupture at the repair site[40].

Although it is generally accepted that tendon excursion is needed to avoid adhesion, the amount of excursion needed is unknown. Duran and Houser[38] suggested that 5 mm of tendon gliding should prevent firm tendon adhesions; however, this has not been experimentally supported. Additionally, the amount of excursion attained during different rehabilitation protocols is unknown.

Current knowledge of flexor and extensor tendon excursion is based primarily on cadaver studies. Although cadaver studies are generally well-controlled, reported tendon excursions vary widely between studies. Excursions for active movement range from 10 mm to 33 mm[78,128,149,189] and from 1 mm to 21 mm for passive movement excursions[149,189]. This suggests that cadaver studies are unreliable in establishing tendon excursion and reference values, especially for passive joint movements.

Much of the variation in cadaver and peri-operative investigations may be due to disrupted physiology of the tendon and surrounding tissues. Therefore, in-vivo tendon movement measurements should provide more reliable and valid excursion data. Thus far, studies of in-vivo flexor digitorum profundus (FDP) tendon gliding have been limited. Using Color Doppler Imaging, Soeters et al.[174] also found that tendon excursion was larger in active versus passive protocols; however, differences in tendon excursion between passive and active movements were not statistically significant and Color Doppler Imaging measurement errors were approximately 10%.

The purpose of this study was to quantify in-vivo middle finger FDP tendon excursion during three rehabilitation protocols used after flexor tendon repair, using a validated tendon tracking ultrasound algorithm.

METHODS

Subjects and measurements

The medical ethics committee approved this study, and informed consent was obtained from each participant. Ten healthy volunteers with a median age of 25.5 years (range 17 to 52), including five males and five females, were enrolled in this study. Height and hand length, as well as wrist, metacarpophalangeal (MCP), proximal interphalangeal (PIP) and distal interphalangeal (DIP) joint thicknesses were measured (see Table 1).

Experimental conditions

Ultrasound video sequences of middle finger FDP tendons were acquired using an iE33 ultrasound system (Philips Electronics, Eindhoven), which used a 7 MHz linear array, probe at 100 frames per second. The image resolution was 0.021 mm/pixel.

The experimental conditions are illustrated in Figure 1. Subjects were positioned on an examination bench and asked to wear a standard medical examination glove (Ansell NitraTex, Ansell Healthcare LLC, Red Bank, NJ, USA). To relate tendon excursion to joint range of motion (ROM), 5 mm spherical reflective markers were placed on the glove on the radial side of the MCP, PIP, and DIP joints of the middle finger. The glove was used to ensure high contrast between markers and background. The index and middle fingers were taped (Leukotape Classic, 2cm, BSN Medical GmbH, Hamburg, Germany) together at the PIP joint level to ensure minimal discrepancy between measured index finger joint angles and actual middle finger joint angles. A digital

Figure 1. Experimental conditions with the subject's arm positioned in the custom-made brace. Four markers on the index finger were used to automatically track the joint angle.

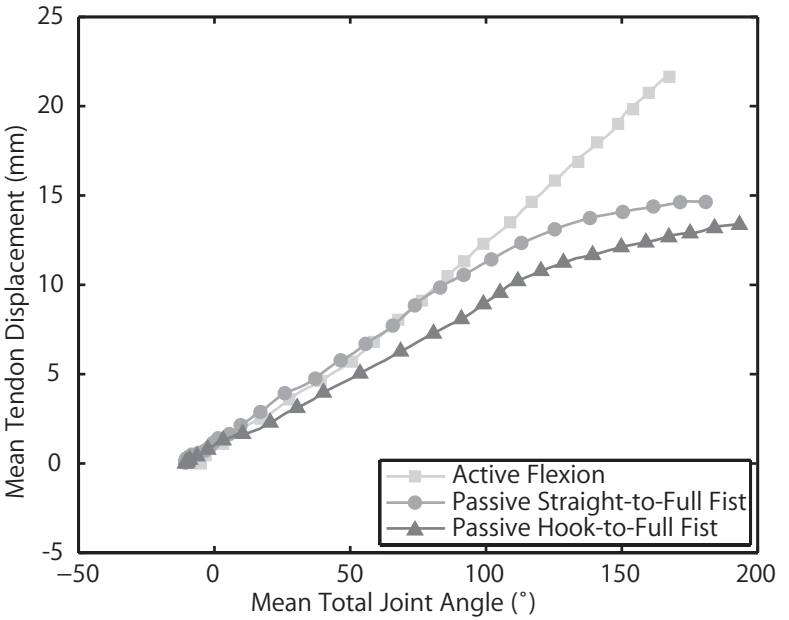

Figure 2. Mean tendon excursion during active and passive protocols as a function of mean total joint angle. During passive hand movement, tendon excursion diminished compared to active hand movement. The cut-off point for the passive straight-to-full fist movement was 130° ($p=0.047$) and the cut-off point for passive hook-to-full fist was at 90° ($p=0.037$).

camera captured finger ROM during flexion at 25 frames/s. Video and ultrasound synchronization was conducted using the audio start signal of the iE33 as the starting point for video analysis.

A custom thermoplastic splint was used to minimize arm and wrist movement without limiting finger ROM. Subjects' right hands were splinted and immobilized in the supine position using Velcro straps. Forearms were fixed to the brace at forearm midpoint, wrist, and just proximal to the MCP joint. The lateral thumb was taped to the brace to prevent it from obscuring the marker view of the camera. The splint was fixed to an x-y-z-table containing a 3-dimensional micro-manipulator, using double-sided adhesive tape. The scanhead of the ultrasound scanner was placed in the 3-dimensional micro-manipulator by using a custom-made plastic holder and was used to position and fix the scanhead to the wrist. The FDP and flexor digitorum superficialis (FDS) muscle locations of the middle finger were identified by palpation and marked on the wrist as the starting point to localize the middle finger FDP using ultrasound. After localizing the FDP tendon and the FDS tendon, the DIP joint was flexed and extended to distinguish between the FDP tendon and FDS tendon based on more FDP excursion during DIP movement. Moreover, the FDP tendon commonly passes through the carpal tunnel at an angle while the FDS tendon does not; this additional feature also distinguished the FDP tendon from the FDS tendon. After analysis, the DIP joint angle was compared to the FDP tendon excursion; if a change in DIP joint angle did not result in FDP tendon excursion it was likely that not the FDP tendon but the FDS tendon was scanned. However, this was not the case in any of the measurements.

An electromyogram (EMG) was used to verify that passive movements were performed without muscle activity. Two electrodes were placed longitudinally at the midpoint of a line between the medial epicondyle and ulnar styloid. The ground electrode was positioned to create an equilateral triangle[11]. Although surface EMG cannot discriminate single muscle activity, all increases in activity were considered as possible FDP activity. Therefore, trials were repeated until fully passive movement was achieved. The EMG threshold for passive movement was set at twice the baseline measured during relaxation.

Motion protocols

Active fist, passive straight-to-full fist, and passive hook-to-full fist protocols were used[205,206]. For the active protocol, subjects were asked to make a fist starting from full extension without using excessive force at the endpoint. To control for possible squeezing forces at the full fist position, we evaluated tendon excursion only to the point where the total joint angle stopped changing. For passive straight-to-full fist movements, all fingers were moved from full extension to full flexion, from MCP joint flexion, through PIP joint flexion, and finally to DIP joint flexion. Passive hook-to-full fist movements started with DIP joint flexion, followed by PIP joint flexion, and concluded with MCP joint flexion. Each movement was executed twice. When the arm moved with respect to the scanhead, measurements were discarded and repeated. A visual check ensured that subjects moved toward the same end position of full extension against the brace.

Ultrasound imaging analyses

Ultrasound images were exported as uncompressed AVIs using Qlab 7 (Philips, Best, The Netherlands). A dedicated two-dimensional multi-kernel block-matching scheme using normalized cross-correlation (NCC) was used to measure tendon excursion. This algorithm has been extensively tested and described elsewhere, and has a mean measurement error of 1.6%[104]. The algorithm is based on the general concept of block-matching schemes, which are frequently used to track cardiac wall movements[34,49,104,110,117,141,154]. Uncompressed AVIs were imported into Matlab (7.5, R2007b). Then, a region of interest (ROI) was manually assigned to the first frame.

Frame-to-frame displacement was estimated by using multiple overlapping small kernels. Each kernel was compared with a search region in a subsequent frame using NCC as a similarity mea-

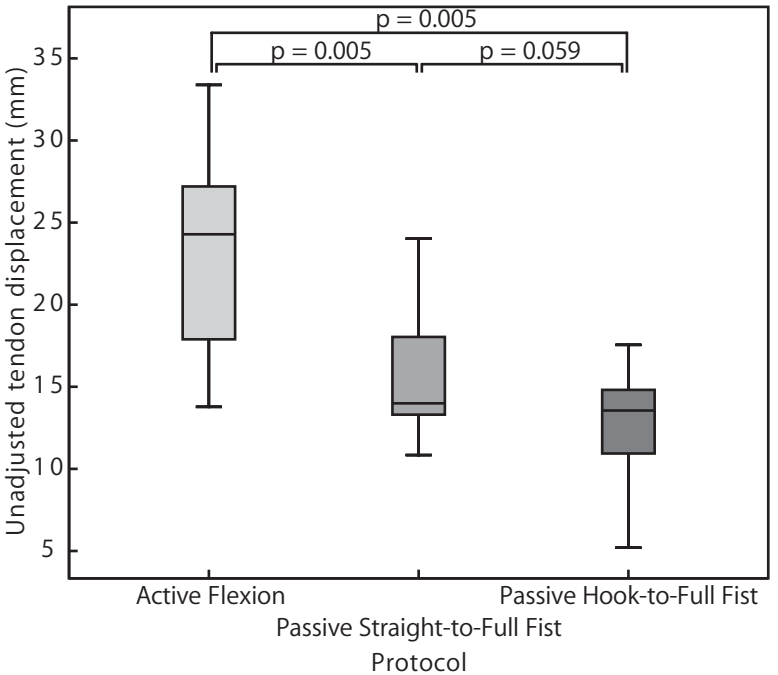

Figure 3. Box plot of the absolute tendon excursion (in mm) for the three movement protocols. Excursion in the active protocol was significantly larger compared to excursion in the passive straight-to-full fist and hook-to-full fist protocols.

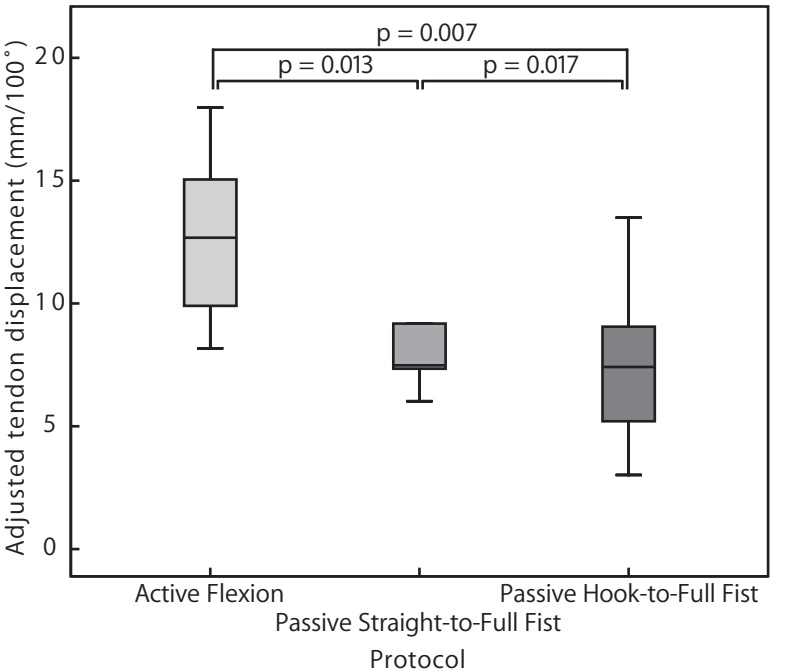

Figure 4. Box plot of the tendon excursion adjusted for the total summed joint angle for the three different protocols. Excursion was significantly larger for active compared to straight-to-full fist and the hook-to-full fist protocols.

sure. A correlation of one indicated a perfect match and a correlation of zero indicated no match. We considered all correlations greater than 0.7 to be good matches. The total 2-dimensional ROI displacement was calculated from all kernel displacements within the ROI that had good correlations. We used a correlation-weighted displacement vector average; such that unreliable estimates were discarded and best estimates were given more weight to the average.

Video recordings of joint movements were imported using Pinnacle Studio 9 (Pinnacle Systems Inc., CA, USA). Simi-motion 7.5 (SIMI Reality Motion Systems, Unterschleissheim, Germany) was used to analyze exported AVIs to identify individual joint ROM. The three phalanges of the fingers were identified using the spherical markers. Angular rotation of the MCP joint was calculated as the angle between the proximal phalanx and the horizontal baseline. Angular rotation of the PIP joint was calculated as the angle between the middle phalanx and the proximal phalanx. DIP joint rotation was calculated as the angle between the distal phalanx and middle phalanx.

Excursions for the three protocols were adjusted for total joint angle by using video tracking. The total excursion was divided by the total ROM and normalized to 100°. Displacements are reported as median excursions and ranges unless otherwise noted.

Statistical analyses

We used Kendall's W test to evaluate the ROM and joint angles for all three protocols. For all significant differences, we subsequently used the Wilcoxon signed rank test to evaluate differences between protocols. We also used the Wilcoxon signed rank to compare excursions between active and passive protocols, for both adjusted and unadjusted excursions. Additionally, the straight-to-full fist and hook-to-full fist protocols were compared. Statistical significance was set at p=0.05.

Figure 2, which illustrates the mean, summed joint angles (MCP joint + PIP joint + DIP joint) versus mean tendon excursions. Total tendon excursions were larger during active movement compared to both passive movements. This difference was more pronounced closer to the full fist position. Differences in tendon excursion between active fist movement and passive straight-to-full fist movement became statistically significant at 130° (p=0.047). Differences in tendon excursion between active fist movement and passive hook-to-full fist movement became statistically significant at 90° (p=0.037).

Table 2 shows angular displacements and joint angular velocities for each protocol. Although the total joint angle did not differ significantly between the three protocols (p=0.905), the MCP joint ROM was significantly smaller for active fist movements compared to passive straight-to-full fist movements (p=0.007). The MCP joint ROM was significantly smaller for passive straight-to-full fist movements compared to hook-to-full fist movements (p=0.007). The joint angular velocity did not differ between the three protocols (p=0.130).

The median absolute tendon excursion for the middle finger FDP was 24.3 mm, 14.0 mm, and 13.6 mm for active, fist straight-to-full fist, and hook-to-full fist movements, respectively. Tendon excursion was increased 74% and 79% in active versus both passive protocols (p=0.005) (Figure 3). There were no significant differences between passive protocols (p=0.059).

Adjusted tendon excursions for total joint angular displacements were 12.7 mm/100º, 7.5 mm/100º, and 7.4 mm/100º for active fist, straight-to-full fist, and hook-to-full fist movements, respectively. All adjusted tendon excursions differed significantly: 1) active to straight-to-full fist (approximately 69% increase in tendon excursion for active fist movement compared to straight-to-full fist, p=0.013); 2) active fist to hook-to-full fist protocol (72% increase in tendon excursion for active movement compared to hook-to-full fist, p=0.017); and 3) straight-to-full fist to hook-to-full fist (6% increase in tendon excursion for straight-to-full fist compared to hook-to-full fist, p=0.007, Figure 4).

Table 1. Participant characteristics (5 males, 5 females)

	Median	Range
Age (yr)	26	17-52
Height (cm)	183	171-203
Hand length (mm)	193	187-220
Metacarpophalangeal joint thickness (mm)[a]	25.5	22.2-28.5
Proximal interphalangeal joint thickness (mm)[a]	16.3	15.0-18.1
Distal interphalangeal joint thickness (mm)[a]	12.7	11.3-21.3

[a] Thickness was measured in the palmo-dorsal plane

Table 2. Median and ranges for middle finger joint angles and angular velocity

	Active	Straight-to-Full Fist	Hook-to-Full Fist
Metacarpophalangeal joint (°)[a]	64.9 (36.1-97.3)[b]	77.1 (61.6-98.0)[c]	67.7 (55.9-89.2)[d]
Proximal interphalangeal joint (°)[e]	53.1 (9.3-63.6)	49.8 (5.5-72.4)	41.4 (34.7-87.4)
Distal interphalangeal joint (°)[f]	71.6 (46.9-81.1)	60.6 (47.2-81.0)	68.5 (49.7-78.9)
Range of motion (°)[g]	176.0 (134.3-231.9)	191.9 (148.0-226.6)	183.3 (157.6-225.1)
Angular velocity (°/s)[h]	41.5 (31.2-52.3)	39.9 (31.2-49.3)	38.4 (34.1-62.6)

[a] p=0.008 (Kendall's W test)
[b] p=0.007, tested between the active and straight-to-full fist protocols (Wilcoxon's signed rank test)
[c] p=0.007, tested between the straight-to-full fist and hook-to-full fist protocols (Wilcoxon's signed rank test)
[d] p=0.508, tested between the active and hook-to-full fist protocols (Wilcoxon's signed rank test)
[e] p=0.905 (Kendall's W test)
[f] p=0.150 (Kendall's W test)
[g] p=0.905 (Kendall's W test)
[h] p=0.130 (Kendall's W test)

Only two studies to date have non-invasively quantified in-vivo tendon excursion during rehabilitation[149,174]. In the present study, we investigated in-vivo tendon excursion by using three rehabilitation protocols in ten healthy subjects. Both unadjusted and adjusted tendon excursions were significantly larger during active compared to passive movements. This difference may result from tendon buckling, as suggested by Horii et al.[79]. Whereas tendons are continuously loaded during active movements, passive flexion shortens the FDS muscle to the point of no passive tension. After that, the tendon may buckle as it is forced through its surrounding sheath without loading.

In comparing passive protocols, we observed a small but significantly larger adjusted tendon excursion during straight-to-full fist compared to hook-to-full fist movement. This difference is likely caused by differences in joint angles at the end of the flexion movement. MCP and PIP joint ranges were larger and the DIP joint range smaller during straight-to-full fist compared to hook-to-full fist protocols. Because the tendon moment arm is largest at the MCP joint, a similar angular change in this joint contributes more to tendon excursion than in the other joints. Although clinicians should consider that different flexion patterns result in different tendon excursions, the small differences between the excursions may have little impact on adhesion formation after tendon repair.

Previous investigations of tendon excursion in cadaver hands produced widely varying tendon excursion results (see Table 3). McGrouther and Ahmed[128] reported a mean middle finger tendon excursion of 17.6 mm during active movement simulated by full extension to 90° PIP joint flexion and 60° DIP joint flexion. Horibe et al.[78] reported larger tendon excursions, but these were mean tendon excursions with no distinction between index and middle finger FDP tendon excursions. In that study, mean tendon excursion was 30.4 mm during active movement (full extension to 105° MCP joint flexion plus 32° PIP joint flexion plus 15° DIP joint flexion). Tanaka et al.[189] reported a mean tendon excursion of 20.9 mm for the index finger FDP in zone II during passive movement from full extension to full flexion. Panchal et al.[149] investigated active and passive tendon excursion cadavers, showing larger tendon excursions during simulated active movement (10 mm) compared to passive movement (1 mm). The ROM was 90° at the PIP joint and 70° at the DIP joint with the MCP joint splinted at 90° flexion. Panchal et al.[149] observed similar tendon excursions during in-vivo studies, with a mean tendon excursion of 11 mm during simulated active movement and 4 mm during passive movement. Soeters et al.[174] reported mean tendon excursions of 13.3 mm during active movement and 11.4 mm during passive movement (PIP joints and DIP joints moved from full extension to full flexion).

Variations in tendon excursion in the above-described studies are much larger than can be expected based on individual differences; the differences more likely relate to experimental conditions such as measurement techniques, tissue changes in cadaver tendons, or surgery-induced changes to tendons (see Table 4). Our in-vivo study yielded larger active and passive tendon excursions compared to those reported in the literature.

The present study has some limitations. We limited FDP tendon excursion measurement to zone V. Because proximal to this point FDP tendons are oriented longitudinally during flexion and extension, measurement biases due to out-of-plane tracking errors are minimized. Another limitation is that the sample was limited to ten healthy subjects. Despite the small size, we found statistically significant differences by using conservative non-parametric Wilcoxon signed rank tests. Future studies will determine whether our findings in healthy controls are applicable to patients who have undergone flexor tendon reconstruction. Also motion was not device-controlled, so motion patterns differed slightly between conditions. Consequently, ROMs differed for MCP, PIP, and DIP joints across protocols. This motion variation may explain differences in tendon excursion between passive protocols. Additionally, joint angular velocities may differ between protocols, although Fu-

Table 3. Middle finger flexor digitorum profundus tendon excursions and tendon excursions normalized to 100° total joint angle in published studies

	Cadaver or in-vivo	Excursion (mm)	Range of Motion (°)	Adjusted excursion (mm/100°)
Active				
McGrouther (1981)	Cadaver	18	150	12.0[a]
Horibe et al. (1990)	Cadaver	30	152	19.7[b]
Panchal et al. (1997)	Cadaver	10	110	9.1[c]
Panchal et al. (1997)	In-vivo	33	160	20.6[d]
Soeters et al. (2004)	In-vivo	13	120	10.8[e]
This study	In-vivo	24	176	12.7[f]
Passive				
Tanaka et al. (2005)	Cadaver	21	210	10.0[g]
Panchal et al. (1997)	Cadaver	1	110	0.9[c]
Panchal et al. (1997)	In-vivo	7	160	4.4[h]
Soeters et al. (2004)	In-vivo	11	120	9.2[e]
This study	In-vivo	14	188	7.4[i]

[a] 90° proximal interphalangeal joint and 60° distal interphalangeal joint flexion
[b] 105° metacarpophalangeal joint, 32° proximal interphalangeal joint and 15° distal interphalangeal joint flexion
[c] 90 ° proximal interphalangeal joint and 40° distal interphalangeal joint flexion
[d] Assuming at least 90 ° proximal interphalangeal joint and 70° distal interphalangeal joint flexion
[e] Assuming 60° proximal interphalangeal joint and 60° distal interphalangeal joint flexion
[f] 65° metacarpophalangeal joint, 53° proximal interphalangeal joint and 72° distal interphalangeal joint flexion
[g] Assuming 90° metacarpophalangeal joint, 60° proximal interphalangeal joint and 60° distal interphalangeal joint flexion
[h] 90 ° proximal interphalangeal joint and 70° distal interphalangeal joint flexion
[i] 72° MCP joint, 46° proximal interphalangeal joint and 65° distal interphalangeal joint flexion

kunaga et al.[59] showed that this velocity does not influence tendon displacement in their studies of the lower leg. A potential limitation is the possibility that examination glove pressure increased tendon friction. However, examination gloves were chosen to closely fit subjects' hands. Another potential limitation is that angle measurements may be less accurate because we taped the index and middle fingers together. However, the relationship between active tendon excursion and total joint angle was nearly linear, as predicted by biomechanical models and experimental data, indicating that the angle measurement were accurate[7]. Finally, our subjects were young and tall with long hands.

In summary, this study demonstrates large and statistically significant differences in tendon excursion during active and passive movements. These baseline data can be used to develop FDP tendon mobilization protocols and the experimental method that we applied may help surgeons and therapists quantify early tendon gliding after tendon repair. The method can be used to assess sufficiency of tendon gliding and modify post-surgical exercises to avoid tendon adhesion.

Table 4. Measurement devices and cadaver conditions

Study	Type	Measurement device	Cadaver conditions
McGrouther (1981)	Cadaver	Suture\Ruler	Complete removal of tissue
Tanaka (2005)	Cadaver	Marker[a]	Open incision\Open sheath\No pretension
Panchal (1997)	Cadaver	Marker/Ruler	Removal of subcutaneous fat\Removal of skin\No pretension
Horibe (1990)	Cadaver	Roentgenograms	Digit separated from hand
Panchal (1997)	In-vivo	Marker/Ruler	NA
Soeters (2004)	In-vivo	Doppler	NA
This study	In-vivo	Ultrasound tracking	NA

[a] Assumed ruler, not otherwise specified
NA Not applicable

Chapter 5

Ultrasonographic Assessment of Different Flexor Tendon Mobilization Protocols; Effect on Long Finger Tendon Excursions Compared to its Surrounding Tissue

Jan-Wiebe H. Korstanje
Johannes N.M. Soeters
Ton R. Schreuders
Peter C. Amadio
Steven E.R. Hovius
Henk J. Stam
Ruud W. Selles

Provisionally accepted
Journal of Bone
and Joint Surgery (Am)

Different mobilization protocols have been proposed for rehabilitation after hand flexor tendon surgery that aim at adhesion prevention by adequate tendon excursion exercises. Several cadaver studies have suggested that the position of the neighboring injured fingers influences tendon excursions of the injured finger. Therefore, the purpose of this study was to determine the influence of different finger positions on the long finger flexor digitorum profundus (FDP) tendon excursions, measured both absolutely and relatively to the surrounding tissue of the tendon. FDP tendon excursions and surrounding tissue movement were measured in Zone V in 12 healthy subjects during three different rehabilitation protocols and two experimental models: 1) Active Four-Finger Mobilization Protocol, 2) Passive Four-Finger Mobilization Protocol, 3) Modified Kleinert Mobilization Protocol, 4) experimental Modified Kleinert Flexion Mobilization Model, and 5) experimental Modified Kleinert Extension Mobilization Model. Tendon excursions were measured using a frame-to-frame analysis of high-resolution ultrasound images. Absolute FDP tendon excursions were 23.4, 17.8, 10.0, 13.9, and 7.6 mm for the Active Four-Finger Mobilization Protocol, the Passive Four-Finger Mobilization Protocol, the Modified Kleinert Mobilization Protocol, the experimental Modified Kleinert Flexion Mobilization Model, and the experimental Modified Kleinert Extension Mobilization Model, respectively; these differences were all statistically significant. Corresponding relative FDP tendon excursions were 11.2, 8.5, 7.2, 10.4, and 5.6 mm. Active Four-Finger Mobilization Protocol excursions were significantly larger than Passive Four Finger Mobilization Protocol excursions, but not significantly larger than Modified Kleinert Flexion Mobilization Protocol excursions. This study demonstrates large and significant differences between the different rehabilitation protocols and experimental models in terms of absolute and relative tendon displacement. More importantly, our study clearly demonstrates the influence of the position of the adjacent fingers on the hand flexor tendon displacement of the finger that is mobilized.

After tendon reconstruction or tendon repair, adhesions are a common problem that contribute significantly to poor hand function outcome. To prevent tendon adhesions two mainstream rehabilitation protocols have been proposed: passive mobilization and active mobilization[159,181,188]. Although active mobilization protocols obtain larger tendon excursions and therefore lead to a decrease in adhesion formation, active mobilization protocols are also associated with a higher incidence of tendon re-ruptures due to higher forces on the tendon[102,181]. Alternatively, it is possible to increase the strength of the sutures by using different suture techniques and therefore enabling the use of an active mobilization protocol. However, increasing the number of sutures is likely to cause more damage to the tendon or compromise its ability to heal1. The ideal mobilization protocol would obtain the tendon excursion of the active mobilization protocol with the forces associated with a passive mobilization protocol.

In the literature, several passive mobilization protocols have been described, such as the modified Kleinert mobilization technique with palmar pulley and the four-fingers mobilization protocol[126,127]. The differences between these two protocols is that while the modified Kleinert uses a rubber band attached to only the injured finger, the four-finger protocol uses rubber bands attached to all four fingers, including the injured finger, thereby increasing tendon excursion and stress (see Figure 1, top two panels)[168]. Neither of these mobilization protocols achieve excursions comparable those during active mobilization[102,149].

The modified Kleinert mobilization protocol is commonly used clinical settings, even though the four-finger mobilization protocol achieves larger excursions than the modified Kleinert mobilization protocol.[168] This indicates that moving all fingers in conjunction with the injured finger, as in the four-finger mobilization protocol, improves excursion compared to the modified Kleinert mobilization protocol, which actually is a single-finger mobilization protocol. Therefore, it might be possible to increase tendon excursion within the modified Kleinert mobilization protocol by placing the adjacent fingers in different positions, such as full flexion or full extension. A number of cadaver studies have compared tendon excursions during passive mobilization and active mobilization, but these cadaver studies may not always represent in-vivo tendon excursions[102]. At present, only a small number of studies assessed tendon excursions in-vivo[149,167,174]. However, none of these studies investigated the biomechanical influence of the adjacent fingers and its surrounding structures on tendon excursions of the finger during the different mobilization protocols.

There has been an increased interest in the tissue surrounding the tendon, reflected by the relatively large number of studies focusing on the repair of the tissue surrounding the tendon and its effect as a barrier to prevent formation of extrinsic adhesions (for review, see[181]). The anatomy and nomenclature of this tissue is still debated. Traditionally, the tissue surrounding the hand flexor tendons was called “paratenon” or “common carpal tunnel sheath”. Ettema et al.[44] launched an anatomical concept of the carpal tunnel focusing on surrounding tissues. They hypothesized that the tendon is surrounded with subsynovium connective tissue (SSCT). Guimberteau launched a similar anatomical concept, hypothesizing that the tendon is surrounded by a multimicrovacuolar collagenous dynamic absorbing system (MCDAS), which interconnects the tendon and the carpal retinaculum[70,71].

Recently, a small number of cadaver studies investigated hand flexor tendon excursions and surrounding tissue movement, suggesting that the surrounding tissue moves in the same direction as the tendon, with excursions ranging from 3 to 13 mm [46,78,128,214,217,220]. Since this surrounding tissue moves in the same direction as the tendon, tendon movement relative to the surrounding tissue may be smaller than absolute tendon movement. It may therefore be misleading to study only absolute excursions, that is, tendon excursions measured with respect to a non-moving reference such as a ruler or a bone. As a result, the 5mm of excursion that has been suggested

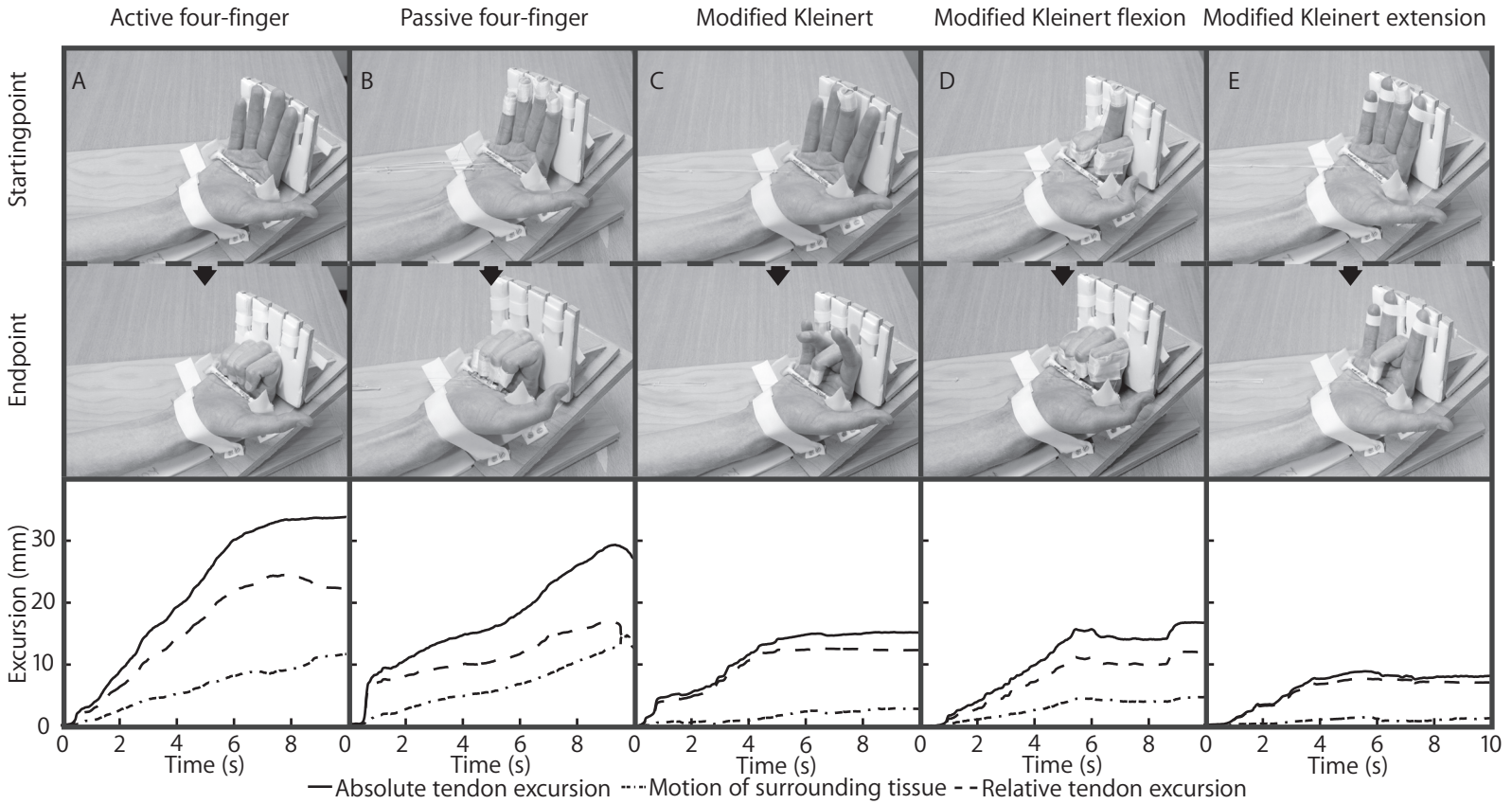

Figure 1. Overview of the active mobilization protocol and the two passive mobilization protocols used in this study, and the two experimental passive mobilization models. (A) The Active Four-Finger Mobilization Protocol. (B) The Passive Four-Finger Mobilization Protocol. (C) The Modified Kleinert Mobilization Protocol. (D) The experimental Modified Kleinert Flexion Mobilization Model. (E) The experimental Modified Kleinert Extension Mobilization Model. The lower panel shows a typical example of absolute hand flexor tendon excursions, surrounding tissue motion, and relative tendon excursions obtained during the corresponding mobilization protocols and experimental models shown in the top two panels.

to be needed to overcome tendon adhesions may be more difficult to meet when considering this relative to the surrounding area.[38].

The purpose of this study was to determine the influence of the uninjured fingers on the long finger flexor digitorum profundus (FDP) tendon excursions, measured both relatively to the stationary ultrasound scanhead as well as relatively to the surrounding tissue of the tendon. To do so, we compared three different finger position protocols already used in a clinical setting: 1) the Active Four-Finger Mobilization protocol, 2) the Passive Four-Finger Mobilization Protocol, and 3) the Modified Kleinert Mobilization Protocol. In addition, we compared the protocols with two experiment models, where we positioned the other fingers in two extreme situations to evaluated the effect of the adjacent fingers on the tendon excursion: 1) an experimental model based on the Modified Kleinert Mobilization protocol, but with the adjacent fingers in full flexion, and 2) and experimental model based on the Modified Kleinert Mobilization Model, but with the adjacent fingers in full extension. We will compare the absolute and relative excursions between the different protocols and experimental models as well as compare them to the minimal excursion of 5mm needed to avoid adhesions, as suggested by Duran and Houser[38].

INTRODUCTION

Subjects and measurements

Our institutional medical ethics committee approved this study, and informed consent was obtained from each participant. Twelve healthy subjects (6 males and 6 females), with a median age of 24 years (range, 21 to 52) and a median BMI of 23.7 kgm^{-2} (range, 18.8 to 34.7) were enrolled in this study. One subject was excluded because of failure to comply with the passive mobilization protocols since he was not able to relax sufficiently during the measurements.

Experimental conditions

Ultrasound video sequences of the long finger FDP tendons were acquired using a Philips iE33 ultrasound system (Philips Electronics, Eindhoven, the Netherlands) with a 7 MHz linear array at 100 frames per second. The image resolution was 0.0166 mm/pixel.

The experimental conditions are illustrated in Figure 1. Subjects dominant forearm was immobilized in the supine position using Velcro straps. Forearms were fixed to the brace at forearm midpoint, just proximal of the wrist, and just proximal to the MCP joints. The wrist was positioned in 30° flexion, MCP joints in 60° flexion, and interphalangeal (IP) joints fully extended. Rubber bands were attached to the tips of all four fingers at the start of the experiments.

To localize the FDP and flexor digitorum superficialis (FDS) tendon with ultrasound we first identified a landmark close to the FDP and FDS tendon. In this case we palpated the FDP and FDS muscle, but another landmark such as the flexor carpi radialis is also suitable as starting point to identify the FDP and FDS tendon with ultrasound. After localizing the FDP and FDS muscle we move the probe along the muscle towards the FDP and FDS tendons. When both the FDP and FDS tendon were visualized, the distal interphalangeal (DIP) joint of each finger was flexed and extended separately by the investigator to determine which FDP and FDS tendon was visualized. The FDP tendon could then be identified based on more FDP excursion during DIP movement compared to the FDS. Moreover, the identification of the FDP tendon was confirmed by its position and its orientation, as the FDP commonly passes through the carpal tunnel at an angle while the FDS tendon passes through more horizontally.

METHODS

Motion protocols and finger positions

In this study we compared one active protocol, which served as reference, two passive protocols already used in a clinical setting, and two experimental passive models. The protocols and experimental models are depicted in Figure 1 and the order of execution was randomized to minimize possible learning effects.

In the Active Four-Finger Mobilization Protocol, subjects were asked to make a fist starting from full extension, which was limited by the splint, and moving to full flexion without

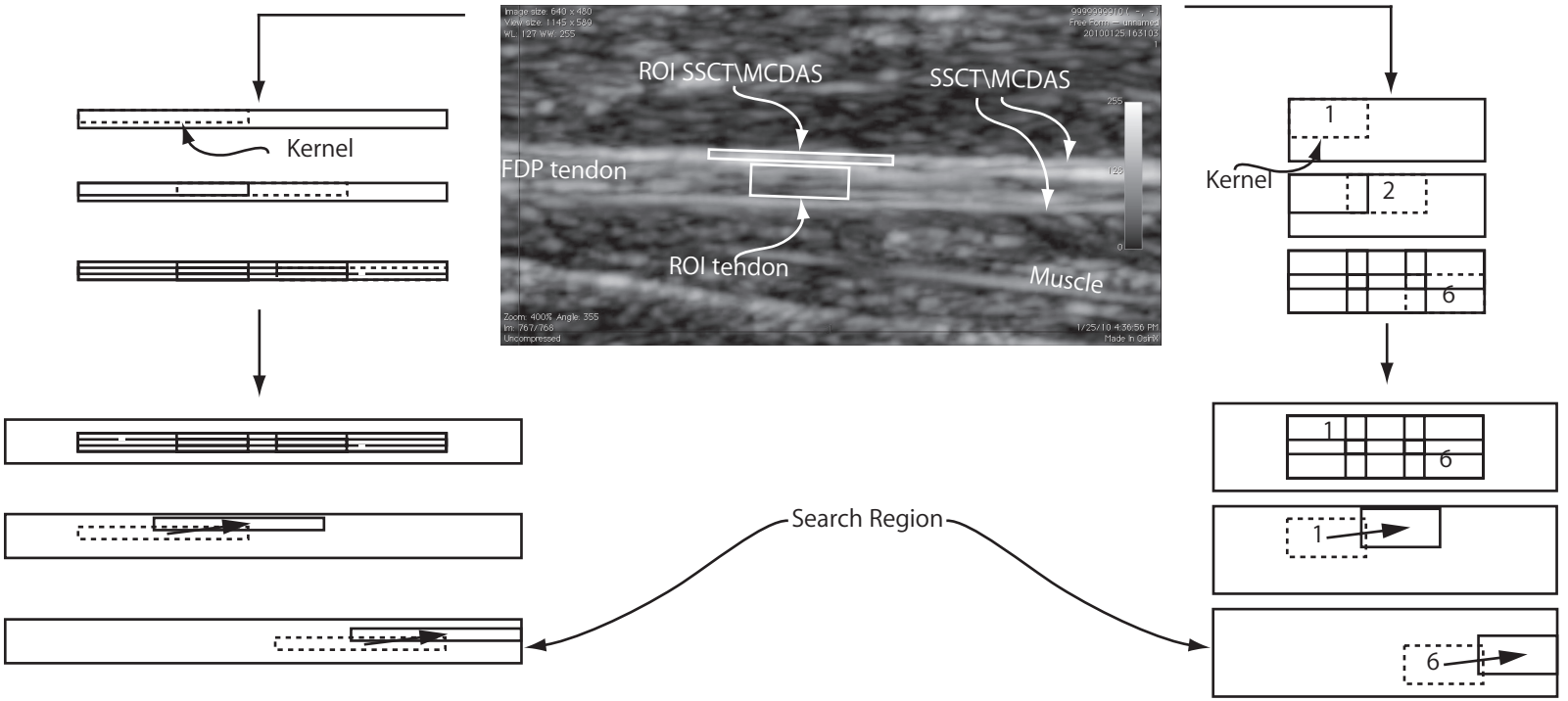

Figure 2. Flowchart of the speckle tracking algorithm to calculate excursions of the tendon and the SSCT\MCDAS. The upper part shows frame #1 of the ultrasound recording of the FDP tendon and its surrounding tissue, mostly referred to as either subsynovial connective tissue (SSCT) or multimicrovacuolar collagenous dynamic absorbing system (MCDAS). The two manually placed white rectangles are the regions of interest (ROI), which depict where the tendon and the SSCT are located. The user places both ROIs in the first frame; in the consecutive frames the ROIs are automatically updated. The second step in the algorithm is the automated placement of six kernels covering both ROIs. The size of the kernels for the tendon and SSCT\MCDAS are optimized based on the properties of the speckle pattern. The third step is that in the frame #2 a search region is defined for both ROIs. Within this search region the algorithm tries to find the pattern that best matches the pattern from the kernel. Matching is performed separately for all kernels for both ROIs. When displacements have been calculated for all kernels, the displacement vector of each kernel is multiplied by its corresponding normalization coefficient (NCC) and all weighted displacement vectors are averaged, resulting in a single displacement vector for both the tendon and the SSCT. For all consecutive frames the algorithm repeats itself, starting with the placement of both ROIs in frame #2.

squeezing at the endpoint. In the Passive Four-Finger Mobilization Protocol, the rubber bands of all four fingers were guided through a guiding system, placed in the palm of the subject, and attached to the splint[126,168]. Subjects were asked to fully extend their fingers followed by full relaxation, which resulted in passive flexion due to the attached rubber bands. They were specifically instructed not to actively flex any of the fingers.

In the Modified Kleinert Mobilization Protocol, the rubber band of the long finger was attached proximally on the splint while all other rubber bands were detached[101]. Again, subjects were asked to fully extend the long finger followed by full relaxation, which resulted in passive flexion due to the attached rubber band. Subjects were specifically instructed not to actively flex any of the fingers and leave the fingers without a rubber band, in a relaxed position. Passive movement of these three fingers was allowed.

In the experimental Modified Kleinert Flexion Mobilization Model, the three fingers were positioned in full flexion and fixed to the splint with Velcro straps. Subsequent steps were the same as for the Modified Kleinert Mobilization Protocol.

In the experimental Modified Kleinert Extension Mobilization Model, the three fingers were positioned in full extension and fixed to the splint with Velcro straps. Again, subsequent steps were the same as for the Modified Kleinert Mobilization Protocol.

Ultrasound imaging analyses

Ultrasound images were exported as uncompressed audio video interleave (.avi) files using OsiriX (Version 3.7.0; (http://www.osirix-viewer.com/). The uncompressed AVIs were then imported into Matlab (7.5, R2009a, the MathWorks Inc., Natick, MA) and analyzed with in-house developed tracking software that can be described as a "dedicated two-dimensional multi-kernel block-matching scheme using normalized cross-correlation (NCC)". The software has been extensively described and validated elsewhere[103,104] and can track tendons with a mean measurement error of 50mm over physiological tendon excursions and velocities. The algorithm is based on the general concept of block-matching schemes, which are frequently used to track cardiac wall movements[34,117,141].

Figure 2 shows the general concept of our software. The user first identifies a Region of Interest (ROI) in the first frame of the AVI. This region of interest is nothing more than a rectangle that describes the location of the tendon and therefore has to be placed on the tendon without capturing any other structure. Then the user identifies a second ROI in the first frame of the AVI, which has to be placed on the surrounding tissue instead of the tendon. The algorithm automatically places several overlapping kernels in the ROI. Kernels are small rectangular shaped blocks that capture a part of the speckle pattern of the structure. In our application, the kernel is a small part of the tendon with sufficient speckle patterns so that the algorithm can find a good match in the next frame. The algorithm searches for a best-matching speckle pattern in the next frame in an automatically defined search region. We avoid searching the entire image to reduce computational load. In the algorithm, each block in a particular frame is matched with a block in the next frame, hence the name block-matching algorithm. The goodness of the match is defined by the normalized cross-correlation measure (NCC), which ranges from 0 to 1. A 0 means that there was no match at all between a kernel and the speckle pattern captured within the search region, while a 1 means a full match. We use multiple kernels to increase accuracy, as more kernels allow for weighting the tendon excursions with the NCC outcome, thereby minimizing the contribution of possible outliers. Only matches with a NCC equal or larger than 0.7 were considered a good match, this lower bound is adopted from Farron et al.[49]

From the displacement estimates, we calculated absolute FDP tendon excursion, absolute surrounding tissue excursion, and FDP tendon excursion relative to its surrounding tissue, that is, the difference between absolute FDP tendon excursion and absolute movement of its surrounding tissue. We also calculated the excursion ratios, defined as the absolute surround-

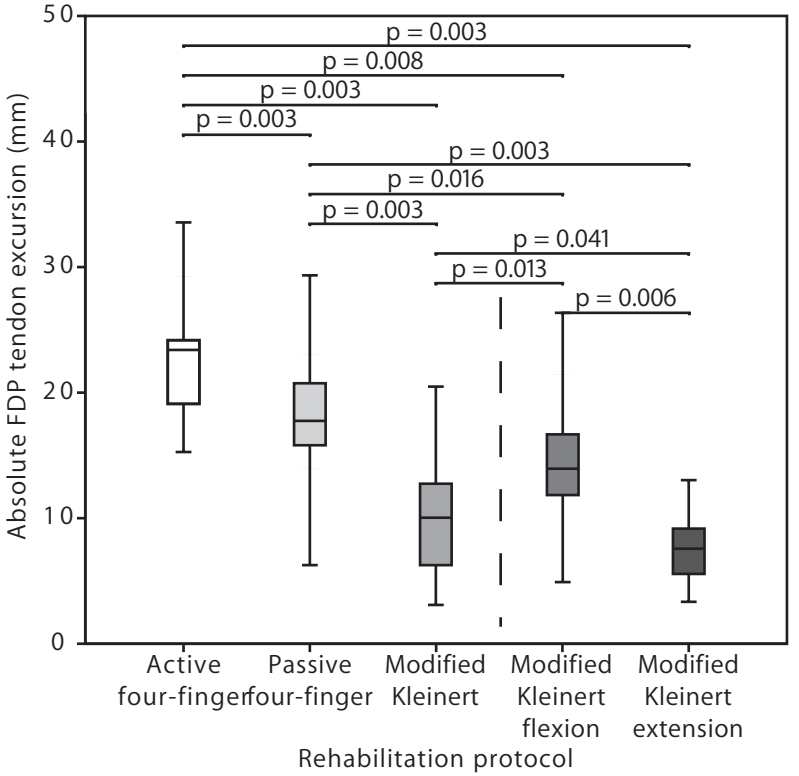

Figure 3. Boxplot of the absolute FDP tendon excursions for the three different mobilization protocols and two experimental mobilization models depicted as medians, inter-quartile ranges, and ranges. Excursions of all protocols were statistically significant.

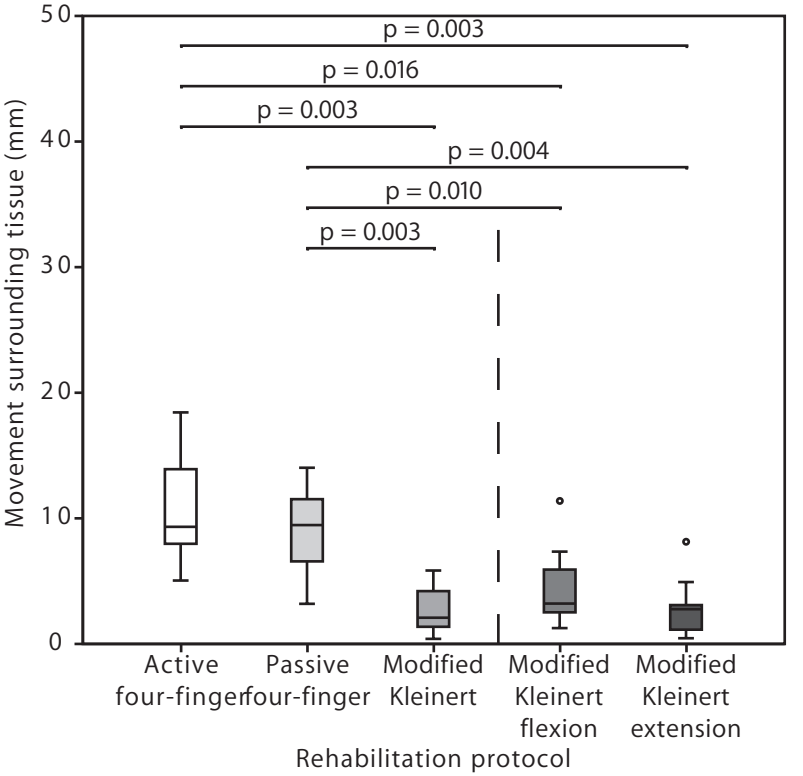

Figure 4. Boxplot of the excursion of the tissue surrounding the FDP tendon depicted as medians, inter-quartile ranges, and ranges. Both the active four-finger protocol and the passive four-finger protocol differed statistically significantly compared to the three modified Kleinert protocols.

ing tissue excursion divided by the absolute tendon excursion, categorized by single digit movement or full fist movement.

Statistical analyses

To perform a power analyses, we extracted excursion data from a study by Silfverskiold et al.[168], who reported a mean excursion for the Passive Four-Finger Mobilization Protocol of 11.9 mm (±4.1) and an excursion of 5.6 mm (±3.5) for the the Modified Kleinert Mobilization Protocol. Based on an effect size of 1.23, an α of 0.05 and a power (1-β) of 0.80, 6 subjects would be needed. Based on this, we decided to include 12 subjects in this study. We used the Wilcoxon signed rank test to evaluate differences in tendon excursions, surrounding tissue movement, and relative tendon excursions between the different protocols and experimental models. Statistical significance was set at $p<0.05$. All results were expressed as median and range.

METHODS

Table 1 shows the excursion ratios during full fist movement (protocol 1 and 2) and single digit movement (protocol 3, 4, and 5) found in this study and compared with findings from literature.

In the top two panels of Figure 1, the extreme positions of the different mobilization protocols and experimental models are depicted while the lower panel depicts the corresponding typical plots of absolute long finger FDP excursion, surrounding tissue excursion, and relative FDP excursion. The absolute excursions of long finger FDP tendon for different mobilization protocols and experimental models for all subjects are summarized in Figure 3. All comparisons between protocols and experimental models showed statistically significant differences in long finger FDP excursions ($p\leq0.041$). Excursions were largest during the Active Four-Finger Mobilization Protocol, followed by the Passive Four-Finger Mobilization Protocol. The excursions obtained during the experimental Modified Kleinert Flexion Mobilization Model were significantly larger than obtained during the Modified Kleinert Mobilization Protocol (p=0.013) and the experimental Modified Kleinert Extension Mobilization Model (p=0.041).

RESULTS

The movements of the tissue surrounding the long finger FDP tendon are depicted in Figure 4. Surrounding tissue excursions obtained during the Active Four-Finger Mobilization Protocol were significantly larger than during the Modified Kleinert Mobilization Protocol (p=0.003), the experimental Modified Kleinert Flexion Mobilization Model (p=0.016), and the experimental Modified Kleinert Extension Mobilization Model (p=0.003). Excursions obtained during the Passive Four-Finger Mobilization Protocol were significantly larger than obtained during the Modified Kleinert Mobilization Protocol (p=0.003), the experimental Modified Kleinert Flexion Mobilization Model (p=0.010), and the experimental Modified Kleinert Extension Mobilization Model (p=0.004)

The FDP tendon excursions relative to its surrounding tissue are depicted in Figure 5. Relative excursions during the experimental Modified Kleinert Flexion Mobilization Model did not differ significantly from the excursions obtained with the Active Four-Finger Mobilization Protocol (p=0.213). The same was found for the Passive Four-Finger Mobilization Protocol and the experimental Modified Kleinert Flexion Mobilization Model (p=0.374). However, excursions obtained during the Active Four-Finger Mobilization Protocol were significantly larger than obtained during the Passive Four-Finger Mobilization Protocol (p=0.013).

RESULTS

When comparing relative FDP tendon excursion with the suggested 5mm minimum excursion needed to prevent tendon adhesions, also depicted in Figure 5, only the Active Four-Finger Mobilization Protocol (p=0.003), the Passive Four-Finger Mobilization Protocol (p=0.021), and the experimental Modified Kleinert Flexion Mobilization Model (p=0.010) showed significantly larger excursions than this threshold. The excursions obtained during the Modified Kleinert Mobilization Protocol (p=0.050) and the experimental Modified Kleinert Extension Model (p=0.859) were not significantly larger than this threshold.

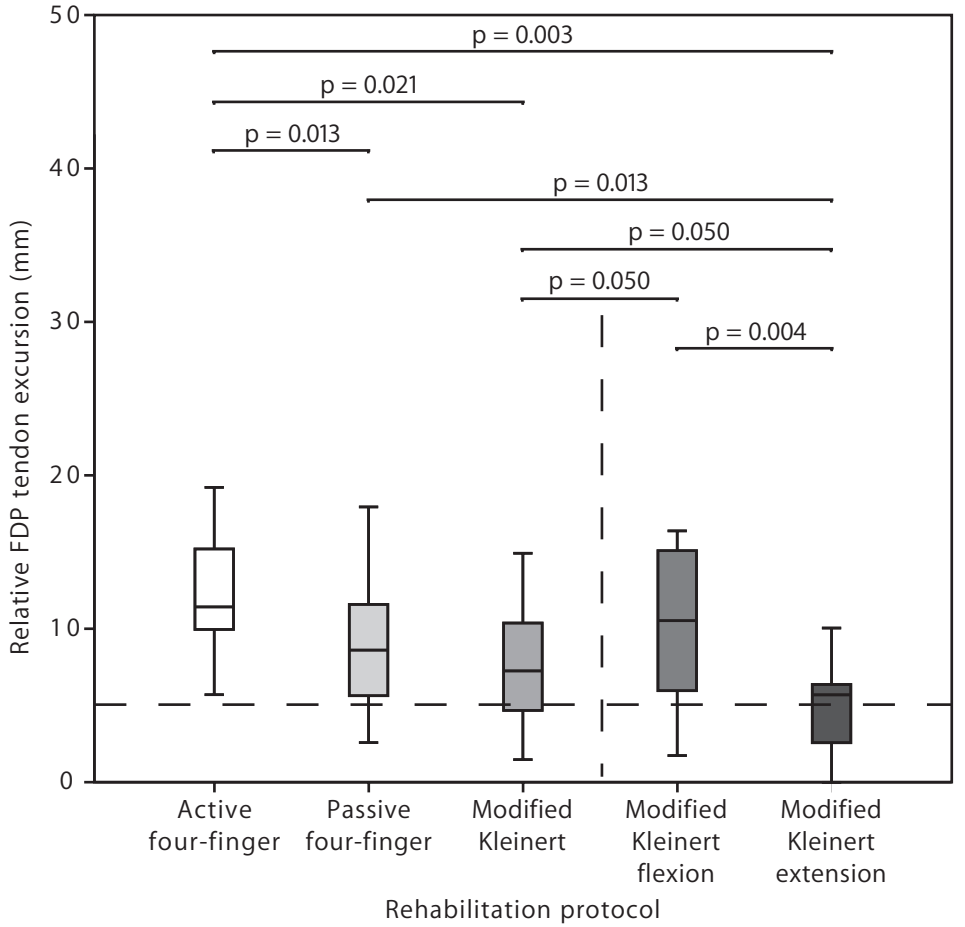

Figure 5. Boxplot of the relative FDP tendon excursions for the five different mobilization protocols depicted as medians, inter-quartile ranges, and ranges. The relative excursion is defined as the FDP excursion relative to its surrounding tissue. The dotted line is the minimum tendon excursion of 5mm, suggested by Duran and Houser (1975) to prevent tendon adhesions.

In the present study, we investigated, in-vivo, the influence of finger positions on the absolute tendon excursions, surrounding tissue excursions, and relative tendon excursions in 12 healthy subjects. We have shown that the different finger positions in the different mobilization protocols and experimental models have a large influence on the absolute and relative flexor tendon excursions. In terms of absolute flexor excursions, the Active Four-Finger Mobilization Protocol is favorable over the Passive Four-Finger Mobilization Protocol, which in turn is favorable over the Modified Kleinert Mobilization Protocol and the two experimental models. When looking at the movement of surrounding tissue, two groups can be distinguished: the Active and Passive Four-Finger Mobilization Protocols have relatively large surrounding tissue movements while in the Modified Kleinert Mobilization Protocol and the two experimental models these movements were relatively small. Consequently, the largest relative flexor tendon excursions (with respect to its surrounding tissue) were obtained during the Active Four-Finger Mobilization Protocol and potentially similar relative tendon excursions were obtained during the experimental Modified Kleinert Flexion Mobilization Model. The latter may be surprising since the Kleinert protocol is commonly thought to be inferior in terms of excursions. Furthermore, we found that excursions larger than 5mm were obtained only during the Active Four-Finger Mobilization Protocol, the Passive Four-Finger Mobilization Protocol, and the experimental Modified Kleinert Flexion Mobilization Model.

Only a few studies have reported tendon excursions relative to their surrounding tissue expressed as a ratio and mostly measured in cadavers (see Table 1). The ratios ranged from 0.10 to 0.44 during active movement, meaning that the surrounding tissue excursion was 10% to 44% of the tendon excursion. In the present study we have found ratios ranging from 0.22 to 0.53, which are comparable although somewhat larger than in the reported studies.

We also compared the ratios obtained during single digit motion and full fist motion from the present study with those in the literature. In the literature, the ratios during single digit motion (ranging from 0.10-0.18) are consistently smaller than during fist motion (0.25-0.30). In this study we also found smaller ratios during single digit motion (ranging from 0.22-0.32) than during full fist motion (0.45-0.53). In this comparison, we excluded the results reported by Horibe et al.[78] as they fully dissected the finger, thereby removing any interaction with the adjacent fingers. The somewhat higher ratios in the present study may result from different experimental conditions, most notably the in-vivo nature of our experiment compared to the cadaver measurements in previous studies, but also differences in the tendons under investigation.

The present study has a number of possible limitations. An important limitation is that we measured FDP tendon excursion in zone V, as at that point the FDP tendon runs almost completely longitudinally, minimizing measurement errors such as out-of-plane motion. For flexor tendon rehabilitation, it would be very valuable to obtain similar data from zone II, since zone II tendon repairs have a high incidence of adhesion formation[111]. Since the tendons are very stiff in the low loading levels applied in the present study, and since the joints between zone II and zone V were fixed, absolute tendon excursion in zone II will be highly comparable to zone V. However, this will not apply to the surrounding tissue. For example, Horibe et al.[78] showed significantly larger tendon sheath excursions more proximally around the tendon compared to distally in cadavers. The results of the relative excursion from zone V can therefore not be generalized towards zone II.

Another limitation is that we evaluated only healthy controls at this point. In patients after flexor tendon reconstruction, the surrounding tissue at the rupture site will be damaged in order to make the anastomosis. However, during rehabilitation most patients have a reasonable range of motion; therefore we can assume that the tendon and thus the anastomosis is able to exhibit excursions far beyond the damaged area of the surrounding tissue, thereby moving through the intact surrounding tissue. It could be argued

Table 1. Surrounding tissue-tendon excursion ratio

Study	Ratio		Active or Passive	FDP or FDS
	Single digit	Fist		
Ettema et al.[46]	0,16	0,3	Active	FDS
Yamaguchi et al.[214]	0,1	0,25	Active	FDS
Horibe et al.[78]	0,44	NA	Active	FDP
Yoshii et al.[219]	0,18	0,3	Active	FDS
This study				
Active Four-Finger	NA	0,45	Active	FDP
Passive Four-Finger	NA	0,53	Passive	FDP
Kleinert	0,22	NA	Passive	FDP
Kleinert in Flexion	0,23	NA	Passive	FDP
Kleinert in Extension	0,32	NA	Passive	FDP

FDS Flexor digitorum superficialis
FDP Flexor digitorum profundus
NA Not applicable

that in patients sutures can negatively influence tendon excursions and it is reasonable to assume that the sutures will affect excursions for all mobilization protocols. Nevertheless, several studies showed that even with sutures in place excursions are well within physiological range and are therefore likely to move far beyond the repair site and mostly through the normal surrounding tissue[167,168].

A third limitation is the relatively small sample size of 12 subjects (11 subjects after exclusion). Albeit small, the results convincingly showed statistically significant differences between different rehabilitation protocols used after tendon repair and the experimental models, while using the most conservative non-parametric statistical tests. This resulted from very consistent effects of the different protocols and experimental models in the different subjects. More importantly than enlarging the study population, we feel that it is important for future studies to evaluate if similar findings would be found in patients with flexor tendon injury where tendon gliding may be reduced and if similar findings would be found in different zones of the hand.

A more technical limitation might be that the accuracy of the speckle tracking approach depends on the kernel size. For the surrounding tissue, we used very thin and elongated kernels. Although the total area of the kernel for the surrounding tissue was smaller than for the tendon, we found similarly high normalized cross-correlations indicating that the surrounding tissue was tracked successfully[103,104].

It should be noted that the two extensions of the Modified Kleinert Mobilization Protocol were designed primarily to study the influence of the positions of the adjacent fingers on the tendon excursion. Therefore, the most important clinical message is to not only focus on the injured finger, but also on the adjacent fingers to optimize tendon excursion during rehabilitation. Especially the experimental Modified Kleinert Flexion Model seems promising due to the high excursion rates. While an a clinical situation, it may be uncomfortable for patients to maintain the this flexed position of the other fingers, this model may serve as a basis for more short-term mobilization exercises to increase excursion.

In addition, our findings may be especially important if extension of one of the adjacent fingers is needed due to, for example, a fracture needing a K-wire PIP-joint immobilization, wound problems with split skin grafts (SSG) or full thickness grafts (FTG), or immobilization after a central slip repair. Our findings indicate that in such a situation, the excursion of the tendons of the involved fingers will be reduced. This may require addition mobilization exercises. In addition, for these patients, in may be especially worthwhile to do practices with the other adjacent fingers in a flexed position.

In conclusion, this study demonstrates large and significant differences between the different rehabilitation protocols and experimental models in terms of absolute hand flexor tendon displacement, movement of surrounding tissue, and relative tendon displacement in healthy subjects. Our study clearly demonstrates the influence of the position of the adjacent fingers on the hand flexor tendon displacement of the finger that is mobilized. Therefore, clinicians should not only focus on the injured finger, but also on the adjacent fingers to optimize tendon excursion during rehabilitation.

Chapter 6
Reliability of Ultrasonographic Measurements of Median Nerve and Flexor Tendons

Anika Filius
Jan-Wiebe H. Korstanje
Yvette Hoendervangers
Ruud W. Selles
Steven E.R. Hovius
Harm. P. Slijper
Submitted

Ultrasound imaging is an increasingly used modality to investigate the median nerve in the carpal tunnel. However, the quality and interpretation of the ultrasound images is rater dependent. In this study we investigated the reliability of ultrasound for measuring shape and displacement parameters of the median nerve and flexor tendons in the carpal tunnel. Furthermore, reference values of shape and displacement parameters are reported. Both wrists of 20 persons without a history of wrist pathology were imaged. Ultrasound scans of the carpal tunnel were acquired during hand movement, starting from extension through flexion of all fingers ending with a forceful grip. Intra- and interrater intraclass correlation coefficients (ICC) were calculated based on measurements of 10 hands. If the ICC was higher than 0.5 the reference values were reported and alterations of the shape and displacement parameters described. For the shape parameters of the median nerve and the flexor digitorum superficialis (FDS) and flexor digitorum profundus (FDP) of both the index finger and the middle finger the interrater ICC was at least 0.51 but for most parameters higher. The ICC of the interrater displacement measurement of the median nerve and all flexor tendons was 0.68 or higher. The largest differences in shape and displacement parameters were found from extension 1 to forceful grip. The following changes were observed when going from extension to flexion and then to forceful gripping: 1) the median nerve flattened and moved ulnar, 2) the tendons became more circular, and 3) each FDS moved towards its corresponding FDP. Ultrasound imaging can reliable measure shape and displacement parameters of the median nerve and flexor tendons. The reported reference values can be used for comparison with measurements in patients with carpal tunnel syndrome or tendinopathies to identify if parameters differ between healthy persons and patients and if discriminating parameters can be distinguished.

Ultrasound is an increasingly used modality for diagnosing abnormalities of the median nerve in the carpal tunnel. Different studies have shown that due to compression of the median nerve the cross sectional area of the nerve increases and the shape of the nerve flattens. Ultrasound measurements of this cross sectional area are potentially sensitive measures for detecting carpal tunnel syndrome (CTS)[109,162].

A number of recent studies have suggested that ultrasound may not only be valuable for detecting changes in the cross sectional area of the median nerve, but also for measuring changes in shape and displacement of the nerve during flexion and extension movements of the hand[197,218]. Increasingly it is suggested that non-inflammatory fibrosis of the connective tissue in the carpal tunnel may play an important role in the development of CTS[45,47,74,142,182,194,222]. Therefore measuring shape and displacement could become diagnostic. The connective tissue between the tendons and the median nerve is called the subsynovial connective tissue (SSCT)[44]. In CTS patients, fibrosis and thickening of this tissue has been observed[44,145]. It has been hypothesized[48,116] that these changes in the properties of the SSCT might be the first step in developing CTS since it may restrict the ability of the nerve and tendons within the carpal tunnel to move, and therefore cause compression of the median nerve[99,100,194,211] by affecting the ability of the nerve to move out of the way of the hand flexor tendons during finger movement[2,134]. Measuring changes in shape and displacement of the nerve and flexor tendons in the carpal tunnel might therefore provide information about possible changes in the properties of the SSCT in CTS patients.

Although ultrasound measurements might provide a powerful tool for understanding the pathophysiology of CTS, the ultrasound image quality and thus the interpretation of the ultrasound images varies between raters[85]. While some studies have reported the measurements of shape and displacement of the nerve and tendons in transversal ultrasound images[197,218], to our knowledge, no study has been conducted of intrarater and interrater reliability of these measurements.

Therefore, in this study, our aim was to establish reliability of measuring shape (area, circularity and perimeter) and displacement parameters of the median nerve and the tendons in the left and right wrist of healthy volunteers using ultrasound. In addition, we will compare the measurements of shape and displacement in different hand postures, namely: 1) extension of the fingers, 2) flexion of the fingers, and 3) flexion of the fingers with forceful grip.

INTRODUCTION

Subjects

We recruited 20 asymptomatic volunteers (10 male and 10 female), with a mean age of 28 years (range 21-72). Subjects were excluded if they had any history of disease that could influence the study (e.g., history of traumatic injuries to the hand or forearm, carpal tunnel syndrome, trigger finger, etc). The local medical ethics committee approved this study and all subjects signed an informed consent.

Ultrasound recordings and measurement protocol

We acquired ultrasound recordings of the carpal tunnel using an Philips iU22 ultrasound system (Philips Electronics, Eindhoven, The Netherlands), equipped with a L12-5 scan head with a frequency band ranging from 5 to 12MHz. The following settings were used: all image enhancers on (Xres, SonoCT, and AGC) with exception of persistence which was turned off to minimize blurring during tendon and nerve displacement, power output was maximized for full penetration, and the pulse repetition frequency was set at high. The frame rate was fixed at 73Hz and the image resolution was 0.083 mm/pixel.

The subjects were seated with the arm positioned on a table. The elbow was flexed approximately 120° with the wrist and phalanges in a neutral position. The investigator placed the scan head at the wrist crease, which is the proximal part of the carpal tunnel,

METHODS

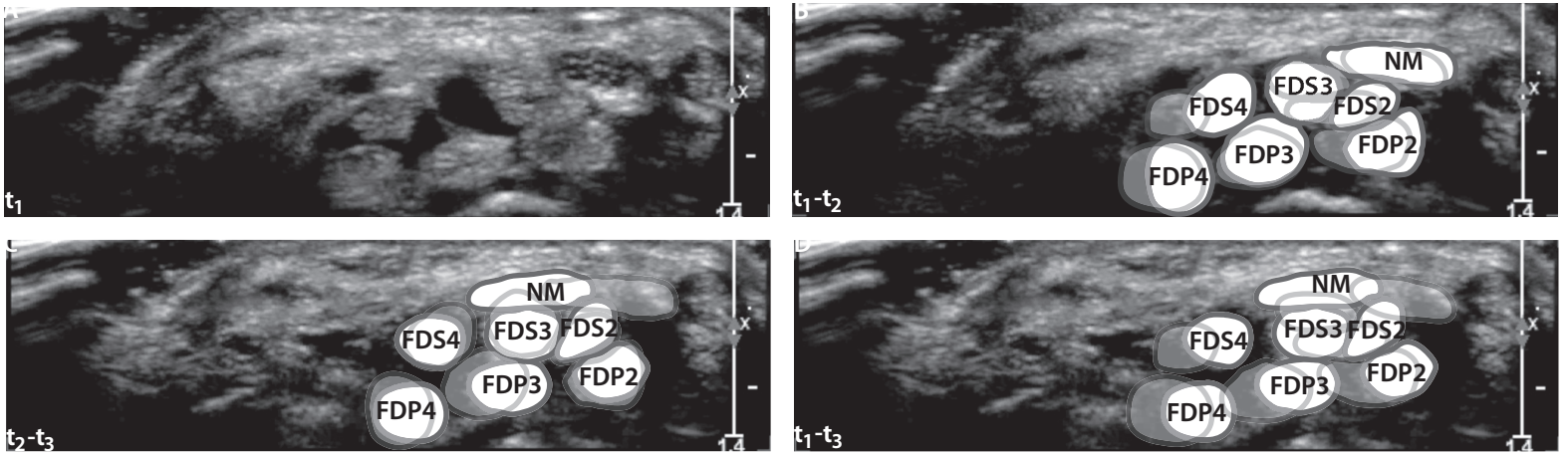

Figure 1. A. Cross-sectional sonography image of the carpal tunnel of the right wrist of a healthy person during extension of all fingers. Figure 1B, C, and D shows an illustration of the median nerve (MN) and the index finger's, middle finger's, and ring finger's flexor digitorum superficialis (FDS) and flexor digitorum profundus (FDP) of one subject during different hand positions. The shape and position of the nerve and flexor tendons during the initial hand posture are displayed in a transparent color and the shape and position of the nerve and tendons during the final hand postures are displayed in an opaque color. B. The initial hand posture is extension of all fingers and the final hand posture is flexion of all fingers. C. Full flexion of the fingers is compared to forceful grip. D. Full extension of the fingers is compared with the hand in a forceful grip.

and imaged the carpal tunnel in the transversal plane. The median nerve was then identified as a superficial hypoechogenic structure with small hyperechogenic speckles compared to the overall more hyperechogenic speckle structure of the tendons. After identification of the median nerve, we identified the flexor digitorum superficialis (FDS) tendon and the flexor digitorum profundus (FDP) tendon of the index finger, middle finger, and ring finger in the longitudinal and transversal plane. After identification an image of the carpal tunnel was stored on the scanner and each of the hand flexor tendons and the median nerve were outlined with an online annotation tool provided by the scanner software package. This ensured that during offline analysis each of the raters started of with the correct placement of each of the flexor tendons and median nerve.

Motion protocol

We made ultrasound scans of 10 seconds, always starting with the right followed by the left hand. Starting from extension of all fingers, subjects were asked to fully flex all fingers within 5 seconds without force and had to maintain this finger position for 2 seconds followed by a forceful grip for 3 seconds. The protocol was repeated for the left hand. Recordings were discarded if subjects did not follow instructions correctly or when the probe did not maintain full skin contact during the measurements due to the hand movements.

Image processing

We exported the ultrasound images as compressed audio-video interleave (AVI) files from the scanner using the MS-CRAM codec with a frame rate of 40Hz. For analysis we used an in-house developed image processing software package based on Matlab (7.10 R2010a; The MathWorks, Inc., Natick, MA). To identify the different structures and to calculate shape and displacement parameters, we manually placed polygons on the outside border of the median nerve and the six flexor tendons in the first frame of the AVI based on the image indicating each starting point made during the scans. Every polygon contained at least 15 nodes with a maximum of 25 nodes. All consecutive frames were analyzed similarly with a frame interval of 40 frames (corresponding to a frame rate of 1Hz) to minimize the computational load. This way, we placed polygons in 11 images during the flexion movement.

After identifying the first structure, the polygon was displayed as an overlay in the original AVI and a new AVI was created. The next step was to identify one of the other tendons in this new AVI including the prior overlay. This ensured minimal overlap between polygons of different structures in the same frame. All steps were repeated until all identifiable structures were analyzed. The resulting AVI thus contained seven overlays outlining the median nerve and the six flexor tendons (FDS and FDP of index finger, middle finger, and ring finger).

Shape and displacement parameters

From the polygons in the different AVI files, the following outcome measures were calculated: area, perimeter, circularity, centre of mass (CoM) and the transversal displacement of the median nerve and tendons. The shape parameter values were calculated for all finger at extension (frame 1), flexion (frame 6), and during forceful grip. For the forceful grip condition, we selected the frame where maximal displacement of the median nerve was seen compared to frame 6. To estimate the transversal displacement of the median nerve and flexor tendons two parameters were calculated: the endpoint displacement and the path displacement. To calculate the endpoint displacement, displacement between frame 1 and frame 6, and from frame 6 to the frame with the largest displacement after frame 6 were calculated. To calculate the path displacement, the displacements between all consecutive frames were used (frame 1 to 11).

Area was calculated based on the number of pixels within the polygon. Perimeter was calculated as the total length of the line segments of the polygon. Circularity was defined as:

$$\text{circularity} = \frac{\text{perimeter}^2}{4\pi \cdot \text{area}} \qquad \text{(Eq.1)}$$

Table 1. The intrarater intraclass correlation coefficients (ICC) with 95% confidence interval (CI) of the measurements of the different parameters of the median nerve (MN) and the index finger's and middle finger's flexor digitorum superficialis (FDS) and flexor digitorum profundus (FDP).

Intrarater reliability	NM	FDS2	FDP2	FDS3	FDP3
	ICC (95% CI)	ICC (95% CI)	ICC (95% CI)	ICC (95% CI)	ICC (95% CI)
Area	0.75 (0.28-0.93)	0.87 (0.56-0.97)	0.72 (0.15-0.93)	0.64 (0.04-0.90)	0.77 (0.28-0.94)
Circularity	0.77 (0.36-0.94)	0.94 (0.80-0.99)	0.86 (0.55-0.96)	0.89 (0.62-0.97)	0.71 (0.23-0.92)
Perimeter	0.87 (0.54-0.97)	0.80 (0.31-0.95)	0.71 (0.21-0.2)	0.97 (0.89-0.99)	0.78 (0.33-0.94)
Center of Mass x-coordinate	0.98 (0.64-0.97)	0.96 (0.85-0.99)	0.99 (0.98-1.00)	0.97 (0.94-0.99)	0.89 (0.57-0.98)
Center of Mass y-coordinate	0.99 (0.94-1.00)	0.89 (0.64-0.97)	0.99 (0.97-1.00)	0.99 (0.94-1.00)	0.97 (0.84-0.99)
Endpoint displacement	0.91 (0.69-0.98)	0.85 (0.42-0.97)	0.65 (0.00-0.93)	0.82 (0.34-0.96)	0.24 (-0.21-0.79)
Path displacement	0.96 (0.85-0.99)	0.99 (0.96-1.00)	0.92 (0.72-0.98)	0.94 (0.79-0.98)	0.95 (0.82-0.99)

Table 2. The interrater correlation coefficients ICC with 95% confidence interval CI of the measurements of the different parameters of the median nerve (MN) and the index finger's and middle finger's flexor digitorum superficialis (FDS) and flexor digitorum profundus (FDP).

Interrater reliability	NM	FDS2	FDP2	FDS3	FDP3
	ICC (95% CI)	ICC (95% CI)	ICC (95% CI)	ICC (95% CI)	ICC (95% CI)
Area	0.75 (0.29-0.93)	0.64 (0.05-0.90)	0.65 (0.12-0.90)	0.51 (-0.18-0.86)	0.26 (-0.44-0.75)
Circularity	0.58 (-0.08-0.88)	0.84 (0.49-0.96)	0.90 (0.48-0.98)	0.83 (0.47-0.96)	-0.17 (-0.82-0.52)
Perimeter	0.83 (0.48-0.95)	0.94 (0.79-0.99)	0.85 (0.54-0.96)	0.88 (0.60-0.97)	0.41 (-0.30-0.82)
Center of Mass x-coordinate	0.94 (0.79-0.99)	0.90 (0.65-0.97)	0.86 (0.52-0.97)	0.92 (0.73-0.98)	0.95 (0.77-0.99)
Center of Mass y-coordinate	1.00 (0.98-1.00)	0.99 (0.95-1.00)	1.00 (0.99-1.00)	0.97 (0.73-0.99)	0.95 (0.77-0.99)
Endpoint displacement	0.96 (0.83-0.99)	0.87 (0.55-0.97)	0.86 (0.27-0.98)	0.71 (0.14-0.93)	0.97 (0.36-1.00)
Path displacement	0.98 (0.90-0.99)	0.99 (0.95-1.00)	0.89 (0.61-0.97)	0.98 (0.93-1.00)	0.92 (0.73-0.98)

A circularity of 1 indicates a perfect circle, while a circularity larger than 1 indicates a deviation from a circle, such as a more ellipsoid shape or a more irregular pattern.

Displacement was calculated based on the displacement of the CoM, which was defined as the gravitational point of the polygon in terms of an x-coordinate (radial-ulnar axis) and y-coordinate (palmar-dorsal axis). The endpoint displacement vector between frame n and frame p was defined as:

$$\vec{d}_{endpoint,n,p} = \sqrt{(x_p - x_n)^2 + (y_p - y_n)^2} \qquad \text{(Eq.2)}$$

Where n and p are the different frame numbers at the start and endpoints (1 to 6 and 6 to maximum displacement frame) and x and y are the corresponding coordinates of the CoM. To calculate the path displacement, Δx_p in Eq. 2 was substituted by x_{n-1} and all separate vectors were summated:

$$\vec{d}_{path,n} = \sum_{1}^{n-1} \sqrt{(x_{n-1} - x_n)^2 + (y_{n-1} - y_n)^2} \qquad \text{(Eq.3)}$$

Since the path displacement includes displacements across a larger number of frames, the path displacement is by definition larger than the endpoint displacement.

Statistical Analysis

To determine the intrarater reliability the first rater analyzed the AVI files of the right hand of ten subjects twice in a randomized order with an interval of at least one day. To determine the interrater reliability, a second rater analyzed the same AVI files for the right hand of the same ten subjects, again in a randomized order and blinded for the results of the first rater. From these data, we calculated for both the intra- and the interrater reliability the intraclass correlation coefficients (ICC) using a two-way random effect model with single measure and absolute agreement. All dynamic parameters (area, circumference, circularity, and displacements) used for the ICC calculations were taken from extension to flexion using a forceful fist.

We calculated reference values for all parameters except if the intrarater or interrater ICC of a specific variable for a specific tendon or nerve was below 0.5. A repeated measure ANOVA with 2 within factors (hand posture and side) was used to determine significant differences between the reference values of the different parameters in the three different hand postures and between the left and right hand. Post hoc tests with Bonferroni correction were used to evaluate differences between hand postures. An alpha of less than 0.05 was deemed significant.

Intrarater reliability

The intrarater reliability of the measurements of the different parameters is shown in Table 1. Overall there was a moderate to excellent intrarater reliability (ICC≥0.64) for area, circularity and perimeter of the median nerve and all tendons. The ICC for CoMx was excellent (ICC≥0.89) for all tendons and the median nerve, while the CoMy was poor to excellent (0.24≤ICC≤0.89). The ICC of the endpoint displacement was excellent (ICC≥0.85) for all tendons and the median nerve except for the index and middle finger FDP (ICC <0.6). The ICC for the path displacement was excellent (ICC≥0.92) for all tendons and the median nerve. The ICCs for the ring finger FDS and FDP were poor (p<0.5) and therefore excluded from further analysis.

Interrater reliability

The results of the interrater reliability analysis are shown in Table 2. The reliability declined only slightly for interrater measurements as compared to the intrarater reliability, with an exception for the CoMx and the endpoint displacement, where the ICCs increased. The ICCs for area of the median nerve and for the FDS and FDP of the index finger and the FDS of the middle finger were moderate (ICC≥0.51). For circularity the ICCs of these structures were higher (ICC≥0.58) compared to the ICCs for area. The ICCs for perimeter were excellent (ICC≥0.83). Most of the ICCs of the shape parameters of the middle finger FDP were poor (ICC<0.5) and therefore excluded from further analy-

Table 3. Shown are the reference values of the median nerve (MN) and the index finger's and middle finger's flexor digitorum superficialis (FDS) and flexor digitorum profundus (FDP) in healthy persons (N=20, 40 wrists) with standard deviation during three hand postures: extension of all fingers, during flexion of all fingers, and during forceful grip. No significant difference was found for area, circularity, and perimeter between the left and right hand for the MN and tendons, except for circularity of the FDS2. Averages of left and right hand are therefore not shown. Significant differences ($p<0.05$) between the reference values of extension and flexion of all fingers and between extension and flexion with forceful grip are indicated with an asterisk (*).

	Area (mm²)			Circularity			Perimeter (mm)		
	extension	flexion	forceful grip	extension	flexion	forceful grip	extension	flexion	forceful grip
NM	9.99 (2.47)	9.74 (2.91)	9.96 (2.86)	1.85 (0.39)	1.96 (0.28)	2.10 (0.43)*	15.00 (2.25)	15.16 (2.19)	15.9 (2.81)*
FDS2	9.20 (2.20)	9.60 (1.96)	9.16 (1.91)	2.00 (0.54)	1.53 (0.34)*	1.35 (0.24)*	15.00 (2.14)	13.42 (1.98)*	12.34 (1.65)*
FDP2	11.65 (2.92)	12.42 (1.93)	11.89 (2.09)	1.65 (0.32)	1.43 (0.23)	1.41 (0.24)*	15.31 (2.01)	14.67 (1.44)	14.31 (1.69)
FDS3	10.63 (2.63)	11.55 (3.02)	12.29 (3.08)	1.82 (0.54)	1.47 (0.20)	1.36 (0.15)*	15.27 (2.48)	14.48 (1.97)	14.33 (1.87)

Table 4. Shown are the displacement reference values of the median nerve (MN) and the index finger's and middle finger's flexor digitorum superficialis (FDS) and flexor digitorum profundus (FDP) in healthy persons (N=20, 40 wrists) with standard deviation. No significant difference was found between the left and right hand for the MN and the flexor tendons; averages across both hands are therefore shown. The first column shows the displacement values of the structure from extension to flexion of all fingers and the second column from extension to forceful grip. The path displacement is significantly larger ($p<0.001$) than the endpoint displacement for the median nerve and the flexor tendons.

	Path Displacement (mm)			Endpoint Displacement (mm)		
	Extension → flexion	Extension → forceful grip	p-value	Extension → flexion	Extension → forceful grip	p-value
NM	2.56 (1.66)	8.00 (3.72)	<0.001	2.08 (1.94)	5.49 (4.01)	<0.001
FDS2	2.02 (0.72)	5.69 (2.37)	<0.001	1.28 (0.77)	2.68 (1.85)	<0.001
FDP2	2.35 (1.31)	6.06 (2.42)	<0.001	1.39 (0.99)	2.94 (2.09)	<0.001
FDS3	2.45 (1.35)	7.28 (2.98)	<0.001	2.18 (1.65)	3.73 (2.32)	0.011
FDP3	2.48 (0.81)	6.46 (2.00)	<0.001	1.36 (0.86)	2.59 (1.65)	<0.001

sis. Overall, the reliability of CoM and displacement of the median nerve and all tendons were excellent (ICC≥0.86), except for ICC of the endpoint displacement of the middle finger FDP (ICC=0.71).

Changes in shape and displacement in the carpal tunnel

In Figure 1, the median nerve and tendons are outlined in the ultrasound image of the carpal tunnel of one of the subjects during the three different hand postures. The figure shows that from extension to flexion the median nerve flattened and moved ulnar, although the position of the nerve remained close to the index finger FDS. The FDS and FDP of the index finger and FDS of the middle finger became more round (circularity closer to 1). Also each FDS moved toward its corresponding FDP, in other words the index finger FDS moved toward, but more palmar to, the index finger FDP, and the middle finger FDS toward the middle finger FDP. From flexion to forceful grip the median nerve moved further ulnar, towards the middle finger FDS.

Reference values: shape

Differences in the shape parameters between the left and right hand were small and did not reach significance. Presented data are therefore shown as averages across the left and right hand. Table 3 shows the reference values of the area, circularity, and perimeter of the median nerve and flexor tendons at the carpal tunnel.

Going from extension to flexion using a forceful grip, the circularity of the median nerve increased with 14%, indicating a less-circular nerve, while the perimeter increased by 6%. The tendons showed an opposite trend; the tendons became on average 25% more circular from extension to flexion using a forceful grip while the perimeter decreased by 11 % on average. This pattern was supported by significant differences in all tendons, except by the change in perimeter in the index finger FDP and middle finger FDS, which did not reach significance ($0.05<p<0.1$).

Reference values: displacement

The displacement parameters between the left and right side were non-significant, except for the right middle finger FDS, which had a significantly lower endpoint displacement. However, this significance disappeared when excluding a single outlier. Therefore, we averaged all displacement reference values over the left and right hand. Table 4 shows the endpoint and path displacements of the median nerve and tendons. The largest path displacement was seen in the median nerve; the path displacement from extension to flexion using a forceful grip was 213% larger ($p<0.001$) than the displacement from extension to flexion. The endpoint displacement of the median nerve from extension to flexion using a forceful grip was 164% ($p<0.001$) larger than the displacement from extension to flexion. The tendons showed, on average, a significant increase of 74% in endpoint displacement ($p\leq0.011$) and a significant increase of 96% in path displacement ($p<0.001$) from extension to flexion using a forceful grip compared to extension to flexion.

RESULTS

Although high-resolution ultrasound allows precise imaging of the carpal tunnel, image quality and therefore the interpretation of the images are rater dependent[85]. While previous studies focused on the reliability of measuring cross sectional area [132,211], in this study, we determined the intrarater and interrater reliability of measurements of the shape and displacement of the median nerve and tendons in de carpal tunnel. In addition, unlike most previous studies[132,197,211], we have not only performed analysis on one static ultrasound image, but also on a series of images (dynamic measurement); for the calculation of transversal displacements we used a series of images taken during hand movement, starting from extension through flexion of all fingers, ending with a forceful grip.

Overall, we found that we were able to reliably measure the parameters of shape of the median nerve, FDS and FDP for the index and the FDS of the middle finger and the displacement parameters of the median nerve and all flexor tendons in these healthy controls. Based on these reliability analyses, we established reference

DISCUSSION

Table 5. The ICCs of different shape parameters of the median nerve reported in ultrasound studies. The reliability values are shown in parentheses. Note: apart from the index finger flexor digitorum superficialis (FDS), no reliability values of parameters of the FDS or the flexor digitorum profundus (FDP) in the carpal tunnel were found. Therefore, reliability tests of the tendons are not shown. N = Number of patients.

Parameter	Intrarater reliability	Interrater reliability	Test-retest reliability
Area	(0.75)[d]	(0.87)[a], (0.81)[b], (0.75)[d]	(>0.75)[c]
Circularity	(0.77)[d]	(0.58)[d]	(>0.75)[c]
Perimeter	(0.87)[d]	(0.83)[d]	(>0.75)[c]
Displacement	(0.98)[d]	(0.89)[d]	(>0.75)[c]

[a] Wong et al. (N = 8)
[b] Moran et al. (N = 20)
[c] Doesburg et al. (N = 30)
[d] This study

values of shape and displacement parameters during the three different hand postures. The largest changes in shape and displacement were observed between extension to flexion using a forceful grip. No differences were found between the left and right hand. For the different tendons and nerves, we found that the total path displacement was, on average, two to three times larger than the displacement between the initial and end point, indicating that the structures do not move in a straight line. This indicates that measurement of only two positions, as done in previous studies, largely underestimates the actual displacement between these positions.

The intrarater and interrater ICCs of the shape parameters of the median nerve and index finger FDS reported in other studies are similar or slightly higher than our ICCs (see Table 5). For the area of the median nerve we found an ICC of 0.75, which is slightly lower than the ICCs reported by Wong et al. and Moran et al. (ICC>0.81)[132,211]. Doesburg et al. found the ICCs for area, circularity, perimeter, and displacement of the median nerve, the flexor pollicis longus, and index finger FDS to be 0.75 or higher[197], similar to the ICC's that we reported. Reliability of the other parameters evaluated in this study, to our knowledge, have not been previously reported.

The ICC for the middle finger FDP and the ring finger FDS and FDP was lower when compared to the median nerve and FDS and FDP of the index finger and FDS of the middle finger. This may be due to the oval form of the wrist and the radial position of the median nerve, making it sometimes difficult to maintain full skin contact with the more ulnar part of the wrist and decreasing the image quality. Despite of this, the ICC of the CoM displacement for these flexor tendons still had good to excellent reliability.

In this study we used cut-off values of ICC>0.50 for reliability to decide if reference values would be reported. Fleiss reported that the ICC<0.40 represents poor reliability, the ICC 0.40-0.75 represents fair reliability and above 0.75 represents excellent reliability[53]. Many other studies used these same cut-off values[41,131,151]. While most ultrasound studies on the carpal tunnel only reported their lowest ICC values[197] or calculated only one ICC[132,211,] we report exact ICC-values of all nerve and tendon parameters so that researchers can choose their own cut-off values.

A limitation of our study is that we focused only on the proximal part of the carpal tunnel, since more distal parts were not accessible with the scan head during movement and therefore no ultrasound measurements for reliability calculations could be made. Especially during flexion with forceful grip the palm of the hand deforms, which makes full skin contact difficult. In addition, previous studies have shown that ultrasound measurements of the distal carpal tunnel were less reliable compared to more proximal measurements. Furthermore, it should be noted that we included healthy subjects and not patients. Based on our experience, the difference in the image quality between healthy subjects and CTS patients is generally small. However, future studies should indicate whether the reliability of ultrasound measurements is similar in CTS patients and patients with tendinopathies. A further limitation is that we report relative displacements of the median nerve and tendons instead of absolute displacements. The reason for using relative displacement is to eliminate any scan head motion, which leads to motion of the entire ultrasound image. Although some studies use a fixating frame [197,218], in our experience, motion of the hand in relation to the scan head is difficult to prevent during dynamic conditions such as in this study, even when using such a frame. Analyzing nerve and tendon movement relative to the FDP of the middle finger or a stationary landmark is therefore a feasible alternative. The last limitation we would like to mention is that we calculated the ICC over a limited set of 10 hands. Although values for most parameters and structures were high (ICC>0.75), in small datasets one aberrant measurement can have a relative great effect on the ICC. However, there is a clear overall tendency of all measurements having a sufficient reliability.

We found significantly larger displacements and changes in

shape parameters in the condition in which the hand is fully flexed with a forceful grip as compared to the flexed position. This suggest that this condition may be more suitable for detecting differences between patients and controls, also because this condition may mimic daily life activities of the hand more closely and because CTS is often associated with labour involving higher forces[184,198].

While not all variables used in this study were reported earlier, our references values are largely in line with the literature. For example, the area of the median nerve found in the present study 9,99 mm² is comparable to Yoshii et al. and Doesburg et al., who reported areas of respectively 9,78 and 9,89 mm²[197,218]. Kamolz et al. reported lower values of the area and perimeter, though they performed ultrasounds in cadaver hands[92]. Sarria et al. found that the area of median nerve was 10.41 mm²[162]. However, rather than outlining the median nerve they calculated the area based on an ellipse of the maximum and minimum cross-section.

In this study we found that circularity was most influenced by different hand postures, while the perimeter was less influenced by this and the cross sectional area was not affected by hand postures. The perimeter increased when the median nerve became less circular and decreased when the tendons became more circular. This is consistent with the findings of Yoshi et al. and Doesburg et al.[197,218].

In conclusion, alterations in shape parameters of the median nerve and the flexor tendons can be reliably measured for the median nerve and the FDP and FDS of the index finger and the FDS of the middle finger. Displacements can be reliably measured for the median nerve and all the flexor tendons in the carpal tunnel. We found that displacements and shape changes are most pronounced when moving the fingers from extension of all fingers to flexion with a forceful grip. The comprehensive dataset of reference values can be used for evaluating possible changes in the displacement and or shape of the median nerve and tendons in CTS patients and patients with tendon pathology.

Chapter 7

Ultrasonographic Assessment of Transversal Tendon and Nerve Dynamics in CTS Patients Versus Healthy Controls

Jan-Wiebe H. Korstanje
Richard van Balen
Marjan Scheltens-de Boer
Joleen H. Blok
Harm P. Slijper
Henk J. Stam
Steven E.R. Hovius
Ruud W. Selles
Submitted

The objective of this study was to improve ultrasound assessment of carpal tunnel syndrome (CTS) by: 1) normalizing data, 2) using forceful gripping of the hand instead of full extension of the hand, and 3) using hand flexor tendon data alongside median nerve data. In a case-control study (51 cases, 25 controls) we evaluated the performance gained by comparing different logistic regression models using LASSO variable selection. Normalizing ultrasound variables increased the correct classification rate with 6%, using forceful gripping instead of full extension resulted in an increase of 3%, and using the hand flexor tendon resulted in an increase of 2%. The best predictive model combines normalization of the median nerve and the hand flexor tendons measured during both full extension and forceful gripping. However, the clinically most practical model only includes the normalized area of the median nerve measured during full extension.

Carpal tunnel syndrome (CTS) is the most common entrapment neuropathy with an estimated prevalence of 3.8%[9]. Symptoms associated with CTS are pain, numbness, and weakness in the median nerve distribution[164,177]. These symptoms can lead to loss of function in an advanced stadium[164]. The combination of a high prevalence and reduced function of the hand makes that CTS has a severe socioeconomic burden[50,94,112].

CTS is commonly diagnosed using clinical symptoms, supported by nerve conduction studies such as electromyography (EMG)[176]. Downside of EMG is that it misses up to 25% of patients suffering from CTS[8,90,164,210]. Therefore, EMG is not considered to be the gold standard[66,68,97] and alternative diagnostic tools have been investigated[8,54].

Multiple studies showed that ultrasound imaging might be an alternative diagnostic approach for CTS[109,162]. Various measures extracted from the transversal plane of the carpal tunnel have been proposed, e.g. the cross-sectional area of the median nerve (MN), the flattening ratio of the MN, and the ratio of the cross-sectional area of the MN measured proximal and distal of the carpal tunnel[37,99,109,197,211,218]. The cross-sectional area of the MN at the proximal part of the carpal tunnel is considered the best predicting measure to diagnose CTS. However, sensitivity (57-94%) and specificity (51-98%) varied largely between studies and a combination of a high sensitivity and high specificity have never been reported[54]. Since the cross-sectional area is only measured optimally when the recordings are consistently made under the same angle between the scan head and the wrist, the large variability in sensitivity and specificity might partly be explained by the variation in this angle during different recordings.

Several studies suggested that CTS patients may have altered properties of the MN shape due to changes in the subsynovial connective tissue (SSCT). The SSCT surrounds and interconnects the median nerve and hand flexor tendons. It is suggested that CTS patients develop fibrosis of the SSCT, thereby stiffening the interconnection between the MN and the hand flexor tendons[44,47,74,142,145,182,194,222]. These changes might therefore restrict movement of the median nerve and the hand flexor tendons within the carpal tunnel. The MN may therefore be at risk for compression as it might not be able to move freely in the carpal tunnel during finger movement; since the hand flexor tendons might impinge the MN[2,135,197].

The purpose of this study was to investigate the added value of assessing hand flexor tendons besides the MN to diagnose CTS as well as to determine if normalization of the MN area might decrease variability and thus increase sensitivity and specificity. To do so we made ultrasound recordings of the transversal plane of the carpal tunnel. Subsequently we used logistic regression classification models to compare performance when 1) using the area of the MN normalized to the area of the carpal tunnel instead of the non-normalized area of the MN, 2) using the normalized ultrasound variables measured during forceful gripping of the hand instead of the normalized ultrasound variables measured during full extension of the hand, 3) using all normalized ultrasound variables, including the flexor tendons of the index finger and middle finger.

INTRODUCTION

Population

A total of 51 patients were enrolled in this study, which were referred to our university medical center suspected of having CTS. Patients were excluded if they were younger than 18 years of age or had a diagnosed ulnaropathy (n=1). After exclusion, 50 patients (13 males and 37 females), with a mean age of 50.5 years (SD 13.1) were enrolled in the study. Data for the control subjects were obtained from a previous study. In summary, control subjects were randomly recruited from the employees of our university medical center. We included 25 asymptomatic controls (10 male and 15 female), with a mean age of 33.2 years (SD 13.8). Controls were excluded if they had a medical history that could interfere with the study (CTS, trigger finger, auto-immune

METHODS

Table 1. Population characteristics

		Cases	Controls	P
No of subjects		50	25	
Males		13/50 (26%)	10/25 (40%)	0.215*
Age group (years)	<20	1(2%)	0	
	20-39	7 (14%)	19 (79%)	
	40-59	30 (60%)	2 (8%)	
	60-79	12 (24%)	3 (13%)	
	≥80	0	0	
	Average age (S.D.)	50.6 (13)	33.4 (14)	<0.001†‡
BMI	<18,5	0	1 (4%)	
	18,5-24,9	14 (30%)	16 (67%)	
	25-29,9	16 (35%)	5 (21%)	
	30-34,9	10 (22%)	2 (8%)	
	35-39,9	4 (9%)	0	
	≥40	2 (4%)	0	
	Average BMI (S.D.)	28.9 (6)	23.4 (4)	<0.001†‡
EMG score	No CTS	48/98 (49%)		
	Possibly CTS	9/98 (9%)		
	Mild CTS	27/98 (27%)		
	Moderate CTS	6/98 (6%)		
	Severe CTS	8/98 (8%)		
Clinical symptoms	No CTS	23/99 (23%)		
	Possibly CTS	45/99 (45%)		
	Probably CTS	23/99 (23%)		
	CTS	8/99 (8%)		

* Chi^2-test, † Mann Whitney U-test, ‡ Independent Student's T-test

disease, pregnancy, infection, fracture, surgery, or deformation of the hand or forearm). Our medical ethics committee approved this study and informed consent was obtained from each participant.

Experimental conditions

Each patient underwent a full clinical examination and EMG by an experienced neurologist and filled out the Boston Carpal Tunnel Questionnaire (BCTQ)[113]. Nerve conduction studies were performed using standard clinical protocols on a Viking Select EMG machine (CareFusion, San Diego, CA) using ring electrodes for recording sensible nerve action potentials (SNAPs) and surface electrodes for recording of compound muscle action potentials (CMAPs) from the abductor pollicis brevis muscle. From the antidromically elicited SNAPs, the distal sensory latency (DSL) was determined automatically by the system and compared between nerves or nerve segments in the following ways: 1) Comparison of the DSL of the median and ulnar nerves between wrist and ring finger, 2) Comparison of the DSL of the median nerve between wrist and palm versus palm and the third finger, and 3) Comparison of the DSL of the median and radial nerve between wrist and thumb. During all measurements electrode distances were kept equal between nerve segments. If necessary, also the distal motor latency (DML) of the median nerve to the abductor pollicis brevis muscle was determined.

If the latency difference of the first test equaled or exceeded 0.5 ms, the EMG was considered positive for CTS. If this difference was smaller than 0.5 ms, the two additional sensory tests were performed. These were considered abnormal if the respective latency differences were ≥ 0.5 ms and CTS was confirmed if both were positive. If SNAPs could not be evoked, the median distal motor latency (DML) to the abductor pollicis brevis muscle was measured. This DML was considered abnormal if it exceeded the age and gender dependent normal value (between 4.4 and 4.7 ms)[22].

Ultrasound imaging

Images of the carpal tunnel were acquired using a Philips iU22 ultrasound system (Philips Electronics, Eindhoven, The Netherlands). The ultrasound system was equipped with a L12-5 scan head with a frequency band ranging from 5 to 12MHz. All subjects were imaged using the same settings profile. The US settings were as follows: all image enhancers were enabled (Xres, SonoCT, and AGC) with the exception of persistence. The latter was disabled to minimize blurring during movement of the structures in the carpal tunnel. Pulse repetition was set at high and the power output was maximized in order to achieve optimal tissue penetration. The frame rate was kept above 40 Hz and the image resolution was on average 0.088 mm/pixel.

Measurement protocol

All subjects were seated with their arms resting on a table. We adjusted the height of the tabletop to bring the subjects elbow in approximately 120 degrees flexion. In order to visualize the transversal plane of the carpal tunnel, the scan head was placed on the proximal part of the carpal tunnel at the level of the wrist crease. We identified the flexor tendons and the median nerve by using a systematic approach. First we identified the flexor carpi radialis tendon, which is located on the radial side of the carpal tunnel, and the ulnar artery, which is located on the ulnar side of the carpal tunnel. Then we distinguished the median nerve from the tendons by visually inspecting the speckle density. The median nerve is predominantly a hypoechogenic structure with small hyperechogenic speckles, while tendons can be recognized by their hyperechogenic structure. Subsequently we identified the different hand flexor tendons by passively moving each finger. Finally we used the vertical alignment of the tendons during forceful gripping to distinguish the superficial flexor digitorum superficialis (FDS) from the deep flexor digitorum profundus (FDP). During forceful gripping the FDSs are located volarly compared to the FDPs. After identification of the median nerve and all the hand flexor tendons the motion protocol was executed.

Table 2. Overview of all measured ultrasound variables during full extension and forceful gripping

	Full Extension					Forceful Gripping				
	Cases		Controls			Cases		Controls		
	Mean	SD	Mean	SD	P-value	Mean	SD	Mean	SD	P-value
Area carpal tunnel	198.90	47.13	183.26	28.55	0.208	NA	NA	NA	NA	NA
Perimeter carpal tunnel	64.02	6.80	66.77	7.72	0.177	NA	NA	NA	NA	NA
Area median nerve	13.01	3.62	9.61	1.82	<0,001	12.78	3.09	9.78	2.38	<0,001
Area index finger FDS	9.07	2.37	8.88	1.72	0.890	8.82	2.03	8.61	1.87	0.854
Area index finger FDP	12.95	3.07	12.17	2.37	0.570	12.18	2.89	11.41	1.95	0.443
Area middle finger FDS	10.64	2.17	10.15	2.10	0.490	10.78	2.30	10.79	2.83	0.878
Area middle finger FDP	14.69	4.04	14.18	3.06	0.724	15.38	4.63	13.97	2.79	0.480
Perimeter median nerve	16.43	2.88	13.85	1.51	<0,001	16.35	2.32	14.57	2.47	0.002
Perimeter index finger FDS	12.95	2.02	13.97	2.43	0.125	12.04	1.43	11.86	1.55	0.591
Perimeter index FDP	15.19	2.09	14.77	1.93	0.480	14.21	1.79	13.87	1.78	0.500
Perimeter middle FDS	13.67	1.81	14.36	2.28	0.297	13.04	1.46	12.94	1.43	0.724
Perimeter middle finger FDP	15.65	2.19	15.08	1.79	0.407	15.49	2.39	15.02	1.86	0.656
Circularity median nerve	1.69	0.30	1.63	0.34	0.244	1.70	0.31	1.76	0.30	0.244
Circularity index finger FDS	1.52	0.37	1.82	0.63	0.075	1.34	0.21	1.34	0.31	0.226
Circularity index finger FDP	1.44	0.22	1.47	0.36	0.570	1.34	0.16	1.36	0.22	0.842
Circularity middle finger FDS	1.41	0.20	1.70	0.63	0.158	1.27	0.12	1.27	0.11	0.927
Circularity middle finger FDP	1.35	0.16	1.29	0.11	0.192	1.27	0.11	1.30	0.14	0.645

SD Standard deviation
NA Not applicable
FDS Flexor digitorum superficialis
FDP Flexor digitorum profundus

Motion protocol

Subjects were asked to fully extend their fingers, which was the starting point for the measurements. We then instructed the subjects to make a fist within 5 seconds without using excessive force, maintain this state for 2 seconds and then grip forcefully for 3 seconds. If subjects failed to comply or the scan head did not maintain full contact during the entire motion protocol the recording was discarded and the measurement was repeated. The protocol was executed twice for both hands, starting with the right hand followed by the left.

Ultrasound image processing

We exported the ultrasound images as compressed audio-video interleave (AVI) files from the scanner using the MS-CRAM codec with a frame rate of 40Hz. For analysis we used an in-house developed image processing software package based on Matlab (7.10 R2010a; The MathWorks, Inc., Natrick, MA). We analyzed one frame out of every 40 frames in the initial recording to reduce analysis time and highly correlated measures, effectively resulting in 11 frames that were analyzed. Starting with frame 1, we manually placed polygons on the border of the five identified structures starting with the median nerve. After identifying the median nerve, the polygon was displayed as an overlay in the original AVI and a new AVI was created. The next step was to identify the FDS of the index finger in this new AVI including the prior overlay. This ensured minimal overlap between polygons of different structures in the same frame. Every step was repeated until all 5 identified structures were analyzed. The resulting AVI thus contained 5 overlays outlining the median nerve and the 4 hand flexor tendons (FDS and FDP of both index finger and middle finger). Every polygon contained at least 14 nodes to minimize estimation errors.

Parameters

Based on the polygons from the AVIS we extracted the following three parameters: area, perimeter, and circularity. Area, perimeter, and circularity were calculated during full extension at frame 1 and during forceful gripping. Due to variability in the applied force during forceful gripping we averaged the ultrasound variables over frame 9, 10, and 11

The area of each structure was calculated based on the number of pixels within the polygon outlining the structure. The area was normalized to the area of the carpal tunnel to minimize variations due to scan angle variations. Perimeter was calculated as the total length of the line segments of the polygon. The perimeter was also normalized to the perimeter of the carpal tunnel, again to minimize variations due to scan angle variations. Circularity was defined as:

$$\text{circularity} = \frac{\text{perimeter}^2}{4\pi \cdot \text{area}} \qquad \text{(Eq.1)}$$

A circularity of 1 indicates a perfect circle, while a circularity larger than 1 indicates a deviation from a circle, such as a more ellipsoid shape or a more irregular pattern.

Statistical methods

As a first step, we compared differences between patients and controls for all individual ultrasound variables using a Mann-Whitney U test. Then, we used univariate logistic regression models to predict CTS by entering the individual ultrasound variables in combination with the confounding variables (age, gender and BMI). Using the Wald test, we determined in each model whether the ultrasound variable contributed significantly to the model to predict CTS. To further inspect the prognostic value and to reduce redundancy of the ultrasound variables, we applied logistic regression analysis using the least absolute shrinkage and selection operator (LASSO) for variable selection[192]. We constructed five separate logistic models: 1) a model with the non-normalized area of the median nerve at full extension, 2) a model with the normalized area of the median nerve at full extension, 3) a model with all ultrasound variables at full extension, followed by LASSO selection of variables, 4) a model with all ultrasound variables at forceful gripping, followed by LASSO selection of variables, and 5) a model with all ultrasound vari-

Table 3. Overview of the logistic regression models

	Model 1		Model 2		Model 3		Model 4		Model 5	
	ß	SE	ß	SE	ß	SE	ß	SE	ß	SE
BMI	0.037	0.092	0.092	0.089	3.238	5.484	5.311	5.003	4.095	5.169
Age	0.085	0.029	0.088	0.030	11.081	5.275	9.696	4.477	10.262	4.860
Gender	-0.688	0.803	-0.108	0.830	-0.548	0.941	-0.552	0.931	-0.531	0.886
Constant	-8.137	2.557	-10.015	3.057	1.690	1.421	1.568	1.369	1.586	1.368
Not normalized area MN at full extension	0.387	0.173								
Area MN at full extension			73.916	31.771						
Perimeter MN at full extension					6.143	2.212			3.973	0.876
Circularity middle finger FDP at full extension					4.984	2.544			3.025	1.173
Perimeter index finger FDP at full extension					0.544	0.970				
Circularity index finger FDP at full extension					0.929	0.914				
Perimeter middle finger FDP at forceful gripping							1.864	1.032	0.415	0.562
Area MN at forceful gripping							0.709	0.944		
Perimeter MN at forceful gripping							1.558	1.086		

Model 1 only included the confounding variables and the non-normalized area of the median nerve
Model 2 only included the confounding variables and the normalized area of the median nerve
Model 3 included the confounding variables and a LASSO selection of all the ultrasound variables during full extension
Model 4 included the confounding variables and a LASSO selection of all the ultrasound variables during forceful gripping
Model 5 included the confounding variables and a LASSO selection of all the ultrasound variables
SE Standard error
MN Median nerve
FDP Flexor digitorum profundus
FDS Flexor digitorum superficialis

ables at both full extension and forceful gripping followed by LASSO selection of variables. The confounding variables BMI, age, and gender were fixed in all models. After selection of the optimal set of ultrasound variables for the five models, a 5-fold cross-validation was used to analyze the performance of the models in terms of the accuracy, sensitivity, specificity, negative predictive value, positive predictive value, and the area under the curve (AUC) of the receiver operator curve (ROC). With 5-fold cross-validation, a balanced group of cases and controls are randomly selected to train the model and the remainder of the group is used to validate the model by repeating the selection, training, and validation 5 times. In addition, we specifically assessed the performance gain of specific models by comparing: 1) model 1 and model 2 to assess whether normalization of the area of the median nerve would improve the performance, 2) model 3 and model 4 to assess whether forceful gripping instead of full extension would improve the model, and 3) model 2 and model 5 to assess if the most complete model with LASSO selection of variables would improve the model. For all analyses, a $p<0.05$ was considered statistically significant.

METHODS

Population characteristic of the 50 cases and 25 controls are summarized in Table 1. The variables BMI ($p<0.001$) and age ($p<0.001$) differed significantly between groups and were therefore considered to be confounding variables and included in all statistical models. Gender ($p=0.215$) was not significantly different but was considered a confounding variable as well due to its skewed distribution.

Ultrasound findings of cases and controls are summarized in Table 2. The area of the MN was significantly larger for CTS patients than healthy subjects, both when measured at full extension ($p<0.001$) and during forceful gripping ($p<0.001$). The perimeter of the MN was significantly larger for CTS patients than healthy subjects, also both during full extension ($p<0.001$) and during forceful gripping ($p=0.002$). All the other ultrasound variables did not show a significant difference between cases and controls.

The univariate logistic regression models to predict CTS by entering the individual ultrasound variables in combination with the confounding variables (age, gender and BMI) indicated that four ultrasound variables contributed significantly to predicting CTS, namely: normalized area of the MN during full extension ($p<0.001$), normalized perimeter of the MN during full extension ($p=0.029$), normalized area of the MN during forceful gripping ($p=0.035$), and normalized perimeter of the MN during forceful gripping ($p=0.024$).

The properties of the five predictive models are summarized in Table 3 and the performance parameters of these models are summarized in Table 4. To evaluate the gained performance when normalizing the area of the MN, we compared model 1 (including the non-normalized area of the MN) with model 2 (including the normalized area of the MN) at full extension. We found that the correct classification rate of model 2 outperformed model 1, while both had a comparable AUC.

To evaluate the gained performance when using forceful gripping instead of full extension, we compared model 3 (including the LASSO selected variables selected from all ultrasound variables measured during full extension) and model 4 (including the LASSO selected variables selected from all ultrasound variables measured during forceful gripping). See Table 3 for the ultrasound variables included in the models. Model 4 outperformed model 3 on the correct classification rate, while model 3 outperformed model 4 on the AUC (Table 4).

Finally, to evaluate the gained performance when including the LASSO selected variables selected from all ultrasound variables, thus including the non-normalized MN, normalized MN and normalized hand flexor tendons measured during full extension and forceful gripping, we compared model 2 (including only the normalized area of the MN) with model 5 (including the LASSO selected variables selected from all ultrasound variables). Again, see Table 3 for the ultrasound variables included in the models.

RESULTS

Table 4. Overview of performance parameters of the logistic regression models

	Model 1	Model 2	Model 3	Model 4	Model 5
Correct classification rate	76.5%	81.0%	80.0%	82.8%	82.3%
Area under receiver operator characteristics	86.8%	86.4%	83.7%	82.0%	81.7%
Sensitivity	74.8%	84.9%	84.0%	88.0%	87.3%
Specificity	81.1%	76.1%	75.7%	76.0%	75.3%
Positive predictive value	86.5%	85.3%	85.5%	85.8%	85.4%
Negative predictive value	68.4%	78.1%	73.8%	79.7%	78.8%

Model 1 only included the confounding variables and the non-normalized area of the median nerve
Model 2 only included the confounding variables and the normalized area of the median nerve
Model 3 included the confounding variables and a LASSO selection of all the ultrasound variables during full extension
Model 4 included the confounding variables and a LASSO selection of all the ultrasound variables during forceful gripping
Model 5 included the confounding variables and a LASSO selection of all the ultrasound variables

Model 5 outperformed model 2 in terms of classification rate, but model 2 outperformed model 5 on the AUC of the ROC (Table 4).

Until today, ultrasound (US) studies were considered inferior compared to EMG studies when diagnosing CTS[163]. The most important reason was the high variation between US studies, which may partially be explained by operator variance[54]. The most considerable improvement in the classification models to diagnose carpal tunnel syndrome (CTS) was normalizing the median nerve (MN). Normalizing the cross-sectional area of the MN to the cross-sectional area of the carpal tunnel minimizes operator variance as it eliminates the dependency of the angle of the scanhead. Any offset in the angle of the scanhead will enlarge the cross-sectional area that is measured. However, both the cross-sectional area of the MN and of the carpal tunnel will increase similarly; therefore normalizing the area of the MN with respect to the area of the carpal tunnel will cancel the distortion and thus minimize operator variance. Furthermore, we have shown that the classification models are only minimally improved by using forceful gripping instead of full extension. Finally, we have shown that the classification model with only the normalized area of the MN performs almost equally as the extensive model 5 including the perimeter of the MN, the circularity of the middle finger FDP both at full extension, and the perimeter of the middle finger FDP at forceful gripping. Interestingly, however, the hand flexor tendons do seem to contain valuable information alongside with the MN to identify CTS, because the ultrasound variables of the hand flexor tendon were selected by LASSO in the extensive prediction model.

A large number of studies have investigated the performance of the cross-sectional area (CSA) of the MN to assess CTS, reporting a wide range in both sensitivity (48-99%) and specificity (39-100%). The two largest studies, Fowler et al.[54] and Visser et al.[204], found a median CSA of 8 mm^2 (7-10) and 13 mm^2 (11-15). In addition, Nakamichi and Tachibana[136] found a median CSA of 14.1 mm^2 (SD 4.7) for patients, compared to 10.0 mm^2 (SD 2.6) for controls. These findings are comparable to our findings of 13.5 mm^2 (SD 4.0) for patients and 9.8 mm^2 (SD 1.8) for controls. The sensitivity and specificity reported by Visser et al. were 78% (71-84) and 91% (85-95) and by Nakamichi and Tachibana were 57% (52-62) and 97% (95-98), thereby showing considerable differences. Findings of the latter study are comparable to findings in the present study, while the sensitivity and specificity reported by Visser et al. are considerably higher. Differences may be due to different reference standards; Visser et al. used clinical findings as a reference standard, while Nakamichi and Tachibana used EMG as a reference standard. Furthermore, Visser et al. did not use a validated questionnaire to assess CTS, which might explain the higher sensitivity and specificity compared to findings in the present study. Nevertheless, the similarity in CSAs between these studies and the present study suggests that our small sample is representative for the population.

Several ultrasound variables in addition to the cross sectional area of the MN have been proposed to improve the performance of CTS assessment, such as the perimeter[218], aspect ratio[136,218], circularity[218], delta CSA[76,99], wrist-to-forearm ratio[75], and nerve density[186]. Yoshii et al. found a mean perimeter of 14.3 mm (SD 1.6), and a mean circularity 1.69 (SD 0.30) for controls, which is similar to our findings. This suggests that these parameters can be reliably measured, which has also been investigated and confirmed by van Doesburg et al.[197].

The present study has a number of limitations. A first limitation is that we included an unbalanced number of cases and controls, resulting in differences in the major confounders (age, gender, BMI) between cases and controls. Although unbalanced confounders should be avoided if possible, they can be well controlled for in a logistic regression model as performed in the present study. Besides the unbalanced cases and controls, the present study is also based on a relatively small sample size. Statistically, small sample sizes can be a major issue when using logistic regression on a relatively large number of parameters. By using LASSO as a variable

selector in conjunction with logistic regression, only one parameter was selected from each group of highly correlated ultrasound variables, as each variable within that group would inherently yield similar predictions. Because we performed cross-validation, it was not possible to statistically test for differences in performance of the individual models. Nevertheless, the cross-validated performance parameters can be interpreted in such a way that clear differences between parameters can be considered as sufficient proof as such.

We have shown that the extensive model including the perimeter of the MN, the circularity of the middle finger FDP both at full extension, and the perimeter of the middle finger FDP at forceful gripping outperformed all other classification models. However, this model is not the most practical model, because it included several different ultrasound variables that need to be measured during both full extension and forceful gripping. Alternatively, the model including only the cross-sectional area of the median nerve, normalized to the area of the carpal tunnel, may be the most useful model to assess CTS with only minimal decrease in performance compared to the extensive model. We have shown that reducing operator variability increases the performance of the classification models dramatically, making ultrasound a more attractive diagnostic tool when assessing CTS. We have also shown with the extensive model that the hand flexor tendons add valuable information to predict CTS. It may therefore be that the hand flexor tendons are involved in CTS possibly due to the fibroses of the SSCT associated with CTS. We believe that our findings are enforced by patient friendliness, ease of use, and lower time consumption of US compared to EMG, thereby making US a more attractive diagnostic tool in the assessment of CTS.

Chapter 8

Ultrasonographic Assessment of Longitudinal Median Nerve and Hand Flexor Tendon Dynamics in Carpal Tunnel Syndrome

Jan-Wiebe H. Korstanje
Marjan Scheltens-de Boer
Joleen H. Blok
Peter C. Amadio
Steven E.R. Hovius
Henk J. Stam
Ruud W. Selles

Submitted

ABSTRACT

Changes in subsynovial connective tissue (SSCT) of carpal tunnel syndrome (CTS) patients may result in altered dynamics; consequently quantification of these dynamics might support an objective diagnosis of CTS. We used ultrasound to measure longitudinal hand dynamics during finger extension-to-fist motion in 51 CTS patients. Results were compared between most affected and least affected hands using EMG or clinical symptoms as discriminator. Excursions of the median nerve and flexor digitorum superficialis tendon of the most affected hands were smaller than in the least affected hands, while the excursions of the flexor digitorum profundus were larger. Similar results were found for the SSCT. Logistic regression models classified between 67% and 86% of the investigated hands correctly on the basis of these excursion data. The dynamics of the hand are altered in CTS patients, therefore using our models based on ultrasound findings may support the diagnose CTS.

Carpal tunnel syndrome (CTS) is the most frequently encountered compression neuropathy. In general terms, CTS is defined as an entrapment of the median nerve, but in the majority of patients diagnosed with CTS its precise etiology is unknown. The traditional diagnosis of CTS is based on clinical symptoms and signs in combination with results of electromyographic (EMG) studies, however, EMG only has moderate specificity and sensitivity with either the sensitivity or the specificity reaching high values but never both[8,9,37,137]. This justifies exploration of new techniques to complement EMG findings.

Because CTS might be associated with an increased cross-sectional area of the median nerve, the additional diagnostic value of ultrasonographic assessment of this area and of the carpal tunnel has been studied extensively over the past years[75,95,107,163,209,215]. However, results were equivocal, probably partly due to the lack of a gold standard for establishing the diagnosis of CTS and the use of EMG as sub-optimal reference[95]. Recently, a number of studies have addressed not only the cross-sectional area of the median nerve, but also the dynamic behavior of the median nerve and hand flexors in CTS patients[42,46,82,213]. It has been suggested that thickening and non-inflammatory fibrosis of the subsynovial connective tissue (SSCT) within the carpal tunnel is an essential part of the pathophysiology. The SSCT surrounds the tendons and is connected to the tendons with fibrils. Thickening and fibrosis of the SSCT might change the excursion of the median nerve and hand flexor tendons during hand movement. Therefore, measuring the movement of the flexors and median nerve may provide important insights into the specific pathology in individual patients.

For the purpose of measuring the longitudinal dynamics of the median nerve and the hand flexor tendons, various approaches have been proposed. Ettema et al. assessed the longitudinal excursion of the relevant structures in cadaver hands and peri-operatively in patients with CTS during carpal tunnel release with a video camera[46,48]. Although usable, this technique is invasive and might, therefore, alter tendon dynamics. Alternatively, ultrasound techniques such as Color Doppler Imaging[23] or speckle tracking[42,217] have been employed to measure longitudinal nerve and tendon movement in-vivo. However, Color Doppler Imaging was found to be only moderately accurate, with tracking errors up to 18%[23]. Similarly, tracking accuracy using an industrial speckle tracking algorithm not optimized for tendons proved to be only moderate compared to model based tendon excursion calculations (r2= 0.313)[217]. Recently, Korstanje et al. introduced and validated a tendon-optimized speckle tracking algorithm with an in-vivo mean tracking error of 1.6%[103]. This accurate approach opens new possibilities.

To our knowledge it has not been investigated whether a change in the longitudinal excursion of the median nerve, hand flexor tendons, or SSCT is associated with CTS. Therefore, the purpose of this study was to study the longitudinal dynamics of the flexor tendons, the median nerve, and the surrounding SSCT in the wrist in a group of CTS patients and to relate the findings to EMG results and clinical symptoms and signs. To do so, we 1) compared the longitudinal excursions of the median nerve and of the tendons of the flexor digitorum profundus (FDP) and flexor digitorum superficialis (FDS) of the least affected hand with those of the most affected hand using either EMG or the clinical symptoms and signs as discriminator, 2) compared the longitudinal excursions of the SSCT of the same structures of the least affected hand with those of the most affected hand using either EMG or the clinical symptoms as discriminator, and 3) developed several decision models based on the longitudinal excursions of the median nerve, FDP and FDS tendons, and the SSCT. The excursions were measured using an in-house developed novel speckle tracking algorithm that was optimized for tendon en nerve tracking[103].

Subjects and measurements

Subjects were recruited at our university medical centre and were invited to participate in this study. With a response rate of 93%, 51 out of 55 invited subjects were included. Fifty-one other-

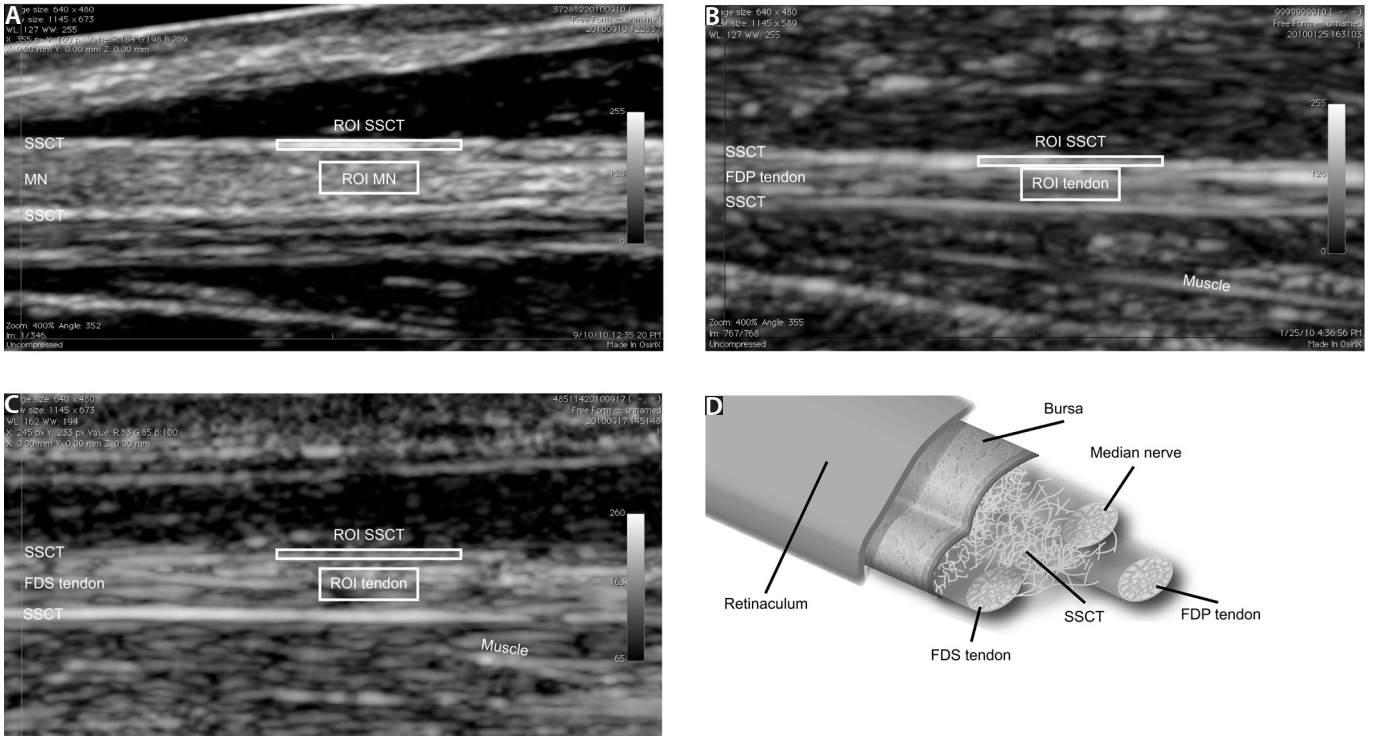

Figure 1. Shows the placement of the region of interest (ROI) for A. the median nerve (MN), B. the flexor digitorum superficialis (FDS) tendon, and C. the flexor digitorum profundus (FDP) tendon and for their corresponding surrounding tissue or subsynovial connective tissue (SSCT). D. The SSCT is a complex fine-meshed structure connecting the MN, FDP, and FDS.

wise healthy adults (14 males and 37 females) with a mean age of 50.6 years (±13.0) were enrolled in this study on referral to the department of Clinical Neurophysiology because of a clinical suspicion of CTS. Subjects were excluded if they were younger than 18 years of age. Each subject underwent a neurological examination and an EMG, and filled out the Boston Carpal Tunnel Questionnaire (BCTQ)[113] for the clinical evaluation. Our medical ethics committee approved this study and informed consent was obtained from each participant.

Nerve conduction studies

Nerve conduction studies were performed using standard clinical protocols on a Viking Select EMG machine (CareFusion, San Diego, CA) using ring electrodes for recording sensible nerve action potentials (SNAPs) and surface electrodes for recording of compound muscle action potentials (CMAPs) from the abductor pollicis brevis muscle. From the antidromically elicited SNAPs, the distal sensory latency (DSL) was determined automatically by the system and compared between nerves or nerve segments in the following ways: 1) Comparison of the DSL of the median and ulnar nerves between wrist and ring finger, 2) Comparison of the DSL of the median nerve between wrist and palm versus palm and the third finger, and 3) Comparison of the DSL of the median and radial nerve between wrist and thumb. During all measurements electrode distances were kept equal between nerve segments. If necessary, also the distal motor latency (DML) of the median nerve to the abductor pollicis brevis muscle was determined.

If the latency difference of the first test equaled or exceeded 0.5 ms, the EMG was considered positive for CTS. If this difference was smaller than 0.5 ms, the two additional sensory tests were performed. These were considered abnormal if the respective latency differences were ≥ 0.5 ms and CTS was confirmed if both were positive. If SNAPs could not be evoked, the median distal motor latency (DML) to the abductor pollicis brevis muscle was measured. This DML was considered abnormal if it exceeded the age and gender dependent normal value (between 4.4 and 4.7 ms)[22].

Ultrasound recordings

Ultrasound video sequences were acquired of the median nerve and of the tendons of the flexor digitorum superficialis (FDS) and the flexor digitorum profundus (FDP) of the middle finger, using a Philips iU22 ultrasound system (Philips Electronics, Best, the Netherlands) with a 5 to 12 MHz linear array transducer at a minimum of 70 frames per second. The image resolution was 0.0166 mm/pixel.

Subjects were seated with the arm positioned on a table. The arm was supinated and the elbow was flexed approximately 90° with the wrist and phalanges in a neutral position. The investigator subsequently placed the scan head at the wrist crease (which overlies the proximal part of the carpal tunnel) and imaged the carpal tunnel in the longitudinal plane.

To localize the FDP and FDS tendons with ultrasound, we first palpated the FDP and FDS muscles and then moved the probe along the muscles towards the tendons. When both the FDP and FDS tendons were identified, the distal interphalangeal (DIP) joint of each finger was flexed and extended separately by the investigator to identify which of the FDP and FDS tendons was visualized. Finally, the FDP tendon could be distinguished from the FDS tendon based on a larger excursion during DIP movement. Moreover, the identification of the FDP tendon was confirmed by its position and orientation, as it commonly passes through the carpal tunnel at an angle while the FDS tendon passes through more horizontally.

To localize the median nerve, we made a transversal image of the proximal part of the carpal tunnel. At that site, the median nerve could be identified as a superficial structure that is hypoechogenic compared to the speckle structure of the tendons. After identification of the median nerve in the transversal plane, the scan head was rotated to image the median nerve longitudinally. In this case, the absence of any noticeable displacement of the imaged structure during passive flexion and extension of the subject's fingers confirmed that we did not image a tendon or muscle.

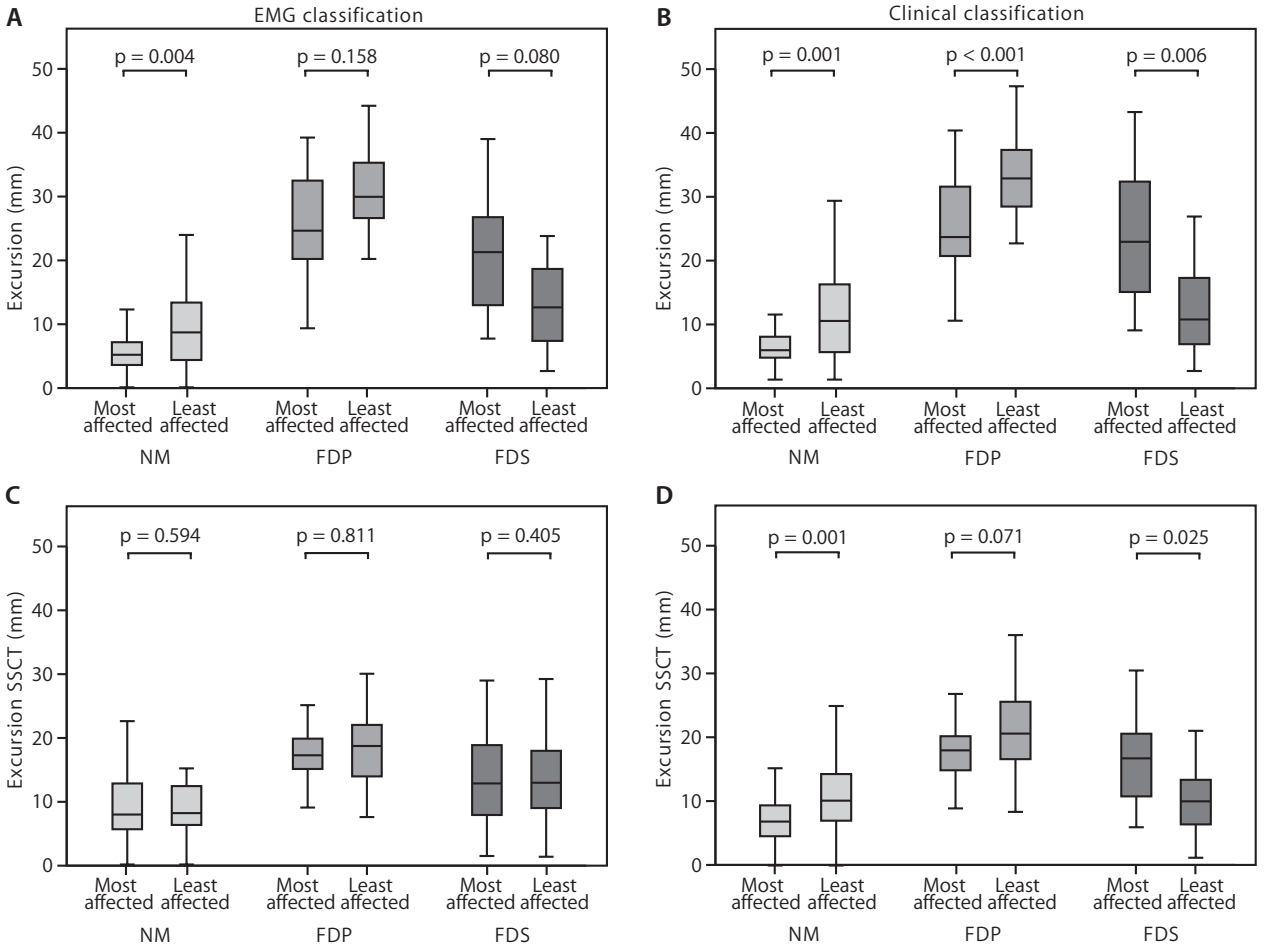

Figure 2. Shows the longitudinal excursions for the median nerve (MN), flexor digitorum profunudus (FDP) tendon, and flexor digitorum superficialis (FDS) tendon (top row) as well as the longitudinal excursions of the surrounding subsynovial connective tissue (SSCT) of these structures (bottom row). EMG was used as discriminator of least and most affected hand in the left column (A and C), clinical symptoms and signs in the right column (B and D).

Motion protocols

In this study we looked at displacements of the FDS and FDP tendons and the median nerve during active flexion of the hand. Each subject was asked to extend his hand fully and keep his wrist in a neutral position. Next, the subject was instructed to make a fist within 10 seconds without using excessive force at the end point. After completion, the motion was repeated. The FDS and FDP tendons and the median nerve were imaged separately; hence, the procedure was executed three times. After completing the six motions the entire protocol was repeated for the other hand.

Ultrasound imaging analyses

Ultrasound images were exported as uncompressed audio video interleave (.avi) files using OsiriX (Version 3.7.0; http://www.osirix-viewer.com). The uncompressed AVIs were then imported into Matlab (7.5, R2010b, the MathWorks Inc., Natick, MA) and analyzed with in-house developed tracking software that can be described as a "dedicated two-dimensional multi-kernel block-matching scheme using normalized cross-correlation (NCC)". This software has been extensively described and validated elsewhere[103]. It can track tendons with a mean measurement error of 0.3 mm over physiological tendon excursions and velocities. The algorithm is based on the general concept of block-matching schemes, which are frequently used to track cardiac wall movements[34,117,141].

Figures 1A, B, and C show typical examples of the ultrasound recordings and the placement of the Regions of Interest (ROIs) on the tendons and median nerve (MN). Figure 1d schematically illustrates the 3D structure of the flexor tendons at wrist level, MN, and the SSCT at the recording site. At the start of the analysis, the user identifies a ROI in the first frame of the AVI. This rectangular ROI marks the location of the tendon or nerve; therefore, it has to be placed on the structure without capturing any other structure. Then, the user identifies a second ROI in the first frame of the AVI, which has to be placed on the surrounding tissue instead of the tendon or nerve. The algorithm automatically places several overlapping kernels in the ROI. Kernels are small rectangular blocks that capture a part of the speckle pattern of the structure. In our application, the kernel is a small part of the structure to be tracked with sufficient speckle patterns to allow the algorithm to find a good match in the subsequent frame. Next, the algorithm searches for the best-matching speckle pattern in this second frame within an automatically defined search region. In the algorithm, each block (kernel) in a particular frame is matched with a block in the next frame; hence the name block-matching algorithm. The goodness of the match is defined by the normalized cross-correlation measure (NCC), which ranges from 0 to 1. A 0 means that there was no match at all between a kernel and the speckle pattern captured within the search region, while a 1 means a full match. We use multiple kernels to increase accuracy: by weighting the excursion per kernel with the NCC outcome, we can minimize the contribution of possible outliers. Only matches with an NCC equal or larger than 0.7 were considered a good match and were included in the weighted average.[49]

From the displacement estimates, we calculated the excursions of the FDS and FDP tendons and the excursion of the MN as well as the corresponding excursions of the surrounding tissue. Based on the excursions of the hand flexor tendons and MN and the excursion of the corresponding surrounding tissue or subsynovial connective tissue (SSCT) we calculated the shear index defined as:

$$SI = \frac{\Delta x_{structure} - \Delta x_{SSCT,structure}}{\Delta x_{structure}} \qquad \text{(Eq.1)}$$

where $\Delta x_{structure}$ is the excursion of the hand flexor tendons or MN and $\Delta x_{SSCT,structure}$ is the excursion of the corresponding SSCT[220].

Statistical analyses

We used the Shapiro-Wilk and Kolmogorov-Smirnov tests to test the data for normality. A paired-samples T-test was used to compare the ultrasonographic variables (excursions of the middle finger FDP and FDS tendons, and MN and corresponding shear strain in-

Table 1. Population characteristics

		Total group	
No of patients		51	
No of hands		102	
Males		14/51 (27.5%)	
Age group (years)	18-20	1(2.0%)	
	20-39	7 (13.7%)	
	40-59	31 (60.8%)	
	60-79	12 (23.5%)	
	Average age (SD)	50.6 (13.0)	
		Total group	Left hands
EMG score	No CTS	48/98 (49.0%)	27/49 (55.1%)
	Possibly CTS	9/98 (9.2%)	3/49 (6.1%)
	Mild CTS	27/98 (27.6%)	10/49 (20.4%)
	Moderate CTS	6/98 (6.1%)	3/49 (6.1%)
	Severe CTS	8/98 (8.2%)	6/49 (12.2%)
	Unilateral involvement	18/49 (36.7%)	
Clinical symptom score	No CTS	13/101 (12.9%)	8/50 (16.0%)
	Possibly CTS	22/101 (21.8%)	10/50 (20.0%)
	Probably CTS	49/101 (48.5%)	24/50 (48.0%)
	CTS	17/101 (16.8%)	9/50 (18.0%)
	Unilateral involvement	13/51 (25.5%)	

SD Standard deviation
EMG Electromyography
CTS Carpal tunnel syndorme

dices) between the least affected and most affected wrist, using either EMG or clinical symptoms and signs as discriminators. For the purpose of determining which hand was least and which most affected, we used the EMG as previously described and the BCTQ. For the BCTQ the grading scale was defined as: 1) no CTS (0-1 points), 2) possible CTS (2-5 points), 3) probable CTS (6-8 points), and 4) definite CTS (9-11 points) in accordance with the American Association of Electrodiagnostic Medicine (AAEM) practice guidelines[3].

To explore the relationship between EMG or clinical symptoms on the one hand and the ultrasonographic variables on the other, binary logistic regression analyses with stepwise elimination using the maximum likelihood function were performed. Four separate models were constructed: 1) a model with the EMG results (positive/negative for CTS) as the dependent variable and the longitudinal excursions of the MN and the FDS and FDP tendons as independent variables; 2) a model with clinical symptoms and signs (consistent or inconsistent with CTS) as the dependent variable and the longitudinal excursions of the MN and the FDS and FDP tendons as independent variables; 3) a model with EMG results as the dependent variable and the excursions of the SSCT of the MN and FDS and FDP tendons as independent variables; 4) a model with clinical symptoms and signs as the dependent variable and the longitudinal excursions of the SSCT of the MN, FDS, and FDP as independent variables.

For the binary logistic regression we defined CTS according to EMG as previously described and defined CTS according to clinical symptoms and signs as a BCTQ score ≥ 2. Binary logistic regression analyses were only performed on the data obtained from the left hands, for two reasons. First, inclusion of both hands from the same patient would render the logistic regression analyses invalid. Second, we choose the left hand over the right hand because the left hand had a more balanced distribution of affected and unaffected hands (see Table 1). Statistical significance was set at $p<0.05$. Results were expressed as means and standard deviations (SD). All statistical analyses were performed with SPSS 18.0.3 (IBM Corporation, Somers, NY, USA).

METHODS

Table 1 gives an overview of the study population characteristics. Of the 51 included subjects, two had an incomplete EMG and one had an incomplete assessment of clinical symptoms and signs. Based on the EMG findings, 51% of the patients had unilateral or bilateral CTS, while clinical symptoms and signs were consistent with CTS (BCTQ ≥ 2 points) in 100% of the patients. Left hand involvement was seen in 45% of the patients based on EMG and 86% based on clinical symptoms and signs.

Using the EMG as discriminator, the excursion of the MN was smaller in the most affected hands than in the least affected hands ($p=0.004$). The excursions of the FDS and FDP tendons in the most affected hands were not significantly different compared to the least affected hands (see Figure 2A). Using clinical symptoms and signs as discriminator, all three excursions differed significantly (see Figure 2B). As with the EMG, the excursion of the MN was smaller in the most affected hands than in the least affected hands ($p=0.001$). The excursion of the FDP tendon was also smaller ($p<0.001$), but that of the FDS tendon was larger ($p=0.006$).

When studying the excursions of the SSCT, we found none of these to be significantly different when discriminating between hands on the basis of the EMG (see Figure 2C). Using clinical symptoms and signs as discriminator, the excursion of the SSCT of the MN was smaller in the most affected hands compared to the least affected hands ($p=0.001$) (see Figure 2D). The excursion of the SSCT of the FDS tendon was larger ($p=0.025$).

To determine the associations between the measured excursions and the EMG results or clinical symptoms, we evaluated four different logistic regression models. In all but the second model (relating clinical symptoms to MN, FDP tendon, and FDS tendon excursions), significant associations were found between the EMG or clinical symptoms and signs on the

RESULTS

Table 2. Explanatory variables included in the logistic regression models

	Logistic regression parameter estimates					
Explanatory variable	ß	SE	EXP(ß)	95% CI		p-value
Model 1*						
Excursion MN	6.026	2.548	413.914	2.808	6,1007	0.018
Excursion FDS tendon	2.743	1.369	15.531	1.061	227.3	0.045
Excursion MN x Excursion FDP tendon	-1.126	0.549	0.324	0.111	0.951	0.040
Excursion MN x Excursion FDS tendon	-2.918	1.303	0.054	0.004	0.695	0.025
Constant	-3.078	1.692	0.046			0.069
Model 3†						
Excursion SSCT FDP tendon	3.308	1.563	27.328	1.277	584.7	0.034
Excursion SSCT MN x Excursion SSCT FDS tendon	3.068	1.252	21.498	1.849	249.9	0.014
Excursion SSCT MN x Excursion SSCT FDP tendon	-1.054	0.497	0.349	0.132	0.923	0.034
Excursion SSCT FDS tendon x Excursion SSCT FDP tendon	-2.147	0.864	0.117	0.021	0.635	0.013
Constant	-3.232	1.738	0.039			0.063
Model 4‡						
Excursion SSCT FDS tendon x Excursion SSCT FDP tendon	4.426	1.986	83.614	1.706	4,098	0.026
Excursion SSCT FDP tendon	2.191	1.171	8.948	0.901	88.8	0.061
Excursion SSCT MN x Exursion SSCT FDP tendon x Excursion SSCT FDS tendon	-1.713	0.833	0.180	0.035	0.923	0.040
Constant	-3.412	2.123	0.033			0.108

SE Standard error
CI Confidence interval
MN Median nerve
FDS Flexor digitorum superficialis
FDP Flexor digitorum profundus
SSCT Subsynovial connective tissue
*EMG as dependent variable and longitudinal median nerve and hand flexor tendon excursions as independent variables
†EMG as dependent variable and longitudinal subsynovial connective tissue excursions as independent variables
‡Clinical symptoms and signs as dependent variable and longitudinal subsynovial connective tissue excursions as independent variables

one hand and excursions or interactions between excursions on the other (see Table 2). The classification accuracy of models 1, 3, and 4 were 70%, 86%, and 67%, respectively (see Table 3).

In the present study, we have demonstrated that longitudinal dynamics of the median nerve and flexor tendon at wrist level in the most affected hand of suspected CTS patients differ significantly from those of the least affected hand. Furthermore, we were able to predict with up to 86% accuracy which of the left hands were affected by CTS using logistic regression models in which the most predictive parameters were the longitudinal excursions of the MN, FDS tendon, and SSCT of the FDP tendon.

An interesting and unexpected finding was the combination of a decreased longitudinal excursion of the MN and the FDP tendon with an increased longitudinal excursion of the FDS tendon in the most affected hand compared to the least affected hand. The same pattern of differences between hands was seen in the longitudinal excursions of the corresponding SSCTs. This is interesting, because in absolute terms the longitudinal excursions of the SSCT of the FDP and FDS tendons were similar. In a normal situation, the longitudinal FDP SSCT excursion is larger than the longitudinal FDS SSCT excursion (as evidenced by our findings in the least affected hand). Apparently, in the most affected hands, the SSCT excursions were equalized. This may point towards adhesions or stiffening of the SSCT, which in turn could be due to fibrosis associated with CTS. Alternatively, a compensatory mechanism induced by, for example, pain in the hand during finger movement might increase the excursion of the FDS at the expense of that of the FDP. Such a mechanism would be similar to previously observed compensatory mechanisms at the MCP and IP joints that result from impaired function of the thenar muscles in CTS patients.[91]

Table 4 compares our findings with those of other studies focusing on longitudinal excursions of the MN, FDS tendon, or SSCT. It should be noted that none of the previous studies reported longitudinal excursions of both the FDS and FDP tendons and the MN in the same subjects. Hough et al. found that the longitudinal MN excursion in CTS patients was smaller than in healthy subjects, which is in line with our study findings[82]. In their study, the longitudinal excursions in both cases and controls were larger than in ours, possibly because of the reversed motion order (from full flexion to full extension). Surprisingly, Erel et al. reported the opposite of the previous results, i.e., a longitudinal MN excursion in CTS patients that was larger than in healthy subjects, although not statistically significant[42]. Again, this might be due to different motion protocols: in the study of Erel et al. the metacarpophalangeal (MCP) joint was extended, while in our study both the MCP joint and the interphalangeal (IP) joints were flexed. Hough et al.[82] and Ettema et al.[46] found an increased longitudinal FDS tendon excursion in CTS patients compared to healthy subjects, which is similar to our findings. However, in their studies, no explanation of this observation was given. One of the strengths of our study is that we also included measurements of longitudinal FDP tendon excursions, which allowed us to propose the novel hypotheses of the preceding paragraph.

The SSCT interconnects the hand flexor tendons and the MN in the carpal tunnel, thereby influencing the dynamics of each of these structures. In several studies it has been hypothesized that CTS is associated with fibrosis of the SSCT. Fibrosis of the SSCT might alter its dynamics and hence also that of the MN and hand flexor tendons[46,48]. Ettema et al. showed that the longitudinal SSCT excursion of the FDS is smaller in CTS patients than in healthy subjects, which is the opposite of our findings. However, a major difference between the two studies is that Ettema et al. compared perioperative excursions in CTS patients with lonogitudinal excursions in cadaver hands, which are likely to have different dynamics.

The fact that we did not include a control group of healthy volunteers may be considered a limitation of our study. Because we compared the most affected hand with the least affected hand of suspected CTS patients, we expect smaller differences

Table 3. Classification characteristics of the logistic models

	Model 1*		Model 3†		Model 4‡	
Parameter	Proportion (%)	95% CI§	Proportion (%)	95% CI§	Proportion (%)	95% CI§
Sensitivity	12/21 (57)	37-76	40/41 (98)	87-100	9/21 (43)	24-63
Specificity	21/26 (81)	62-91	2/6 (25)	10-70	23/27 (85)	68-94
Positive predictive value	12/17 (71)	47-87	41/47 (87)	75-94	9/13 (69)	42-87
Negative predictive value	21/30 (70)	52-83	2/3 (67)	21-94	23/35 (66)	49-79
Accuracy	33/47 (70)	56-81	43/50 (86)	74-93	32/48 (67)	53-78

CI Confidence interval
*EMG as dependent variable and longitudinal median nerve and hand flexor tendon excursions as independent variables
†EMG as dependent variable and longitudinal subsynovial connective tissue excursions as independent variables
‡Clinical symptoms and signs as dependent variable and longitudinal subsynovial connective tissue excursions as independent variables
§Wilson score method

between our groups than when comparing patients with controls. Nevertheless, we were able to demonstrate significant differences in dynamic parameters between the two hands. Another limitation is the relatively small sample size in the present study, which prohibits subgroup analysis based on the severity of CTS.

The major contribution of our study is that it demonstrates the existence of considerable changes in the longitudinal excursions of the FDP and FDS tendons, the MN and their associated SSCT in the hands of CTS patients. Our comprehensive in-vivo approach enabled us to better understand these dynamic changes. More specifically, our findings of an increased longitudinal FDS tendon excursion and decreased longitudinal FDP tendon excursion suggest activation of compensatory mechanisms and/or increased adhesions in the SSCT. Furthermore, we have proposed several decision models that can assist in diagnosing CTS. As a next step, we recommend investigations of the full dynamics of the hand including all hand flexor tendons and the thumb as well as a study of the added value of our technique in diagnosing CTS.

Table 4. Study overview

		Longitudinal excursion mm (SD)			Longitudinal excursion SSCT mm (SD)		
Study	n	FDP	FDS	MN	FDP	FDS	MN
Erel[14] cases*	19			2.6 (1.6-4.5)			
Erel[14] controls*	17			2.2 (1.1-4.8)			
Ettema[12] cases†	8		26.1 (16.3-35.9)			6.9 (-7.1-20.9)	
Ettema[12] controls†	8		24.4 (14.2-34.6)			9.0 (0.6-17.4)	
Hough[13] cases‡	19		37.1 (23.9-49.6)	10.2 (4.9-15.8)			
Hough[13] controls‡	37		34.9 (23.1-41.7)	12.5 (6.9-17.4)			
Present study cases	49	26.2 (9.20-44.3)	19.8 (2.8-38.8)	5.3 (0.0-12.2)	17.9 (8.9-26.9)	15.5 (1.3-33.5)	9.8 (0.0-22.5)
Present study controls	49	28.9 (10.0-46.0)	13.8 (0.0-36.6)	8.1 (0.0-23.8)	19.1 (7.5-30.0)	13 (0.0-29.1)	8.8 (0.0-21.8)

SD Standard deviation
SSCT Subsynovial connective tissue
FDS Flexor digitorum superficialis
FDP Flexor digitorum profundus
MN Median nerve
* Hand movement from full extension to full flexion of the metacarpophalangeal (MCP) joint
† Hand movement from full extension to full flexion of the MCP, proximal interphalangeal (PIP) joint, and distal interphalangeal (DIP) joint
‡ Hand movement from full flexion to full extension of the MCP joint, PIP joint, and DIP joint

Chapter 9
Quantification of Digital Nerve Movement During Upper Limb Extension Using Modern Ultrasonography Analysis

Dirk Jan J.C. van der Avoort
Jan-Wiebe H. Korstanje
Pieter H.C. Leliefeld
Ruud W. Selles
Steven E.R. Hovius
Henk H. Coert
Submitted

Mechanical irritation is one of the reasons for a neuroma to become symptomatic. During movement of the elbow and wrist the three major nerves demonstrate a considerable excursion. This can be quantified using modern ultrasonography and custom-made speckle tracking techniques. The aim of this study was to quantify the excursion of digital nerves during movement of the wrist and elbow. In 15 healthy persons the digital nerve was imaged at the base of the second phalanx using ultrasound. The subjects made a full range of motion with the upper limb and the digital nerve movement was captured. Digital nerve excursion was calculated using a validated speckle tracking algorithm with an accuracy of 0.05 mm. We performed a test re-test. In all subjects the digital nerve was moving in relation to its surrounding tissue. We found a median excursion of 0.65 mm (range 0.11-1.60). Based on the test re-test we found an interrater correlation coefficient of 0.948. Digital nerves move in relation to their surrounding tissues from flexion to extension with relatively small excursions. The results in these healthy controls may serve as a basis for comparison of the excursion in patients with symptomatic nerve injuries.

Painful neuromas after peripheral nerve trauma of the upper extremity have a reported incidence of 2-30%[52,138,183]. The pathophysiology of a painful neuroma is largely unknown. Chemical and mechanical irritations are suggested to be the main cause for a neuroma to become painful and to develop spontaneous and disturbing sensory symptoms. These symptoms are caused by persistent stimulation of the axons within the neuroma and are accompanied by the development of spontaneous activity of neurons within the dorsal horn of the spinal cord: the dorsal root ganglion. Chemical irritation may be caused by, for example, the presence of neuronal growth factor (NGF). This NGF thus has a paradoxical effect on the nerve regeneration since it helps the nerve to regenerate but is also associated with the development of a symptomatic neuroma.

Mechanical irritation may be caused by scar tissue deposition, causing changes in the surrounding tissue of the nerve. For example, adhesions of the nerve to the surrounding tissue may increase the strain on the nerve since it may prevent physiological movement of the nerve. In addition, a neuroma that moves relative to its surrounding tissue may cause hyperesthesia.

In recent years, a number of studies have focused on nerve displacement during limb movement using ultrasonography, showing relatively large displacement of the median nerve during arm movement. Longitudinal displacements ranged from 0.6 mm to 2.5 mm in healthy subjects. Erel et al found in their study that in patients following nerve repair longitudinal displacement was significantly smaller, 2.15 mm[43]. In cadaveric studies a range of 1.5 mm up to 5 mm is reported[195]. It is hypothesized that restriction of nerve movement causes non-specific arm pain or carpal tunnel syndrome (CTS)[43].

Since the digital nerves are attached to the median or ulnar nerve, it could be argued that the digital nerve also moves during upper limb movement. Consequently, it might be that restriction in either the median nerve or the digital nerve also leads to pain or painful neuromas. However, to our knowledge, this movement has never been quantified. In an effort to understand the role of possible mechanical irritation in a neuroma, the first step is to quantify digital nerve movement in healthy control subjects in-vivo. To do so, we will use high-frequency ultrasonography and a recently validated speckle tracking algorithm[103]. We have chosen to measure the radial digital nerve of the second finger since this nerve is anatomically attached to the median nerve and is easy accessible with the ultrasonography head.

Subjects

After approval of the Medical Ethical Committee we included 17 healthy controls. Prior to the ultrasonographic measurements, all healthy subjects were physically examined and screened for cervical and upper limb pathology and informed consent was obtained. The examinations confirmed that none of the subjects showed any form of dysfunction of the upper extremities, had a history of hand trauma or were diabetic.

Subject set-up

The hand of each subject was fixed with the device. With this device, we were able to fixate all fingers while subjects could move their wrist, elbow and shoulder freely over the full range of motion. Subjects were seated on a chair on castors in front of the device. For fixation of the third to fifth finger we used modified mallet splints with a vessel loop attached to the device by a clamp on the back side of the fixation plate. Due to the size of the ultrasound probe, the second digit had to be fixed with one vessel loop only. In addition, a Velcro strap was used for fixation of the palm of the hand. Subjects were asked if they experienced any inconvenience as a result of the fixation; if so, the straps were adjusted.

All images of the second digit were made by a single observer. First the digital artery was identified using Color Doppler imaging . Then, the scanhead was moved to antero-lateral to where the digital nerve was located in the neurovascular bundle.

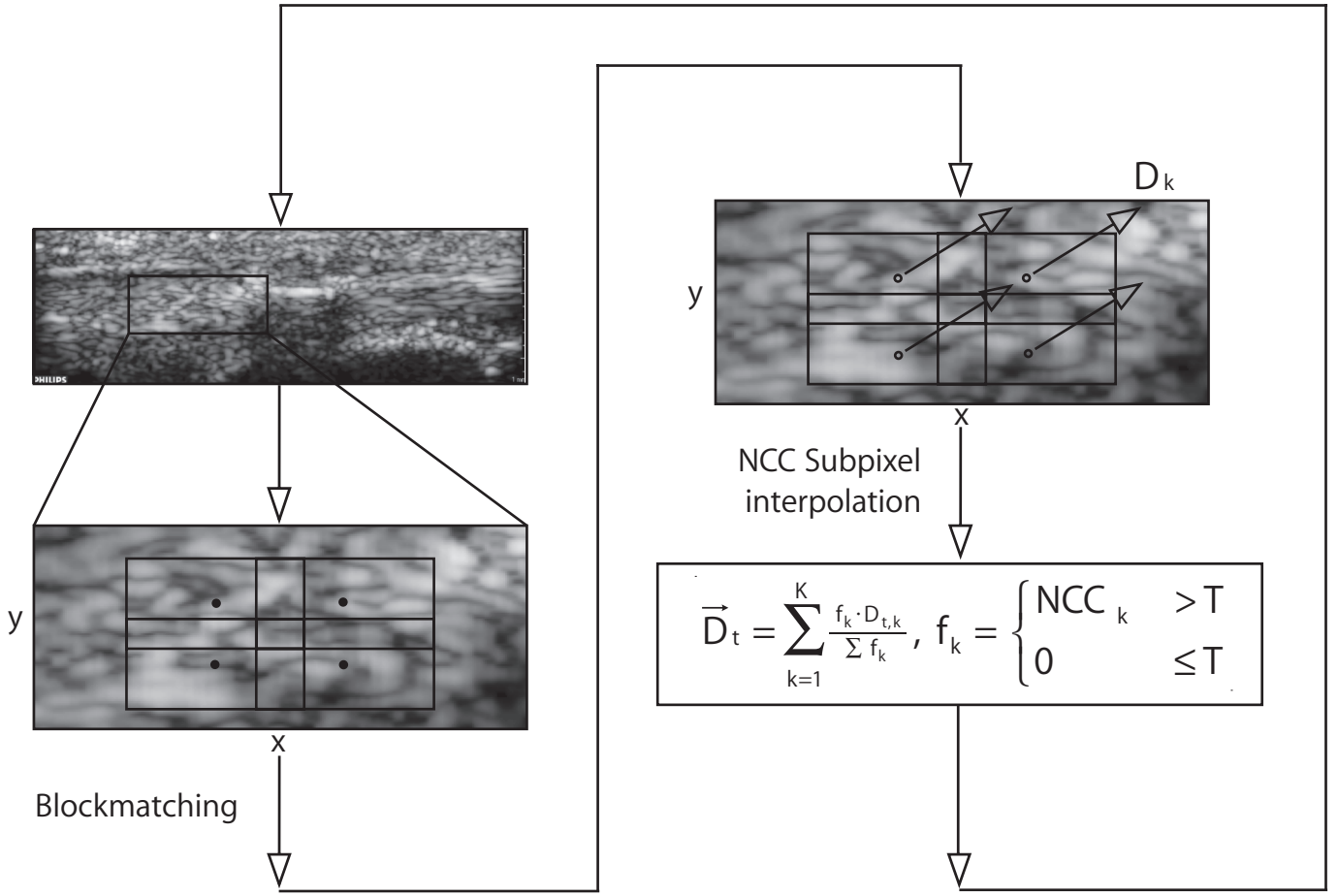

Figure 1. The developed algorithm based on block matching with the normalized cross-correlation (NCC) as similarity measure. The user manually defines a region-of-interest (ROI) after which the algorithm automatically places a predefined number of kernels in the ROI. The algorithm automatically evaluates the different displacement estimates for each kernel. After subpixel interpolation of the NCC output matrix a correlation-weighted kernel displacement vector average is calculated. For each frame the ROI was kept stationary.

After fixation of the hand and visualization of the digital nerve, subjects were asked to obtain a position of maximum flexion of the upper limb (maximum flexion of shoulder, elbow, wrist and MCP joint). From this position, within ten seconds, a second researcher moved the subjects from maximum flexion to maximum extension of the upper limb on a chair on castors. During this movement we made ultrasound movies of the nerve using an Philips iU22 ultrasound system (Philips Electronics, Eindhoven, The Netherlands), with a L17-7io linear array probe with a frequency ranging from 7 to 17MHz. Frames were captured with a minimum frame rate of 70Hz and the image resolution was 0.0056 pix/mm. To establish the intra rater reliability, the same observer measured 12 healthy subjects a second time. This was done with a time interval of at least one hour.

Movement analysis by speckle tracking

For appropriate use of the speckle tracking algorithm, it is of major importance that the nerve is visible during the whole range of motion of the patient. Furthermore, out-of-plane motion can occur when the nerve is moving out of the scanning plane, thus moving in the transversal plane, and consequently the median nerve displacement might be underestimated. Therefore, we carefully inspected all movies after the recordings and excluded movies in which out of plane movement was present.

Ultrasound images were exported as uncompressed audio video interleave (.avi) files using OsiriX (Version 3.7.0; http://www.osirix-viewer.com). The uncompressed AVIs were then imported into Matlab (7.5, R2009a, the MathWorks Inc., Natick, MA) and analyzed with in-house developed tracking software that can be described as a "dedicated two-dimensional multi-kernel block-matching scheme using normalized cross-correlation (NCC)". The software has been extensively described and validated elsewhere[103,104] and can track tendons with a mean measurement error of 50mm over physiological tendon excursions and velocities. The algorithm is based on the general concept of block-matching schemes, which are frequently used to track cardiac wall movements[34,117,141].

Figure 1 shows the general concept of our software. The user first identifies a Region of Interest (ROI) in the first frame of the AVI. This region of interest is nothing more than a rectangle that describes the location of the tendon and therefore has to be placed on the tendon without capturing any other structure. Then the user identifies a second ROI in the first frame of the AVI, which has to be placed on the surrounding tissue instead of the tendon. The algorithm automatically places several overlapping kernels in the ROI. Kernels are small rectangular shaped blocks that capture a part of the speckle pattern of the structure. In our application, the kernel is a small part of the tendon with sufficient speckle patterns so that the algorithm can find a good match in the next frame. The algorithm searches for a best-matching speckle pattern in the next frame in an automatically defined search region. We avoid searching the entire image to reduce computational load. In the algorithm, each block in a particular frame is matched with a block in the next frame, hence the name block-matching algorithm. The goodness of the match is defined by the normalized cross-correlation measure (NCC), which ranges from 0 to 1. A 0 means that there was no match at all between a kernel and the speckle pattern captured within the search region, while a 1 means a full match. We use multiple kernels to increase accuracy, as more kernels allow for weighting the tendon excursions with the NCC outcome (ranging between 0 and 1), thereby minimizing the contribution of possible outliers. Only matches with a NCC equal or larger than 0.7 were considered a good match[49]. Displacements are reported as digital nerve excursions and ranges, unless otherwise noted.

Statistical analysis

Data were analyzed using SPSS 16.0 statistic analysis software (windows). An intraclass correlation coefficient (ICC) was calculated to determine the test-retest reliability of the ultrasonography technique using a two-way random effect model with single measure and absolute agreement, also known as ICC(3,1)[165].

After judging all ultrasonographic movies, two movies of

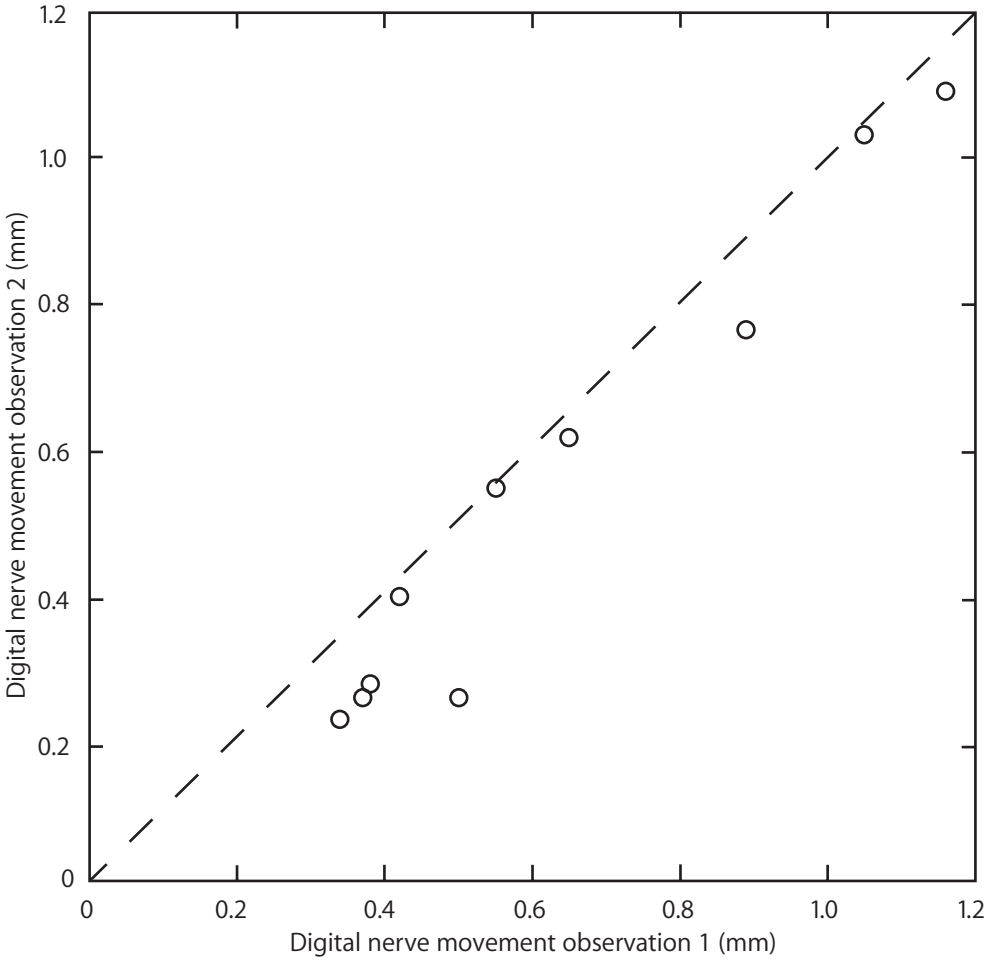

Figure 2. Test-retest plot of the digital nerve excursions from two separate measurements on the same 10 subjects.

two different volunteers were excluded because of out of plane motion was present. These were two re-test observations; this resulted in available test-retest data in ten healthy volunteers. All included movies following speckle tracking analysis showed an average cross-correlation of at least 0.9, which is very high.

RESULTS

Figure 2 shows the digital nerve movement recorded in ten subjects from which two recordings were successfully made. As can be seen there is a large variation between the subjects in digital nerve movement. However all data were highly similar between both observations. This was confirmed by a high intra-rater ICC between these two observations (0.948)

Summarizing the digital nerve movement for the whole group of 17 subjects (see Table 1), we found a mean displacement of 0.79 mm with a median of 0.65 mm. The range was 0.11-1.60 mm with a standard deviation of 0.43 mm.

DISCUSSION

Aim of this study was to quantify movement of the radial digital nerve in healthy control subjects using modern ultrasound image analysis. Imaging the nerve throughout the full extension movement of the upper extremity in combination with a relatively long learning curve is difficult. , The displacement could be reliably measured, as indicated by a high ICC of 0.95 between the first and second observation. In the group of 17 healthy controls digital nerve excursion was considerable compared to its surrounding tissue during upper limb movement, with excursions ranging from 0.11 to 1.60mm.

In the last decade, median nerve movement in the carpal tunnel during wrist movement and during different wrist positions has been extensively studied, resulting in highly variable outcomes. Yoshii et al.[222] used markers attached to the median nerve in cadavers and measured the movement of the markers while pulling the four FDS tendons. They found that the median nerve has the most excursion (9.3 mm) during movement around the neutral position of the wrist. Canuto et al assessed the neurovascular bundle movement using magnetic resonance imaging (MRI) in cadaver specimens. The bundle moved from a dorsal position to a ventral position with respect to the flexor tendons. However, no exact displacements were reported[24]. Ugbolue described median nerve movement during finger movements in a cadaver study and found median nerve excursion of up to 5 mm during index finger excursion[195]. Erel et al. studied longitudinal median nerve movement using ultrasonography and found a significantly reduced excursion in peripheral nerve repair patients compared to healthy controls, with a median excursion in healthy controls of 2.54 mm and 2.15 mm in nerve repair patients[43]. To our knowledge, findings on digital nerves have not been reported earlier. However, based on the approximately 3 mm excursion reported for the median nerve, in studies using a comparable technique to our study, the approximately 0.8 mm movement reported in our study seems plausible.

The visualization of the digital nerve in our study is relatively difficult to learn. Knowledge of the digital anatomy is essential, together with familiarization of the technical procedure and equipment. Out-of-plane motion during the recordings was the most important technical problem since the nerve is not only moving in longitudinal direction but also in a combination of transverse and anterior-dorsal direction. Therefore, in some cases, out of plane motion is inevitable and the movie had to be excluded.

The strength of this study is the ability to test our technique on healthy volunteers instead of cadavers. While in-vivo measurements will generally provide more accurate information about the actual physiology in human, this may be even more so when studying tendon or nerve gliding where the natural gliding can easily be altered in a cadaver specimen. The main limitation of this study is the relatively small number of subjects. Also we were obliged to exclude two movies out of 29 movies made in total. However, despite the relatively small number of subjects, we have shown that with the present technique we can measure digital nerve movement reliably. Further studies could evaluate

Table 1. Digital nerve movements (mm)

Volunteer	Observation 1	Observation 2
1	1.05	1.03
2	0.55	0.54
3	0.34	0.22
4	0.42	0.39
5	1.16	1.09
6	0.38	0.27
7	0.65	0.61
8	0.50	0.25
9	0.89	0.76
10	0.37	0.25
11	0.97	
12	1.02	
13	0.62	
14	1.21	
15	1.65	
16	0.11	
17	1.60	
Median	0.65	
range	0.11-1.60	
Standard deviation	0.43	
Mean	0.79	

both the reliability as well as the reference values for digital nerve movement in larger populations and well as in patients groups, such as patients at risk for developing a symptomatic neuroma.

The results of this study indicate that the combination of ultrasonography and "speckle tracking" is reliable for measuring digital nerve movement. Speckle tracking is already validated by Korstanje et al for tendon movement measurements[103], using the same properties of the ultrasonography movies as we used in nerve movements, which is the natural speckle pattern present in ultrasonography images. Dilley et al validated a similar tracking technique on nerves also using a frame to frame cross-correlation algorithm and gave accurate estimates for median nerve movement[34]. Therefore, we can consider this approach as a valid technique for ultrasonographic measurements of movement of either tendons or nerves. The high ICC of 0.95 we found in our study implies a high reliability of this approach as well.

The clinical implications of these findings are dual. First of all, the knowledge of digital nerve movements can be of influence for developing rehabilitation programs after digital nerve trauma. This is a frequently discussed topic in rehabilitation papers. The latest research on this topic gives no significant changes in outcome between early active rehabilitation versus fixation after digital nerve trauma[26,121,203]. For these programs, it is important to know if nerves move during upper limb movements at the various injury sites. Secondly, hypothetically, either a moving nerve, or a lack of movement of the nerve, might induce mechanical irritation. In nerve injuries scar tissue may impede nerve movements, which may result in an increased strain on the nerve during upper limb movement and therefore lead to mechanical irritation. On the other hand, if the nerve is not attached distally anymore after a nerve injury or amputation, the nerve may move even more proximally during upper limb movement. Using the present approach, we may in the future answer questions on, for example, the range of movement of the digital nerve differs per flexion zone in the palm of the hand and the mechanical irritation on different levels of nerve injury.

Chapter 10
General Discussion

Impairment of hand function is commonly diagnosed using clinical symptoms, physical examination, and static imaging. However, in specific diseases of the hand, such as carpal tunnel syndrome (CTS) or adhesion formations around tendons or nerves, a physical examination or static imaging is inadequate. This is because in the early onset of these diseases changes in hand function are commonly not yet present, whereas dynamics of the tendons and nerves might already have changed. For example, the clinical assessment of adhesions that can develop after hand flexor tendon reconstruction or repair is mainly based on a lacking range of motion (ROM) of the injured finger. Unfortunately, lacking of ROM is by definition a late symptom of tendon adhesions: before hand function is impaired, there will already be subtle changes in the dynamics of the associated tendons. Another example is the assessment of CTS, where changes in electromyography (EMG) are more commonly present in patients with more severe CTS while patients can already have disabling symptoms without EMG changes[93]. EMG is only moderately sensitive in diagnosing asymptomatic CTS, while small changes in the hand flexor tendons and median nerve (MN) might already be present. These examples illustrate the need for new ways to objectively and more accurately assess early changes in tendon and nerve dynamics in the hand. The following sections will discuss the main findings, generalizability, clinical importance, and directions for future research based on the studies described in the previous eight chapters.

Main findings

We developed and extensively validated an ultrasound (US) tracking algorithm specifically optimized for tracking tendons without using any anatomical landmarks (Chapters 2 and 3). We found that the US tracking algorithm is capable of measuring tendon excursions with high accuracy (<0.3mm mean absolute error, <2.7% mean relative error) over a broad range of velocities (4-16 mm/s) and displacements (5-15 mm). Because the US tracking algorithm does not use any anatomical landmark, its scope can be broadened to almost any tissue. For the general concept of block matching, this broadening is already seen by the increasing body of literature on US tracking of different tissues, e.g. heart, muscle, brain, and vessel wall[14,31,65,155]. We have also shown that the US tracking algorithm can be applied to images acquired with very different types of US configurations (mechanical probe versus linear array probe, very high center frequency versus medium to high center frequency, medium temporal resolution versus high temporal resolution) while maintaining high tracking accuracy. Furthermore, the algorithm is highly customizable to track different structures such as subsynovial connective tissue (SSCT) (see Chapters 5 and 8) and nerves (see Chapter 9), while maintaining high reliability (ICC>0.9). The most important parameters that need to be customized are kernel movement restriction (x-coordinate fixed, y-coordinate fixed, or both fixed), kernel size, kernel shape, number of overlapping kernels, and frame difference. The applicability of our US tracking algorithm and the effect of these parameters on tracking accuracy will be discussed in the following subsection

Applicability and generalizability

In this thesis we applied our US tracking algorithm to three specific structures: tendons, nerves, and SSCT. However, our US tracking algorithm was optimized specifically for tendons, which may therefore affect accuracy when applied to other structures. Another factor that could affect accuracy is the sensitivity of the US tracking algorithm to parameter settings, e.g. frame rate or frame difference, block size, contrast, and image enhancement. The following paragraphs will discuss these factors in relation to tracking accuracy.

The first factor that might influence tracking accuracy is the application of our US tracking algorithm to tissues other than tendons. Our US tracking algorithm was optimized for tendons, using the stiffness of tendons as a key feature. Because tendons show a highly coherent movement and small deformations, their stiffness can be exploited by using larger and elongated blocks in the

US tracking algorithm. This in contrast to commercially available block matching algorithms, which are mostly optimized for cardiac purposes using square-shaped and smaller kernels due to the relatively large deformation of the heart during contraction. When applying our US tracking algorithm to nerves, the exploit might be less effective as nerves are less stiff compared to tendons[63]. As a result, the kernel might be more prone to deformation and could therefore yield poorer matches and possibly poorer tracking accuracy[13,34]. On the other hand, under relatively low loading conditions of the nerve, the impact of the deformation on tracking accuracy might be relatively small. Moreover, the general concept had already been proven to achieve reasonable to good accuracy on nerves and tendons in a previous study[34].

The same reasoning might apply to tracking SSCT, as SSCT is even less stiff than nerves and might therefore also suffer from reduced tracking accuracy[63,64,145]. In addition, it should be noted that the SSCT is not a single structure but a layered structure[44,71], which inherently makes tracking of the complete structure less accurate because the displacement estimates becomes an average of the displacement of the different layers. Tracking several layers separately might not be feasible yet as the thickness of the total layer of the SSCT is already very thin (approximately 0.5 mm ≈ 7-25 pixels)[145] and therefore challenging for our US tracking algorithm. In summary, although SSCT tracking will give average displacements of the entire SSCT, it still provides valuable information on the overall dynamics of the SSCT and on the overall interaction between the SSCT and the hand flexor tendons and the MN.

Other factors that could have influenced tracking accuracy are physical limitations and parameter settings, either of the US machine or in the US tracking algorithm. The most important and potentially most influential parameters are out-of-plane motion, frame rate or frame difference, movement out of the region-of-interest (ROI), kernel shape, and kernel size.

Out-of-plane motion is caused by a misalignment of the scan head with respect to the tracked structure. Because of this misalignment, the structure moves in and out-of-plane and consequently the speckles move in and out-of-plane. The velocity of change in speckles is directly related to the out-of-plane velocity. So, a large misalignment will result in a large out-of-plane velocity, thereby rapidly changing the speckles. The consequence is that matching might be hampered. Although out-of-plane motion is not the only contributor to a lower normalized cross-correlation (NCC), out-of-plane motion can be identified by a drop in the NCC. The hampered matching is due to the speckles changing too rapidly to find a reasonable match from frame to frame, resulting in reduced tracking accuracy[55]. Fortunately, the effect of out-of-plane velocity on the matching accuracy is defined by an s-shape. Therefore, small misalignments will most likely have a small effect on matching accuracy and tracking accuracy while large misalignments will most likely have a very large effect on matching accuracy and tracking accuracy. It is thus important to prevent large misalignments, which can primarily be achieved by visual inspection. The most important visual aspect to identify out-of-plane motion is the rapid change in speckles, which can best be checked by visually following one speckle. If the speckle can be followed visually over a large portion of the motion than it is reasonable to assume minimal out-of-plane motion. For all studies using the US tracking algorithm, a visual inspection was performed during scanning to minimize out-of-plane motion.

It is also possible to further reduce the effect of out-of-plane motion by increasing the frame rate. Out-of-plane motion will result in rapid changes in the speckle pattern, but by increasing the frame rate the frame-to-frame change in the speckle pattern will be reduced. So, effectively, the frame-to-frame change in the speckle pattern is reduced by increasing the frame rate and could therefore reduce the effect of out-of-plane motion on the matching accuracy. However, the upper bound of the frame rate is mostly lim-

ited by hardware. Therefore, in a clinical setting, a high-end US scanner is needed to achieve high frame rates with minimal to no loss of spatial resolution. Although increasing the frame rate seems a successful approach to counteract reduced tracking accuracy, the downside could be a reduced tracking accuracy when the frame-to-frame displacement drops to 1-2 pixels[34], although the underlying mechanism is not understood. Therefore, very small frame-to-frame displacements should be avoided. This can be achieved by adapting the frame difference, which defines if the algorithm compares adjacent frames or frames further apart. For all studies in this thesis, the frame difference was kept constant while ensuring that small frame-to-frame displacements were kept to a minimum. Nevertheless, it is inevitable that the frame-to-frame displacement drops below the 1-2 pixels lower bound as tendons accelerate and decelerate during finger motion, assuming that the frame difference is kept constant. For future studies, it may therefore be valuable to automate the selection of the frame difference to prevent human biasing and increase tracking accuracy.

Besides out-of-plane motion, also structures moving out of the region of interest (ROI) influence tracking accuracy. Movement out of the ROI is common when tracking tendons, as tendons tend to move palmar during full gripping. As such, the tendon moves outside the original ROI. To prevent this, the algorithm is capable of moving the ROI in the y-direction of the image, following the movement in the axial direction.

Other parameters that influence tracking accuracy are the kernel shape and kernel size. The kernel shape used in our study was specifically optimized to track tendons by using an elongated rectangular shape. This allows capturing a number of full speckles of only the tendon within the US image. Squared kernels capturing full speckles might result in capturing more than the tendon alone. The advantage of capturing a number of full speckles is the unambiguousness of the kernel content, thereby lowering the number of false peaks in the 3D-NCC output (see Fig. 1) and thus increasing tracking accuracy[13]. False peaks are peaks in the 3D-NCC output that might mask the true peak corresponding to the best match. Consequently, the algorithm might give the wrong displacement estimate. As for the kernel shape, also the kernel size influences tracking accuracy. Similar as with the kernel shape, increasing the kernel size increases the number of speckles captured within the kernel. Again, the content of a larger kernel is less unambiguous, thereby lowering the number of false peaks and again increases tracking accuracy[13].

In summary, the US tracking algorithm is capable of accurately tracking tendons, but also other tissues such as nerves and SSCT. However, users should visually inspect the US recordings for out-of-plane motion and carefully select a suitable frame difference to minimize tracking errors by carefully analyzing tracking parameters such as the normalized cross correlation and the similarity of displacement estimates of the different kernels that are analyzed.

Future research towards clinical implementation

There has been an increasing interest in office-based US in the field of rehabilitation and physical medicine for a broad spectrum of diseases, conditions, or applications, e.g. soft tissue trauma, guided musculoskeletal interventions, and pain management[166,172,223]. The use of office-based US instead of MRI in soft tissue trauma could reduce costs dramatically.

Chapters 2 and 3 have shown that the US tracking algorithm is capable of measuring excursions of different structures. Although the present algorithm can already provide valuable insight in dynamics of tendons and nerves, the algorithm may be further extended by adding the ability to perform strain measurements. The present algorithm is already capable of tracking multiple kernels, enabling strain measurements as the difference in excursion between two kernels, normalized by the distance between the two kernels. Strain measurements can give added insight into changes in the dynamic behavior in, for example, the SSCT in CTS patients or tendon stiffness after reconstruction or repair. In CTS patients it is hypothesized that the SSCT becomes fibrotic and thus becomes stiffer. With

ULTRASOUND TRACKING

strain measurements this could be assessed in-vivo and possibly assessed locally within the SSCT. In tendon injury patients, for example, strain measurements could give more insight in the in-vivo loading capabilities of different suture techniques and of tendons during rehabilitation. Therefore, future research may focus on validating and optimizing the US tracking algorithm for strain measurements.

The new US tracking algorithm presented in this thesis could be the next step in office-based US. The algorithm enables physicians and therapists to accurately assess and follow tendon and nerve dynamics during recovery following trauma or surgery or to accurately diagnose diseases involving changes in tendon and nerve dynamics.

As a next step in developing an office-based technique, future research should focus on further automating and optimizing the US tracking algorithm to minimize inter-operator variance. Although almost fully automated, the present algorithm still requires manual tweaking of parameters such as the frame difference and search region. It has been shown by Dilley et al. that the frame difference can have a large influence on tracking accuracy and should therefore have priority to automate frame difference selection[34].

Besides increasing accuracy, also decreasing calculation time is essential. Overall, a single analysis of an audio-video interleave (AVI) or DICOM takes up to 30 minutes. When analyzing multiple patients with multiple recordings, calculation time increased to problematic levels. Automated adaptation of, for example, the size of the search region might decrease computational load and possibly calculation time.

Furthermore, it is important to keep track of the ongoing improvements of clinical US scanners, as some scanners already have the ability to measure displacements and sometimes strain, as discussed in the previous sections. Although these applications will mostly be optimized for cardiac tracking, the growing body of literature on US imaging of tendons and nerves might tip the scale towards other optimization paths on clinical US scanners.

Main findings

Several rehabilitation protocols can be used following hand flexor tendon reconstruction or repair, e.g. early active mobilization, passive Kleinert mobilization, or passive four-finger mobilization [1,33,101,126,127,170]. Although commonly accepted based on in-vitro studies and in-vivo studies with crude measures[78,128,149,174], it is still questionable whether active mobilization protocols facilitate larger tendon excursions compared to passive mobilization protocols in-vivo. With our novel ultrasound tracking algorithm we are now able to measure hand dynamics in-vivo with very high accuracy. In Chapter 4 and 5 we have shown a difference does exist in tendon excursion between active and passive mobilization protocols. However, differences in excursion between active and passive flexion were subtler than would be expected from literature. We have also demonstrated that the positions of the uninjured fingers are of great importance as they influence the excursion of the tendons of the injured finger or fingers significantly (see Chapter 5). Furthermore, we have shown it is possible to facilitate approximately the same tendon excursions with the modified Kleinert mobilization protocol with the uninjured fingers in full flexion compared to an active mobilization protocol. We have also demonstrated it is important to discriminate between excursion with respect to an external reference frame, e.g. bone or the hand as a whole (which is common practice) and excursion with respect to its surrounding tissue (see Chapter 5). When measuring excursion with respect to its surrounding tissue, only the active mobilization protocol, passive four-finger mobilization, and the modified Kleinert with uninjured fingers in flexion facilitated excursions larger than 5mm, which is a threshold thought to be sufficient to overcome tendon adhesions.

Study design, methodology, and generalizability

The study design of the hand flexor tendon studies was ex-

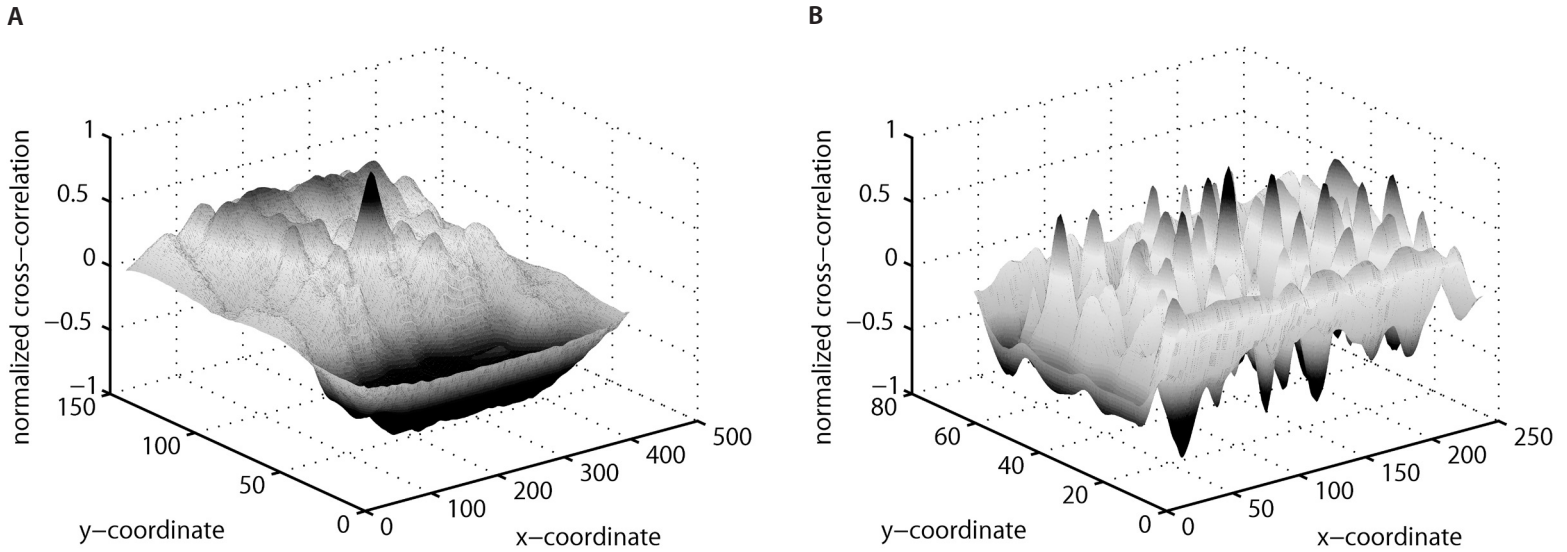

Figure 1. Showing the 3D-normalized cross-correlation (NCC) output matrix, which is the similarity measure used in the tracking algorithm to determine the best match for one kernel. A. The highest peak corresponds to the best match B. while with false peaks there are several high peaks that may lead to a wrong displacement estimate of one kernel. If the peak of the 3D-NCC output matrix is shifted with respect to the center of the graph, this shift is the actual displacement estimate of one kernel.

perimental and was primarily designed as a proof of concept. Because the design was primarily experimental, the number of subjects included in the studies was relatively low (n=10 and n=12). Nevertheless, even with a relatively small group size, we have shown significant differences are present between active and passive mobilization protocols, as discussed in Chapter 3 and 4.

Beside the small study size, there are some issues which could limit generalizability of our findings, such as the dynamic behavior of the SSCT more distal in the hand, the absence of SSCT in zones I and II, the clinical usability of the presented mobilization conditions, and the possible mismatch in population characteristics. These issues will be discussed in the following paragraphs.

The most important question is whether our findings in Zone V can be generalized towards more distal zones. In terms of absolute tendon excursion this seems straightforward as the hand flexor tendons are fairly stiff and, consequently, tendon elongation due to physiological loading is small. As elongation is very small with respect to the excursions of hand flexor tendons, it is reasonable to discard the influence of loading on the hand flexor tendon excursion and to extrapolate excursions found in Zone V towards Zones II, III, and IV.

However, in case of the SSCT excursion, this may not be true. The SSCT is a more elastic structure, consisting of layered bundles of collagen fiber running parallel to the surface of the tendon. The different layers are interconnected through smaller fibers, running perpendicular to the layered bundles of collagen[57]. This loose structure propagates the excursion of one layer to the next, creating a sort of telescopic structure. It is obvious that this structure is less stiff than the tendon to which it is connected[196]. Consequently, it is not straightforward to discard elongation of the SSCT with respect to its excursion. Although different from the SSCT in zone IV and V, it has been reported that the tendon sheath excursion in Zone II increases when measuring more proximally[214]. As much as a 4-fold increase in excursion was found measured at the metacarpal bone when compared at the MCP joint and approximately the same was observed at the MCP joint when compared to the proximal phalanx. This suggests that interpolating sheath excursions distally are not straightforward. Furthermore, the SSCT in Zone IV and V is essentially different from the tissue surrounding the tendons in Zone I and II[71]. Therefore, generalizability from zone V towards more distal zones seems limited and needs further research.

An aspect which should also be acknowledged, following the introduction of the two new mobilization models is patient comfort. The firm immobilization of the uninjured or adjacent fingers will inevitably decrease patient compliance, as it is very uncomfortable over longer periods of time. This is especially important as patient compliance during rehabilitation after tendon injuries is already a concern[160]. Therefore, a different approach should be considered when using these mobilization models. An alternative could be to use the mobilization models with the larger tendon excursion as an exercise instead of a full mobilization protocol. However, its effect in hand function outcome should still be studied before the mobilization model can be applied in a clinical setting.

Important to mention is also the mismatch of our sample with respect to the general population. In our studies we included relatively young, tall, and healthy volunteers. In the next three paragraphs we will discuss these three factors in relation to generalizability.

Data on the effect of aging on hand flexor tendon excursion is scarce. There are, however, a few studies, though conflicting. In-vitro analysis has shown that there are alterations in tendons with increasing age, such as increased collagen cross-linking and increased elastin content[143]. The increased cross-linking would suggest stiffening of the tendon while the increased elastin content would suggest the opposite effect. Also, a decrease

in collagen fibril diameter was found in an in-vitro animal study, suggesting thinner tendons with increasing age[28,86,89]. In contrast to the in-vitro studies, in-vivo studies showed that with increasing age the tendons were thicker by 22% and less stiff[143]. Although there might be an effect of age on tendon excursion, for our studies this was not of influence as we compared all excursions within individuals. However, when comparing between groups it would be advisable to crudely match by age.

The influence of hand length on hand flexor tendon excursion may be intuitively misperceived. Body height is related to hand length, which intuitively would suggest larger hand flexor tendon excursions. However, the opposite seems more plausible: it is not the finger length that directly dictates the tendon excursion but the finger depth. The linear relationship between finger depth and tendon excursion determines the moment arm, assuming the tendon follows the articular curvature tightly. Assuming that the articular curvature approximates a circle, then the radius of the curvature is approximately the joint depth[4,87,108]. Since it has been shown that the correlation between hand length and finger depth is low[133], body height is not likely to have any influence on tendon excursion and will therefore not limit generalizability.

The influence of asymptomatic volunteers on the measured excursion is without doubt a limitation. However, the studies in this thesis aimed at getting insight in tendon excursions facilitated by different mobilization protocols, not on clinical outcome after tendon reconstruction or repair. Nevertheless, healthy subjects do not suffer from edema, ROM limitation due to stiffness after surgery, altered tendon dynamics, and pain. While all these factors do influence tendon excursion and might therefore restrict generalizability, our results provide insight in the performance of different mobilization protocols following tendon reconstruction or repair. Hopefully, our findings may initiate new studies on improving clinical outcome after hand tendon lacerations in patients.

Clinical implications and future research

Results demonstrated that passive mobilization protocols, such as the four-finger mobilization protocol and the Kleinert mobilization protocol with the uninjured fingers in flexion, facilitate hand flexor tendon excursions similar to an active mobilization protocol (Chapter 5). These findings should encourage hand surgeons, rehabilitation physicians, and hand therapists to: 1) be aware that the adjacent fingers are important in obtaining maximal excursion, 2) consider the newly introduced mobilization models as a possibly valuable additional exercise, and 3) be aware that relative excursion gives valuable information when looking at tendon gliding in relation to adhesion formation.

In theory, the Modified Kleinert Flexion Mobilization Model combines the positive features of an active mobilization protocol (large excursions) and the positive features of a passive mobilization protocol (low rupture rates). However, in clinical practice, it is still unknown if this model will be more beneficial than an active mobilization protocol or the passive four-finger mobilization protocol and if the mobilization model is of real added value as an exercise. Future research should therefore focus on clinical outcome studies including the Modified Kleinert Flexion Mobilization Model, the four-finger mobilization protocol, and active mobilization protocol. Most preferably, this would be investigated in a randomized control trial (RCT) to increase the level of evidence and minimize biasing, although downsides would be the costs and administrative complexity of an RCT. A good first step would be to do a follow-up study to assess the associations between clinical outcome, patient comfort, patient compliance, and the modified Kleinert with uninjured fingers in flexion and compare these findings with conventional therapy found in literature. If the clinical outcome between the new Kleinert protocol and conventional therapy seems comparable, an RCT could be considered.

Main findings

It is already well established that CTS patients suffer from compression of the median nerve (MN) with changes in signal conduction through the MN and progressive hand function impairment. CTS is also associated with an increased cross-sectional area (CSA) of the MN. However, sensitivity and specificity showed a large variance when assessing the CSA of the MN using ultrasound. Several other parameters based on the MN also failed to decrease the large variance. The main contributor to this large variance may be the operator variability of US. We have shown that it is possible to measure parameters such as CSA, perimeter, and displacement of the MN and the hand flexor tendons reliably in healthy subjects. In addition, we have also created a set of normative values for the excursion of the MN and the hand flexor tendons (see Chapter 6). Supported by these findings, we have found (see Chapter 7) that normalizing the MN size parameters to the carpal tunnel size decreased operator variability and increased performance. Performance increased even more by adding hand flexor tendon variables to the prediction model. The clinically most suitable model included the normalized CSA of the MN, BMI, age, and gender and has a correct classification rate of 81.0%. The most extensive model including the perimeter of the MN, circularity of the middle finger FDP, and the perimeter of the middle finger FDP had a correct classification rate of 82.3%.

Furthermore, we established changes in the longitudinal excursion of the middle finger FDP and FDS in CTS patients (see Chapter 8); the most prominent finding was the decreased FDP excursion and increased FDS excursion, suggesting a compensatory mechanism that has already been established for the thumb but not for the fingers (James et al., 52nd Annual meeting of the orthopedic research society, Chicago, IL, 2006). Furthermore, we presented decision models for assessing CTS based on the longitudinal displacement data. However, we were able to correctly classify patients suspected of having CTS in approximately 70% of cases. The longitudinal excursion parameters most strongly associated with CTS were an increased MN excursion, an increased FDS excursion, and an increased SSCT FDP excursion.

Study design, methodology, and generalizability

The CTS studies focused on ultrasound as a new diagnostic tool using transversal images or longitudinal images. The transversal imaging study was a retrospective case-control study, while the longitudinal imaging study was a cross-sectional study comparing the most involved hand with the least involved hand.

One of the disadvantages of both the transversal and longitudinal imaging studies was the potential for recall bias and sampling bias. Recall bias is a type of bias in retrospective studies in which participants are asked to recall certain events or habits. Patients have the tendency to recall past events more rigorously than healthy people. In our studies, recall bias may not be an important problem because we used questionnaires that focused on symptoms and complaints that patients had on that specific moment or during the last few days (Chapter 7 and 8). However, sampling bias might be more of a problem. For the transversal imaging study, the control group consisted of mostly highly educated, relatively young subjects all working and having a relatively healthy lifestyle. This group might therefore not be representative for the overall population. Nevertheless, the CSA of the MN for the control group was consistent with literature (Chapters 6 and 7) and therefore sampling bias is less likely in the transversal imaging study. For both the transversal and longitudinal imaging studies, patients suspected of CTS were recruited at Erasmus MC, which is a university medical center and could therefore have more severe cases of CTS. However, all patients were referred to the Erasmus MC by the general practitioner; it could therefore be argued that sampling bias is minimal.

A possible disadvantage of the transversal imaging study is possible confounding, which is a general disadvantage of a case-control study design. BMI, age, and gender are risk factors for the

CARPAL TUNNEL SYNDROME

development of CTS and are associated with changes in the CSA of the MN (see Chapter 8)[95,148,150]. The case group was on average older, had a higher BMI, and the percentage of males not similar to the control group. Significant changes in the regression coefficients after correcting for age, gender, and BMI confirmed possible confounding; therefore, all models were corrected for age, gender, and BMI, making the models more robust and less prone to invalid generalizability.

For the longitudinal study we only included CTS patients to determine whether changes in the dynamics of the hand flexor tendons and MN can predict the outcome of clinical findings or EMG. To do so, we first compared the least affected hand with the most affected hand to see which parameters were potentially interesting for predicting CTS. Then we used logistic regression analysis using only the left hands to predict CTS based on clinical symptoms, EMG or a combination of both. We only used the left hands because combining both left and right hands would statistically be invalid. Moreover the left hand had a more balanced distribution of affected and unaffected hands. Downside to this study design is that clinical symptoms, EMG, or a combination of both are considered the gold standard, while this is still questionable[66,67,97]. To establish if ultrasound is suitable to diagnose CTS or at least can differentiate between CTS patients and healthy subjects, a future matched case-control study would be needed. Again, however, the lack of a gold standard would still be a problem.

In Chapter 8 we used logistic regression analysis, as the dependent variable was binary and we were interested in the performance of US variable to predict EMG and clinical outcomes. Due to the small group size, the logistic regression analysis relating hand dynamics and CTS should be interpreted with caution. This is reflected in relatively large confidence intervals of the regression coefficients. Additionally, the regression analyses included 2-term and 3-term interactions, which are less likely to be plausible explanatory variables, as more independent variables included in a model are more likely to better predict the dependent variable. On the other hand, interaction between hand flexor tendons and the MN is plausible because of the SSCT that connects these structures. Although the conclusions need to be interpreted with caution, we have shown that the prediction models can correctly classify patients suspected of having CTS in approximately 70% of cases using longitudinal excursions of the MN, hand flexor tendons, and SSCT.

Clinical implications and future research

Results from the transversal imaging study showed that CTS could be detected with relatively high sensitivity and specificity. This suggests that US could have added value to the existing suboptimal diagnostic tools in CTS or may even have the potential to replace EMG. Future research should focus on a larger group of cases and controls to define subgroups and establish whether asymptomatic CTS patients can also be identified correctly and consistently. Although expanding the original case-control study seems logical and most feasible, a longitudinal cohort study might also be valuable. The advantage of cohort study over a case-control study is that it enables for detecting timing and directionality of events.

In the longitudinal imaging study, results showed that CTS patients have small but detectable changes in hand flexor tendon and MN dynamics compared to their contralateral hand. Although this would allow easy assessment of CTS as the patient itself is both the case and the control, the classification model is very complex and has to be interpreted with caution. Therefore, the clinical impact of the present longitudinal imaging findings will be less significant than of the transversal imaging study, discussed in the next paragraph. Nevertheless, results have shown that small alterations in the tendon and MN dynamics are already present in CTS patients.

The lack of a proper golden standard makes it more complicated to assess new diagnostic tools [66,67,97]. A possible solution would be using the outcome after carpal tunnel release (CTR) as

a reference standard in a prospective longitudinal cohort study. The downside of such a study design could be that carpal tunnel release (CTR) is only successful in 75% of CTS patients and might also be beneficial for other diseases as well[16]. The 25% unsuccessful CTRs might be caused by the group of patients with severe CTS, in which the MN may be irreversibly damaged. Therefore, future research may focus on the assessment of US tracking as a diagnostic tool in a pre- and post-operative follow-up study excluding the severe CTS patients.

Obviously both the longitudinal imaging study and transversal imaging study have separately shown that there are detectable changes in tendon and nerve dynamics. Both studies included the same cases. Combining both studies to further improve the classification models to diagnose CTS is thus a relatively easy step forward. Therefore, future research could also focus on combining both longitudinal and transversal ultrasound findings both using a case-control study design to improve the classification models to diagnose CTS.

Main findings

In Chapter 9 we have demonstrated the US tracking algorithm is not only capable of tracking a thicker median nerve, but it can also track the digital nerve consistently and with very high reliability. On average, the digital nerve had an excursion of 0.59 mm and the intrarater correlation coefficient (ICC) was high (>0.9). It thereby demonstrates its broad versatility and applicability in tracking tendon and nerves of different sizes. Furthermore, we have gained valuable insight in digit nerve dynamics, which can be used for more in-depth research towards factors causing neuromas to become painful, such as mechanical irritation due to displacement of the nerve ending relative to its surrounding area.

Study design, methodology, and generalizability

The main study design was experimental, although, if continued, it could serve as the controls in a case-control study. From an experimental point of view, the study lacked a good reference standard to validate tracking accuracy on very small structures. Nevertheless, we found a high ICC, demonstrating that the US tracking is very reliable. Although reliability does not give information on accuracy, tracking parameters such as the NCC can help assess tracking accuracy. In our study, the NCC was always at least 0.9 or higher, suggesting that tracking was not hampered. In addition, it indicates there was minimal out-of-plane motion and that the deformation due to loading was minimal. Therefore, it is reasonable to assume that tracking the digital nerve is accurate and may therefore be pursued in a case-control study. Furthermore, if the study would be continued in a case-control design, sampling bias might be an issue as the controls were young, highly educated, had a healthy lifestyle, and did not perform hard labor. This would than be a poor reflection of the general population and might jeopardize generalizability. Therefore, when pursuing a case-control design, more suitable controls could be added to overcome selection bias.

In summary, we have shown that even for very small and elastic structures tracking is possible and reliability is very high. This suggests that generalizability is valid and the tendon-optimized US tracking algorithm is capable of tracking not only tendons but also small nerves.

Clinical implications and future research

Our study has demonstrated the US tracking algorithm is capable of tracking very small structures. One clinical implication is that the US tracking algorithm can be applied to very small structures such as the digital nerve or the superior median nerve. It should be noted, however, it took very extensive practice sessions by the examiner (DJJC van der Avoort) to be able to visualize the nerve and to maintain the nerve in field of view during its complete motion. The next logical step would be to do a case-control study as data of the controls are already available and a cohort study might be too cumbersome, as painful neuromas are

relatively rare. As discussed in the tracking section, strain measurements would be an added value in this case-control study, because not only excursion but also strain might lead to mechanical irritation.

Summary

Chapter 1 discussed why dynamic imaging of the hand and wrist would give valuable insight in the complex interaction between tendons, nerves, and their surrounding tissue during hand movements. Dynamic imaging could provide clinicians and therapists with valuable information to objectively diagnose patients, or to follow progress in patients over time. However, the dynamic behavior of the hand and its tendons and nerves is hard to capture with a clinical imaging modality, let alone to quantify its behavior. Several studies focused on the development of ultrasound tracking algorithms, mainly on cardiac tracking and some on nerve tracking. The main challenge in using these algorithms for measuring dynamics of tendons and nerves lies in the optimization needed for soft tissue tracking, which leaves room for further optimization towards tendon tracking. The following chapters tried to answer the question whether quantifying dynamic behavior of tendons and nerves in the hand and wrist during hand movements is possible using ultrasound. If so, is it also possible to differentiate between normal and abnormal dynamic behavior for a number of diseases of the hand using ultrasound?

The development of the ultrasound tracking algorithm optimized for tracking tendons was described in Chapters 2 and 3. The tracking algorithm was extensively validated in-vitro, ex-vivo, and in-vivo and was capable of tracking tendons with high accuracy over a broad range excursions and velocities. Furthermore, the ultrasound tracking algorithm was capable of tracking excursions larger than the field of view of the ultrasound scanhead and the ultrasound tracking algorithm was successfully used on different ultrasound scanners. The average tracking accuracy in-vitro was 1.3%, ex-vivo was 1.0%, and in-vivo was 1.6%. These promising results were the start of the implementation of the ultrasound tracking algorithm in a clinical setting, thereby focusing on 1) tendon dynamics in the hand and wrist, 2) tendon and nerve dynamics in the hand and wrist, and 3) nerve dynamics in the hand.

In Chapters 4 and 5 we focused on the hand tendon flexor dynamics in the hand and wrist, specifically during mobilization protocols used following hand flexor tendon reconstruction or repair. There are two mainstream mobilization protocols, namely early active mobilization and passive mobilization. Although commonly accepted based on in-vitro studies and in-vivo studies with crude measures, it is still questionable whether active mobilization protocols facilitate larger tendon excursions compared to passive mobilization protocols in-vivo. Findings presented in Chapter 4 showed that in-vivo excursions obtained during active finger movement were significantly larger than obtained during passive finger movement.

Based on these findings the passive mobilization protocols were extended to determine adjacent finger dependency on the absolute excursion and relative excursion and were compared with each other and the active mobilization protocol. The rationale behind the adjacent finger dependency was that the subsynovial connective tissue surrounds and interconnects the hand flexor tendons and median nerve and may therefore transfer forces from one tendon or nerve to the other. Findings presented in Chapter 5 showed that absolute excursions obtained during the active mobilization protocol were significantly larger than obtained during passive mobilization protocols. Furthermore, the positioning of the adjacent fingers in full flexion resulted in larger absolute excursions compared to a neutral position or in full extension. More importantly, relative excursions were very dependent on the position of the adjacent fingers. Relative excursions obtained during the active mobilization protocol were comparable to the excursion obtained during the passive mobilization protocol with the fingers in full flexion, thereby showing the influence of the subsynovial connective tissue and the importance of adjacent finger position during mobilization with respect to tendon excursion.

In Chapters 6, 7, and 8 we focused on the hand flexor tendons and median nerve dynamics in the hand and wrist, specifically on the diagnostic value of ultrasound to assess carpal tunnel syndrome (CTS). Up until now, the diagnose CTS is

mainly based on clinical symptoms supported by electromyography (EMG) findings. Although EMG is becoming more commonly accepted as gold standard, it still performs only reasonable as EMG still misses between 16% and 34% present of cases.

In Chapter 6 we presented a validation study to assess CTS using ultrasound images of the carpal tunnel transversally. In these images we outlined the hand flexor tendons and median nerve several times by several investigators to assess the operator dependency. We showed that for the variables area, perimeter, and circularity of the hand flexor tendons and median nerve we found an intrarater correlation coefficient ranging from 0.64 up to 0.97 and an interrater correlation coefficient of -0.17 up to 0.94. We thereby showed that the there is considerable operator dependency.

Based on these findings we assessed different approaches to increase the performance of the classification models based on logistic regression using transversal ultrasound images of the hand flexor tendons and the median nerve in a case-control study. In Chapter 7, we showed that the classification model was greatly improved when normalizing the area of the MN with respect to the area of the carpal tunnel to reduce operator variance. Furthermore, we showed that assessing the ultrasound variables during forceful gripping instead of full extension of the hand only minimally improved the classification model. Finally, the classification model with only the normalized area of the MN performed almost equally well as the extensive model. This model included the perimeter of the MN, the circularity of the middle finger FDP both at full extension, and the perimeter of the middle finger FDP at forceful gripping. Interestingly, however, the hand flexor tendons do seem to contain valuable information alongside with the MN to identify CTS, because the ultrasound variables of the hand flexor tendon were selected the classification model.

In Chapter 8 we assessed the diagnostic value of longitudinal hand flexor tendon and median nerve dynamics using the ultrasound tracking algorithm discussed in Chapters 2 and 3. In this study we compared the most affected hand with the least affect hand of CTS patients. We showed that there were considerable changes in the excursions of the FDP and FDS tendons and the median nerve. Interestingly, we found an increased FDS tendon excursion and decreased FDP tendon excursion in the most affect hand of CTS patients compared to the least affect hand, which may suggest activation of compensatory mechanisms and/or increased adhesions in the subsynovial connective tissue. Furthermore, the developed classification models to diagnose CTS had a correct classification rate ranging from 67% up to 86%.

In Chapter 9 we focused on the nerve dynamics in the hand, specifically the digital nerve. In this study we assessed the reproducibility of measurements of digital nerve excursions and thereby assessed the robustness of our ultrasound tracking algorithm. We found that our ultrasound tracking algorithm is capable of tracking very small structures consistently and reliable, thereby showing the broad applicability of our ultrasound tracking algorithm.

Finally, in Chapter 10 we discussed the main findings with respect to the main questions discussed in Chapter 1, methodological issues, generalizability of the main findings, clinical implications, and the recommendations for future research. In Chapters 2, 3, and 9 we demonstrated that the ultrasound tracking algorithm was capable of accurately tracking tendons, large nerves, and very small nerves during different hand movements. In Chapters 4 and 5 we demonstrated that using the ultrasound tracking algorithm we were capable of identifying which mobilization protocol used after tendon repair or reconstruction facilitates the largest tendon excursions in terms of absolute and relative tendon excursions. We thereby demonstrated that when positioning the adjacent fingers correctly passive mobilization protocols are capable of facilitating relative tendon excursions comparable to active mobilization. We thereby answered the question if it would be possible to quantify the dynamic behavior of tendons and nerves in the hand during hand movement using ultrasound, which was the first aim

of this thesis. The next aim of this thesis was to determine whether the ultrasound tracking algorithm was capable of differentiating between normal and abnormal dynamic behavior of hand flexor tendons and nerves. In Chapter 7 we demonstrated that using transversal ultrasound images we were capable of correctly classifying 83% of CTS patients and healthy controls. In Chapter 8 we demonstrated that using the ultrasound tracking algorithm we were capable of differentiating between the most and least affected hands of CTS patients based on longitudinal excursions of the middle finger FDP and FDS tendons and the median nerve. Using these parameters we can correctly classify up to 86% of the hands. We thereby demonstrated that using ultrasound we were able to differentiate between normal and abnormal dynamic behavior of the hand flexor tendons and the median nerve in CTS.

Samenvatting

Hoofdstuk 1 beschrijft hoe dynamische beeldvorming van de hand en pols waardevol inzicht kan geven in de complexe interactie tussen pezen, zenuwen en het omliggende weefsel. Dynamische beeldvorming kan clinici en therapeuten waardevolle informatie geven om patiënten objectiever te diagnosticeren of om genezing van patiënten over de tijd te volgen. Echter, de dynamica van de hand en meer specifiek van de pezen en zenuwen is moeilijk te vangen met klinische beeldvormende modaliteiten, laat staan het kunnen kwantificeren van de dynamica. Verschillende studies richtten zich op de ontwikkeling van ultrageluid *tracking* algoritmes, veelal specifiek gericht op het *tracken* van het hart en in sommige gevallen gericht op het *tracken* van zenuwen. De grootste uitdaging in de doorontwikkeling van deze algoritmes voor het meten van pees- en zenuwdynamica is de optimalisatie voor zacht weefsel; dit laat ruimte over voor optimalisatie voor pezen. De volgende hoofdstukken zullen trachten de vraag te beantwoorden of het mogelijk is om pees- en zenuwdynamica in de hand en pols te kwantificeren tijdens handbewegingen gebruikmakende van ultrageluid. Vervolgens zal getracht worden antwoord te geven op de vraag of ultrageluid het mogelijk maakt om te differentiëren tussen normale en abnormale pees- en zenuwdynamica in verschillende ziekten. Als laatste zal getracht worden antwoord te geven op de vraag wat de prestatie van ultrageluid is wanneer deze gebruikt wordt als diagnosticum.

Hoofdstukken 2 en 3 beschrijft de ontwikkeling van het ultrageluid *tracking* algoritme welke is geoptimaliseerd voor pezen. Het ultrageluid *tracking* algoritme hebben we zowel in-vitro, ex-vivo en in-vivo zeer uitvoerig gevalideerd en het bleek mogelijk om pezen te *tracken* met zeer hoge nauwkeurigheid in een groot bereik van excursies en snelheden. Bovendien bleek via het ultrageluid *tracking* algoritme om peesexcursies groter dan het *field of view* van de scanhead te meten en was het ultrageluid *tracking* algoritme te gebruiken op beelden van verschillende ultrageluidscanners. De gemiddelde *tracking* nauwkeurigheid in-vitro was 1,3%, ex-vivo was 1,0% en in-vivo was 1,6%. Deze veelbelovende resultaten luidden de start in voor implementatie van het ultrageluid *tracking* algoritme in een klinische setting, waarbij de focus lag op: 1) peesdynamica in de hand en pols, 2) pees- en zenuwdynamica in de hand en pols en 3) de zenuwdynamica in de hand.

Hoofdstukken 4 en 5 waren gericht op de flexorpees dynamica in de hand en pols, specifiek tijdens mobilisatie protocollen die werden ingezet na hand flexorpees reconstructie of reparatie. De mobilisatie protocollen zijn op te delen in twee hoofdgroepen, namelijk de vroege actieve mobilisatie en de passieve mobilisatie. Alhoewel het algemeen geaccepteerd is op basis van in-vitro en in-vivo studies gebruikmakende van grove schattingen, is het tot op heden nog steeds twijfelachtig of actieve mobilisatie protocollen leiden tot meer peesexcursie dan passieve mobilisatie protocollen. De resultaten gepresenteerd in Hoofdstuk 4 laten zien dat in-vivo peesexcursies gemeten tijdens actieve vingerbeweging significant meer is dan gemeten tijdens passieve vingerbeweging.

Gebaseerd op de in Hoofdstuk 4 gepresenteerde resultaten hebben we de passieve mobilisatie protocollen uitgebreid om te bepalen wat de invloed van de positie van de naastliggende vingers is op de absolute en relatieve peesexcursie. De redenatie hierachter is dat de naastliggende vingers invloed uitoefenen op elkaar door het *subsynovial connective tissue*; dit weefsel verbindt namelijk de hand flexorpezen en de nervus medianus waardoor krachten mogelijk overgebracht kunnen worden van de ene pees of zenuw op de andere. De resultaten gepresenteerd in Hoofdstuk 5 laten zien dat de absolute peesexcursie gemeten tijdens het actieve mobilisatie protocol significant hoger was dan gemeten tijdens verschillende passieve mobilisatie protocollen. Verder bleek dat de positionering van de naastliggende vingers in flexie leidde tot meer absolute peesexcursie dan wanneer gepositioneerd in een neutrale stand of in extensie. Belangrijker nog, de relatieve excursie blijkt zeer afhankelijk te zijn van de positie van de naastliggende vingers. De tijdens het actieve mobilisatie protocol

gemeten relatieve excursies bleken in grote mate gelijkwaardig te zijn aan de relatieve excursies gemeten tijdens het passieve mobilisatie protocol met de vingers in flexie gepositioneerd. Dit suggereert dat het *subsynovial connective tissue* van invloed is op de peesexcursie en dat het daarbij belangrijk is om de naastliggende vingers te positioneren in flexie tijdens mobilisatie. Dit impliceert namelijk een mogelijk verlaagde kans op verklevingen en dus sneller herstel.

Hoofdstukken 6, 7 en 8 beschrijven de pees- en zenuwdynamica in de hand en pols en met name de diagnostische waarde van ultrageluid in de diagnostisering van carpaal tunnel syndroom (CTS). Tot op heden is de diagnostisering van CTS gebaseerd op klinische symptomen en kenmerken ondersteund met bevindingen verkregen door elektromyografisch (EMG) onderzoek. Alhoewel EMG steeds meer geaccepteerd wordt als gouden standaard, blijkt dat middels EMG tussen de 16% en 34% van de CTS patiënten niet correct worden gediagnosticeerd.

Hoofdstuk 6 presenteert de validatie van ultrageluid als diagnosticum in CTS gebruikmakende van de transversale beelden van de carpale tunnel. In deze beelden werden de hand flexorpezen en nervus medianus meerdere malen handmatig door verschillende gebruikers aangegeven om zodoende de gebruikersafhankelijkheid te bepalen. Voor oppervlakte, omtrek en rondheid van de hand flexorpezen en nervus medianus hebben wij een intra-beoordelaarsbetrouwbaarheid van 0,64 tot 0,97 gevonden en een inter-beoordelaarsbetrouwbaarheid -0,17 tot 0,94. Daarbij hebben wij aangetoond dat de beoordelaarsafhankelijkheid groot is.

Op basis van de bevindingen beschreven in Hoofdstuk 6 hebben we verschillende methoden gebruikt om de prestaties van de classificatie modellen te verbeteren. Hierbij hebben we gebruik gemaakt van logistische regressie op transversale ultrageluid analyses van de carpale tunnel. Dit hebben we onderzocht in een patiënt-controle-onderzoek. In Hoofdstuk 7 laten wij zien dat de classificatie modellen grote prestatie verbeteringen laat zien wanneer de oppervlakte van de nervus medianus wordt genormaliseerd; normalisatie van de oppervlakte van de nervus medianus naar de oppervlakte van de carpale tunnel reduceert namelijk beoordelaarsafhankelijkheid. Verder hebben wij vastgesteld dat wanneer de ultrageluid variabelen gemeten worden tijdens een krachtige vuist de classificatie modellen minimaal verbeteren ten opzichte van ultrageluid variabelen gemeten tijdens een hand in volle extensie. Als laatste hebben wij laten zien dat het classificatie model met alleen de genormaliseerde oppervlakte van de nervus medianus bijna vergelijkbaar presteert als het uitgebreide classificatie model. Dit model omvatte de omtrek van de nervus medianus en de rondheid van de middelvinger FDP beide gemeten tijdens volledige extensie en de omtrek van de middelvinger FDP gemeten tijdens een krachtige vuist. Een interessante bevinding was dat de hand flexorpezen naast de nervus medianus waardevolle informatie bevatten, dit bleek uit het feit dat de ultrageluid variabelen van de hand flexorpezen werden geselecteerd in de classificatie modellen om CTS te voorspellen.

In Hoofdstuk 8 hebben we de diagnostische waarde van ultrageluid bij CTS geëvalueerd; hierbij hebben we gebruik gemaakt van het ultrageluid *tracking* algoritme om de longitudinale hand flexorpees en nervus medianus dynamica te kwantificeren. We hebben laten zien dat er duidelijke veranderingen zijn in de excursie van de FDP en FDS pees en de nervus medianus. Een interessante bevinding was een grotere FDS pees excursie en een kleinere FDP pees excursie in de meest aangedane hand van CTS patiënten in vergelijking met de minst aangedane hand. Dit zou kunnen suggereren dat er een compenserend mechanisme wordt geactiveerd en\of meer verklevingen van de *subsynovial connective tissue* zijn. Verder hebben we laten zien dat de door ons ontwikkelde classificatie modellen om CTS te diagnosticeren tussen de 67% en 86% van de CTS patiënten correct classificeerden.

Hoofdstuk 9 was gericht op de zenuw dynamica in de hand, specifiek de digitaal zenuw. In dit hoofdstuk hebben we de reproduceerbaarheid en robuustheid van het ultrageluid *tracking* algoritme geëvalueerd door excursies te meten van de di-

gitaal zenuw. Hierbij hebben we aangetoond dat het ultrageluid *tracking* algoritme in staat is om zeer kleine structuren consistent en betrouwbaar te meten en daarmee breed inzetbaar is.

Afsluitend hebben we in Hoofdstuk 10 de algemene bevindingen in het licht van de algemene onderzoeksvragen geplaatst en bediscussieerden we de algemene methodologische problemen, generaliseerbaarheid van de algemene bevindingen, klinische impact en de aanbevelingen voor verder onderzoek. In Hoofdstukken 2, 3 en 9 hebben we aangetoond dat het ultrageluid *tracking* algoritme in staat is om pezen en grote en kleine zenuwen nauwkeurig te volgen tijdens verschillende handbewegingen. In Hoofdstuk 4 en 5 hebben we aangetoond dat gebruikmakend van het ultrageluid *tracking* algoritme het mogelijk is om te bepalen welk mobilisatie protocol de grootste absolute en relatieve pees excursie oplevert. We hebben daarbij ook aangetoond dat wanneer de aanliggende vingers correct worden gepositioneerd de passieve mobilisatie protocollen relatieve pees excursies kunnen opleveren die vergelijkbaar zijn met actieve mobilisatie protocollen. Daarmee beantwoorden we direct de eerste algemene vraag in dit proefschrift, namelijk of het mogelijk zou zijn om pees- en zenuwdynamica in de hand te kwantificeren middels ultrageluid. De tweede algemene vraag in deze thesis was of het mogelijk zou zijn om middels ultrageluid te differentiëren tussen normale en abnormale dynamica van de flexorpezen en de zenuwen in de hand. In Hoofdstuk 7 hebben we aangetoond dat door middel van transversale ultrageluidbeelden we in staat zijn 83% van de CTS patiënten en gezonde controles correct te classificeren. In Hoofdstuk 8 hebben we aangetoond dat middels het ultrageluid tracking algoritme we in staat zijn te differentiëren tussen de meest en minst aangedane hand in CTS patiënten gebaseerd op longitudinale excursies van de FDP en FDS van de middel vingers en de nervus medianus. Daarmee hebben we antwoord gegeven op de tweede algemene vraag in dit proefschrift, namelijk dat we in staat zijn om te differentiëren tussen normale en abnormale dynamica van de hand flexorpezen en de nervus medianus in CTS.

PhD Portfolio

Presentations	Year	ECTS
Meten van de dynamica van pees bewegingen met behulp van echografie	2007	0.2
Praktijk Opleiding Handtherapie 2007		
Ultrasound imaging of tendon dynamics in arm and hand	2008	0.2
Biomedical Engineering, Thoraxcenter, Erasmus MC.		
Meten van dynamica van pees bewegingen met behulp van echografie	2008	0.2
Dept. of Rehabilitation Medicine and Physical Therapy		
Meten van dynamica van pees bewegingen met behulp van echografie	2008	0.2
Dept. of Plastic and Reconstructive Surgery		
Ultrasound imaging of tendon dynamics in arm and hand	2008	0.2
Dept. of Biomedical Engineering, Delft University of Technology		
Handiness of ultrasound	2010	0.2
Dept. of Plastic and Reconstructive Surgery		
Highly accurate speckle tracking for measurement of tendon and nerve dynamics in the hand	2010	1.1
Dept. of Orthopedic Surgery, Mayo Clinic, Rochester (MN), USA		
Oral presentations at conferences		
Dedicated ultrasound speckle tracking to study displacement	2009	1.1
SPIE Medical Imaging 2009, Lake Buena Vista (FL), USA		
Accuracy of dedicated ultrasound speckle tracking to quantify tendon displacement	2009	0.2
2nd Dutch BME Conference 2009, Egmond aan Zee, The Netherlands		
Influence of finger positions on tendon excursions during different passive mobilization protocols	2010	0.6
World Congress on Biomechanics 2010, Singapore		
Dedicated ultrasound speckle tracking to study tendon displacement	2010	0.6
World Congress on Biomechanics 2010, Singapore		
Novel tracking algorithm to objectively and accurately asses tendon gliding	2009	0.4
13th European Conference of Scientist and Plastic Surgeons (ECSAPS), Rotterdam, The Netherlands		

Supervising students	Year	ECTS
Supervising medical student (Niels Noordzij)	2008-2009	2.9
Supervising medical student (Jors van der Sijde)	2009-2010	2.9
Supervising Delft University of Technology students (Esma Safiue and Jonathan Zoentrum)	2009-2010	1.4
Supervising Haagse Hogeschool students (Jordi Evers and Evelien Dubbeldeman)	2009-2010	1.4
Supervising medical student (Richard van Balen)	2010-2011	2.9
Supervising medical student (Joris Snijders)	2010-2011	1.4
Supervising medical student (Anika Filius)	2010-2011	1.4
Lecturing		
Medical students third year (keuze onderwijs thema 3.2)	2009	0.2
Courses\Lectures		
Principles or reasearch in medicine and epidemiology (ESP01)	2009	0.7
Introduction to data-analysis (ESP03)	2010	1.0
Integrity in scientific research	2010	2.0
English biomedical writing	2010	2.0
Research meetings		
Dept. of Rehabilitation Medicine and Physical Therapy	2007-2011	5.6
Dept. of Plastic and Reconstructive Surgery	2009-2010	1.0
Dept. of Plastic and Reconstructive Surgery and Rehabiliation (labmeeting)	2011	1.0
Total ECTS		31.2

Dankwoord

DANKWOORD

Na vier jaar onderzoeken ligt dan nu voor u mijn dissertatie, gekscherend mijn boekje genoemd. U leest het goed: onderzoeken, niet onderzoek. Als gup word je aangesteld om onderzoek te gaan verrichten, niet beseffende dat het neer komt op onderzoeken. Onderzoeken van je proefpersonen, patiënten, data, artikelen, mede-onderzoekers, bazen, bazen boven bazen en bovenal jezelf. Wat je allemaal wel niet te weten komt over jezelf is een wonder op zich. Specifieke karakter eigenschappen komen te pas en te onpas boven borrelen, om zich te doen laten gelden om je vervolgens ontredderd achter laten mogelijk met het nodige schaamrood op de kaken. Neem nou eigenwijsheid, iets wat mij niet onbekend is; het komt en het gaat zoals zijn gegeven naam, namelijk op zijn eigen wijze. Vele om mij heen hebben meerdere malen mogen ervaren hoe ik op eigen wijze of eigenwijs hetgeen onderzocht wat onderzocht moest worden of juist wat niet onderzocht had hoeven worden. Een kenmerkend bewijs hiervan ligt voor u, een eigenwijs boekje welke niet in de kast past zoals u het wellicht zou willen. Het weerspiegelt wellicht de visie van haar eigenaar of wellicht die van haar maker. In dezelfde eigenwijsheid is dit dankwoord ook niet geheel zoals u het wellicht zou verwachten. Zo correct als ik poog te zijn zal het speelse kleine kind in mij en aan mijn hand de wereld tegemoet treden. Het speelse in dit dankwoord is de *wordcloud* waarin praktisch alle namen staan van mensen met wie ik in meer of mindere mate mail contact heb onderhouden. Het gestileerde element in deze zal niemand zijn ontgaan, een hand welke als thema van mijn boekje kan worden betiteld als ook een hand bij wijze van dank en afscheid. Terugkomende op mijn gepoogde correctheid, mogelijk soms als keurslijf ervarende, zal ook ik mij conformeren om in een verwoede poging te komen tot een waardig dankwoord. Veelal zijn dankwoorden prachtige stukken proza waarin elke gelaten traan en aderlating zijn verworden tot ware heldendaden of triomftochten ontstaan in een zucht van verlichting. Echter, onderzoek leerde mij dat verwoede pogingen tot hoogstaande proza, wellicht in je stoutste dromen reikend tot aan de hemel, vaak hebben geleid tot droge romannetjes. Iets wat ook niet al te best samen gaat. Welnu, ik zal pogen u op correcte wijze mee te nemen in mijn dankbaarheid richting een aantal individuen zonder welke de totstandkoming van dit proefschrift, mijn boekje, niet mogelijk zou zijn geweest.

Allereerst en principieel om wie het echt gaat in welk klinisch onderzoek dan ook is de patiënt. Mijn dank gaat uit naar alle patiënten die zich vrijwillig overgaven aan al mijn onderzoeken. U was vaak het gouden randje om een dag in de kliniek en was nooit te beroerd om enkele en soms vele verhalen uit de spreekwoordelijke stoffige oude doos te halen.

Alvorens patiënten bloot te stellen aan mijzelf en mijn onderzoeken waren veelal vrienden en collegae de eerste proefpersonen. Ook hier ben ik dankbaar voor al uw geduld wanneer ik u voor de zoveelste keer vastbond aan mijn “martelwerktuig” in de naam van de wetenschap (zie de foto’s in de betreffende artikelen voor een impressie).

Vooruitlopende op de zaken gaat mijn dank uit naar de heren commissieleden welke de tijd en moeite hebben genomen en nog zullen nemen om deze dissertatie grondig te ontleden ware het een anatomisch preparaat. Dit geschreven hebbende, gaat mijn dank uit naar prof. dr. Kleinrensink, prof. dr. Veeger en dr. ir. Bosch als leden van zowel de kleine als ook de grote commissie. Daarnaast gaat mijn dank uit naar prof. dr. Amadio, prof. dr. van Doorn en prof. dr. French, mijn TU Delft afstudeer professor welke mij de mogelijkheid heeft geboden mijn onderzoek te verschuiven richting het Erasmus MC.

Uiteraard wordt een promotie vanuit hogere hand gestuurd en geschuurd om deze tot een succes te laten geworden. Allereerst gaat mijn dank uit naar mijn eerste promotor prof. dr. H.J. Stam. Hartelijk dank voor het vertrouwen in mij en de mogelijkheid die u mij heeft gegeven om naast mijn studie geneeskunde een promotie aan te durven. Uw eigenzinnige en vrijelijke manier van leiding geven was en is voor een eigenwijze promovendus als mijzelf een ware ver-

ademing. Daarnaast gaat mijn dank uit naar mijn tweede promotor, prof. dr. S.E.R. Hovius. Ook voor u geldt dat ik u zeer dankbaar ben voor het gegeven vertrouwen en alle mogelijkheden die u heeft geboden. Uw correcte en strakke manier van leiding geven maakte en maakt dat elk overleg altijd als succesvol kon worden geschouwd.

Als eerste en uiteindelijk enige copromotor ben ik dr. R.W. Selles veel dank verschuldigd. Ruud, mijn eigenwijze, wellicht soms koppige manier van aanpakken en doorpakken is niet altijd een makkelijke taak om in goede banen te leiden. Ik refereer onder andere aan mijn eindeloze gepruts in de marge wat schrijven betreft. Gelukkig kon ik in het proces leunen op de begenadigd schrijver die je bent. Deze dissertatie is daar mede het ultieme bewijs van dat dit alles gelukt is.

In de aanloop naar een promotie ben ik dr. ir. J.G. Bosch veel dank verschuldigd. Hans, als begeleider tijdens mijn afstuderen aan de TU Delft bleek al snel dat mijn accuraatheid al snel verwelkte tot een zakhorloge zonder tourbillon in vergelijking met het Zwitserse uurwerk als jij bent. Bijna vanzelfsprekend gaat de tijd uit de pas lopen en is het bijstellen van het loopwerk wenselijk. Zo geschreven, zo gedaan. Zie deze dissertatie als bewijs.

Deze gehele dissertatie berust op geluid, ultrageluid wel te verstaan. Mijn dank is daarbij groot voor W. van 't Leven op wie ik dagelijks een beroep kon doen wanneer er problemen waren rondom de ultrageluid techniek in de kliniek. Daarnaast hebben de afdelingen, mede dankzij jouw inzet, een prachtige Philips iU22 als ultrageluid scanner!

Daarnaast heb ik in het begin van mijn onderzoek veel op de 23e gezeten, ofwel de dames en heren van het échte ultrageluid! De gezelligheid, vooral na werk, was altijd een aangename afwisseling! Mijn tijd op de 23e was een mooie afsluiting van jaren in de ingenieurs-wereld, al zal ik de ingenieur in mij nooit vaarwel zeggen.

De laatste artikelen in deze dissertatie zijn mede tot stand gekomen door de tomeloze inzet van de afdeling Neurologie en Klinische Neurofysiologie. In het bijzonder gaat mijn dank uit naar dr. J.H. Blok en drs. M. Schelten-de Boer. Beide hebben jullie veel moeten verduren met het stroomlijnen van patiëntenzorg richting onderzoek, het beoordelen van patiënten en het lezen van de manuscripten en vele andere zaken rondom het onderzoek. Daarnaast ben ik veel dank verschuldigd aan R.J. Veldhuizen en alle baliemedewerkers van de beide afdelingen.

De artikelen met betrekking tot peesletsel en mobilisatie protocollen leunen sterk op de inbreng van de mannen uit de kliniek: dr. A.R. Schreuders en J.N.M. Soeters. Ton, jouw sereniteit en expertise waren altijd een goede afwisseling op de "fast lane" van het onderzoek. Hans, jouw ongelofelijke precisie en enthousiasme met betrekking tot handtherapie en mobilisatie protocollen was keer op keer een welkome aanvulling!

Locatie-technisch gezien lopen de gangen ietwat door elkaar, maar aan de overkant van de handtherapie resideren de senioren van de revalidatie. De open deur mentaliteit van alle senioren is altijd een goede eigenschap van een afdeling en komt ook zeker ten goede van de sfeer. Iedereen hartelijk dank voor de open en vriendelijke sfeer al deze jaren. In het bijzonder wil ik nog dr. H.P. Slijper bedanken. Harm, thanks voor alle koffietjes en lunches waarin we zo af en toe zalig de rest van de wereld konden afzeiken en allemaal zo goed wisten hoe het allemaal wél had gemoeten, een beetje zoals de twee oude opaatjes uit de muppets! Ik hoop je nog vaak tegen te komen op het Erasmus MC of in alle andere ziekenhuizen waar je de patiënttevredenheid aan de top wilt krijgen! Daarnaast wil ik Betty Koehorst, Hetty Mulder en Carin Oostdijk bedanken voor alle secretariële afhandelingen!

Als we nu de afslag links nemen komen we bij het handenlab, waar veelal patiënten in en uit lopen om "gemeten" te worden. Daarnaast was de snoeppot en de gezelligheid altijd vast prik om toch even snel naar beneden te gaan! Emiel, Herwin en Carlijn bedankt voor alle gezelligheid en borrels! Ik hoop jullie nog regelmatig tegen te komen in de kliniek!

Steeds dichter komen we dan bij mijn dagelijkse verblijf op de 16e, maar niet voordat we eerst op de 15e komen. Mijn dubbelaanstelling op zowel de "plastische" als de "reva" leek wat weg te hebben van een gespleten persoonlijkheid. De snelle wereld van de plastische staat in schril contrast met de rust overdenkende wereld van de reva. Het was dan ook een zeer aangename afwisseling om dan eens koffie te drinken, te lunchen, te dineren of te borrelen met de plastici en dan weer met de reva's. Daarvoor allen dank en in het bijzonder Hester, Dirk Jan, Tim, Ernst, Liron en Anika. Ik zie jullie snel weer in de kliniek en vast nog vaker in de DE! Speciaal voor de laatste, Anika: ik wens je heel veel sterkte met het vervolg van dit onderzoek. De "fast lane" zit duidelijk in je en ik zie er naar uit om samen met het hele team je te begeleiden om je promotie tot een waar huzarenstuk te maken!

Nu zijn we dan echt aangekomen op mijn dagelijkse verblijf, de 16e! Het was eerst even wennen om in een omgeving gedomineerd door bewegingswetenschappers m'n weg te vinden. Ik wist dat ingenieurs elkaar altijd konden herkennen en vaak elkaar aantrokken, maar voor de bewegingswetenschapper is dit niet minder waar. Maar wat een relaxte tijd heb ik gehad op de 16e. Er was altijd wel tijd om weer een goeie grap uit te halen, een thuisbioscoop op het werk in te richten om de tour of de olympische spelen te volgen of om gewoon lekker een filmpje te pakken! Daarnaast waren jullie altijd wel in om te borrelen of gewoon even een hapje ergens te eten! De FRANK borrel was daarbij altijd een mooie gelegenheid om nog maar eens een biertje te doen. Plots kwam dit geheel tot een abrupte stilstand door het afschuwelijke verlies van Marian.

Lieve Marian, vanaf het begin zaten we bij elkaar op de kamer en was je de hardwerkende en goedlachse onderzoekster! Altijd was je op zoek naar nieuwe spannende uitdagingen, welke zowel in als buiten je onderzoek tot uiting kwamen. Binnen je onderzoek bleek je een ware analyticus te zijn en bestreed je vurig alle onkunde rondom je onderzoek. Buiten je onderzoek was je altijd bezig om mensen aan te sporen om te gaan sporten of om even gezellig te gaan borrelen of ergens even te eten. Dit alles was plots slechts een herinnering toen we het bericht te horen kregen dat je nooit meer zou terug keren van je geliefde berg. De stilte die je achterlaat is oorverdovend…

Maar zoals met alles zijn de fysische wetten door niets of niemand te buigen en bleef de aarde met zijn almachtige snelheid van 1031 km/u doordraaien. Nu dit dankwoord schrijvende gaan we straks dan toch maar weer naar de FRANK borrel als afsluiting van mijn jaren op de 16e. Monique, Jorrit, Karin, Javad, Carla, Nienke, Diana, Robert, Lyam, Sjel, Hedwig en Helmi, het was fantastisch en ik zie uit naar de volgende borrel!

Naast promoveren moest er ook nog gestudeerd worden. Samen met o.a. Milly, Jeroen, Jors en Richard hebben we een briljante tijd gehad in de niet-live zalen, maar ook daarbuiten in alle kroegen. Samen met Jors heb ik mijn eerste klinische artikel gepubliceerd en met Richard heb ik een jaar lang samen gewerkt aan één van de kroonstukken van dit boekje. Richard, thanks voor de fantastische inzet en zie het resultaat!

Gelukkig bestond de dag niet geheel uit werken, maar was er 's avonds zo nu en dan ook nog tijd voor gezelligheid met oude en nieuwe vrienden. In het verlengde van werk hebben we elkaar leren kennen, Markus en Thomas. Inmiddels zien we elkaar regelmatig onder het genot van goed eten en fantastische gesprekken reikend van toch weer ons werk tot en met de volgende vakantietrips naar verre bestemmingen. Dank jullie beide voor jullie enorme warmte en interesse en ik hoop dat we nog jaren elkaar kunnen verrassen met toch weer nieuwe interessante en spannende gerechten. Ennuh: het is geen wedstrijd, het is genieten!

Indirect toch via werk leren kennen, maar dan via Lydi: Gijs & Janine en Emma & Egbert. Als oude studievrienden van Lydi en nu goede vrienden van ons beide is het altijd genieten als we

weer eens samen zijn om bij te praten over alle spannende dingen die ons allemaal zijn overkomen. Veelal gaat het over coschappen, opleidingen, promotie en uiteindelijk de grote toekomst! Dank jullie voor alle gezelligheid en de onuitputtelijk bron aan informatie over alles wat mij in de kliniek nog te wachten staat.

Met een kleine stap precies tussen oude en nieuwe vrienden in zijn we bij onze oude buren aangekomen. Rob, Chloë en kleine Yanne! Alle etentjes, koffietjes en oppas acties waren en zijn nog steeds een gezellige en leuke afleiding. Snel weer eens afspreken om te zien hoe groot Yanne al weer is geworden!

Nu komen we dan langzaam aan in het gebied dat echt buiten werk valt. Mijn oude vrienden. Jan Jaap, man wat hebben we toch een hoop meegemaakt. Het begon allemaal zo rond de ontgroening toen we als kleine guppen bedacht hadden toch maar lid te worden. De jaren die volgde waren overladen met borrels, feesten, wedstrijden, etentjes, vakanties en altijd weer die vrouwen of soms misschien wel het tekort er aan! Inmiddels zijn we het tijdperk van onze studententijd voorbij en zijn we toch verdacht veel gaan lijken op echte burgers. Had je dat ooit gedacht? Topmanager geworden verantwoordelijk voor alles wat spoort of misschien wel ontspoort, vrouwlief Marijke voor het leven op de kop getikt en eindelijk dan volop gelukkig! Ik hoop dat we nog decennia lang kunnen praten over vroeger, nu en over de toekomst!

Ergens in de jaren tussen sjaars en burger kwam jij, Jan bij ons clubje. Samen met je toen nog bijna vrouw en nu al weer een aantal jaren je échte vrouw, Nelja, was je altijd de echte goede nuchtere Fries. Je was stiekem ons geweten en was altijd onze steun en toeverlaat als iemand van ons clubje het weer eens niet zo goed kon vinden met z'n toekomst! Jan en ook Nelja, spannende tijden wachten op jullie in het krijgen van jullie eerste kind én bovenal misschien wel het avontuur in het buitenland. In alles staan ik en natuurlijk Lydi altijd voor jullie klaar en we komen jullie zeker achterna!

Bastiaan, als tweedejaars vonkentrekkers leerde we elkaar kennen. Als goede studenten was de studie bijzaak en waren borrels en feesten de gelegenheden waar de studiepunten te scoren waren. Wat dat betreft liepen we ruim nominaal. Vele studentensteden en studentenverenigingen waanden zich veilig totdat de Delftenaren zich aankondigde. Realiteit haalde ons echter bijna in en beide werden we toch wat serieuzer. Alvorens echt het studentenleven de rug toe te keren hebben we als afsluiting de sjaars nog een mooie week bezorgd of toch misschien onszelf? Nu hebben we toch mooi onze bul op zak, al was het voor beide in een andere studierichting dan waar we mee begonnen waren. Inmiddels ben je duidelijk de burger zelve: woont samen met een fantastische vrouw Heleen, zijn de borrels terug gedraaid tot gezellige avondjes thuis met vrienden, en ben je de werkende man geworden. Binnenkort maar weer burgerlijk een gezellige avond met z'n vieren plannen!

Vrienden zijn letterlijk dicht bij en familie figuurlijk dicht bij. Lieve schone ouders, wat gaat de tijd toch snel als je lol hebt. Ruim vier jaar geleden leerde ik Lydi kennen en was mijn ervaring met schoonouders niet om over naar huis te schrijven. Echter, vanaf de eerste kennismaking met jullie was het een thuis weg van huis. Jullie zijn fantastische schone ouders; staan altijd klaar voor ons, willen altijd het naadje van de kous weten en zijn echte lieverds met een eigenwijze twist! Behalve het leren kennen van schone ouders krijg je daar altijd ook je zwagers en schoonzus bij cadeau… en wat voor een cadeautjes! Lieve Pieter, Charly en Arthur, jullie grote zus "inpikken" is niet niks natuurlijk, maar ik ben super blij dat we het zo relaxt met elkaar kunnen vinden. Pieter en Anne, super ambitieus, maar altijd oog voor anderen! Bewonderenswaardig! Charly en Sander, een supercombo van zorgzaamheid en focus! Wat wil je nog meer als schoonzus en zwager! Arthur en Ruby, de keiharde marinier en de zachtaardige dame, bijna sprookjesachtig. Jullie doorzettingsvermogen is ontzag waard.

Mijn lieve bruder, ik heb nu al vier jaar de nodige pakken cornflakes zitten versmaden en wat blijkt… t zat er niet in. Ik moest m'n boekje toch echt zelf schrijven en zie hier, het ligt er

dan toch! Je bent en blijft m'n kleine broertje, de slimmere van de twee alleen niet de snelste ;)! Vroeger liep je fier achter je grote broer aan, ik volleyballen, jij volleyballen. Ik skiën, jij skiën. Ik studeren, jij studeren. Ik roeien, jij roeien. Ik vriendin, jij vriendin. Ik samenwonen, jij samenwonen. Ik promoveren, jij promoveren. Ik een gepromoveerde partner, jij een bijna gepromoveerde partner. Ok, hier loopt de vergelijking dan langzaam spaak. Ik ben super trots op je broertje van me! Lieve Suzan, perfect passend bij mijn kleine broertje. Let je goed op 'm als ie weer eens meent Einstein te zijn en zichzelf bijna ten gronde richt om de Nobelprijs binnen te halen? Ik bewonder je enorme doorzettingsvermogen en je fantastische focus op de kleinere op deze wereld!

Lieve pa en ma, wat een jaar hebben we met z'n allen meegemaakt. De omslag van altijd gezond naar plots ernstig ziek was niet misselijk. De achtbaan waarin we met z'n allen raakte van polibezoeken, naar UMCs, naar opname voor chemo, bestralingen, opname voor OK, nogmaals OK en plotse IC opname kon op zijn zachts gezegd niet tippen aan een six-flags bezoekje. Gelukkig konden we als gezin de boel super draaiende houden en pa elke dag bij staan! Het leek ook bijna alsof iemand boven de pionnen zo had bespeeld dat ik en Lydi als medici de medische kant konden regisseren, Ties en Suzan de stabiele factor waren en de zorg rondom pa konden regisseren, en dat jij, ma, je volledig kon bezig houden met pa alleen! Ik ben dan ook super trots op ons gezin en vooral op jullie beide! Hoe jullie je door deze periode hebben heen geslagen was fenomenaal en geeft de sterkte van ons gezin weer! Ik hou van jullie!

De laatste alinea is natuurlijk alleen voor jou: dokter Piefie! Jij bent mijn grootste voorbeeld en inspirator! Mijn sparringpartner en mentor. Mijn paranimf en oppositie. Professioneel gezien ben je magistraal en probeer ik je bij te benen waar ik kan en te leren wat ik kan. Arts, doctor, master of science en ook nog even zonder blikken of blozen de enige externe AIOS van de MDL dit jaar! Hoe fantastisch is het om jou als partner te hebben. Privé gezien ben je mijn piefie. Je bent mijn geweten en mijn duiveltje op mijn schouder. Hoe geweldig is het om een zorgzame, lieve, slimme, eigenwijze en mooie vrouw te hebben waar je van mag zeggen dat jij haar partner bent! Ik ben zo onnoemelijk trots op je en dat vergeet ik nog wel eens te zeggen. Lieve pief, ik ben trots op jou! Op alles wat je

bereikt hebt, op wie je bent, op hoe je in het leven staat en op hoe je mooi alles voor elkaar hebt in je leven als dokter! Ik kijk uit naar alle dagen dat we samen ergens op de wereld rose-tjes drinken, patienten casussen bespreken en ondertussen fantastisch kunnen genieten van elkaar tussen al het dokteren door! Lieverd, ik hou van jou!

List of Publications

D.J.J.C. van der Avoort, **J.-W.H. Korstanje**, P.H.C. Leliefeld, R.W. Selles, S.E.R. Hovius, H.H. Coert. Quantification of Digital Nerve Movement During Upper Limb Extension Using Modern Ultrasonography Analysis. Submitted to Journal of Orhtopedic Research.

J.-W.H.Korstanje, M. Scheltens-de Boer, J.H. Blok, P.C. Amadio, S.E.R. Hovius, H.J. Stam, R.W. Selles. Ultrasonographic Assessment of Longitudinal Median Nerve and Hand Flexor Tendon Dynamics in Carpal Tunnel Syndrome. Submitted to Muscle and Nerve

J.-W.H. Korstanje, R. van Balen, M. Scheltens-de Boer, J.H. Blok, H.P. Slijper, H.J. Stam, S.E.R. Hovius, R.W. Selles. Ultrasonographic Assessment of Transversal Tendon and Nerve Dynamics in CTS Patients Versus Healthy Controls.

A. Filius, **J.-W.H. Korstanje**, Y. Hoendervangers, R.W. Selles, S.E.R. Hovius, H.P. Slijper. Reliability of Ultrasonographic Measurements of Median Nerve and Flexor Tendons. Submitted to Journal of Ultrasound in Medicine and Biology.

J.-W.H. Korstanje, J.N.M. Soeters, T.A.R. Schreuders, P.C. Amadio, S.E.R. Hovius, H.J. Stam, R.W. Selles. Ultrasonographic Assessment of Different Flexor Tendon Mobilization Protocols; Effect on Long Finger Tendon Excursions Compared to its Surrounding Tissue. Submitted to Journal of Bone and Joint Surgery American Edition

J.-W.H. Korstanje, T.A.R. Schreuders, J. van der Sijde, S.E.R. Hovius, J.G. Bosch, R.W. Selles. Ultrasonographic Assessment of Third Finger Tendon Excursion During Passive and Active Tendon Gliding Exercises in zone V. American Journal of Hand Surgery 35A (2010) 559–565.

J.**-W.H. Korstanje**, R.W. Selles, H.J. Stam, S.E.R. Hovius, J.G. Bosch. Development and Validation of Ultrasound Speckle Tracking to Quantify Tendon Displacement. Journal of Biomechanics 43 (2010) 1373–1379.

J.-W.H. Korstanje, R.W. Selles, H.J. Stam, S.E.R. Hovius, J.G. Bosch. Dedicated Ultrasound Speckle Tracking to Study Tendon Displacement. Proc. SPIE 7265, 726505 (2009).

ARTICLES

J.N.M. Soeters, **J.-W.H. Korstanje**, A.R. Schreuders, S.E.R. Hovius, H.J. Stam, R.W. Selles. Influence of the Position of the Adjacent Fingers on the Excursion of the FDP Tendon in a Kleinert Mobilization Protocol. Abstracts of the Xth International Congress of EFSHT.

A. Filius, **J.-W.H. Korstanje**, Y. Hoendervangers, R.W. Selles, S.E.R Hovius, H.P. Slijper. Changes in Shape and Displacement of the Median Nerve and Tendons in the Carpal Tunnel. Abstracts of the XVIth International Congress of FESSH.

J.-W.H. Korstanje, R.W. Selles, H.J. Stam, S.E.R. Hovius, J.G. Bosch. Novel Automated Tendon Tracking to Assess Tendon Movement Without Anatomical Landmarks. Book of Abstracts of the World Congress on Biomechanics 2010.

J.-W.H. Korstanje, J.N.M. Soeters, T.A.R. Schreuders, H.J. Stam, S.E.R. Hovius, R.W. Selles. Influence of Finger Positions on Tendon Excursions and Excursions of Surrounding Tissue During Different Passive Mobilization Protocols. Book of Abstracts of the World Congress on Biomechanics 2010.

J.-W.H. Korstanje, T.A.R. Schreuders, J. van der Sijde, S.E.R. Hovius, H.J. Stam, J.G. Bosch, R.W. Selles. Differences Between Passive and Active Movements of the Hand in Tendon Excursion in Zone V with Accurate In-vivo Ultrasound Measurement. Abstracts of the XVth International Congress of FESSH.

D.J.J.C. van der Avoort, **J.-W.H. Korstanje**, P. Leliefeld, R.W. Selles, S.E.R. Hovius, J.H. Coert. Neurodynamics of the Digital Nerve. Abstracts of the XVth International Congress of Federation of FESSH.

J.-W.H. Korstanje, J.G. Bosch, H.J. Stam, S.E.R. Hovius, R.W. Selles. Accuracy of Dedicated Ultrasound Speckle Tracking to Quantify Tendon Displacement. Book of Abstracts of the First Dutch Conference on Bio-Medical Engineering 2009.

N.A.Noordzij, **J.-W.H. Korstanje**, J.G. Bosch, S.E.R. Hovius, G.J. Kleinrensink, R.W.Selles. Validating Tendon Gliding Measurement Without the Presence of Anatomical Landmarks Using Ultrasound Imaging. Book of Abstracts of the XIVth International Congress of FESSH.

R. Selles , **J.-W.H. Korstanje** , H. Stam , S. Hovius , H. Bosch. Quantification of Tendon Movement Without the Presence of Anatomical Landmarks Using Ultrasound Imaging. Gait & Posture,Volume 28, Supplement 2, September 2008, Pages S15-S16 Abstracts of the 17th Annual Meeting of ESMAC.

R.W. Selles, J.G. Bosch, **J.-W.H. Korstanje**, H.J. Stam, S.E.R Hovius, P.J. French, N. de Jong. Quantification of Tendon Dynamics in the Hand Flexors Using High-Frequency Ultrasound Imaging. Book of Abstracts of the First Dutch Conference on Bio-Medical Engineering 2007.

R.W. Selles, **J.-W.H. Korstanje**, H.J. Stam, S.E.R. Hovius, J.G. Bosch. Quantification of Tendon Dynamics in the Hand Flexors Using High-Frequency Ultrasound Imaging. Book of Abstracts of European Conference of handsurgery and handtherapy 2007.

ABSTRACTS

References

1. **Allen BN, Frykman GK, Unsell RS, Wood VE. Ruptured flexor tendon tenorrhaphies in zone II: repair and rehabilitation.** *J. Hand Surg. [Am.].* **Jan 1987;12(1):18-21.**

2. **Allmann KH, Horch R, Uhl M, et al. MR imaging of the carpal tunnel.** *Eur. J. Radiol.* **Sep 1997;25(2):141-145.**

3. **American Association of Electrodiagnostic Medicine, American Academy of Neurology, and American Academy of Physical Medicine and Rehabilitation. Practice parameter for electrodiagnostic studies in carpal tunnel syndrome: summary statement.** *Muscle Nerve.* **Jun 2002;25(6):918-922.**

4. **An KN, Chao EY, Cooney WP, 3rd, Linscheid RL. Normative model of human hand for biomechanical analysis.** *J. Biomech.* **1979;12(10):775-788.**

5. **An KN, Takahashi K, Harrigan TP, Chao EY. Determination of muscle orientations and moment arms.** *J. Biomech. Eng.* **Aug 1984;106(3):280-282.**

6. **Arampatiz A, Stafilidis S, DeMonte G, Karamanidis K, Morey-Klapsing G, Brüggeman GP. Strain and elongation of the human gastrocnemius tendon and aponeurosis during maximal plantarflexion effort** *J. Biomech.* **2005;38(4):833-841.**

7. **Armstrong TJ, Chaffin DB. An investigation of the relationship between displacements of the finger and wrist joints and the extrinsic finger flexor tendons.** *J. Biomech.* **1978;11(3):119-128.**

8. **Atroshi I, Gummesson C, Johnsson R, Ornstein E. Diagnostic properties of nerve conduction tests in population-based carpal tunnel syndrome.** *BMC Musculoskelet Disord.* **May 7 2003;4:9.**

9. **Atroshi I, Gummesson C, Johnsson R, Ornstein E, Ranstam J, Rosen I. Prevalence of carpal tunnel syndrome in a general population.** *JAMA.* **Jul 14 1999;282(2):153-158.**

10. **Bal S, Oz B, Gurgan A, et al. Anatomic and functional improvements achieved by rehabilitation in Zone II and Zone V flexor tendon injuries.** *Am. J. Phys. Med. Rehabil.* **Jan 2011;90(1):17-24.**

11. **Basmaijan JV.** *Biofeedback: principles and practice for clinicians***. Baltimore: Williams & Wilkins; 1989.**

12. **Beekman R, Visser LH. Sonography in the diagnosis of carpal tunnel syndrome: a critical review of the literature.** *Muscle Nerve.* **Jan 2003;27(1):26-33.**

13. **Behar V, Adam D, Lysyansky P, Friedman Z. The combined effect of nonlinear filtration and window size on the accuracy of tissue displacement estimation using detected echo signals.** *Ultrasonics.* **Mar 2004;41(9):743-753.**

14. **Behar V, Adam D, Lysyansky P, Friedman Z. Improving motion estimation by accounting for local image distortion.** *Ultrasonics.* **Oct 2004;43(1):57-65.**

15. **Bircan C, El O, Akalin E, et al. Functional outcome in patients with zone V flexor tendon injuries.** *Arch. Orthop. Trauma Surg.* **Jul 2005;125(6):405-409.**

16. **Bland JD. Treatment of carpal tunnel syndrome.** *Muscle Nerve.* **Aug 2007;36(2):167-171.**

17. **Bohs LN, Trahey GE. A novel method for angle independent ultrasonic imaging of blood flow and tissue motion.** *IEEE Trans. Biomed. Eng.* **1991;38(3):280-286.**

18. **Bor-Ray L, Huihua Kenny C, Cheng-Deng K, Win-Li L, San-Kan L. Doppler angle and flow velocity estimations using the classic and transverse Doppler effects.** *IEEE Trans. Ultrason., Ferroelectr., Freq. Control.* **1999;46(1):252-256.**

19. **Boyer MI, Goldfarb CA, Gelberman RH. Recent progress in flexor tendon healing. The modulation of tendon healing with rehabilitation variables.** *J. Hand Ther.* **Apr-Jun 2005;18(2):80-86.**

20. **Buck-Gramcko D, Dietrich FE, Gogge S. [Evaluation criteria in follow-up studies of flexor tendon therapy].** *Handchirurgie.* **1976;8(2):65-69.**

21. **Bunnell S. Repair of tendons in the fingers.** *Surg. Gynecol. Obstet.* **1922;35(88-97).**

22. **Buschbacher RM, Prahlow ND.** *Manual of nerve conduction studies***. Second ed: New York, N.Y.: Demos Medical Publishing; 2006.**

23. **Buyruk HM, Holland WPJ, Snijders CJ, et al. Tendon excursion measurements with colour doppler imaging: A calibration study on an embalmed human specimen.** *J. Hand Surg. [Br.].* **1998;23(3):350-353.**

24. **Canuto HC, Oliveira ML, Fishbein KW, Spencer RG. Tendon and neurovascular bundle displacement in the palm with hand flexion and extension: an MRI and gross anatomy correlative study.** *J. Magn. Reson. Imaging.* **May 2006;23(5):742-746.**

25. **Cetin A, Dincer F, Kecik A, Cetin M. Rehabilitation of flexor tendon injuries by use of a combined regimen of modified Kleinert and modified Duran techniques.** *Am. J. Phys. Med. Rehabil.* **Oct 2001;80(10):721-728.**

26. **Chao RP, Braun SA, Ta KT, et al. Early passive mobilization after digital**

nerve repair and grafting in a fresh cadaver. *Plast. Reconstr. Surg.* **Aug 2001;108(2):386-391.**

27. Chen H, Shi H, Varghese T. Improvement of elastographic displacement estimation using a two-step cross-correlation method. *Ultrasound Med. Biol.* **Jan 2007;33(1):48-56.**

28. Chino O, Osamura Y, Kise Y, et al. Acceleration of the proliferative activity of esophageal carcinoma with invasion beyond the muscularis mucosae; immunohistochemical analysis using MIB-1 for the Ki-67 antigen. *Tokai J. Exp. Clin. Med.* **Dec 2007;32(4):115-120.**

29. Cigali BlS, Buyruk HM, Snijders CJ, et al. Measurement of tendon excursion velocity with colour Doppler imaging: a preliminary study on flexor pollicis longus muscle. *Eur. J. Radiol.* **1996;23(3):217-221.**

30. Cinthio M, Ahlgren AR, Jansson T, Eriksson A, Persson HW, Lindstrom K. Evaluation of an ultrasonic echo-tracking method for measurements of arterial wall movements in two dimensions. *IEEE Trans Ultrason Ferroelectr Freq Control.* **Aug 2005;52(8):1300-1311.**

31. Clatz O, Delingette H, Talos IF, et al. Robust nonrigid registration to capture brain shift from intraoperative MRI. *IEEE Trans. Med. Imaging.* **Nov 2005;24(11):1417-1427.**

32. Cobb TK, Cooney WP, An KN. Aetiology of work-related carpal tunnel syndrome: the role of lumbrical muscles and tool size on carpal tunnel pressures. *Ergonomics.* **Jan 1996;39(1):103-107.**

33. Cullen KW, Tolhurst P, Lang D, Page RE. Flexor tendon repair in zone 2 followed by controlled active mobilisation. *J. Hand Surg. [Br.].* **Nov 1989;14(4):392-395.**

34. Dilley A, Greening J, Lynn B, Leary R, Morris V. The use of cross-correlation analysis between high-frequency ultrasound images to measure longitudinal median nerve movement. *Ultrasound Med. Biol.* **Sep 2001;27(9):1211-1218.**

35. Dimitriou M, Edin BB. Discharges in human muscle receptor afferents during block grasping. *J. Neurosci.* **Nov 26 2008;28(48):12632-12642.**

36. Doyle FH, Gore JC, Pennock JM, et al. Imaging of the brain by nuclear magnetic resonance. *Lancet.* **Jul 11 1981;2(8237):53-57.**

37. Duncan I, Sullivan P, Lomas F. Sonography in the diagnosis of carpal tunnel syndrome. *Am. J. Roentgenol.* **Sep 1999;173(3):681-684.**

38. Duran R, Houser R. Controlled passive motion following flexor tendon repair in zones 2 and 3. Paper presented at: AAOS Symposium on Tendon Surgery in the Hand1975; St. Louis.

39. Edinburg M, Widgerow AD, Biddulph SL. Early postoperative mobilization of flexor tendon injuries using a modification of the Kleinert technique. *J. Hand Surg. [Am.].* **Jan 1987;12(1):34-38.**

40. Elliot D, Moiemen NS, Flemming AF, Harris SB, Foster AJ. The rupture rate of acute flexor tendon repairs mobilized by the controlled active motion regimen. *J. Hand Surg. [Br.].* **Oct 1994;19(5):607-612.**

41. Ellis R, Hing W, Dilley A, McNair P. Reliability of measuring sciatic and tibial nerve movement with diagnostic ultrasound during a neural mobilisation technique. *Ultrasound Med. Biol.* **Aug 2008;34(8):1209-1216.**

42. Erel E, Dilley A, Greening J, Morris V, Cohen B, Lynn B. Longitudinal sliding of the median nerve in patients with carpal tunnel syndrome. *J. Hand Surg. [Br.].* **Oct 2003;28(5):439-443.**

43. Erel E, Dilley A, Turner S, Kumar P, Bhatti WA, Lees VC. Sonographic measurements of longitudinal median nerve sliding in patients following nerve repair. *Muscle Nerve.* **Mar 2010;41(3):350-354.**

44. Ettema AM, Amadio PC, Zhao C, Wold LE, An KN. A histological and immunohistochemical study of the subsynovial connective tissue in idiopathic carpal tunnel syndrome. *J. Bone Joint Surg. Am.* **Jul 2004;86-A(7):1458-1466.**

45. Ettema AM, Amadio PC, Zhao C, et al. Changes in the functional structure of the tenosynovium in idiopathic carpal tunnel syndrome: a scanning electron microscope study. *Plast. Reconstr. Surg.* **Nov 2006;118(6):1413-1422.**

46. Ettema AM, An KN, Zhao C, O'Byrne MM, Amadio PC. Flexor tendon and synovial gliding during simultaneous and single digit flexion in idiopathic carpal tunnel syndrome. *J. Biomech.* **2008;41(2):292-298.**

47. Ettema AM, Belohlavek M, Zhao C, Oh SH, Amadio PC, An KN. High-resolution ultrasound analysis of subsynovial connective tissue in human cadaver carpal tunnel. *J. Orthop. Res.* **Oct 2006;24(10):2011-2020.**

48. Ettema AM, Zhao C, Amadio PC, O'Byrne MM, An KN. Gliding characteristics of flexor tendon and tenosynovium in carpal tunnel syndrome: a pilot study. *Clin. Anat.* **Apr 2007;20(3):292-299.**

49. Farron J, Varghese T, Thelen DG. Measurement of tendon strain during

muscle twitch contractions using ultrasound elastography. *IEEE Trans Ultrason Ferroelectr Freq Control.* **Jan 2009;56(1):27-35.**

50. Feuerstein M, Miller VL, Burrell LM, Berger R. Occupational upper extremity disorders in the federal workforce. Prevalence, health care expenditures, and patterns of work disability. *J. Occup. Environ. Med.* **Jun 1998;40(6):546-555.**

51. Fincham AM, Spedding GR. Low cost, high resolution DPIV for measurement of turbulent fluid flow. *Exp. Fluids.* **1997;23(6):449-462.**

52. Fisher GT, Boswick JA, Jr. Neuroma formation following digital amputations. *J. Trauma.* **Feb 1983;23(2):136-142.**

53. Fleiss JL. *Design and Analysis of Clinical Experiments***. New York: John Wiley and Sons; 1986.**

54. Fowler JR, Gaughan JP, Ilyas AM. The Sensitivity and Specificity of Ultrasound for the Diagnosis of Carpal Tunnel Syndrome: A Meta-analysis. *Clin. Orthop.* **Apr 2011;469(4):1089-1094.**

55. Friemel BH, Bohs LN, Nightingale KR, Trahey GE. Speckle decorrelation due to two-dimensional flow gradients. *IEEE Trans. Ultrason., Ferroelectr., Freq. Control.* **1998;45(2):317-327.**

56. Friemel BH, Bohs LN, Trahey GE. Relative performance of two-dimensional speckle-tracking techniques: normalized correlation, non-normalized correlation and sum-absolute-difference. Paper presented at: Ultrasonics Symposium, 1995. Proceedings., 1995 IEEE1995.

57. Fujii Y, Yamane T, Orito K, Osamura K, Wakao Y. Increased chymase-like activity in a dog with congenital pulmonic stenosis. *J Vet Cardiol.* **May 2007;9(1):39-42.**

58. Fujita M, Yasuda M, Kitatani K, et al. An up-to-date anti-cancer treatment strategy focusing on HIF-1alpha suppression: its application for refractory ovarian cancer. *Acta Histochem Cytoc.* **Dec 18 2007;40(5):139-142.**

59. Fukunaga T, Ito M, Ichinose Y, Kuno S, Kawakami Y, Fukashiro S. Tendinous movement of a human muscle during voluntary contractions determined by real-time ultrasonography. *J. Appl. Physiol.* **Sep 1996;81(3):1430-1433.**

60. Geiman B, Bohs L, Anderson M, Breit S, Trahey G. A comparison of algorithms for tracking sub-pixel speckle motion. Paper presented at: Ultrasonics Symposium, 1997. Proceedings., 1997 IEEE1997.

61. Gelberman RH, Hergenroeder PT, Hargens AR, Lundborg GN, Akeson WH. The carpal tunnel syndrome. A study of carpal canal pressures. *J. Bone Joint Surg. Am.* **Mar 1981;63(3):380-383.**

62. Giachetti A. Matching techniques to compute image motion. *Image Vision Comput.* **2000;18(3):247-260.**

63. Goetz JE, Main EK, Rudert MJ, Goreham-Voss CM, Brown TD. Apparent transverse compressive material properties of the digital flexor tendons and the median nerve in the carpal tunnel. *J. Biomech.* **Mar 15 2011;44(5):863-868.**

64. Goldberg SH, Jobin CM, Hayes AG, Gardner T, Rosenwasser MP, Strauch RJ. Biomechanics and histology of intact and repaired digital nerves: an in-vitro study. *J. Hand Surg. [Am.].* **Apr 2007;32(4):474-482.**

65. Golemati S, Sassano A, Lever MJ, Bharath AA, Dhanjil S, Nicolaides AN. Carotid artery wall motion estimated from B-mode ultrasound using region tracking and block matching. *Ultrasound Med. Biol.* **2003;29(3):387-399.**

66. Graham B. The value added by electrodiagnostic testing in the diagnosis of carpal tunnel syndrome. *J. Bone Joint Surg. Am.* **Dec 2008;90(12):2587-2593.**

67. Graham B, Dvali L, Regehr G, Wright JG. Variations in diagnostic criteria for carpal tunnel syndrome among Ontario specialists. *Am. J. Ind. Med.* **Jan 2006;49(1):8-13.**

68. Graham B, Regehr G, Naglie G, Wright JG. Development and validation of diagnostic criteria for carpal tunnel syndrome. *J. Hand Surg. [Am.].* **Jul-Aug 2006;31(6):919-924.**

69. Grechenig W, Clement H, Egner S, Tesch NP, Weiglein A, Peicha G. Musculo-tendinous junction of the flexor carpi ulnaris muscle. An anatomical study. *Surg. Radiol. Anat.* **2000;22(5-6):255-260.**

70. Guimberteau J. How does the sliding system work. *New ideas in hand flexor tendon surgery***. Bordeaux, France: Aquitaine Domaine, Forestier; 2001:16-44.**

71. Guimberteau J. How is anatomy adapted for tendon sliding. *New ideas in hand flexor tendon surgery***. Bordeaux, France: Aquitaine Domaine, Forestier; 2001:47-90.**

72. Guimberteau JC, Sentucq-Rigall J, Panconi B, Boileau R, Mouton P, Bakhach J. [Introduction to the knowledge of subcutaneous sliding system in humans]. *Ann. Chir. Plast. Esthet.* **Feb 2005;50(1):19-34.**

73. Hendee WR. Cross sectional medical imaging: a history. *Radiographics.*

Nov 1989;9(6):1155-1180.

74. Hirata H, Nagakura T, Tsujii M, Morita A, Fujisawa K, Uchida A. The relationship of VEGF and PGE2 expression to extracellular matrix remodelling of the tenosynovium in the carpal tunnel syndrome. *J. Pathol.* Dec 2004;204(5):605-612.

75. Hobson-Webb LD, Massey JM, Juel VC, Sanders DB. The ultrasonographic wrist-to-forearm median nerve area ratio in carpal tunnel syndrome. *Clin. Neurophysiol.* Jun 2008;119(6):1353-1357.

76. Hobson-Webb LD, Padua L. Median nerve ultrasonography in carpal tunnel syndrome: findings from two laboratories. *Muscle Nerve.* Jul 2009;40(1):94-97.

77. Hoeks AP, Arts TG, Brands PJ, Reneman RS. Comparison of the performance of the RF cross correlation and Doppler autocorrelation technique to estimate the mean velocity of simulated ultrasound signals. *Ultrasound Med. Biol.* 1993;19(9):727-740.

78. Horibe S, Woo SL, Spiegelman JJ, Marcin JP, Gelberman RH. Excursion of the flexor digitorum profundus tendon: a kinematic study of the human and canine digits. *J. Orthop. Res.* Mar 1990;8(2):167-174.

79. Horii E, Lin GT, Cooney WP, Linscheid RL, An KN. Comparative flexor tendon excursion after passive mobilization: an in-vitro study. *J. Hand Surg. [Am.].* May 1992;17(3):559-566.

80. Hossack JA. Influence of elevational motion on the degradation of 2D image frame matching. Paper presented at: IEEE Ultrasonics Symposium2000; San Juan, Puerto Rico.

81. Hough AD, Moore AP, Jones MP. Peripheral nerve motion measurement with spectral Doppler sonography: a reliability study. *J. Hand Surg. [Br.].* Dec 2000;25(6):585-589.

82. Hough AD, Moore AP, Jones MP. Reduced longitudinal excursion of the median nerve in carpal tunnel syndrome. *Arch. Phys. Med. Rehabil.* May 2007;88(5):569-576.

83. Huang XS, Moore J, Guiraudon G, et al. Dynamic 2D Ultrasound and 3D CT Image Registration of the Beating Heart. *IEEE Trans. Med. Imaging.* Aug 2009;28(8):1179-1189.

84. Hung LK, Chan A, Chang J, Tsang A, Leung PC. Early controlled active mobilization with dynamic splintage for treatment of extensor tendon injuries. *J. Hand Surg. [Am.].* Mar 1990;15(2):251-257.

85. Impink BG, Gagnon D, Collinger JL, Boninger ML. Repeatability of ultrasonographic median nerve measures. *Muscle Nerve.* Jun 2010;41(6):767-773.

86. Inomoto C, Umemura S, Egashira N, et al. Granulogenesis in non-neuroendocrine COS-7 cells induced by EGFP-tagged chromogranin A gene transfection: identical and distinct distribution of CgA and EGFP. *J. Histochem. Cytochem.* May 2007;55(5):487-493.

87. Inomoto C, Umemura S, Sasaki Y, Yasuda M, Terachi T, Osamura RY. Renal cell carcinoma arising in a long pre-existing angiomyolipoma. *Pathol. Int.* Mar 2007;57(3):162-166.

88. Ito M, Akima H, Fukunaga T. In-vivo moment arm determination using B-mode ultrasonography. *J. Biomech.* Feb 2000;33(2):215-218.

89. Itoh J, Osamura RY. Quantum dots for multicolor tumor pathology and multispectral imaging. *Methods Mol. Biol.* 2007;374:29-42.

90. Jablecki CK, Andary MT, So YT, Wilkins DE, Williams FH. Literature review of the usefulness of nerve conduction studies and electromyography for the evaluation of patients with carpal tunnel syndrome. AAEM Quality Assurance Committee. *Muscle Nerve.* Dec 1993;16(12):1392-1414.

91. James ER, Tang J, Goitz RJ, Kaufmann RA, Li ZM. Carpal tunnel syndrome causes motion deficits in thumb joints. Paper presented at: 52nd Annual meeting of the orthopeadic research society2006; 52nd Annual meeting of the orthopeadic research society in Chicago, IL.

92. Kamolz LP, Schrogendorfer KF, Rab M, Girsch W, Gruber H, Frey M. The precision of ultrasound imaging and its relevance for carpal tunnel syndrome. *Surg. Radiol. Anat.* 2001;23(2):117-121.

93. Karadag YS, Karadag O, Cicekli E, et al. Severity of Carpal tunnel syndrome assessed with high frequency ultrasonography. *Rheumatol. Int.* Apr 2010;30(6):761-765.

94. Katz JN, Lew RA, Bessette L, et al. Prevalence and predictors of long-term work disability due to carpal tunnel syndrome. *Am. J. Ind. Med.* Jun 1998;33(6):543-550.

95. Kaymak B, Ozcakar L, Cetin A, Candan Cetin M, Akinci A, Hascelik Z. A comparison of the benefits of sonography and electrophysiologic measurements

as predictors of symptom severity and functional status in patients with carpal tunnel syndrome. *Arch. Phys. Med. Rehabil.* Apr 2008;89(4):743-748.

96. Keith LG, Ngorima T, Tsar OM. Hyperfertility, obesity, and stillbirth: new considerations for clinical practice. *J. Exp. Clin. Assist. Reprod.* 2009;6:2.

97. Keith MW, Masear V, Chung KC, et al. American Academy of Orthopaedic Surgeons Clinical Practice Guideline on diagnosis of carpal tunnel syndrome. *J. Bone Joint Surg. Am.* Oct 2009;91(10):2478-2479.

98. Kessler I, Nissim F. Primary repair without immobilization of flexor tendon division within the digital sheath. An experimental and clinical study. *Acta Orthop. Scand.* 1969;40(5):587-601.

99. Klauser AS, Halpern EJ, De Zordo T, et al. Carpal tunnel syndrome assessment with US: value of additional cross-sectional area measurements of the median nerve in patients versus healthy volunteers. *Radiology.* Jan 2009;250(1):171-177.

100. Kleindienst A, Hamm B, Lanksch WR. Carpal tunnel syndrome: staging of median nerve compression by MR imaging. *J. Magn. Reson. Imaging.* Sep-Oct 1998;8(5):1119-1125.

101. Kleinert HE, Kutz JE, Atasoy E, Stormo A. Primary repair of flexor tendons. *Orthop. Clin. North Am.* Oct 1973;4(4):865-876.

102. Korstanje J-WH, Schreuders TAR, van der Sijde J, Hovius SER, Bosch JG, Selles RW. Ultrasonographic Assessment of Long Finger Tendon Excursion in Zone V during Passive and Active Tendon Gliding Exercises. *J. Hand Surg. [Am.].* 2010;35(4):559-565.

103. Korstanje J-WH, Selles RW, Stam HJ, Hovius SER, Bosch JG. Development and validation of ultrasound speckle tracking to quantify tendon displacement. *J. Biomech.* 2010;43(7):1373-1379.

104. Korstanje JWH, Selles RW, Stam HJ, Hovius SER, Bosch JG. Dedicated ultrasound speckle tracking to study tendon displacement. Paper presented at: In conference proceedings of SPIE Medical Imaging 2009: Ultrasonic Imaging and Signal Processing2009; Lake Buena Vista, FL, USA.

105. Koyuncuoglu HR, Kutluhan S, Yesildag A, Oyar O, Guler K, Ozden A. The value of ultrasonographic measurement in carpal tunnel syndrome in patients with negative electrodiagnostic tests. *Eur. J. Radiol.* Dec 2005;56(3):365-369.

106. Kumaki N, Umemura S, Kajiwara H, Itoh J, Itoh Y, Osamura RY. Immunohistochemical analysis of neuroendocrine (NE) differentiation in testicular germ cell tumors (GCTs): use of confocal laser scanning microscopy (CLSM) to demonstrate direct NE differentiation from GCTs. *Acta Histochem Cytoc.* Dec 21 2007;40(6):143-151.

107. Kwon BC, Jung KI, Baek GH. Comparison of sonography and electrodiagnostic testing in the diagnosis of carpal tunnel syndrome. *J. Hand Surg. [Am.].* Jan 2008;33(1):65-71.

108. Landsmeer JM. Studies in the anatomy of articulation. I. The equilibrium of the "intercalated" bone. *Acta Morphol. Neerl. Scand.* 1961;3:287-303.

109. Lee CH, Kim TK, Yoon ES, Dhong ES. Correlation of high-resolution ultrasonographic findings with the clinical symptoms and electrodiagnostic data in carpal tunnel syndrome. *Ann. Plast. Surg.* Jan 2005;54(1):20-23.

110. Lee SS, Lewis GS, Piazza SJ. An algorithm for automated analysis of ultrasound images to measure tendon excursion in-vivo. *J. Appl. Biomech.* Feb 2008;24(1):75-82.

111. Lehfeldt M, Ray E, Sherman R. MOC-PS(SM) CME article: treatment of flexor tendon laceration. *Plast. Reconstr. Surg.* Apr 2008;121(4 Suppl):1-12.

112. Leigh JP, Miller TR. Job-related diseases and occupations within a large workers' compensation data set. *Am. J. Ind. Med.* Mar 1998;33(3):197-211.

113. Levine DW, Simmons BP, Koris MJ, et al. A self-administered questionnaire for the assessment of severity of symptoms and functional status in carpal tunnel syndrome. *J. Bone Joint Surg. Am.* Nov 1993;75(11):1585-1592.

114. Lim BH, T.M. T. The six-strand technique for flexor tendon repair. *Atlas Hand Clin.* 1996;1:65-76.

115. Lipton MJ, Higgins CB, Farmer D, Boyd DP. Cardiac imaging with a high-speed Cine-CT Scanner: preliminary results. *Radiology.* Sep 1984;152(3):579-582.

116. Lluch AL. Thickening of the synovium of the digital flexor tendons: cause or consequence of the carpal tunnel syndrome? *J. Hand Surg. [Br.].* Apr 1992;17(2):209-212.

117. Loram ID, Maganaris CN, Lakie M. Paradoxical muscle movement in human standing. *J. Physiol.* May 1 2004;556(3):683-689.

118. Loram ID, Maganaris CN, Lakie M. Use of ultrasound to make noninvasive in-vivo measurement of continuous changes in human muscle contractile length. *J. Appl. Physiol.* Apr 2006;100(4):1311-1323.

REFERENCES

119. Maganaris CN, Baltzopoulos V, Tsaopoulos D. Muscle fibre length-to-moment arm ratios in the human lower limb determined in-vivo. *J. Biomech.* **2006;39(9):1663-1668.**

120. Maganaris CN, Paul JP. Tensile properties of the in-vivo human gastrocnemius tendon. *J. Biomech.* **2002;35(12):1639-1646.**

121. Malczewski MC, Zamboni WA, Haws MJ, Johnson RM, Smoot EC, Russell RC. Effect of motion on digital nerve repair in a fresh cadaver model. *Plast. Reconstr. Surg.* **Dec 1995;96(7):1672-1675.**

122. Mallouhi A, Pulzl P, Trieb T, Piza H, Bodner G. Predictors of carpal tunnel syndrome: accuracy of gray-scale and color Doppler sonography. *Am. J. Roentgenol.* **May 2006;186(5):1240-1245.**

123. Manente G, Torrieri F, Di Blasio F, Staniscia T, Romano F, Uncini A. An innovative hand brace for carpal tunnel syndrome: a randomized controlled trial. *Muscle Nerve.* **Aug 2001;24(8):1020-1025.**

124. Manske PR. Flexor tendon healing. *J. Hand Surg. [Br.].* **Aug 1988;13(3):237-245.**

125. Marshall S, Tardif G, Ashworth N. Local corticosteroid injection for carpal tunnel syndrome. *Cochrane Database Syst. Rev.* **2007(2):CD001554.**

126. May EJ, Silfverskiold KL, Sollerman CJ. Controlled mobilization after flexor tendon repair in zone II: a prospective comparison of three methods. *J. Hand Surg. [Am.].* **Sep 1992;17(5):942-952.**

127. May EJ, Silfverskiold KL, Sollerman CJ. The correlation between controlled range of motion with dynamic traction and results after flexor tendon repair in zone II. *J. Hand Surg. [Am.].* **Nov 1992;17(6):1133-1139.**

128. McGrouther DA, Ahmed MR. Flexor tendon excursions in "no-man's land". *Hand.* **Jun 1981;13(2):129-141.**

129. McLarney E, Hoffman H, Wolfe SW. Biomechanical analysis of the cruciate four-strand flexor tendon repair. *J. Hand Surg. [Am.].* **Mar 1999;24(2):295-301.**

130. Meunier J, Bertrand M. Ultrasonic texture motion analysis: theory and simulation. *IEEE Trans. Med. Imaging.* **1995;14(2):293-300.**

131. Migrino RQ, Harmann L, Woods T, Bright M, Truran S, Hari P. Intraventricular dyssynchrony in light chain amyloidosis: a new mechanism of systolic dysfunction assessed by 3-dimensional echocardiography. *Cardiovasc Ultrasound.* **2008;6:40.**

132. Moran L, Perez M, Esteban A, Bellon J, Arranz B, del Cerro M. Sonographic measurement of cross-sectional area of the median nerve in the diagnosis of carpal tunnel syndrome: correlation with nerve conduction studies. *J. Clin. Ultrasound.* **Mar-Apr 2009;37(3):125-131.**

133. Nag A, Nag PK, Desai H. Hand anthropometry of Indian women. *Indian J. Med. Res.* **Jun 2003;117:260-269.**

134. Nakamichi K, Tachibana S. Restricted motion of the median nerve in carpal tunnel syndrome. *J. Hand Surg. [Br.].* **Aug 1995;20(4):460-464.**

135. Nakamichi K, Tachibana S. Restricted Motion of the Median Nerve in Carpal-Tunnel Syndrome. *J. Hand Surg. [Br.].* **Aug 1995;20B(4):460-464.**

136. Nakamichi KI, Tachibana S. Enlarged median nerve in idiopathic carpal tunnel syndrome. *Muscle Nerve.* **Nov 2000;23(11):1713-1718.**

137. Nathan PA, Keniston RC, Meadows KD, Lockwood RS. Predictive value of nerve conduction measurements at the carpal tunnel. *Muscle Nerve.* **Dec 1993;16(12):1377-1382.**

138. Nelson AW. The painful neuroma: the regenerating axon verus the epineural sheath. *J. Surg. Res.* **Sep 1977;23(3):215-221.**

139. Ng ACT, Tran DT, Newman M, et al. Comparison of Myocardial Tissue Velocities Measured by Two-Dimensional Speckle Tracking and Tissue Doppler Imaging. *Am. J. Cardiol.* **2008;102(6):784-789.**

140. Oda T, Himeno R, D CH, et al. In-vivo behavior of muscle fascicles and tendinous tissues in human tibialis anterior muscle during twitch contraction. *J. Biomech.* **2007;40(14):3114-3120.**

141. Ofer N, Akselrod S, Nyska M, Werner M, Glaser E, Shabat S. Motion-based tendon diagnosis using sequence processing of ultrasound images. *J. Orthop. Res.* **2004;22(6):1296-1302.**

142. Oh J, Zhao C, Zobitz ME, Wold LE, An KN, Amadio PC. Morphological changes of collagen fibrils in the subsynovial connective tissue in carpal tunnel syndrome. *J. Bone Joint Surg. Am.* **Apr 2006;88(4):824-831.**

143. Oh S, Belohlavek M, Zhao C, et al. Detection of differential gliding characteristics of the flexor digitorum superficialis tendon and subsynovial connective tissue using color Doppler sonographic imaging. *J. Ultrasound Med.* **Feb 2007;26(2):149-155.**

144. Ophir J, Cespedes I, Ponnekanti H, Yazdi Y, Li X. Elastography: a

quantitative method for imaging the elasticity of biological tissues. *Ultrason. Imaging.* **Apr 1991;13(2):111-134.**

145. Osamura N, Zhao C, Zobitz ME, An KN, Amadio PC. Evaluation of the material properties of the subsynovial connective tissue in carpal tunnel syndrome. *Clin. Biomech.* **Nov 2007;22(9):999-1003.**

146. Osamura N, Zhao C, Zobitz ME, An KN, Amadio PC. Permeability of the subsynovial connective tissue in the human carpal tunnel: a cadaver study. *Clin. Biomech.* **Jun 2007;22(5):524-528.**

147. Oshiro M, Nishimura T. US Image Improvement Using Fuzzy Neural Network with Epanechnikov Kernel. *2009 35th Annual Conference of IEEE Industrial Electronics, Vols 1-6.* **2009:2005-2010.**

148. Padua L, Aprile I, Caliandro P, et al. Symptoms and neurophysiological picture of carpal tunnel syndrome in pregnancy. *Clin. Neurophysiol.* **Oct 2001;112(10):1946-1951.**

149. Panchal J, Mehdi S, Donoghue JO, O'Sullivan ST, O'Shaughnessy M, O'Connor TP. The range of excursion of flexor tendons in Zone V: a comparison of active vs passive flexion mobilisation regimes. *Br. J. Plast. Surg.* **Oct 1997;50(7):517-522.**

150. Phalen GS. The carpal-tunnel syndrome. Clinical evaluation of 598 hands. *Clin. Orthop.* **Mar-Apr 1972;83:29-40.**

151. Qvistgaard E, Torp-Pedersen S, Christensen R, Bliddal H. Reproducibility and inter-reader agreement of a scoring system for ultrasound evaluation of hip osteoarthritis. *Ann. Rheum. Dis.* **Dec 2006;65(12):1613-1619.**

152. Rappaport D, Adam D, Lysyansky P, Riesner S. Assessment of myocardial regional strain and strain rate by tissue tracking in B-mode echocardiograms. *Ultrasound Med. Biol.* **2006;32(8):1181-1192.**

153. Rempel D, Dahlin L, Lundborg G. Pathophysiology of nerve compression syndromes: response of peripheral nerves to loading. *J. Bone Joint Surg. Am.* **Nov 1999;81(11):1600-1610.**

154. Revell J, Mirmehdi M, McNally D. Combined Ultrasound Speckle Pattern Similarity Measures. *Medical Image Understanding and Analysis***: BMVA Press; 2004:149-153.**

155. Revell J, Mirmehdi M, McNally D. Musculoskeletal motion flow fields using hierarchical variable-sized block matching in ultrasonographic video sequences *J. Biomech.* **2004;37(4):511-522.**

156. Revell J, Mirmehdi M, McNally D. Computer vision elastography: speckle adaptive motion estimation for elastography using ultrasound sequences. *IEEE Trans. Med. Imaging.* **Jun 2005;24(6):755-766.**

157. Riederer SJ, Tasciyan T, Farzaneh F, Lee JN, Wright RC, Herfkens RJ. MR fluoroscopy: technical feasibility. *Magn. Reson. Med.* **Sep 1988;8(1):1-15.**

158. Roh YH, Chung MS, Baek GH, Lee YH, Rhee SH, Gong HS. Incidence of clinically diagnosed and surgically treated carpal tunnel syndrome in Korea. *J. Hand Surg. [Am.].* **Sep 2010;35(9):1410-1417.**

159. Rosenthal EA, Stoddard CW. Questions hand therapists ask about treatment of tendon injuries. *J. Hand Ther.* **Apr-Jun 2005;18(2):313-318.**

160. Sandford F, Barlow N, Lewis J. A study to examine patient adherence to wearing 24-hour forearm thermoplastic splints after tendon repairs. *J. Hand Ther.* **Jan-Mar 2008;21(1):44-52; quiz 53.**

161. Sandow MJ, McMahon MM. Single cross-grasp six-strand repair for acute flexor tenorrhaphy: modified Savage technique. *Atlas Hand Clin.* **1996;1:41-64.**

162. Sarria L, Cabada T, Cozcolluela R, Martinez-Berganza T, Garcia S. Carpal tunnel syndrome: usefulness of sonography. *Eur. Radiol.* **2000;10(12):1920-1925.**

163. Seror P. Sonography and electrodiagnosis in carpal tunnel syndrome diagnosis, an analysis of the literature. *Eur. J. Radiol.* **Jul 2008;67(1):146-152.**

164. Shapiro BE, Preston DC. Entrapment and compressive neuropathies. *Med. Clin. North Am.* **Mar 2009;93(2):285-315, vii.**

165. Shrout PE, Fleiss JL. Intraclass correlations: uses in assessing rater reliability. *Psychol. Bull.* **Mar 1979;86(2):420-428.**

166. Siddique J, Lauderdale DS, VanderWeele TJ, Lantos JD. Trends in prenatal ultrasound use in the United States: 1995 to 2006. *Med. Care.* **Nov 2009;47(11):1129-1135.**

167. Silfverskiold KL, May EJ. Flexor tendon repair in zone II with a new suture technique and an early mobilization program combining passive and active flexion. *J. Hand Surg. [Am.].* **Jan 1994;19(1):53-60.**

168. Silfverskiold KL, May EJ, Tornvall AH. Tendon excursions after flexor

tendon repair in zone. II: Results with a new controlled-motion program. *J. Hand Surg. [Am.].* **May 1993;18(3):403-410.**

169. Silva MJ, Hollstien SB, Fayazi AH, Adler P, Gelberman RH, Boyer MI. The effects of multiple-strand suture techniques on the tensile properties of repair of the flexor digitorum profundus tendon to bone. *J. Bone Joint Surg. Am.* **Oct 1998;80(10):1507-1514.**

170. Small JO, Brennen MD, Colville J. Early active mobilisation following flexor tendon repair in zone 2. *J. Hand Surg. [Br.].* **Nov 1989;14(4):383-391.**

171. Smidt MH, Visser LH. Carpal tunnel syndrome: clinical and sonographic follow-up after surgery. *Muscle Nerve.* **Aug 2008;38(2):987-991.**

172. Smith J, Hurdle MF. Office-based ultrasound-guided intra-articular hip injection: technique for physiatric practice. *Arch. Phys. Med. Rehabil.* **Feb 2006;87(2):296-298.**

173. Soeters JN, Roebroeck ME, Holland WP, Hovius SE, Stam HJ. Non-invasive measurement of tendon excursion with a colour Doppler imaging system: a reliability study in healthy subjects. *Scand. J. Plast. Reconstr. Surg.* **2004;38(6):356-360.**

174. Soeters JN, Roebroeck ME, Holland WP, Hovius SE, Stam HJ. Reliability of tendon excursion measurements in patients using a color Doppler imaging system. *J. Hand Surg. [Am.].* **Jul 2004;29(4):581-586.**

175. Sofka CM, Pavlov H. The history of clinical musculoskeletal radiology. *Radiol. Clin. North Am.* **May 2009;47(3):349-356.**

176. Stevens JC. AAEM minimonograph #26: the electrodiagnosis of carpal tunnel syndrome. American Association of Electrodiagnostic Medicine. *Muscle Nerve.* **Dec 1997;20(12):1477-1486.**

177. Stevens JC, Smith BE, Weaver AL, Bosch EP, Deen HG, Jr., Wilkens JA. Symptoms of 100 patients with electromyographically verified carpal tunnel syndrome. *Muscle Nerve.* **Oct 1999;22(10):1448-1456.**

178. Strickland JW. Results of flexor tendon surgery in zone II. *Hand Clin.* **Feb 1985;1(1):167-179.**

179. Strickland JW. Flexor Tendon Injuries: II. Operative Technique. *J. Am. Acad. Orthop. Surg.* **Jan 1995;3(1):55-62.**

180. Strickland JW. Development of flexor tendon surgery: twenty-five years of progress. *J. Hand Surg. [Am.].* **Mar 2000;25(2):214-235.**

181. Strickland JW. The scientific basis for advances in flexor tendon surgery. *J. Hand Ther.* **Apr-Jun 2005;18(2):94-110.**

182. Sud V, Tucci MA, Freeland AE, Smith WT, Grinspun K. Absorptive properties of synovium harvested from the carpal tunnel. *Microsurgery.* **2002;22(7):316-319.**

183. Sullivan DJ. Results of digital neurorrhaphy in adults. *J. Hand Surg. [Br.].* **Feb 1985;10(1):41-44.**

184. Szabo RM. Carpal tunnel syndrome as a repetitive motion disorder. *Clin. Orthop. Relat. Res.* **Jun 1998(351):78-89.**

185. Szabo RM, Chidgey LK. Stress carpal tunnel pressures in patients with carpal tunnel syndrome and normal patients. *J. Hand Surg. [Am.].* **Jul 1989;14(4):624-627.**

186. Tagliafico A, Tagliafico G, Martinoli C. Nerve density: a new parameter to evaluate peripheral nerve pathology on ultrasound. Preliminary study. *Ultrasound Med. Biol.* **Oct 2010;36(10):1588-1593.**

187. Takei M, Suzuki M, Kajiya H, et al. Immunohistochemical detection of somatostatin receptor (SSTR) subtypes 2A and 5 in pituitary adenoma from acromegalic patients: good correlation with preoperative response to octreotide. *Endocr. Pathol.* **Winter 2007;18(4):208-216.**

188. Talsma E, de Haart M, Beelen A, Nollet F. The Effect of Mobilization on Repaired Extensor Tendon Injuries of the Hand: A Systematic Review. *Arch. Phys. Med. Rehabil.* **2008;89(12):2366-2372.**

189. Tanaka T, Amadio PC, Zhao C, Zobitz ME, An KN. Flexor digitorum profundus tendon tension during finger manipulation. *J. Hand Ther.* **Jul-Sep 2005;18(3):330-338; quiz 338.**

190. Thien TB, Becker JH, Theis JC. Rehabilitation after surgery for flexor tendon injuries in the hand. *Cochrane Database Syst. Rev.* **2004(4):CD003979.**

191. Thijssen JM, Oosterveld BJ. Texture in tissue echograms. Speckle or information? *J. Ultrasound Med.* **Apr 1990;9(4):215-229.**

192. Tibshirani R. Regression shrinkage and selection via the Lasso. *J. R. Sta. Soc. Ser. B Stat. Methodol.* **1996;58(1):267-288.**

193. Trumble TE, Vedder NB, Seiler JG, 3rd, Hanel DP, Diao E, Pettrone S. Zone-II flexor tendon repair: a randomized prospective trial of active place-and-hold therapy compared with passive motion therapy. *J. Bone Joint Surg. Am.* **Jun 2010;92(6):1381-1389.**

194. **Uchiyama S, Itsubo T, Yasutomi T, Nakagawa H, Kamimura M, Kato H. Quantitative MRI of the wrist and nerve conduction studies in patients with idiopathic carpal tunnel syndrome.** *J. Neurol. Neurosurg. Psychiatry.* **Aug 2005;76(8):1103-1108.**

195. **Ugbolue UC, Hsu WH, Goitz RJ, Li ZM. Tendon and nerve displacement at the wrist during finger movements.** *Clin. Biomech.* **Jan 2005;20(1):50-56.**

196. **Umemura S, Yoshida S, Ohta Y, Naito K, Osamura RY, Tokuda Y. Increased phosphorylation of Akt in triple-negative breast cancers.** *Cancer Sci.* **Dec 2007;98(12):1889-1892.**

197. **van Doesburg MH, Yoshii Y, Villarraga HR, et al. Median nerve deformation and displacement in the carpal tunnel during index finger and thumb motion.** *J. Orthop. Res.* **Oct 2010;28(10):1387-1390.**

198. **van Rijn RM, Huisstede BM, Koes BW, Burdorf A. Associations between work-related factors and the carpal tunnel syndrome--a systematic review.** *Scand. J. Work. Environ. Health.* **Jan 2009;35(1):19-36.**

199. **Varghese T, Bilgen M, Ophir J. Multiresolution imaging in elastography.** *IEEE Trans Ultrason Ferroelectr Freq Control.* **1998;45(1):65-75.**

200. **Varghese T, Konofagou EE, Ophir J, Alam SK, Bilgen M. Direct strain estimation in elastography using spectral cross-correlation.** *Ultrasound Med. Biol.* **Nov 2000;26(9):1525-1537.**

201. **Verdan C. Practical Considerations for Primary and Secondary Repair in Flexor Tendon Injuries.** *Surg. Clin. North Am.* **Aug 1964;44:951-970.**

202. **Viola F, Walker WF. A spline-based algorithm for continuous time-delay estimation using sampled data.** *Ultrasonics, Ferroelectrics and Frequency Control, IEEE Transactions on.* **2005;52(1):80-93.**

203. **Vipond N, Taylor W, Rider M. Postoperative splinting for isolated digital nerve injuries in the hand.** *J. Hand Ther.* **Jul-Sep 2007;20(3):222-230; quiz 231.**

204. **Visser LH, Smidt MH, Lee ML. High-resolution sonography versus EMG in the diagnosis of carpal tunnel syndrome.** *J. Neurol. Neurosurg. Psychiatry.* **Jan 2008;79(1):63-67.**

205. **Wehbe MA, Hunter JM. Flexor tendon gliding in the hand. Part I. In-vivo excursions.** *J. Hand Surg. [Am.].* **Jul 1985;10(4):570-574.**

206. **Wehbe MA, Hunter JM. Flexor tendon gliding in the hand. Part II. Differential gliding.** *J. Hand Surg. [Am.].* **Jul 1985;10(4):575-579.**

207. **Weinberg SM, Scott NM, Neiswanger K, Marazita ML. Intraobserver error associated with measurements of the hand.** *Am J Hum Biol.* **2005;17(3):368-371.**

208. **Wiebe C, Brodland GW. Tensile properties of embryonic epithelia measured using a novel instrument.** *J. Biomech.* **Oct 2005;38(10):2087-2094.**

209. **Wiesler ER, Chloros GD, Cartwright MS, Smith BP, Rushing J, Walker FO. The use of diagnostic ultrasound in carpal tunnel syndrome.** *J Hand Surg Am.* **May-Jun 2006;31(5):726-732.**

210. **Witt JC, Hentz JG, Stevens JC. Carpal tunnel syndrome with normal nerve conduction studies.** *Muscle Nerve.* **Apr 2004;29(4):515-522.**

211. **Wong SM, Griffith JF, Hui AC, Lo SK, Fu M, Wong KS. Carpal tunnel syndrome: diagnostic usefulness of sonography.** *Radiology.* **Jul 2004;232(1):93-99.**

212. **World Health Organization.** *Towards a common language for functioning, disability, and health: ICF - The international classification of functioning, disability, and health.* **Geneva: World Health Organization;2002.**

213. **Yamaguchi T, Osamura N, Zhao C, An KN, Amadio PC. Relative longitudinal motion of the finger flexors, subsynovial connective tissue, and median nerve before and after carpal tunnel release in a human cadaver model.** *J. Hand Surg. [Am.].* **Jul-Aug 2008;33(6):888-892.**

214. **Yamaguchi T, Osamura N, Zhao C, Zobitz ME, An KN, Amadio PC. The mechanical properties of the rabbit carpal tunnel subsynovial connective tissue.** *J. Biomech.* **Dec 5 2008;41(16):3519-3522.**

215. **Yesildag A, Kutluhan S, Sengul N, et al. The role of ultrasonographic measurements of the median nerve in the diagnosis of carpal tunnel syndrome.** *Clin. Radiol.* **Oct 2004;59(10):910-915.**

216. **Yeung F, Levinson SF, Parker KJ. Multilevel and Motion Model-Based Ultrasonic Speckle Tracking Algorithms.** *Ultrasound Med. Biol.* **1998;24(3):427-441.**

217. **Yoshii Y, Villarraga HR, Henderson J, Zhao C, An KN, Amadio PC. Speckle tracking ultrasound for assessment of the relative motion of flexor tendon and subsynovial connective tissue in the human carpal tunnel.** *Ultrasound Med. Biol.* **Dec 2009;35(12):1973-1981.**

218. **Yoshii Y, Villarraga HR, Henderson J, Zhao C, An KN, Amadio PC. Ultrasound assessment of the displacement and deformation of the median nerve in the human carpal tunnel with active finger motion.** *J. Bone Joint Surg. Am.* **Dec 2009;91(12):2922-2930.**

219. **Yoshii Y, Zhao C, Henderson J, Zhao KD, An KN, Amadio PC. Velocity-dependent changes in the relative motion of the subsynovial connective tissue in the human carpal tunnel.** *J. Orthop. Res.* **Jul 6 2010;29(1):62-66.**

220. **Yoshii Y, Zhao C, Henderson J, Zhao KD, An KN, Amadio PC. Velocity-dependent changes in the relative motion of the subsynovial connective tissue in the human carpal tunnel.** *J. Orthop. Res.* **Jan 2011;29(1):62-66.**

221. **Yoshii Y, Zhao C, Henderson J, et al. Effects of carpal tunnel release on the relative motion of tendon, nerve, and subsynovial connective tissue in a human cadaver model.** *Clin. Biomech.* **Nov 2008;23(9):1121-1127.**

222. **Yoshii Y, Zhao C, Zhao KD, Zobitz ME, An KN, Amadio PC. The effect of wrist position on the relative motion of tendon, nerve, and subsynovial connective tissue within the carpal tunnel in a human cadaver model.** *J. Orthop. Res.* **Aug 2008;26(8):1153-1158.**

223. **Zempsky WT, Schechter NL. Office-based pain management. The 15-minute consultation.** *Pediatr. Clin. North Am.* **Jun 2000;47(3):601-615.**

224. **Zhou P, Goodson KE. Subpixel displacement and deformation gradient measurement using digital image/speckle correlation (DISC).** *Opt Eng.* **2001;40(8):1613-1620.**